

**N 84 - 20684**

**NASA CR-168320  
BAC D180-28273-1**



**National Aeronautics and  
Space Administration**

**EVALUATION OF PROPELLANT TANK INSULATION  
CONCEPTS FOR LOW-THRUST CHEMICAL  
PROPULSION SYSTEMS**

**BOEING AEROSPACE COMPANY**

**prepared for**

**NASA Lewis Research Center  
Contract NAS3-22824**



NASA CR-168320  
BAC D180-28273-1



National Aeronautics and  
Space Administration

# **EVALUATION OF PROPELLANT TANK INSULATION CONCEPTS FOR LOW-THRUST CHEMICAL PROPULSION SYSTEMS**

by T.J. Kramer, E.W. Brogren, and B.L. Siegel

**BOEING AEROSPACE COMPANY**

prepared for

NASA Lewis Research Center  
Contract NAS3-22824





1. Report No. CR 168320		2. Government Accession No.		3. Recipient's Catalog No.	
4. Title and Subtitle EVALUATION OF PROPELLANT TANK INSULATION CONCEPTS FOR LOW-THRUST CHEMICAL PROPULSION SYSTEMS				5. Report Date March 1984	
				6. Performing Organization Code	
7. Author(s) T. Kramer, E. Brogren, B. Siegel				8. Performing Organization Report No. BAC D180-28273-1	
9. Performing Organization Name and Address Boeing Aerospace Company P.O. Box 3999 Seattle, WA 98124				10. Work Unit No.	
				11. Contract or Grant No. NAS3-22824	
12. Sponsoring Agency Name and Address NASA Lewis Research Center 21000 Brookpark Road Cleveland, OH 44135				13. Type of Report and Period Covered Contractor Report	
				14. Sponsoring Agency Code	
15. Supplementary Notes Project Manager, J. C. Aydelott Lewis Research Center Cleveland, OH 44135					
16. Abstract An analytical evaluation of cryogenic propellant tank insulations for liquid oxygen/liquid hydrogen low-thrust 2224N (500 lbf) propulsion systems (LTPS) was conducted. The insulation studied consisted of combinations of N <sub>2</sub> -purged foam and multilayer insulation (MLI) as well as He-purged MLI-only. Heat leak and payload performance predictions were made for three Shuttle-launched LTPS designed for Shuttle bay packaged payload densities of 56 kg/m <sup>3</sup> (3.5 lbf/ft <sup>3</sup> ), 40 kg/m <sup>3</sup> (2.5 lbf/ft <sup>3</sup> ) and 24 kg/m <sup>3</sup> (1.5 lbf/ft <sup>3</sup> ). Foam/MLI insulations were found to increase LTPS payload delivery capability when compared with He-purged MLI-only. An additional benefit of foam/MLI was reduced operational complexity because Orbiter cargo bay N <sub>2</sub> purge gas could be used for MLI purging. Maximum payload mass benefit occurred when an enhanced convection, rather than natural convection, heat transfer was specified for the insulation purge enclosure. The enhanced convection environment allowed minimum insulation thickness to be used for the foam/MLI interface temperature selected to correspond to the moisture dew point in the N <sub>2</sub> purge gas. Experimental verification of foam/MLI benefits was recommended. A conservative program cost estimate for testing a MLI-foam insulated tank was 2.1 million dollars. It was noted this cost could be reduced significantly without increasing program risk.					
17. Key Words (Suggested by Author(s))  Heat Transfer, Foam Insulation, Space Propulsion, Cryogenics				18. Distribution Statement  Unclassified - Unlimited	
19. Security Classif. (of this report) Unclassified		20. Security Classif. (of this page) Unclassified		21. No. of Pages	
				22. Price*	

\* For sale by the National Technical Information Service, Springfield, Virginia 22161



## **FOREWORD**

This final report was prepared by the Boeing Aerospace Company, under Contract NAS3-22824. The contract was administered by the National Aeronautics and Space Administration Lewis Research Center. Mr. J. C. Aydelott provided technical direction. The period of study was from October 1981 to October 1982.



## TABLE OF CONTENTS

	Page
LIST OF FIGURES	ix
LIST OF TABLES	xiii
SUMMARY	1
1.0 INTRODUCTION	3
1.1 STUDY OBJECTIVES	4
1.2 STUDY SCOPE	4
1.3 REPORT ORGANIZATION	6
2.0 INSULATION CONCEPTS	9
2.1 FOAM INSULATION	14
2.1.1 Properties of Foam Insulations	14
2.1.2 Foam Insulation Application	15
2.1.3 Foam Insulation Design	19
2.2 MULTILAYER INSULATION	19
2.2.1 Multilayer Insulation Design	21
2.2.2 Insulation Properties	23
2.2.3 MLI Venting	23
3.0 LTPS CONCEPTUAL DESIGNS	27
3.1 GROUND RULES AND ASSUMPTIONS	28
3.2 LTPS MISSION	30
3.3 LTPS CONCEPTUAL DESIGN APPROACH	36
3.4 TASK I LTPS CONCEPTUAL DESIGN	43
3.5 TASK II LTPS CONCEPTUAL DESIGNS	46
4.0 PREDICTED PROPELLANT THERMAL LOADS	55
4.1 THERMAL MODELING APPROACH	55
4.1.1 LTPS Environments	56
4.1.2 LTPS Thermal Models	60
4.1.2.1 Thermal Model Description	60
4.1.2.2 Typical Thermal Math Model Results	72
4.1.2.3 Enhanced Convection Thermal Modeling	79
4.2 PREDICTED INSULATION PERFORMANCE	82
4.2.1 Ground Hold and Initial Launch Phases	83
4.2.2 Initial Launch Phase to Orbiter Separation	90
4.2.3 LTPS Free-Flight	90

## TABLE OF CONTENTS (Continued)

	Page
4.3 PREDICTED TANK PENETRATION HEAT LEAK	90
4.4 PREDICTED TANK SUPPORT HEAT LEAK	95
5.0 INSULATION OPTIMIZATION	97
5.1 OPTIMIZATION GROUNDRULES AND ASSUMPTIONS	98
5.2 OPTIMIZATION APPROACH	100
5.3 LTPS SIZING MODEL	101
5.3.1 Model Variables	101
5.3.2 Computer Model Logic Flow	103
5.3.3 Algorithms and Calculation Details	109
5.4 LTPS DESIGN PARAMETRICS	111
5.4.1 Insulation Parametrics	112
5.4.2 Propellant Tank Parametrics	115
5.4.3 Propellant Density	115
5.4.4 Self Pressurization	118
5.4.5 Structural Mass	118
5.5 INSULATION OPTIMIZATION RESULTS	124
6.0 EXPERIMENTAL PROGRAM PLAN	141
6.1 EXPERIMENTAL APPROACH	141
6.2 EXPERIMENT PLAN	142
6.2.1 Test Preparations	142
6.2.2 Test Sequence	145
6.2.3 Measurements	148
6.2.4 Analysis and Conclusions	150
6.3 EXPERIMENTAL HARDWARE DESIGN	151
6.3.1 Cryogenic Tank	151
6.3.2 Tank Support System	151
6.3.3 Thermal Shroud	161
6.3.4 Insulation System(s)	161
6.3.5 Test Facility	165
6.3.6 Instrumentation System	169
6.4 COST ESTIMATES	173
6.5 PROGRAM SCHEDULE AND COSTS	177
6.6 TEST PROGRAM RECOMMENDATIONS AND ALTERNATIVE PLANS	183
7.0 STUDY CONCLUSIONS AND RECOMMENDATIONS	185

## TABLE OF CONTENTS (Continued)

	Page
APPENDIX A      RADIATION INTERCHANGE FACTOR AND ENVIRONMENTAL HEATING ANALYSIS PROGRAMS	189
APPENDIX B      TANK SUPPORT STRUT OPTIMIZATION	191
APPENDIX C      TRADE PROGRAMS FOR LTPS SIZING AND INSULATION OPTIMIZATION	199
APPENDIX D      PROPELLANT EFFECTIVE TANKING DENSITY ANALYSIS	237
APPENDIX E      PROPELLANT TANK SELF PRESSURIZATION MODEL	245
APPENDIX F      SYMBOLS AND DEFINITIONS	249
REFERENCES	251





## LIST OF FIGURES

	Page
2-1	17
2-2	18
2-3	20
2-4	22
2-5	24
2-6	25
2-7	26
	Across Venting MLI
3-1	32
3-2	33
3-3	34
3-4	35
	Mass, Inertial Properties and Projected Areas of the Baseline LTPS/LSS
3-5	42
3-6	44
3-7	48
3-8	49
3-9	50
4-1	57
4-2	59
4-3	61
	Geometric Model of Orbiter Cargo Bay and Stowed LSS/LTPS Used for Radiation Heat Transfer Analysis
4-4	62
4-5	63
4-6	64
	Nodal Map of Thermal Model for 56 kg/m <sup>3</sup> (3.5 lbm/ft <sup>3</sup> ) Payload Density LTPS
4-7	65
	Nodal Map of Thermal Model for 40 kg/m <sup>3</sup> (2.5 lbm/ft <sup>3</sup> ) and 24 kg/m <sup>3</sup> (1.5 lbm/ft <sup>3</sup> ) Density LTPS
4-8	70
4-9	71
4-10	73
	Comparison of Predicted MLI Interstitial Pressure with the Assumed External Boundary (Orbiter Cargo Bay) Pressure History as a Function of Time After Launch
4-11	74
	Predicted Heat Leak for a He-Purged MLI System with a Natural Convection Ground-Hold Environment
4-12	76
	Predicted Heat Leak for a He-Purged MLI System with a Natural Convection Ground Hold Environment; First 20 Hours of Mission
4-13	77
	Predicted Heat Leak for a N <sub>2</sub> -Purged MLI/Foam System with a Natural Convection Ground-Hold Environment
4-14	78
	Predicted Heat Leak for a N <sub>2</sub> -Purged MLI/Foam System with a Natural-Convection Ground Hold Environment; First 20 Hours of Mission
4-15	80
	Typical LH <sub>2</sub> Tank MLI Outer Layer Temperature History Natural-Convection Ground-Hold Environment, He-Purged MLI
4-16	80
	Typical LO <sub>2</sub> Tank MLI Outer Layer Temperature History, Natural-Convection Ground-Hold Environment, He-Purged MLI

## LIST OF FIGURES

		Page
4-17	Typical LH <sub>2</sub> MLI Outer Layer Temperature History, Natural-Convection Ground-Hold Environment, N <sub>2</sub> -Purged MLI/Foam	81
4-18	Typical LO <sub>2</sub> MLI Outer Layer Temperature History, Natural-Convection Ground-Hold Environment, N <sub>2</sub> -Purged MLI/Foam	81
4-19	Minimum MLI Exterior Surface Temperatures for Ground-Hold in a Natural Convection Purge Enclosure Environment	85
4-20	LH <sub>2</sub> Tank Insulation Thicknesses for Various MLI/Foam Interface Temperatures	86
4-21	Toroidal LO <sub>2</sub> Tank Insulation Thicknesses for Various MLI/Foam Interface Temperatures	87
4-22	Ellipsoidal LO <sub>2</sub> Tank Insulation Thicknesses for Various MLI/Foam Interface Temperatures	88
4-23	Predicted Heat Flux Through Helium-Purged MLI During the Ground-Hold Mission Phase	89
4-24	Predicted Heat Flux Through Nitrogen-Purged MLI/Foam Insulations During the Ground-Hold Mission Phase	91
4-25	Time-Averaged Heat Flux Through Helium-Purged MLI for Mission Phase Extending from Insulation Evacuation Through LMSS/LTPS Separation from the Orbiter	92
4-26	Time-Averaged Heat Flux Through Nitrogen-Purged MLI/Foam Insulation for Mission Phase Extending from Insulation Evacuation Through LMSS/LTPS Separation from the Orbiter	93
4-27	Time-Averaged Heat Flux Through Propellant Tank Insulation for Mission Phase Extending from LMSS/LTPS Separation from the Orbiter Through Insertion of LTPS in Disposal Orbit	94
5-1	Insulation Optimization Model Logic Flow	105
5-2	LTPS Payload Calculation Logic Flow	107
5-3	Tank Mass Dependency on Internal Pressure	116
5-4	Tank Mass Dependency on Tank Volume	117
5-5	Effect of Heat Flux on Density of Tanked LH <sub>2</sub>	119
5-6	Effect of Heat Flux on Density of Tanked LO <sub>2</sub>	120
5-7	Effect of Heat Flux on LH <sub>2</sub> Tank Self-Pressurization	121
5-8	Effect of Heat Flux on LO <sub>2</sub> Tank Self-Pressurization	122
5-9	Effect of Foam Thickness on Payload and LTPS Subsystem Mass	127
5-10	Effect of MLI Thickness on Payload and LTPS Length for Volume-Limited Payloads	128
5-11	Effect of MLI Thickness and Ullage Volume on Payload Mass for Helium-Purged MLI for 56 kg/m <sup>3</sup> (3.5 lbm/ft <sup>3</sup> ) Payload Packaged Density	130
5-12	Effect of Foam Thickness and Ullage Volume on Payload Mass for Nitrogen-Purged MLI/Foam Insulations—56 kg/m <sup>3</sup> (3.5 lbm/ft <sup>3</sup> ) Payload Packaged Density	131
5-13	Effect of Foam Thickness and Ullage Volumes on Payload Mass for Nitrogen-Purged MLI/Foam Insulations—24 kg/m <sup>3</sup> (1.5 lbm/ft <sup>3</sup> ) Payload Packaged Density	132
5-14	Effect of MLI/Foam Interface Temperature on Optimized Payload Mass—56 kg/m <sup>3</sup> (3.5 lbm/ft <sup>3</sup> ) Payload Packaged Density	133

## LIST OF FIGURES

		Page
5-15	Effect of MLI/Foam Interface Temperature on Optimized Payload Mass—40 kg/m <sup>3</sup> (2.5 lbm/ft <sup>3</sup> ) Payload Packaged Density	134
5-16	Effect of MLI/Foam Interface Temperature on Optimized Payload Mass—24 kg/m <sup>3</sup> (1.5 lbm/ft <sup>3</sup> ) Payload Packaged Density	135
5-17	Comparison of Optimized LTPS Payload Mass for Insulation Using BX250A and Rohacell 31 Foams	137
6-1	Test Configuration Schematic	143
6-2	Test Timeline	146
6-3	Desired Chamber Pressure History (Based on STS-III Measured Cargo Bay Pressure)	147
6-4	Thermal Shroud Temperature Versus Time	149
6-5	LH <sub>2</sub> Pressure Vessel	153
6-6	Test Tank Parts List	155
6-7	Test Tank Construction Notes	157
6-8	Tank Transportation and Handling Stand	159
6-9	Tank Support Straps	160
6-10	Tank and Thermal Shroud in Stand	162
6-11	Insulation Design Concepts	163
6-12	Insulation Installation	164
6-13	Typical Fastner for MLI Insulation	166
6-14	Insulation Assembly Typical Thermocouple Set Installation and Wire Routing	167
6-15	Vacuum Chamber	168
6-16	Facility Layout and Requirements	170
6-17	Hydrogen Back Pressure and Vent System	171
6-18	Laboratory Activity Schedule	175
6-19	Experimental Program Task Breakdown—Engineering and Administration	178
6-20	Experimental Program Task Breakdown—Fabrication and Assembly	179
6-21	Experimental Program Task Breakdown—Facility Preparation	180
6-22	Experimental Program Task Breakdown—Test Activities	181
C-1	Example of TRADE Program(s) Input and Output	200
C-2	TRADE Computer Program Listing	202
C-3	TRADE2 Computer Program Listing	221
D-1	Terminal Velocity and Volume-Average Velocity for Bubbles in LH <sub>2</sub>	240
D-2	Bubble Terminal Velocity and Minimum Effective Radius	241
D-3	M <sub>V</sub> /q <sub>L</sub> as a Function of Percent Ullage Volume for Baseline LTPS LH <sub>2</sub> Tanks	242
D-4	M <sub>V</sub> /q <sub>L</sub> as a Function of Percent Ullage Volume for Baseline LTPS LO <sub>2</sub> Tanks	243
E-1	Correlation of LH <sub>2</sub> Tank Self-Pressurization Data	247
E-2	Measured Pressure Rise in the Centaur 5 LH <sub>2</sub> Tank During Lockup	248



## LIST OF TABLES

	<b>Page</b>
2-1 Task I Candidate Insulations	11
2-2 Moisture Content and Dew Point of N <sub>2</sub> Purge Gas Candidates	12
2-3 Task II Insulations Selected for Application to LTPS Designs	13
2-4 Candidate Foam Materials	16
3-1 Results of Study to Evaluate the Number of Perigee Burns for LTPS LEO-GEO Transfer	37
3-2 Task I Mission Timeline	38
3-3 Task II Mission Timeline	39
3-4 Task II Orbit Transfer Parameters	40
3-5 Task I LTPS Design Features	45
3-6 Task I LTPS Mass Summary	47
3-7 Task II LTPS Mass Summaries	52
3-8 Tank Support Strut Data	53
4-1 Radiative Properties of the LPTS External Surfaces	58
4-2 Radiative Properties of LTPS Internal Surfaces	68
4-3 Tank Support System Heat Leak	96
5-1 LTPS Sizing Model Dependent Variables	104
5-2 Insulation Designs Optimized in Task II	125
5-3 Optimum LTPS Conceptual Design Summary for Natural- Convection Ground-Hold Purge Enclosure Environments	138
5-4 Optimum LTPS Conceptual Design Summary for Enhanced Convection Ground-Hold Purge Enclosure Environments	139
6-1 Instrumentation List	172
B-1 Tank Support Strut Sizing	193
B-2 Support Strut Thermal Configuration(s)	198



## SUMMARY

An analytical evaluation of cryogenic propellant tank insulations for liquid oxygen/liquid hydrogen low-thrust 2224N (500 lbf) propulsion systems (LTPS) was conducted. Insulations, consisting of combinations of foam and multilayer insulation (MLI), as well as MLI-only, were investigated. The purpose of the study was to analytically assess the benefits of a combined foam/MLI system relative to MLI alone and develop an experimental technology development plan for a combined MLI/foam propellant tank insulation system concept.

Helium-purged MLI with no foam substrate was selected as the baseline insulation concept. The MLI/foam combination insulations studied were purged with nitrogen.

Thermal analysis models of three baseline LTPS conceptual designs were developed to predict heat leak into the propellant tanks during ground-hold, launch, and orbital mission phases. The three LTPS studied were designed for shuttle orbiter launch and packaged payload densities of  $56 \text{ kg/m}^3$  ( $3.5 \text{ lbm/Ft}^3$ ),  $40 \text{ kg/m}^3$  ( $2.5 \text{ lbm/Ft}^3$ ) and  $24 \text{ kg/m}^3$  ( $1.5 \text{ lbm/Ft}^3$ ).

Heat leak information generated by the thermal analysis models was used to evaluate the influence of tank insulation design variables on LTPS and payload size and mass. The insulation design variables studied included were; 1) foam and MLI thickness, 2) foam/MLI interface temperature, 3) purge gas, 4) foam material and 5) purge enclosure heat transfer environment during prelaunch operations. Insulation designs which maximized payload mass were identified.

It was found that LTPS payload mass could be increased by replacing He-purged MLI with MLI/foam combination insulations. Enhanced convection heat transfer in the purge enclosure was required during purging to achieve the desired MLI/foam interface temperature with a minimum thickness of foam. Purging with  $\text{N}_2$  rather than He reduced tank heat leak during ground hold. Boiloff losses were therefore reduced and the effective propellant density was increased due to a lower rate of boiling. Optimum insulation thickness depended on payload density and whether or not foam was used. Typically, He-purged MLI thickness ranged from 2.3 to 5.1 cm (0.91 to 2.0 in.). Optimum MLI/foam insulations ranged from 3.3 to 5.8 cm (1.3 to 2.3 in.). In evaluating the effect of MLI/foam interface temperature on payload mass, the lowest temperature considered ( $144^\circ\text{K}$  ( $-100^\circ\text{F}$ )) gave the highest mass. Of the two foam materials studied, the adhesively bonded Rohacell 31 was preferred over spray-on BX 250A due to its lower density.

A preliminary test plan, conceptual test hardware designs and cost estimates for an experimental program were developed. The objectives of the experimental program are to measure the performance of foam-plus-MLI cryogenic insulation and to verify the analysis of Task I. The plan provides for testing a one-half scale liquid hydrogen tank in an existing vacuum chamber facility. The foam-plus-MLI system and, for comparison purposes, a MLI-only system would be tested separately. Each test would simulate the pressure and temperature environment of a complete STS ground hold, launch, ascent, and orbit. The cost of the 24-month program was estimated as just over two million 1982 dollars. Possible variations on the plan and their effect on costs were briefly investigated.





## 1.0 INTRODUCTION

This report describes a study of propellant tank insulations for cryogenic low-thrust propulsion systems (LTPS). The work was performed for the National Aeronautics and Space Administration Lewis Research Center (NASA LeRC) under contract NAS3-22824.

A 12 month technical effort was conducted to analyze multilayer insulations (MLI) and MLI/foam combination insulations for application to LH<sub>2</sub> and LO<sub>2</sub> tanks on low thrust propulsion systems launched from the Space Transportation System (STS) or Space Shuttle as it is more commonly known. Insulation thermal performance, weight, volume and impact on payload delivery to geosynchronous Earth orbit (GEO) were predicted and an experimental plan to determine the thermal performance of combined MLI/foam insulations was developed.

NASA and DOD studies have forecast the need for low-thrust chemical orbit-to-orbit propulsion systems to transport acceleration-sensitive large space structures (LSS) from low Earth to geosynchronous orbit. These propulsion systems will likely utilize the cryogenic propellants liquid hydrogen and oxygen, thus requiring high performance insulation systems to minimize propellant losses due to environmental heating.

MLI combines the advantages of low weight and excellent on-orbit thermal performance. Disadvantages of MLI are high pre-launch heating rates and the complexity of a helium purge system which is required to preclude the condensation and solidification of water vapor and air within the MLI blankets. The high pre-launch heating rates for MLI cause not only high vent rates, but also yield lower-density propellants due to the boiling of the cryogenic liquids, and thus the requirement for larger volume tanks. The use of foam as an insulating material eliminates the need for a helium purge system and greatly reduces the pre-launch heating rates. However, foam has unacceptable on-orbit thermal performance for the multi-day missions anticipated for the low-thrust chemical propulsion systems.

NASA's current technology program is focused on LTPS/LSS combinations which will utilize a single Space Shuttle launch for transport to low Earth orbit. Shuttle constraints add two additional considerations to the selection criteria for LTPS cryogenic propellant tank insulation systems: 1) some LSS have such low densities when packaged within the Shuttle cargo bay that the total LTPS/LSS payload is volume-limited so that emphasis on minimizing the LTPS weight is not warranted, 2) purging of a LTPS cryogenic tank MLI system within the confines of the Shuttle cargo bay adds the complexity of warm purge requirements for other occupants of the cargo bay which cannot tolerate a low temperature environment.

The work described in this report provides an analytical evaluation of cryogenic tank insulation systems which combine MLI with a foam substrate. The purpose of the study was to: 1) select combined insulation systems which encompass the advantages of each insulation component and 2) assess the combined systems' relative benefits as compared to MLI alone and, 3) plan further technology development for combination insulations for cryogenic propellant tanks. Although the results are generally applicable to any STS-transportable tankage, the study was restricted to the consideration of low-thrust propulsion systems. These systems were assumed to employ a single 2224 N (500 lbf) LO<sub>2</sub> and LH<sub>2</sub> rocket engine in all cases. Specific impulse, at a 6:1 mixture ratio, was set at 4560 N-sec/kg (465 seconds). The LTPS and its LSS payload were assumed to form a

single STS Orbiter payload. Size and mass of the combined LTPS/LSS were restricted by the Orbiter cargo bay volume and the STS payload placement capability. In developing mission timelines for the study, it was assumed that LTPS/LSS erection, deployment and checkout in the Orbiter cargo bay would require slightly less than 43 hours of mission time. The LSS payload was assumed to be transported to GEO in the fully deployed configuration.

## 1.1 STUDY OBJECTIVES

The objectives of this study were to:

- a. Analyze and compare MLI and MLI/foam insulations for LTPS propellant tanks on the basis of mass, volume, payload placement capability and vehicle complexity.
- b. Plan an experimental program to measure the thermal performance of MLI/foam insulations applied to cryogenic propellant tanks and verify thermal performance prediction.

These study objectives were established to provide NASA LeRC with benefit/cost information for planning insulation technology development programs for future low-thrust propulsion systems and similar STS-transportable cryogenic tankage.

## 1.2 STUDY SCOPE

This study consisted of 3 technical tasks. The objective of Task I was to perform a preliminary analysis to predict the thermal performance of candidate LH<sub>2</sub> and LO<sub>2</sub> propellant tank insulations and evaluate the potential benefits of MLI/foam insulation. The effect of foam substrates on propellant vent losses, and the density of tanked propellants prior to launch, were determined. Combined MLI/foam insulations were compared with MLI only. Comparisons were made on the basis of LTPS operational complexity and on LTPS volume, mass and payload placement capability.

In Task I, 9 sets of propellant tank insulation designs were investigated. They consisted of one design in which MLI was used to insulate both the LH<sub>2</sub> and LO<sub>2</sub> tanks, 2 designs in which MLI was used for the LO<sub>2</sub> tank and MLI/foam used for the LH<sub>2</sub> tank and 6 designs in which MLI/foam was applied to both tanks. Two foam materials were studied: BX 250A, manufactured by the Stepan Chemical Company of the U.S.A.; and Rohacell 31, manufactured by Rohm-GMBH Chemische Fabrik Company of Germany.

The insulations were assumed to be applied to the propellant tanks of a single baseline LTPS design. The LTPS design selected for the Task I studies was a Boeing-developed expendable orbit transfer vehicle (OTV) which is described in Reference 1. The OTV was modified by replacing its RL10-IIB engines with a 2224 N (500 lbf) thrust engine and reducing tank size. A single large space structure (LSS) payload and mission were selected for the Task I studies. Thermal analysis models of the STS Orbiter cargo bay, payload, LTPS, propellant tanks and insulation candidates were developed and LH<sub>2</sub> and LO<sub>2</sub> tank heat leaks predicted for the 9 insulation candidates. Heat leak predictions covered the entire mission, from ground-hold through payload separation at GEO and insertion of the LTPS into a disposal orbit.

The results of the Task I thermal analyses were used to select 3 sets of MLI/foam candidate insulation designs for further detailed analysis in Task II. A fourth insulation

design, MLI only, was also included in the Task II studies as a baseline concept, representing current state-of-the-art. The objective of Task II was to compare the operational complexity, volume, mass and payload delivery capability of LTPS point designs. Designs incorporating MLI-insulated tanks were compared with designs in which combined MLI/foam insulations were used. For each of the LTPS point designs developed, propellant tank insulation systems were optimized for maximum payload placement capability.

During ground-hold operations, the MLI in the MLI/foam combinations was assumed to be purged with  $N_2$ . The 3 MLI/foam insulation combinations were designed for 3 temperature levels at the foam-MLI interface during ground hold purging. The interface temperatures selected were slightly above the moisture dew point level in 3 grades of commercially available  $N_2$ . The baseline MLI was assumed to be purged with dry helium.

Three LTPS designs were considered in the Task II insulation studies. Each design was developed for a specific packaged payload density. The 3 densities selected were  $56 \text{ kg/m}^3$ ,  $40 \text{ kg/m}^3$  and  $24 \text{ kg/m}^3$  ( $3.5 \text{ lbm/ft}^3$ ,  $2.5 \text{ lbm/ft}^3$  and  $1.5 \text{ lbm/ft}^3$ ). Packaged-payload density is defined as the mass of the payload divided by its volume in the stowed configuration for launch in the STS Orbiter cargo bay.

Detailed thermal analyses similar to those performed in Task I were conducted for the 3 LTPS designs. The LSS payload defined in Task I was used in the Task II thermal analysis models. Parametric thermal performance, mass and dimensional (thickness) data was generated for the 4 insulation designs, as applied to each of the 3 LTPS. In addition, parametric data was developed relating LTPS size and mass to propellant tank volume, pressure and overall external length (including insulation). The parametric insulation and LTPS data was incorporated into two payload prediction computer programs, TRADE and TRADE2. These programs, described in detail in section 5, were developed to predict the maximum LTPS payload for each insulation design. The predictions were used to determine the insulation designs that optimized LTPS payload mass. The two programs differed only in the assumed thermal environment in the purge enclosure during ground-hold operations. The purge enclosure is an enclosed volume surrounding an insulated propellant tank and is filled with purge gas. Typically a purge enclosure is formed by a loosely fitting bag of plastic film (e.g., Kapton) fastened around the insulated tank. The two thermal environments considered in the computer programs represented the two extremes of the range of conditions that could occur in a purge enclosure. In one extreme there would be no appreciable flow of gas in the enclosure and heat transfer between the purge enclosure surface and outer layer of tank MLI would be by natural convection and radiation. In the other extreme, forced, or enhanced, convection heat transfer between warm purge gas and the cool MLI would dominate and the temperature of the outer layer of the MLI would be at that of the purge gas. The assumed purge enclosure thermal environment was an important consideration because it was found to have a profound effect on tank insulation design and its impact on LTPS payload. Further discussions of the effect of purge enclosure thermal environment on insulation design and performance are contained in sections 4.2.1 and 5.5.

In Task III, a calorimetric test program was designed and planned to experimentally evaluate the thermal performance of an insulated  $LH_2$  tank. The specific objectives of this effort were to: 1) identify the test variables and determine the range of variation of each needed to evaluate insulation performance and verify thermal performance predictions; 2) define instrumentation requirements; 3) develop preliminary test hardware

designs; 4) develop a test plan and schedule, and 5) estimate test program cost. The insulation test program developed in Task III employed a ½ scale "boilerplate" aluminum ellipsoidal dome LH<sub>2</sub> tank. The tank was approximately 209.6 cm (82.5 in) in diameter and 185.2 cm (72.9 in) in length.

Two tests were specified. The first test would be performed with the tank insulated with helium-purged MLI. The results of this test would provide a comparison baseline for the second test in which the tank would be insulated with a N<sub>2</sub>-purged MLI/foam insulation. Testing would simulate a mission timeline including ground-hold purging, ascent, the Orbiter bay doors-open condition, and free flight. Orbital average thermal environments would be imposed on the exterior of the insulated tank by temperature controlled panels surrounding the test article. Thermal performance of the insulation would be determined by measuring LH<sub>2</sub> boiloff and venting during each mission phase. Temperature sensors mounted on the test article would allow the determination of specific heat leaks through insulation, supports, lines, and electrical feed-throughs.

A 24 month program was identified with actual testing occurring in the 17th and 20th months. Test program costs were broken down by major task, subtask and included labor and nonlabor cost estimates. The total predicted cost for the test program, in 1982 dollars, was slightly more than 2 million dollars.

### 1.3 REPORT ORGANIZATION

Study details are presented in the following sections of this report. Section 2 covers specification and selection of candidate insulation materials. This section describes the thermophysical properties of foam insulations, briefly discusses processes for the application of foams to cryogenic tanks and describes foam substrate insulation conceptual designs. Multilayer insulation is also discussed in section 2. Specific topics covered are multilayer insulation design, insulation properties and venting characteristics.

Section 3 describes the LTPS conceptual designs developed to evaluate propellant tank insulations. Design groundrules and assumptions are summarized and the LTPS mission is then described. The technical approach followed in developing the LTPS conceptual designs for Task I and Task II studies is described. Then, in the following two subsections, the Task I and Task II LTPS design details are presented.

Section 4 covers the preliminary thermal analyses and prediction of propellant tank thermal loads. The first topic in this section is the approach followed in developing thermal analysis models. Then the predicted performance of insulations is presented. Following the discussion of insulation performance, predicted heat leaks through insulation penetration and tank supports are presented and discussed.

Section 5 describes the Task II tank insulation system optimization. Groundrules and assumptions are described and the optimization approach is presented. Then, the computer program developed to predict the impact of insulation thickness and type on LTPS payload mass and size is briefly described. Parametric LTPS design data used in the computer programs are described and the results of the insulation optimization study are presented and discussed.

Section 6 describes a plan for an experimental program to measure the performance of MLI and MLI/foam insulation systems and verify insulation performance prediction

models. Topics covered in this section include the recommended experimental approach, a description of the experiment, preliminary designs of experimental hardware, cost estimates, program schedule and recommendations and alternative approaches.



## 2.0 INSULATION CONCEPTS

This section describes the LTPS propellants tank insulation concepts selected in Task I of this study. As described in the preceeding section, two basic generic types of insulation were investigated. One generic type studied was multilayer insulation consisting of alternating layers of metallized Kapton (polyimide) film and Dacron net spacers. This insulation has been used as a cryogenic tank insulation for over 20 years. It was selected as the baseline insulation because it is low-risk and is well-characterized. When used to insulate cryogenic propellant tanks, MLI must be purged of all gases that would liquify or freeze at liquid hydrogen or liquid oxygen temperatures. Helium is normally used for purging because;

- a. it can be easily purified to eliminate contaminants
- b. its condensation temperature at sea level pressure is well below the temperature of liquid hydrogen ( $21^{\circ}\text{K}$  ( $-422^{\circ}\text{F}$ )) and liquid oxygen ( $92^{\circ}\text{K}$  ( $-294^{\circ}\text{F}$ )) and
- c. it has a high mass diffusivity and readily diffuses through the MLI.

An important disadvantage of using helium as a purge gas is its relatively high thermal conductivity. This characteristic of helium causes high heat leaks into the propellants during fill and hold operations on the ground. Large heat leaks are undesirable because:

- a. Boiling occurs, and the presence of bubbles in the liquid propellant reduces its effective density. A lower density reduces the amount of useable liquid propellant that can be placed in a given volume of tankage.
- b. After liquid replenishment is terminated, vaporized propellant must be vented and is therefore lost. The tanks must be oversized to allow for this boiloff.
- c. More reserve propellant must be loaded to account for boiloff losses during a contingency hold that could occur in the countdown following termination of tank replenishment. In the event this hold does not occur the extra propellant is essentially inert weight.
- d. Tank self-pressurization is more rapid during prelaunch and launch vent lockup. Higher ullage pressures require heavier tanks.

The second generic type of insulation evaluated in this study consisted of a combination of closed-cell foam and MLI. The foam covers the exterior of the tank and the MLI attached over it. The presence of the foam between the MLI and tank wall raises the minimum temperature of the MLI during ground hold purging. Therefore, nitrogen gas can be used to purge both the hydrogen and oxygen tank MLI blankets. The principal advantage of using nitrogen rather than helium is that its thermal conductivity is one sixth that of helium. Hence, ground-hold heat leak is diminished. The thicknesses of the foam and MLI can be selected to give the desired interface temperature during purging operations. The performance gain achieved through the use of foam/MLI combinations is countered by the greater density of the foam which increases the overall insulation system mass.

In the selection of candidate insulation concepts, the objective was to identify and characterize foam insulations which could be combined with nitrogen-purged MLI to form an alternative to conventional helium-purged MLI for propellant tank insulation. Following a literature survey and discussions with industry and government experts, two candidate foams were selected, one applied by spraying, and the other applied by adhesive bonding. These materials are described in detail in the following section (section 2.1). In

addition, a single MLI design was selected for use as the helium-purged insulation as well as for the nitrogen-purged insulation in combination with foam. Construction and performance details of the selected MLI design are summarized in section 2.2.

Initially, 9 sets of candidate insulations (each set consisting of a LH<sub>2</sub> and a LO<sub>2</sub> tank insulation design) were studied. These candidate insulations are summarized in Table 2-1. They consist of 8 sets using foam/MLI combinations of varying thicknesses and one set in which only MLI was used with helium purging. In the case of foam/MLI combinations, 4 MLI thicknesses were selected, ranging from 1.40 cm to 2.72 cm. Foam thicknesses were chosen for each tank to provide foam/MLI interface temperature ranging from 83°K (-311°F) (for the LH<sub>2</sub> tank only) to a maximum of 244°K (-20°F). Two foam materials were studied, BX250A and Rohacell 31.

Following the Task I thermal analysis of the 9 candidate insulations, 5 insulation designs were selected for further study in Task II. Helium-purged MLI was retained as the baseline insulation representing state-of-the-art technology. The other 4 insulation designs selected for further study were foam/MLI combinations. Rohacell 31 was chosen as the foam material for three of the insulations because its density is less than that of BX250 A and it has essentially the same thermal conductivity and specific heat. One foam/MLI combination incorporating BX250A was retained for the Task II study so the relative benefits of the 2 foams could be compared for optimized insulation designs.

Instead of specifying MLI thickness, in Task II it was decided to specify foam/MLI interface temperature for each design. This decision was prompted by the fact that the water content of the N<sub>2</sub> purge gas determined the minimum temperature it could be allowed to reach during purging. Hence, the dew point of the N<sub>2</sub> purge gas determined the foam/MLI interface temperature, since it was assumed no condensation would be allowed in the MLI. Table 2-2 summarizes the water vapor content and dew point temperature of 3 grades of N<sub>2</sub>. The N<sub>2</sub> used to purge the STS cargo bay has a moisture content of 140 parts per million and a dew point of 238°K (-31°F). Water content in higher purity N<sub>2</sub> ranges from less than 16 parts per million to less than 5 for 99.998% pure gas. However, even for the 99.998 pure gas, the dew point is between 200°K and 211°K (-100°F and -80°F).

Three values of foam/MLI interface temperature were specified, based on the dew point data summarized in Table 2-2. The two highest interface temperatures were approximately equal to the dew points of orbiter cargo bay purge gas and the 99.998% purity N<sub>2</sub>. A third, lower temperature, was chosen so the benefit of incorporating a thin layer of foam into the insulation design could be determined. In this case, the interface temperature would probably be below the dew point and a small amount of ice could occur on the MLI layers nearest the foam. The amount of ice and its effect on MLI vacuum performance would have to be determined experimentally. The presence of ice would raise the emissivity of the radiation shields and would also raise the interstitial pressure in the MLI during space operations.

The interface temperatures chosen for the three foam/MLI candidate insulations were, 244°K (-20°F), 200°K (-100°F) and 144°K (-200°F). Table 2-3 summarizes the insulation designs that were selected for Task II optimization studies. The helium-purged MLI and Rohacell 31/MLI combinations were applied to all three LTPS/payload designs. The BX250A/MLI insulation was applied only to the LTPS designed for a packaged payload density of 40kg/m<sup>3</sup> (2.5 lbm/ft<sup>3</sup>).



CONFIGURATION ◆	TYPE PURGE GAS	MLI THICKNESS cm (in )	FOAM ■ TYPE	LH <sub>2</sub> TANK		LO <sub>2</sub> TANK	
				FOAM THICKNESS cm (in )	INTERFACE TEMPERATURE K (F)	FOAM THICKNESS cm (in )	INTERFACE TEMPERATURE K (F)
1 △	HELIUM	4.19 (1.65)	—	0	22 (-420)	0	92 (-294)
2	NITROGEN	2.72 (1.07)	BX 250A	0.33 (0.13)	83 (-311)	0	92 (-294)
3	NITROGEN	2.72 (1.07)	ROHACELL 31	0.26 (0.10)	83 (-311)	0	92 (-294)
4	NITROGEN	2.21 (0.87)	BX 250A	1.48 (0.58)	167 (-159)	1.01 (0.40)	167 (-159)
5	NITROGEN	2.21 (0.87)	ROHACELL 31	1.21 (0.48)	167 (-159)	0.85 (0.33)	167 (-159)
6	NITROGEN	1.80 (0.71)	BX 250A	2.61 (1.03)	211 (-80)	2.09 (0.82)	211 (-80)
7	NITROGEN	1.80 (0.71)	ROHACELL 31	2.21 (0.87)	211 (-80)	1.79 (0.70)	211 (-80)
8	NITROGEN	1.40 (0.55)	BX 250A	3.86 (1.52)	244 (-21)	3.23 (1.27)	244 (-21)
9	NITROGEN	1.40 (0.55)	ROHACELL 31	3.54 (1.39)	244 (-21)	3.04 (1.20)	244 (-21)
◆ All configurations are purged by gas diffusion during the ground-hold mission phase.							
■ Foam type; Manufacturer:		BX 250A; Stepan Chemical Co., USA Rohacell 31; ROHM-GMBH, Chemische Fabrik Co., Germany					
• Predicted ground-hold temperature at the MLI/foam or the MLI/tank interface.							
△ Baseline configuration							

Table 2-1: Task 1 Candidate Insulations

Source	Moisture content (parts/million)	Dew point, K (°F)
Nitrogen gas used for STS payload compartment during ground hold <span>1</span>	140	238 (-31)
Available from gas suppliers <span>2</span> 99.995 % purity 99.998 % purity	10.5 to 16 1.5 to < 5	217 to 219 (-70 to -65) 200 to 211 (-100 to -80)

1 Reference: "Spacelab Payload Accomodation Handbook", Document No. SLP/2104, June 1977

2 Suppliers contacted: ARCO Industrial Gases and Linde Division, Union Carbide Corporation

*Table 2-2: Moisture Content and Dew Point of N<sub>2</sub> Purge Gas Candidates*

PAYLOAD PACKAGE DENSITY kg/m <sup>3</sup> (lb <sub>m</sub> /ft <sup>3</sup> )		HYDROGEN-OXYGEN TANK CONFIGURATION	MLI – HELIUM PURGE (CHOSEN AS BASELINE)	MLI/FOAM – NITROGEN PURGE				
				TYPE FOAM				BX250A 200 (-100)
				MINIMUM PURGE GAS TEMPERATURE K (°F)				
				ROHACELL 31 244 (-20)	ROHACELL 31 200 (-100)	ROHACELL 31 144 (-200)		
56 (3.5)	TANDEM ELLIPSOIDAL	X	X					
40 (2.5)	ELLIPSOIDAL H <sub>2</sub> – TOROIDAL O <sub>2</sub>	X	X				X	
24 (1.5)	ELLIPSOIDAL H <sub>2</sub> – TOROIDAL O <sub>2</sub>	X	X					

Table 2-3: Task II Insulations Selected for Application to LTPS Designs

The following sections describe the details of the insulations evaluated in this study. Foams are discussed in section 2.1 which covers physical and thermal properties, application to tankage and foam insulation design. Section 2.2 describes the MLI design selected for this study, MLI properties and venting performance.

## **2.1 FOAM INSULATION**

Two foam insulations were selected for detailed analysis in this study. These foams were:

- a. Rohacell 31
- b. BX250A

The principal difference between these foams is application technique. Rohacell 31 is cut and preformed from sheet stock and bonded to the insulated surface. BX250A is applied by mixing and spraying the liquid foam material onto the insulated surface. Foaming and curing occurs after the material is applied. Physical and thermal properties of the two materials are similar.

A literature survey was conducted at the beginning of the study to evaluate and select candidate foams. The primary considerations in selecting candidates were:

- a. low thermal conductivity at temperatures ranging from liquid hydrogen temperature to room temperature
- b. low density
- c. low specific heat
- d. demonstrated capacity to withstand multiple thermal cycling between cryogenic and room temperature without failing, cracking or debonding from the insulated surface
- e. low flammability in accordance with NASA Handbook 1700.7a for materials used on STS Orbiter payloads
- f. availability of measured and documented properties and performance data.

Reference 2 reported the results of an experimental study which examined the feasibility of applying 12 foam materials to liquid hydrogen tanks. Three foams from this study were initially selected for further evaluation as potential insulations for LTPS propellant tanks. These foams were Rohacell 31, BX250A and CPR 488. All three materials had low thermal conductivity, low density and were demonstrated to perform satisfactorily as cryogenic insulations. In addition, BX250A and CPR 488 are currently used as the insulation on the STS launch system external tank. Hence, the performance, properties and application processes for these foams are well documented. However, CPR 488 is protected as a proprietary material and obtaining information on it was difficult.

Since both BX250A and Rohacell 31 have properties comparable to CPR 488, it was decided to eliminate CPR 488 as a candidate foam.

### **2.1.1 Properties of Foam Insulations**

Physical and thermal property information for the two candidate foams were obtained from data supplied by the manufacturers and from the literature. The foams are manufactured by the following companies:

- a. BX250A - Stepan Chemical Co.  
USA
- b. Rohacell 31 - ROHM-GMBH  
Chemische Fabrik Co.,  
Germany

Table 2-4 presents the room temperature densities of Rohacell 31, BX250A and CPR 488 foams and shows the basic material from which the insulations are formed. BX250A can be seen to have essentially the same density as CPR 488 while Rohacell 31 is about 16% lighter.

Thermal conductivities of Rohacell 31 and BX250A are plotted as a function of temperature in Figure 2-1. The information shown is based on test measurements. The Rockwell International data for Rohacell 31 agrees fairly well with the manufacturer's data for three versions of the foam. The straight line, labeled Rohacell (Baseline), was used as an approximate representation of this data.

An apparent discontinuity can be seen to exist in the plotted data for BX250A. The sharp increase in thermal conductivity between 280°K and 200°K is possibly due to condensation of freon propellant and gases in the closed cells of the foam. Freon, is used to propel the liquid foam material in the spraying process, and becomes entrapped in the insulation as it foams.

Specific heat of Rohacell 31 and BX250A are plotted as a function of temperature in Figure 2-2. Both foams have almost identical values of specific heat at temperatures below 180°K (-136°F). Above this temperature, Rohacell 31 specific heat is slightly higher than that of BX250A.

### 2.1.2 Foam Insulation Application

Foam insulation is applied directly to the propellant tank outer surface. In the case of BX250A, the insulation would be sprayed onto the prepared surface under closely controlled conditions. Surface preparation processes including cleaning, degreasing and etching have been developed by NASA and Martin Marietta Corp. for the application of spray-on foams to 2219 aluminum tanks. Spray process specifications have also been developed to control application variables, including temperature, humidity, application rate and amount of overlap on each spray pass. Care must be taken in application and cure to ensure uniformity of foam properties (density and thermal conductivity) as well as thickness.

Rohacell 31 is available from the manufacture in sheets. A range of thicknesses, are available from 0.254 cm (0.1 inches) to more than a 2.54 cm (1.0 inch). Application of this foam to propellant tanks would be accomplished in 3 steps. First the sheet stock would be cut to the desired shape. Then the pieces would be fit to the contour of the tank by heat forming and then adhesively bonded to the prepared surface. An adhesive manufactured by the Crest Chemical Company of Texas has been found by Boeing to provide the required bond strength at cryogenic temperatures. In test, this adhesive was found to maintain bond integrity under repeated temperature cycling. The insulation would be held against the tank during adhesive cure by vacuum bagging. In this technique, a flexible, leak tight plastic film is placed over the insulated area and taped down to seal off any leakage. The enclosure between the insulation and film is then evacuated and atmospheric pressure on the outside of the film forces the insulation against the tank.

Foam	Material	Manufacturer	Density	
			Kg/m <sup>3</sup>	lb <sub>m</sub> /ft <sup>3</sup>
Rohacell 31	Polymethacrylimide	RÖHM, GMBN, Germany	30	1.9
Stepan Foam BX250A	Polyurethane	Stepan Chemical Company	37	2.3
CPR 488	Polymetric Isocyanate	The Upjohn Company	36	2.3

*Table 2-4: Candidate Foam Materials*

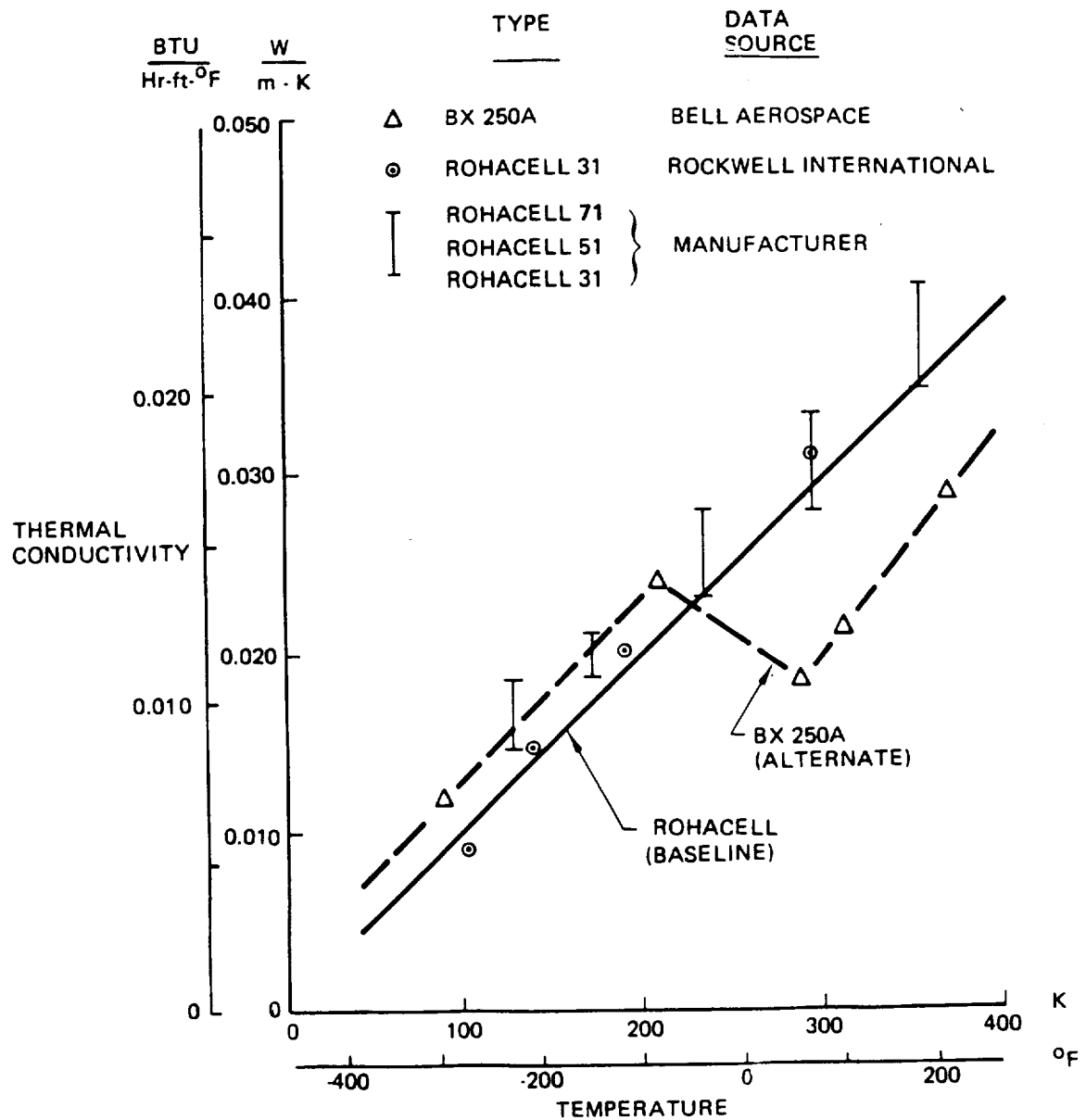


Figure 2-1: Foam Thermal Conductivity Characteristics

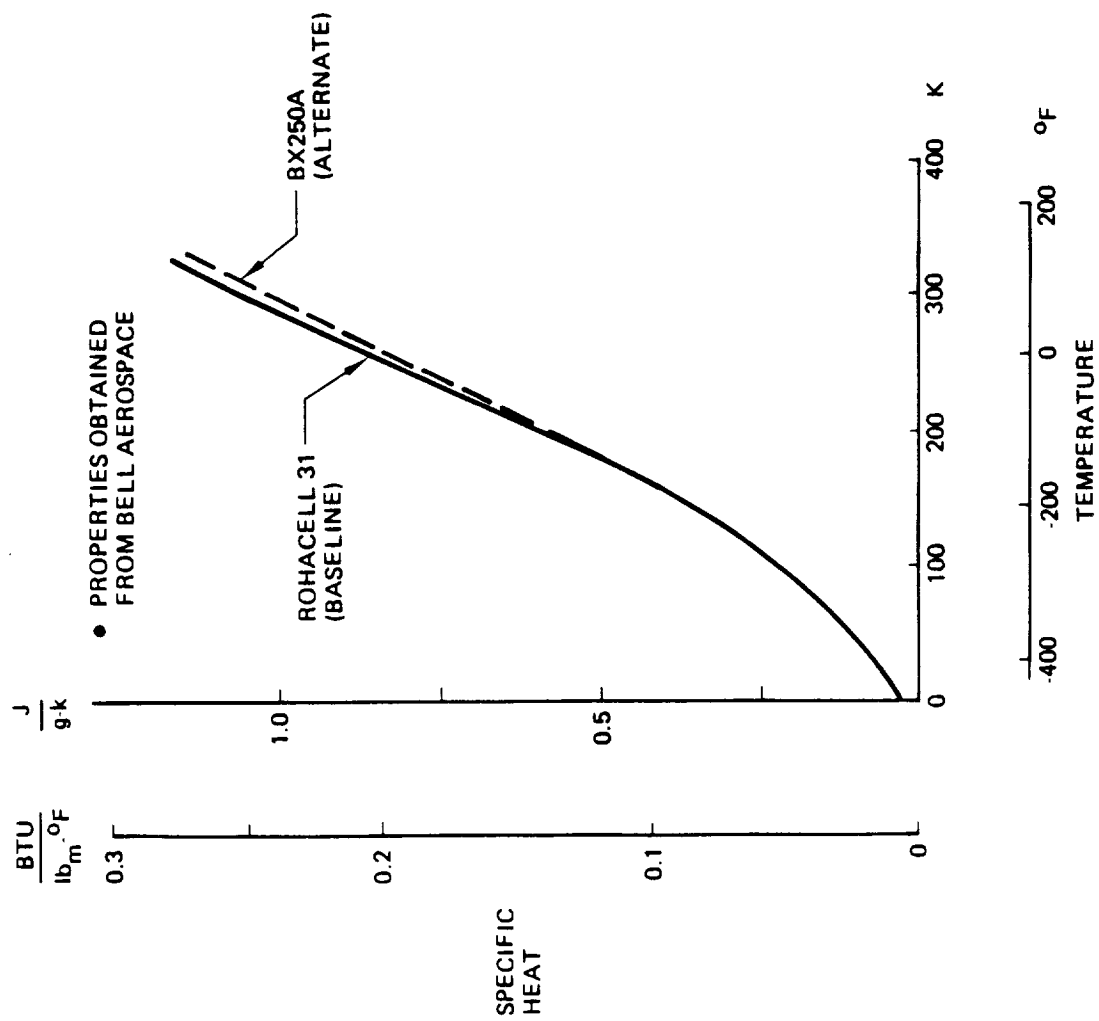


Figure 2-2: Temperature Dependency of Rohacell 31 and BX250A Specific Heats



### 2.1.3 Foam Insulation Design

As shown in Figure 2-3, foam insulation is placed between the propellant tank wall and the MLI. A gas-impervious barrier film is bonded over the outside of the foam. This film serves two purposes. First, it entraps volatile materials in the foam that could otherwise escape into the MLI and degrade its vacuum performance. Second, it keeps the N<sub>2</sub> purge gas from direct contact with the foam. In the case of the LH<sub>2</sub> tank, if there were no barrier, the N<sub>2</sub> purge gas would liquify in any cracks or seams in the foam. This process would increase the ground-hold heat leak into the LH<sub>2</sub> tank and the entrapped N<sub>2</sub> would be a gas source which would degrade MLI performance in space.

Candidate barrier materials are:

- a. Aluminized Kapton
- b. Aluminum foil - Kapton laminate
- c. Aluminum foil - polyester laminate.

A low temperature adhesive such as Crest adhesive would be used to bond the barrier to the foam. Adhesive bonding, or heat sealing in the case of the aluminum foil-polyester laminate, would be used to achieve a vacuum seal on the seams of the barrier.

The foam insulation around tank mounting supports would have to allow for movement of the support struts. This movement arises from:

- a. thermal contraction and expansion of the tank and supports,
- b. tank pressurization and,
- c. vibration due to dynamic launch loads.

One possible design concept for foam insulation at support struts would be to form a barrier film sleeve around a portion of the strut. Inside the sleeve, the strut would be insulated with a layer of foam. The foam on the strut and tank wall would be cut away so they could not interfere under maximum movement of the strut. The length of the insulated sleeve and the thickness of insulation would be determined by the requirement that the purge gas not condense on the exterior of the barrier. The sleeve would be pleated near its attachment to the tanks insulation barrier to allow for movement of the strut.

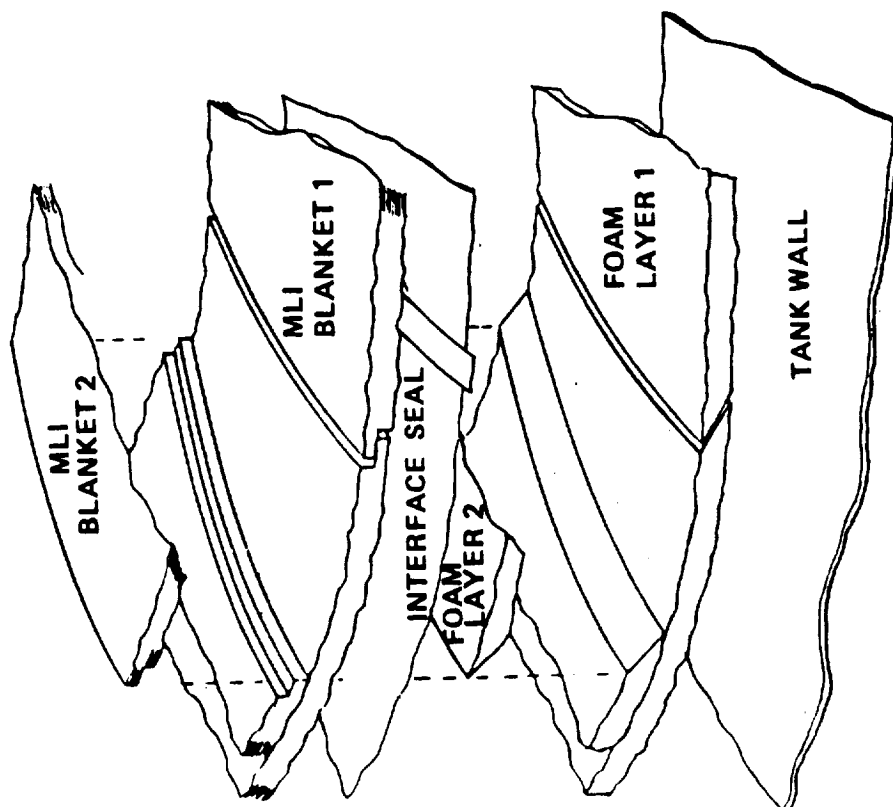
## 2.2 MULTILAYER INSULATION

The MLI design selected for this study consisted of alternating layers of double aluminized Kapton (DAK), and Dacron net spacers. The outer layer of MLI was a laminate of Dacron scrim and double-aluminized Kapton.

This design was selected because:

- a. it is state-of-the-art,
- b. it has been flown and tested extensively as a cryogenic insulation,
- c. its performance is well documented, and
- d. test-validated equations have been developed to characterize its performance.

Kapton was selected over Mylar as the radiation shield material because Kapton meets the flammability requirements of NASA Handbook 1700.7a and Mylar does not. Metalliza-



(a)  
MLI-FOAM SYSTEM  
(PURGE BAG NOT SHOWN)

Figure 2-3: MLI/Foam Insulation Assembly

tion of both sides of the shields is desired to minimize layer-to-layer energy transfer. For the shields to be opaque, a metal deposit at least 600 to 800 Angstroms thick is required.

The Kapton shields were assumed to be metallized with vapor-deposited aluminum rather than gold. Although optical characteristics and durability of gold produce superior shields, aluminized surfaces can be obtained with performance characteristics rivaling those of gold at a substantially reduced cost. At cryogenic temperatures, for example, the emittance of aluminized Kapton is 0.02 versus 0.01 for goldized Kapton. Anti-oxidation coatings have been developed by metallized film manufacturers which provide environmental protection for aluminized shields with little affect on reflectivity. Care must be taken in handling aluminized shields however because, unlike goldized surfaces, the metal layer can fracture if the film is crinkled. Fracturing causes the effective emissivity of the shield to increase.

Dacron net was selected for the shield spacer material because:

- a. It is environmentally inert as shown in Reference 3 and does not outgas appreciably when exposed to vacuum.
- b. It offers low resistance to gas flow and diffusion during MLI purging and venting.
- c. It maintains positive separation of radiation shields in the presence of gravity and launch loads.
- d. Performance predictions for MLI with Dacron net spacers are based on a large volume of experience and should be more accurate than predictions for other MLI designs.

### 2.2.1 Multilayer Insulation Design

Specific design features of the MLI selected for this study were the following:

- a. Inner radiation shields - 0.0076 mm (0.00033 in.) thick double-aluminized Kapton.
- b. Outer layer - laminated 0.025 mm (0.001 in.) thick double-aluminized Kapton and Dacron scrim.
- c. Spacers - Dacron net.
- d. Number of radiation shields per unit of insulation thickness - 24 shields/cm (60 shields/in.).
- e. Blanket thickness control - nylon pins and buttons.
- f. Method of attachment - Velcro tabs.
- g. Installation configuration - two separate blanket layers. Gores and polar caps on ellipsoidal domes, peripheral blankets around cylindrical surfaces and preformed gores on toroidal tanks. Figure 2-4 shows a typical insulation blanket configuration for ellipsoidal tanks. Adjacent blanket segments would be butted together with sufficient space provided for purge gas egress. Inner and outer blanket joints would be staggered.
- h. Purging - removal of condensible gases from MLI blankets would be accomplished by diffusing either helium ( $H_2$ ) or nitrogen ( $N_2$ ) between radiation shields in both inner and outer blankets. Purge gas would be introduced into the blankets by small perforated tubes penetrating all but the outer most shield of each blanket. These tubes or purge pins, would be centrally located in each blanket segment or gore, and the purge gas would diffuse toward the blanket edges where it would escape to the purge enclosure. This enclosure is a volume around the outside of the insulated tank that is filled with purge gas. For the LTPS configuration considered in this study, it was assumed the purge enclosure would be formed by the outer body shell of the LTPS. A reinforced Kapton membrane on each end of the body shell, would

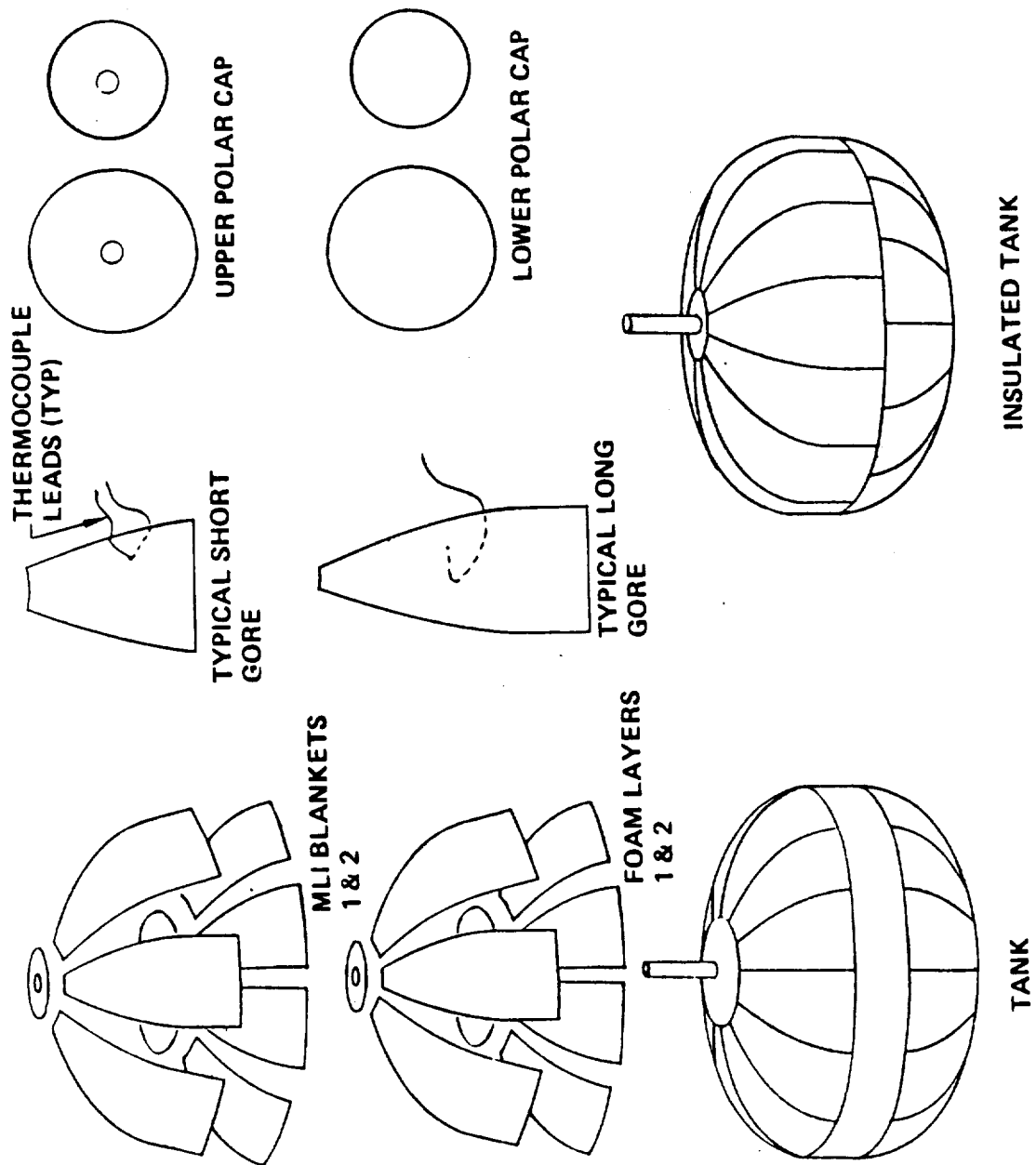


Figure 2-4: Tank Insulation Configuration

complete the enclosure. Purge gas would exit from the enclosure through holes provided in the Kapton closeouts and through leakage paths in the body shell.

### **2.2.2 Insulation Properties**

Physical and thermal properties of MLI used in this study were based on Boeing experience as well as published data. The density of the MLI blankets, was assumed to be  $35.1 \text{ kg/m}^3$  ( $2.19 \text{ lbm/ft}^3$ ). This value included the 0.0076 mm thick inner shields, Dacron spacers, 0.025 mm thick Kapton outer layers and all hardware (pins, buttons, etc.,) as well as Velcro attachment tabs.

MLI blanket specific heat was assumed to be  $1.09 \text{ J/g-}^\circ\text{K}$  ( $0.26 \text{ BTU/lbm-}^\circ\text{R}$ ) in this study. This value is an average of the specific heats of Kapton and Dacron at  $274^\circ\text{K}$ .

The thermal conductivity of MLI is dependent on temperature, the number of radiation shields per unit thickness and interstitial gas species and pressure. In addition, thickness control hardware, seams and penetrations degrade the effective thermal conductivity of the installed insulation. Figure 2-5 shows the predicted vacuum performance of installed MLI used in this study to model propellant tank heat leak. Thermal conductivity is plotted as a function of insulation outer surface temperature for MLI installed on  $\text{LH}_2$  and  $\text{LO}_2$  tanks. This data is for interstitial gas pressure less than  $10^{-5}$  torr. For pressures above this value, the conductivity of the gas influences the effective thermal conductivity of the MLI. Figure 2-6 shows the effect of interstitial gas pressure on heat flux through 3.8 cm thick MLI blankets on  $\text{LH}_2$  and  $\text{LO}_2$  tanks. At atmospheric pressures, during ground-hold purging, the effective thermal conductivity through the MLI was essentially that of the purge gas. The gas velocity between blanket radiation shields was assumed to be so small that convective effects could be neglected. The equations used to predict insulation performance in Figures 2-5 and 2-6 are summarized in Figure 4-9 of section 4.0 of this report.

### **2.2.3 MLI Venting**

MLI internal pressure decay, upon exposure to external vacuum conditions, is dependent on blanket design and installation, materials, entrapped gas species and the degree of cleanliness maintained during blanket construction, storage and handling. In this study, a pressure decay model was developed for the propellant tank insulation. This model was used to predict the MLI interstitial pressure following launch and depressurization of the Orbiter cargo bay.

Effective MLI thermal conductivity during blanket venting could then be calculated, once the interstitial pressure history was established.

The MLI pressure decay model used in this study was developed under a Boeing IR&D program. The model was correlated with test data and compared with published MLI venting measurements. Figure 2-7 shows comparison of model predictions and test results from Reference 4. Differential pressure in Figure 2-7 is the difference between MLI interstitial pressure and the pressure of the local external environment. The measured Orbiter cargo bay depressurization rate is sufficiently slow that the difference between MLI predicted interstitial pressure and the cargo bay pressure is small. Hence, to a good approximation, the interstitial pressure could have been represented by the pressure in the Orbiter cargo bay.

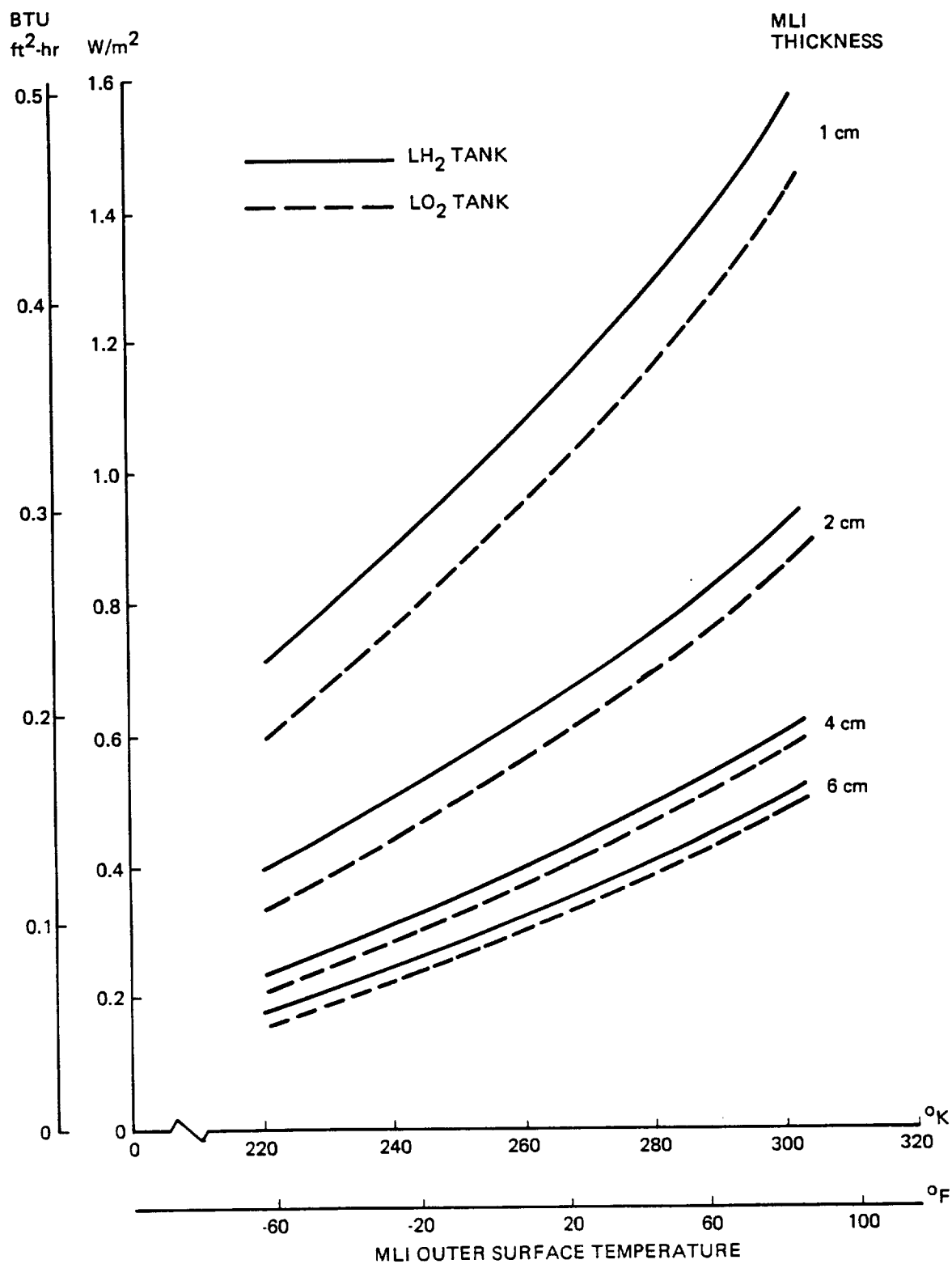


Figure 2-5: Predicted Vacuum Performance of Installed MLI

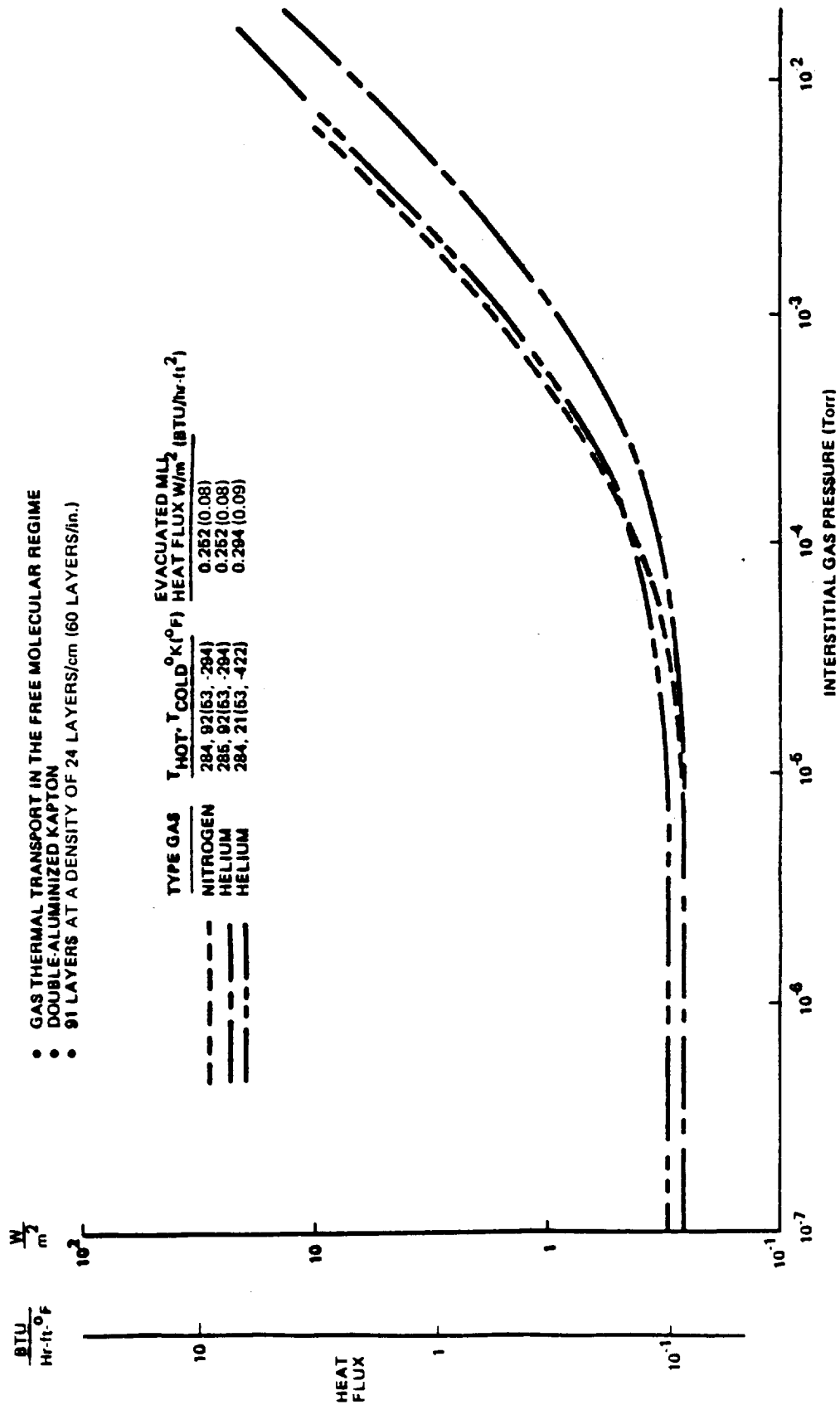


Figure 2-6: The Effect of Interstitial Gas Pressure on  $\text{MLI}$  Thermal Performance

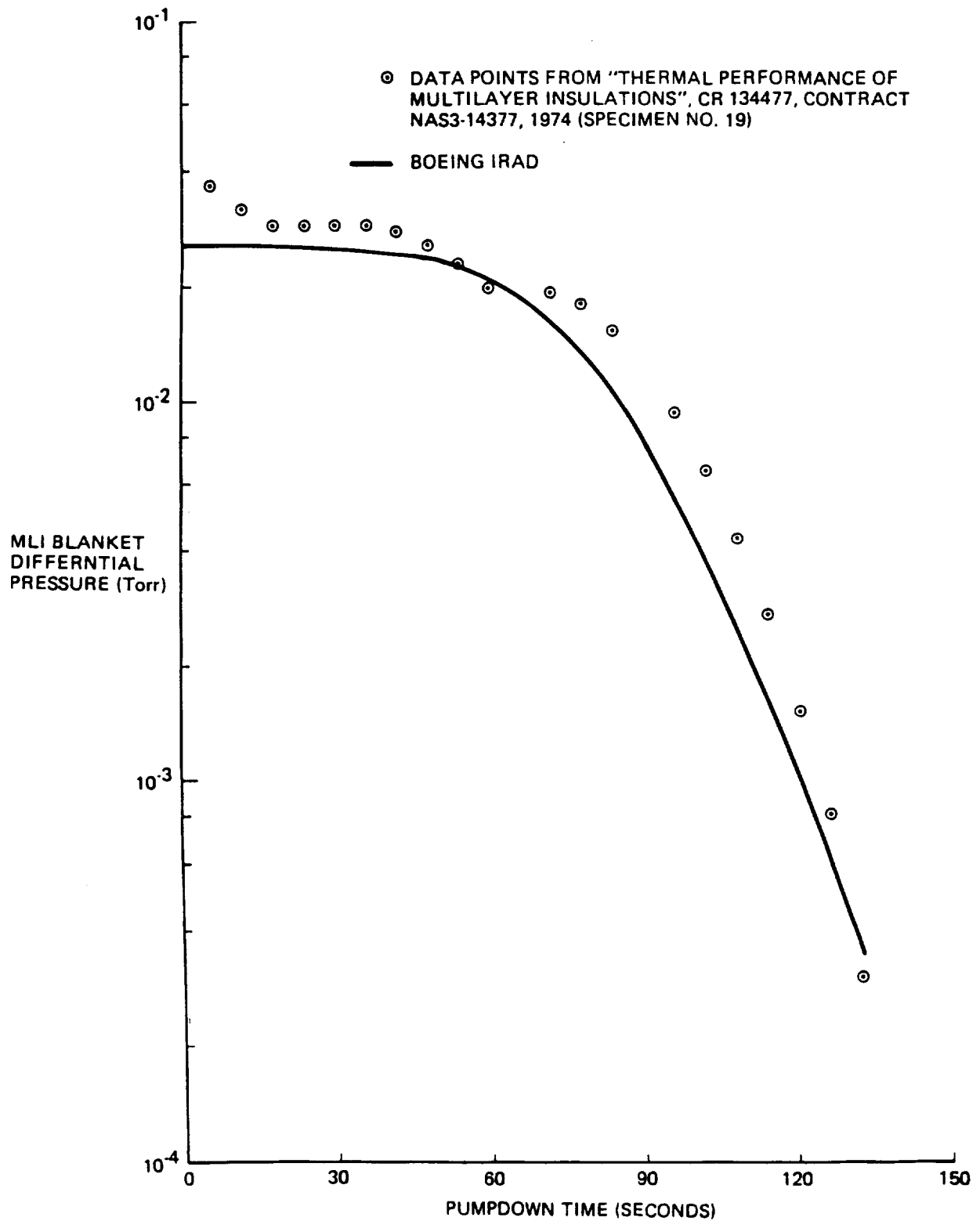


Figure 2-7: Comparison of Predicted and Measured Differential Pressure Across Venting MLI



### 3.0 LTPS CONCEPTUAL DESIGNS

This section describes the low-thrust propulsion system designs developed to support Tasks I and II. These designs were used to determine the impact of propellant tank insulation options on LTPS payload delivery capability. Design data was developed in sufficient detail to allow the benefits and costs of foam/MLI combinations to be compared with those of MLI only. In order to accomplish this objective, the following LTPS design information was developed:

- a. Configuration - general shape and physical arrangement of major subsystem elements
- b. Size - overall envelope dimensions and the dimensions of major subsystem elements
- c. Mass - total system mass and the masses of tanks, structure, engine, avionics, insulation, propellant and miscellaneous inert elements and consumables.
- d. Materials - materials of construction for major subsystems including structure, tanks, insulation, tank supports, and thermal control coatings.

The objectives of preparing this design information were to:

- a. Provide the data needed to develop thermal analysis models of LTPS propellant tanks. These models were used to predict tank heat leak and the resulting loss of useable propellants during the LTPS mission.
- b. Provide mass and size data which, along with propellant loss, was used to predict LTPS payload delivery capability.
- c. Provide parametric mass and size data to be used in the TRADE and TRADE2 computer models to predict optimum insulation designs. (A detailed discussion of these two computer models is presented in section 5.0.)

In Task I of this study, a single LTPS point design was defined. The design was based on the expendable, STS Orbiter-launched OTV developed by Boeing under contract NAS8-33532, "Orbital Transfer Vehicle Concept Definition Study", Reference 1. This particular design was selected for the Task I study because:

- a. It was defined to the level of detail needed to accomplish the Task I thermal analyses and initial insulation performance assessments.
- b. It satisfied all the requirements for an LTPS designed for a 56 kg/m<sup>3</sup> payload density.
- c. It required minimal modification (replacing the 66720 N (15,000 lbf) thrust engine with a 2224 N (500 lbf) thrust engine) to convert it to a low thrust system.
- d. It incorporated the results of detailed structural, environmental and STS interface studies.
- e. A detailed mass statement (including airborne support equipment (ASE) and consumables) and performance model were available.
- f. Schedule time and costs were reduced by using an established design.

Details of the Task I LTPS point design are presented in section 3.4.

In Task II, 3 LTPS designs were developed. Each design was developed for a specific value of payload packaging density. The 3 values of payload density were 56 kg/m<sup>3</sup> (3.5 lbf/ft<sup>3</sup>), 40 kg/m<sup>3</sup> (2.5 lbf/ft<sup>3</sup>) and 24 kg/m<sup>3</sup> (1.5 lbf/ft<sup>3</sup>). The LTPS designed for the 56 kg/m<sup>3</sup> payload density incorporated tandem ellipsoidal dome propellant tanks. This tank shape and arrangement were chosen because:

- a. The high payload density caused the LTPS and payload size to be limited by the STS Orbiter payload launch mass capacity rather than the cargo bay length. Hence there was no need to use a more compact tank arrangement.
- b. Ellipsoidal dome tanks are structurally efficient and are therefore lighter in weight than the alternative tank shapes.

The 2 LTPS designed for the  $40 \text{ kg/m}^3$  and  $24 \text{ kg/m}^3$  payload densities employed toroidal  $\text{LO}_2$  tanks. This tank shape shortened the length of the LTPS. The reduction in length was accomplished by nesting the rocket engine in the center of the torus. By shortening the LTPS for the less-dense payload applications, it was possible to increase the payload mass delivered to GEO. This increase was possible because the Orbiter cargo bay length, rather than the total LTPS/payload launch mass, constrained the weight of the LTPS payload.

The 3 point designs developed for Task II served as baselines, or starting points, for the sizing of LTPS for each of the propellant tank insulation concepts studied. These point designs established the materials, configurations, and physical arrangement of all the LTPS versions studied. Thermal analysis models were built for the 3 point designs and propellant tank heat fluxes were predicted for a range of insulation thicknesses. In addition to heat flux predictions, the point designs also provided parametric data used to calculate the masses of resized LTPS in the insulation optimization studies.

The following sections describe the LTPS conceptual designs developed for this study. Groundrules and assumptions adopted for developing the LTPS point designs to support the Task I thermal analyses and the Task II insulation optimization studies are presented in section 3.1. Section 3.2 summarizes LTPS design requirements and section 3.3 briefly describes the technical approach followed in establishing the LTPS point designs. Section 3.4 describes the LTPS design developed to evaluate tank insulation concepts in Task I. The 3 LTPS conceptual designs developed for the Task II optimization studies are described in section 3.5.

### 3.1 GROUND RULES AND ASSUMPTIONS

A number of groundrules and assumptions were established prior to developing LTPS conceptual designs. The following applied to both Task I and Task II LTPS designs:

- a. Mission
  1. Launch in STS Orbiter
  2. Maximum STS Orbiter payload launch mass of 29,484 kg (65,000 lbm).
  3. Payload delivery to GEO
  4. Replenishment of liquid propellant to the tanks terminated 4 minutes prior to liftoff.
  5. A 5 minute countdown hold could occur after termination of tank replenishment. If the hold were to exceed 5 minutes, the countdown would be set back and tank replenishment resumed.
  6. Propellant tank venting would cease at liftoff and resume after 90 seconds.

7. LTPS/payload erection, deployment and checkout would require 43 hours.
8. The spent LTPS would be transferred to a disposal orbit (GEO + 1852 km) by two main engine burns.
9. Attitude control required during coast as well as powered flight.

b. Payload

1. The Harris hoop column Land Mobile Satellite System (LMSS), described in Reference 5 was used as the payload configuration for all LTPS designs considered. The impact of deployed payload configuration on propellant tank insulation performance was assumed to be minor. The deployed payload configuration was used in:
  - (a) determining reaction control system (RCS) propellant and main engine thrust vector control (TVC) requirements during orbit transfer.
  - (b) modeling the thermal environment of the LTPS during deployment and checkout while attached to the Orbiter and during orbit transfer.
2. Payload densities in the stowed configuration for Orbiter launch were  $56 \text{ kg/m}^3$ ,  $40 \text{ kg/m}^3$  and  $24 \text{ kg/m}^3$ .

c. Interfaces

1. The LTPS interface with the erecting ASE mechanism was at a ring on the aft end of the body shell. The erecting ASE was located just forward of the cargo bay aft bulkhead.
2. The erecting ASE structure and clearance space consumed the following amount of Orbiter cargo bay length:

<u>LTPS CONCEPT</u>	<u>ASE LENGTH</u>
(a) Tandem ellipsoidal tanks	244 cm (95.9 in.)
(b) Toroidal LOX tank	102 cm (40.1 in.)

The assumed dimensions and shapes of the ASE system used in this study are shown as dashed lines in Figures 3-9, 3-10 and 3-11 of this report.

3. A volume 134 cm in length directly aft of the cargo bay forward bulkhead was reserved for stowage of two manned maneuvering units (MMU's).
4. The maximum diameter of the LTPS and stowed payload was 427 cm. This diameter allowed for a clearance of 15 cm between the LTPS/payload and Orbiter bulkheads.

d. Propulsion System Performance

1. Main engine thrust was 2224 N (500 lbf).

2. Oxidizer-to-fuel ratio was 6:1.
  3. Specific impulse was 4560 N sec/kg (465 sec).
- e. Environment
1. The launch environment was as defined in Reference 6, "Space Shuttle System Payloads Accommodation," JSC 07700, Vol XIV Revision F.
  2. Solar heat flux was 1352 W/m<sup>2</sup>.
  3. Earth average radiosity was 221 W/m<sup>2</sup>.
  4. Earth average albedo factor was 0.36.
  5. STS Orbiter cargo bay depressurization characteristics based on modified STS-III flight measurements. Figure 4-2 in section 4.0 of this report shows measured cargo bay history during the first 300 seconds of the STS-III launch and the estimated curve used to extend the pressure decay to longer range times. The Saturn V ascent pressure profile is included for reference.

The following groundrule pertained only to the Task I LTPS:

- a. The elapsed time from completion of orbit transfer to payload release and separation was 24 hours.

The following groundrule pertained only to the three Task II LTPS point designs:

- a. The elapsed time from completion of orbit transfer to payload release and separation was 14 hours. This coast period was reduced from the 24 hours assumed for the Task I mission timeline because it was felt that all final deployment and vernier burns could be completed in a shorter amount of time by optimal phasing at the beginning of transfer.

### 3.2 LTPS MISSION

This section describes three aspects of the LTPS mission established prior to the development of conceptual designs. The three topics addressed are:

- a. Payload
- b. Orbit Transfer
- c. Mission Timelines

In section 3.1 Groundrules and Assumptions, it was stated that a single payload configuration was selected for all LTPS missions considered. However, the mass and packaged density of the payload were assumed to vary.

The selection of a representative payload configuration was necessary to determine the size of the RCS propellant tanks and to determine the additional main impulse propellant required for TVC during powered flight. A payload configuration was also needed to define the radiative thermal environment imposed on the LTPS during LTPS/payload

erection and deployment from the Orbiter cargo bay and during orbit transfer. LTPS thermal environment models, described in section 4.3, included the effect of payload shadowing, reflections, and emitted energy.

Figure 3-1 shows the LMSS chosen as the LTPS payload configuration. This design, developed by Harris Engineering, incorporates a deployable structure and is packaged with the LTPS for a single STS launch. Further details on this proposed satellite design are contained in Reference 5. When deployed, the LMSS mast is 92.2m in length and the parabolic antenna disk 122.2m in diameter. The mass baseline LMSS is 4689 kg. This mass and the resulting inertias, were used in calculating RCS and TVC propellant requirements and in determining the optimum number of engine burns for orbit transfer. It was assumed that the results of this mission optimization were valid for all other payload masses considered.

The packaged LMSS is shown in Figure 3-2. Its package length for stowage in the Orbiter cargo bay is 9.8m. Cargo bay volume occupied by the packaged LMSS, assuming a maximum diameter of 4.47m, is  $154\text{m}^3$ . For the baseline mass of 4689 kg, the packaged density of the LMSS is  $30.5\text{ kg/m}^3$ .

Figure 3-3 shows the LMSS and LTPS in the erected position in the Orbiter cargo bay. Checkout of both the payload and LTPS would be accomplished with the systems in this configuration.

Mass and inertial characteristics of the combined LTPS/LMSS are summarized in Figure 3-4 for start of orbit transfer (LEO) and end of transfer (GEO). The values of mass and inertia shown were used in the determination of RCS and TVC propellant requirements and optimization of main engine firings for orbit transfer. Projected areas shown were used in calculating solar pressure and aerodynamic drag.

An orbit-transfer mission analysis was conducted to determine the optimum number of main engine firings. The objective of the analysis was to minimize the total main impulse, TVC and RCS propellants required for transfer. The optimum number of engine firings for maximum payload delivery was needed to estimate the elapsed time required for orbit transfer; the more firings, the longer the transfer time. Since the total propellant vent loss due to heat leak was dependent on mission time, the orbit transfer time affected tank insulation design trades. Therefore, a realistic transfer time was required for the subsequent insulation performance predictions and payload optimization studies. The effect of number of engine restarts and trip time on system reliability and radiation protection requirements for electronics, solar cells, etc., was not included in the analysis.

A LEO to GEO orbit-transfer optimization model developed by J. V. Breakwell (Reference 7) was used to predict trip times and total main impulse propellants required for transfers of 6, 8, and 16 engine firings. TVC and RCS propellant requirements were predicted for each case, using the LMSS/LTPS inertial and mass properties summarized in Figure 3-4. It was assumed that TVC was required for yaw and pitch control during main engine burn, when the LMSS/LTPS was within  $30^\circ$  of perigee. Roll control during main engine burn and three axis control during coast were assumed to be accomplished by the RCS. It was also assumed the RCS employed 133.4 N thrusters with a specific impulse of 1618 N-sec/kg. Pointing accuracy was set at  $1^\circ$  and the minimum impulse bit for limit cycle calculations was 20 msec. Disturbance torques were calculated for aerodynamic forces, solar pressure and gravity gradient forces. In calculating aerodynamic torques it was assumed the LMSS drag coefficient was 3.0. Solar pressure predictions were based on

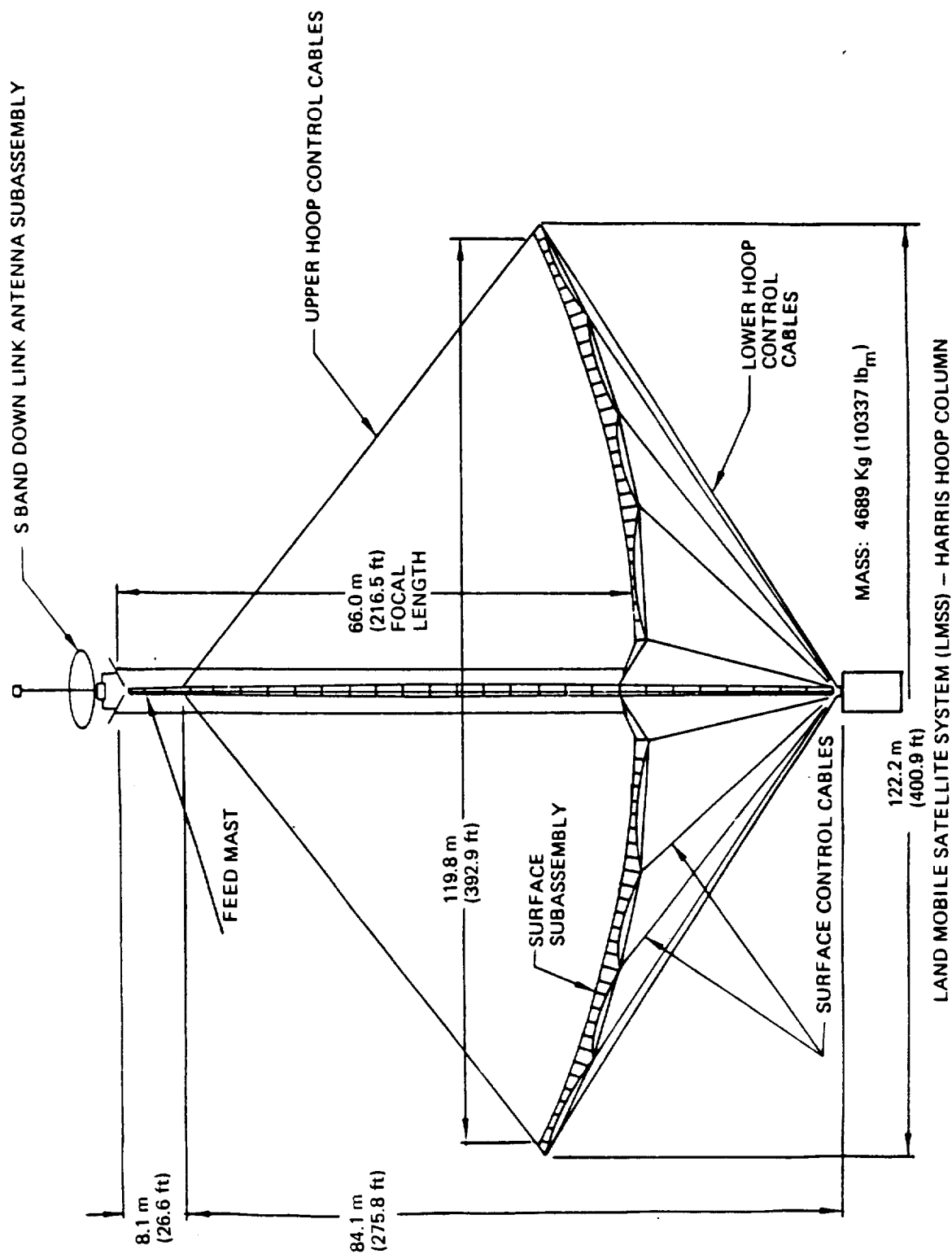


Figure 3-1: Baseline LSS Payload

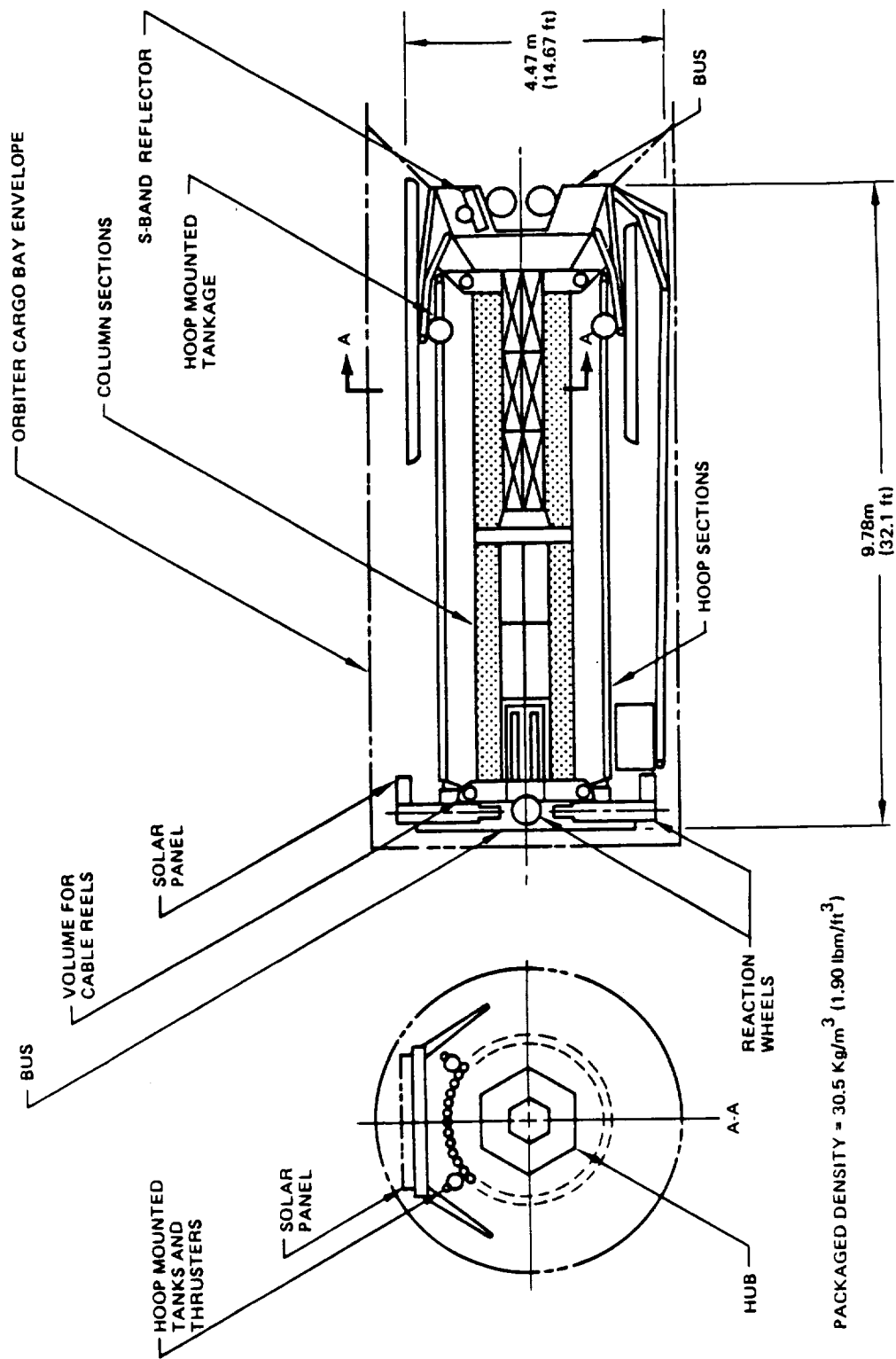
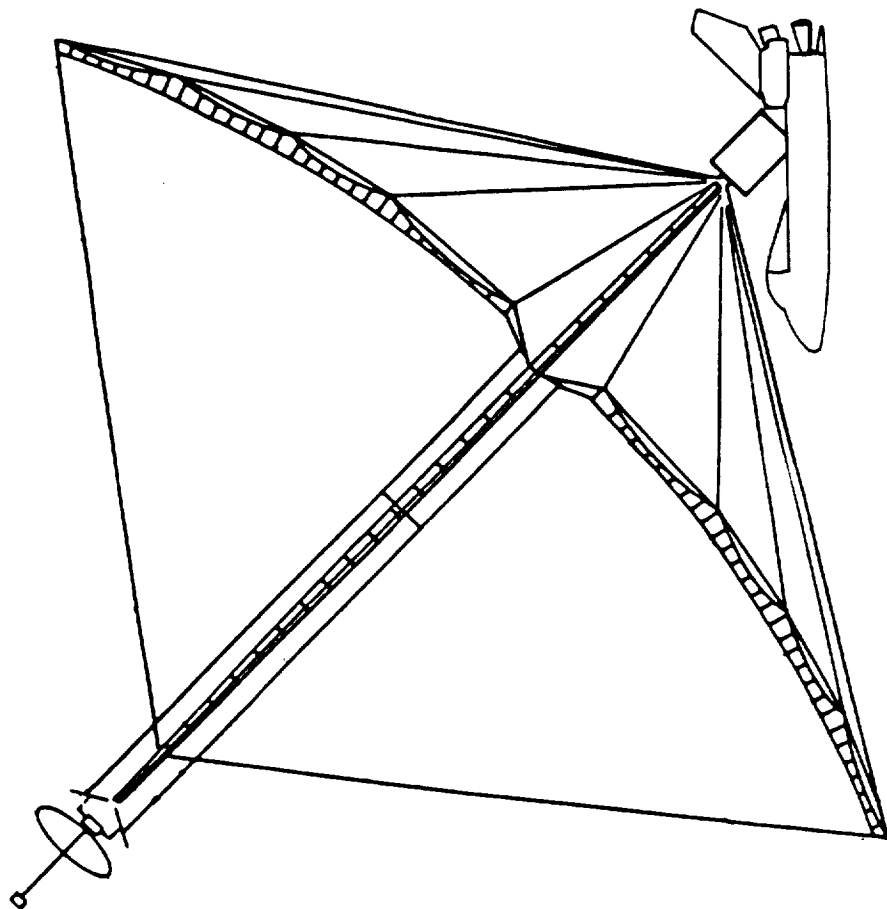


Figure 3-2: Packaged Baseline LSS Payload



*Figure 3-3: LTPS/LSS Erected in Orbiter Bay*



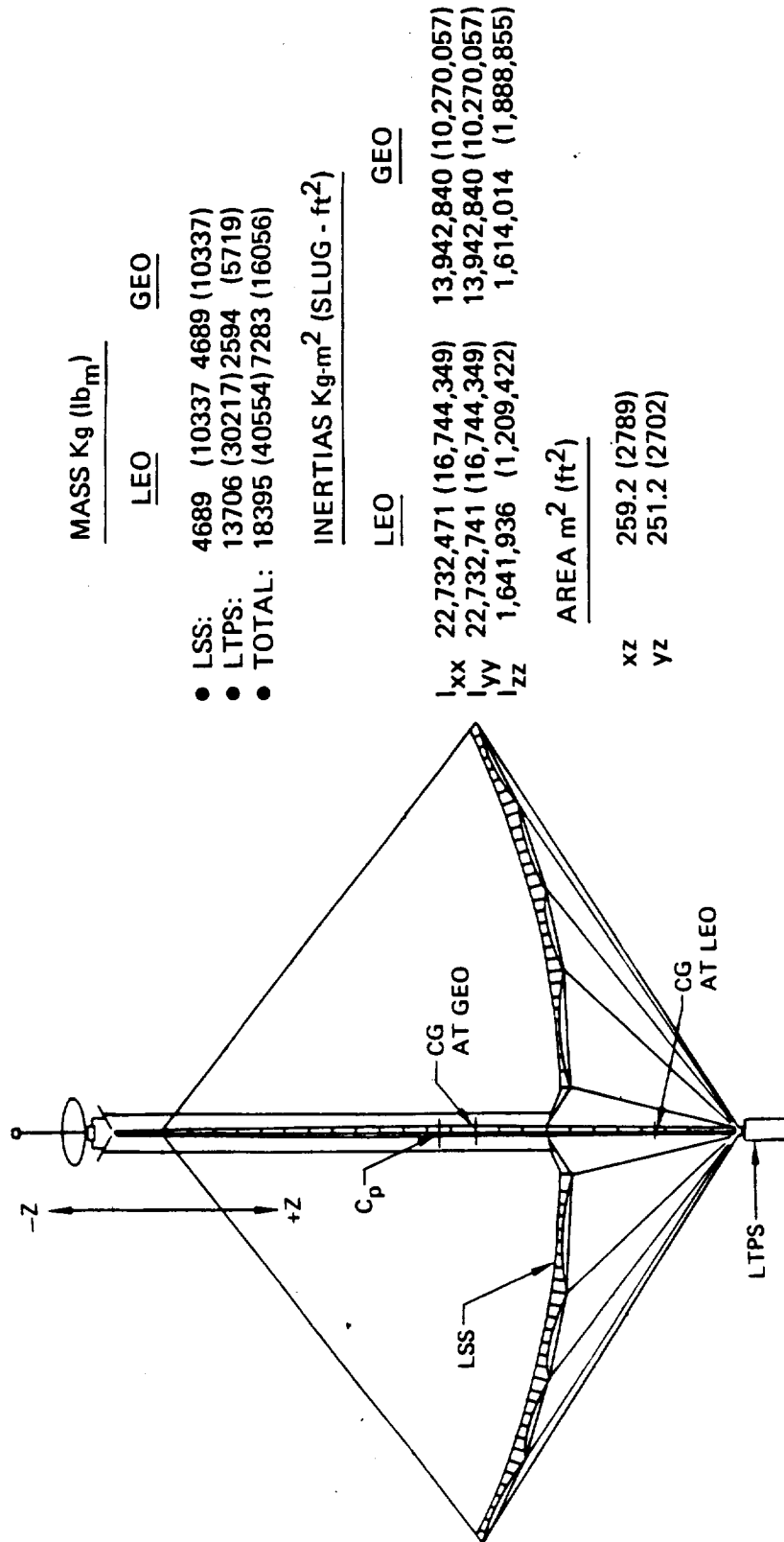


Figure 3-4: Mass, Inertial Properties, and Projected Areas of the Baseline LTPS/LSS

an assumed reflectivity of 1.0. Maximum gravity gradient orientation in pitch and yaw was 20 degrees.

Table 3-1 summarizes the results of the orbit-transfer mission analysis. It can be seen that the 16 perigee burn transfer required the least total propellant mass. A propellant mass savings of 313 kg was predicted in going from 8 to 16 perigee burns. However, trip time increased by 26.3 hours. Since the impact of reliability and additional shielding were not included in the analysis, a complete evaluation of the benefits of a 16 burn mission could not be made. It was therefore decided to adopt the 8 burn transfer for LTPS design and thermal analysis. It was found in the subsequent thermal analyses, that the propellant boiloff rate due to insulation heat leak during orbit transfer was less than 2.27 kg/hr for most cases studied. Hence, trip time did not have a strong influence on total propellant vent loss in orbit and therefore did not have a major affect on insulation design. For example, the total propellant vented during a 29 hour transfer would be approximately 66 kg as opposed to 125 kg for a 55 hour transfer. The additional 59 kg of propellant vent loss would decrease payload mass by approximately 26 kg.

Mission timelines were developed to support the Task I and Task II LTPS design and analysis efforts. One objective of establishing these timelines was to define the time spent in each unique thermal environment of the LTPS mission. There were essentially three thermal environments imposed on the LTPS; they were 1) ground hold, 2) STS Orbiter bay, and 3) free flight orbit transfer. The second objective of establishing mission timelines was to define the operational sequences which influenced propellant tank insulation design trades. Specifically, there were two timeline events of primary importance. One was the amount of time elapsed between termination of liquid replenishment to propellant tanks and MLI evacuation following launch. The second timeline event was the amount of time the propellant tank vent lines were locked up during launch.

Tables 3-2 and 3-3 summarize the mission timelines developed for Task I and Task II studies. They are almost identical with the exception of the elapsed time from completion of orbit transfer to payload release. In the Task I timeline this period was 24 hours while in the Task II timeline it was 14 hours. The time between arrival at GEO and payload release was shortened in Task II because it was determined that the period between the circularization burn and payload separation could be reduced by optimal phasing at the beginning of the transfer in LEO.

Mission parameters for the LEO to GEO transfer are presented in Table 3-4. This table summarizes the velocity increments for each engine firing and shows the apogees and perigees of the transfer orbits. Total velocity increment for the entire LTPS mission following Orbiter separation was 4751.1 m/sec. The data shown in Table 3-4 was used in the Boeing performance and mission simulation program, PMSP, to predict LTPS payload delivery capability.

### **3.3 LTPS CONCEPTUAL DESIGN APPROACH**

The preceding sections described the information established prior to the development of LTPS conceptual designs. This information consisted of groundrules and assumptions, interfaces, environments and mission requirements. A brief summary of the procedure followed in the development of LTPS conceptual designs for the Task I and Task II studies is presented in this section.

● EFFECT OF NUMBER OF PERIGEE BURNS ON PROPELLANT REQUIREMENTS

NUMBER OF PERIGEE BURNS	TRIP TIME (Hr)	ATTITUDE CONTROL PROPELLANT			TOTAL IMPULSE PROPELLANT Kg (lb <sub>m</sub> )	TOTAL PROPELLANT REQUIRED Kg (lb <sub>m</sub> )
		RCS Kg (lb <sub>m</sub> )	TVC Kg (lb <sub>m</sub> )	TOTAL Kg (lb <sub>m</sub> )		
6	25.3	38 (84)	19 (42)	57 (126)	13,433 (29,614)	13,490 (29,740)
8	28.6	48 (106)	21 (46)	69 (152)	13,343 (29,415)	13,412 (29,567)
16	54.9	85 (187)	33 (72)	118 (259)	12,981 (28,619)	13,099 (28,878)

- EFFECT OF INCREASING NUMBER OF PERIGEE BURNS
- SYSTEM RELIABILITY DECREASES
- RADIATION PROTECTION MASS INCREASES

Table 3-1: Results of Study to Evaluate the Number of Perigee Burns for LTPS LEO-GEO Transfer

NO.	EVENT DESCRIPTION	ET AT END OF EVENT	CONSIDERATIONS
1	TERMINATE LO <sub>2</sub> TOPPING	T - 4 MIN.	• PROVIDE TIME TO PURGE THE CARGO BAY CRYOGENIC LINES
2	TERMINATE LH <sub>2</sub> TOPPING	T - 4 MIN.	
3	LOCKUP TANKS	T - ZERO	• REFERENCE - NASA CONTRACTOR REPORT 166283, CONTRACT NAS3-21954, MARTIN-MARIETTA
4	RESUME VENTING OF TANKS	T + 90 SEC.	
5	STS IN LEO (278 x 278 km)	T + 47 MIN.	• BAC IUS STUDIES
6	OPEN PAYLOAD BAY DOORS	T + 100 MIN.	
7	ORBIT AND PAYLOAD CHECKOUT WITH GROUND STATIONS	T + 6 HR.	
8	ERECT LTPS/LSS	T + 17 HR.	• CREW WORK/REST CYCLE CONSTRAINTS - NASA CONTRACTOR REPORT 160861, CONTRACT NAS9-15718, ROCKWELL
9	DEPLOY AND CHECKOUT LSS	T + 46 HR.	
10	CHECKOUT LTPS	T + 46 HR.	• LSS COMPRISED OF DEPLOYABLE STRUCTURES AND APPENDAGES
11	MANEUVER ORBITER AND DISCONNECT	T + 50 HR.	
12	PHASE FOR ORBIT TRANSFER	T + 61 HR.	
13	TRANSFER FROM LEO TO GEO (8 PERGEE BURNS)	T + 89 HR.	• J.V. BREAKWELL STUDIES, STANFORD UNIVERSITY
14	COAST PERIOD	T + 112 HR.	• TYPICAL FOR NON-CIRCULAR FINAL ORBITS
15	RELEASE LSS AND SEPARATE	T + 113 HR.	
16	REMOVE LTPS TO DISPOSAL ORBIT (GEO + 1150 N.Mi.)	T + 125 HR.	• NASA/MSFC OTV STUDIES

Table 3-2: Task 1 Mission Timeline

NO.	EVENT DESCRIPTION	ET AT END OF EVENT	CONSIDERATIONS
1	TERMINATE LO <sub>2</sub> TOPPING	T - 4 MIN.	• PROVIDE TIME TO PURGE THE CARGO BAY CRYOGENIC LINES
2	TERMINATE LH <sub>2</sub> TOPPING	T - 4 MIN.	
3	LOCKUP TANKS	T - ZERO	• REFERENCE - NASA CONTRACTOR REPORT 165293, CONTRACT NAS3-21964, MARTIN-MARIETTA
4	RESUME VENTING OF TANKS	T + 90 SEC.	
5	STS IN LEO (278 x 278 km)	T + 47 MIN.	• BAC IUS STUDIES
6	OPEN PAYLOAD BAY DOORS	T + 100 MIN.	
7	ORBIT AND PAYLOAD CHECKOUT WITH GROUND STATIONS	T + 6 HR.	
8	ERECT LTPS/LSS	T + 17 HR.	• CREW WORK/REST CYCLE CONSTRAINTS - NASA CONTRACTOR REPORT 160881, CONTRACT NAS9-15718, ROCKWELL
9	DEPLOY AND CHECKOUT LSS	T + 46 HR.	
10	CHECKOUT LTPS	T + 46 HR.	• LSS COMPRISED OF DEPLOYABLE STRUCTURES AND APPENDAGES
11	MANEUVER ORBITER AND DISCONNECT	T + 50 HR.	
12	PHASE FOR ORBIT TRANSFER	T + 61 HR.	
13	TRANSFER FROM LEO TO GEO (8 PERGEE BURNS)	T + 89.6 HR.	• J.V. BREAKWELL STUDIES, STANFORD UNIVERSITY
14	COAST PERIOD	T + 102 HR.	• TYPICAL FOR NON-CIRCULAR FINAL ORBITS
15	RELEASE LSS AND SEPARATE	T + 103 HR.	
16	REMOVE LTPS TO DISPOSAL ORBIT (GEO + 1150 N.Mi.)	T + 115 HR.	• NASA/MSFC OTV STUDIES

Table 3-3: Task II Mission Timeline

Orbit Transfer Event	Hours After Launch	Velocity Increment m/s (ft/sec)	Altitude, km (mi)	
			Perigee	Apogee
Orbiter Separation	50	3.1 (10.2)	222 (138)	222 (138)
Perigee Burn No. 1	51	277.4 (910.1)	222 (138)	1031 (640)
2	62.7	292.0 (957.8)	472 (293)	2066 (1283)
3	64.5	309.8 (1016.1)	663 (412)	3430 (2131)
4	66.7	330.9 (1084.4)	845 (525)	5292 (3287)
5	69.3	356.2 (1168.3)	1024 (636)	7971 (4952)
6	72.4	386.5 (1267.7)	1205 (749)	12131 (7536)
7	76.6	423.4 (1388.8)	1390 (863)	19419 (12063)
8	86.6	469.1 (1538.6)	1579 (981)	35389 (21984)
GEO Circularization Burn	87.2	1742.0 (5713.8)	—	35863 (22279)
Orbit Trim and Unload Payload	103	106.7 (350.0)	—	—
Burn to Disposal Orbit	103 +	28.7 (94.1)	35863 (22279)	37715 (23429)
Disposal Orbit Circularization	115	28.4 (93.2)	—	37715 (23429)

*Table 3-4: Task II Orbit Transfer Parameters*

Figure 3-5 shows the principal steps of the design development process. Input data included, in addition to the system requirements, initial LTPS design concepts. These concepts were developed from preliminary modeling estimates of LTPS performance and simplified orbit mechanics.

Four computer analysis programs were used to support the design process. These analysis programs were:

- a. OPERA - thermal radiation environment prediction. (Appendix A)
- b. RADSIM - radiation interchange factor calculation. (Appendix A)
- c. SINDA - temperature and heat leak prediction.
- d. PMSP - LTPS performance and mission analysis.

Geometric models of the principal structural elements of the LTPS were developed from the LTPS design concepts established at the beginning of the design process. These conceptual designs consisted of a general layout, or arrangement, of principal LTPS subsystems and preliminary estimates of tank size. Thermal radiation properties of the LTPS surfaces were established from published data for the initially selected materials and coatings. Highly simplified geometrical models of the Orbiter cargo bay and LMSS payload were also developed and radiative properties defined for their surfaces. The geometrical models and surface property information were the principal input data for the OPERA and RADSIM computer programs.

OPERA was used to predict the thermal radiation flux on external LTPS surfaces during orbit transfer and prior to separation from the Orbiter. Radiation interchange factors between the LTPS surfaces and between radiatively interacting surfaces of the payload, Orbiter and LTPS were calculated with the RADSIM program.

Simple thermal models of each LTPS design concept were developed. These models defined the principal radiative, conductive and convective heat flow paths between major LTPS/LMSS/Orbiter elements. They also characterized the thermal storage capacity of the principal LTPS subsystem masses including propellants, tanks, insulation, structure, engines and avionics. The thermal models, along with thermal radiation environment predictions supplied by OPERA and radiation interchange information provided by RADSIM, were input to the SINDA program. SINDA was used to predict heat leaks into the LH<sub>2</sub> and LO<sub>2</sub> propellants from the beginning of the mission, at ground hold, to the end of mission following insertion of the LTPS into disposal orbit.

Predicted propellant tank heat fluxes were used to calculate values of propellant density, mass loss due to vapor venting, and pressure rise during vent line lockup at launch. Effective densities of the propellants were affected by heat flux because the volume of bubbles in the liquid was dependent on boiling rate. The greater the heat flux, the greater the bubble volume and therefore the less volume available for liquid. Vent loss was directly proportional to heat flux because it was assumed all heat leak into the propellant tanks resulted in vaporization and subsequent venting of the vapor. Larger heat leaks resulted in more initial propellant mass and larger tanks to account for the loss of propellant during the mission.

Heat leak into the tanks during vent line lockup at launch caused the ullage pressure of the tanks to rise. The greater the heat leak, the greater the pressure rise. Peak tank

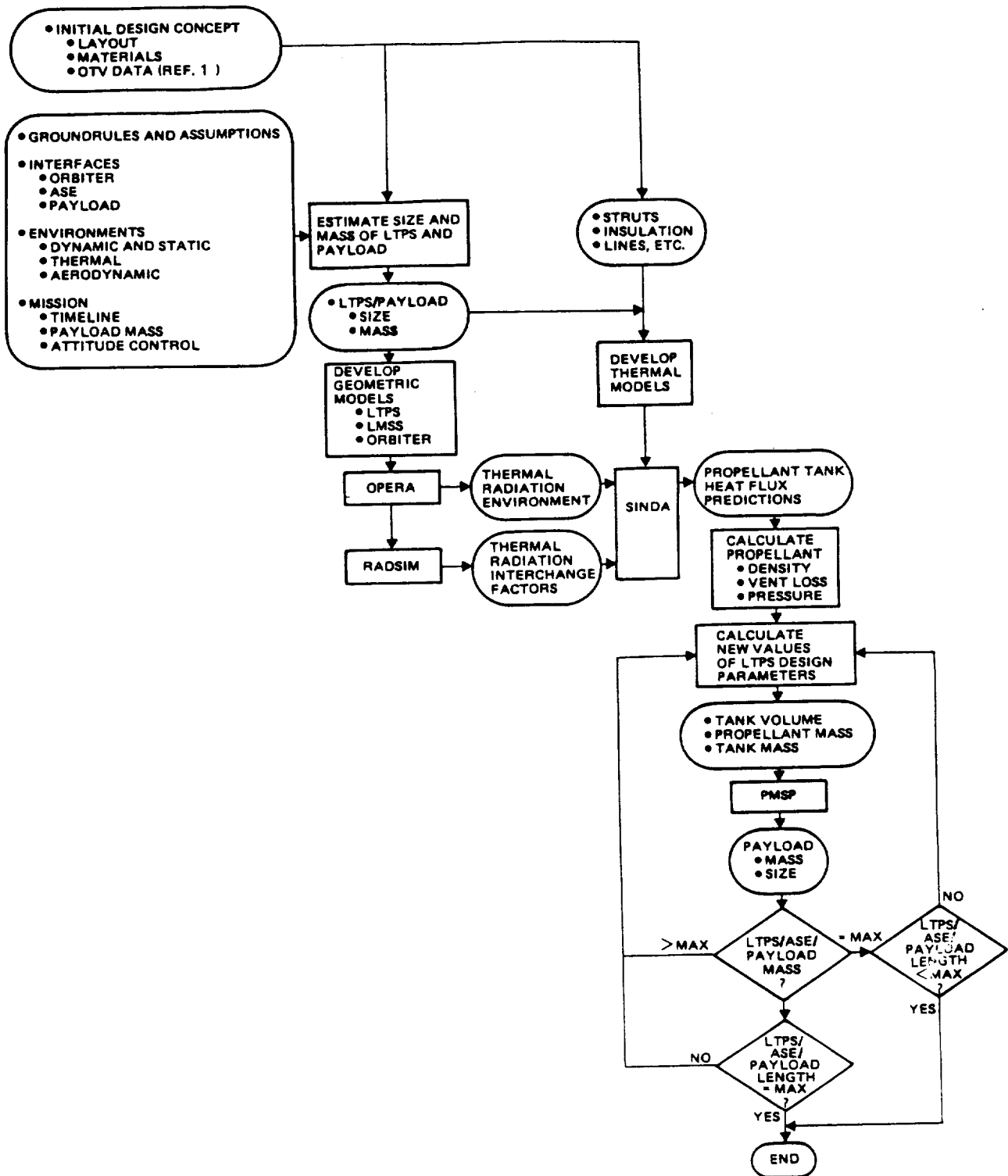


Figure 3-5: LTPS Conceptual Design Approach



pressure depended on assumed ullage volume as well as heat leak. During the vent lockup period the insulation interstitial pressure was essentially at sea level conditions and therefore the heat leak into the tanks was approximately the same as during MLI purging. Hence tank wall thickness and mass depended on the rate of heat leak into the tank during the ground-hold phase of the mission.

Following the prediction of propellant density and vent loss, new estimates of LTPS tank volumes, initial propellant mass and tank mass were incorporated into the design model and new performance predictions were calculated with the PMSP computer program. The PMSP program employs an iterative technique to converge on a specified mass for the combined upper stage and payload. Program inputs are orbit characteristics, mission sequence, propellant loss estimates, engine performance, stage inert mass and tankage nonpropellant mass relationships. The values of payload mass predicted by the PMSP program were used to calculate payload packaged length for the particular packaging density of interest. Then the combined mass and packaged length of the LTPS/ASE/payload were compared with the constraining values for STS launch. If the maximum constraining values of either mass or length were not satisfied, new values of tank size and mass were estimated and the design iterated until the maximum value of payload mass or length was found. The resulting conceptual designs developed for the Task I and Task II studies are described in the following sections.

### 3.4 TASK I LTPS CONCEPTUAL DESIGN

The LTPS design developed for the Task I insulation preliminary thermal analysis is shown in Figure 3-6. This design is a resized version of an expendable, STS-launched orbit transfer vehicle developed under contract NAS8-33532 and described in Reference 1. The total length of the stage is 739 cm, and its diameter is 447 cm. Avionics, RCS propellant tanks, fuel cells and miscellaneous support equipment are mounted to an aluminum girth ring located between the LH<sub>2</sub> and LO<sub>2</sub> tanks. The 2224 N thrust engine is mounted to the LO<sub>2</sub> tank by graphite epoxy struts. Thrust loads are carried through the tank walls to the tank support struts. The engine is 101.6 cm long with a nozzle exit diameter of 40.6 cm, and it weighs 38.8 kg. A complete description of this engine design is contained in Reference 8.

The propellant tanks are sized to carry a total useable propellant mass of 17256 kg. Volume of the LH<sub>2</sub> tank is 38.47 m<sup>3</sup>. The ratio of major-to-minor axes for the ellipsoidal domes is  $\sqrt{2}$ . The height of each dome is 157.8 cm and the length of the cylindrical center section is 63.5 cm. The LH<sub>2</sub> tank diameter is 419.4 cm. Volume of the LO<sub>2</sub> tank is 13.7 m<sup>3</sup>. The axis ratio of the two ellipsoidal domes which form the tank is  $\sqrt{2}$  and the total length of the LO<sub>2</sub> tank is 244.3 cm. At the start of the mission, the total LTPS mass is 20025 kg and at burnout its mass is 2393 kg. Payload delivery capability for GEO missions is 7075 kg for a specific impulse of 4560 N-sec/kg and an 8-burn orbit transfer.

Table 3-5 summarizes specific design features and characteristics of the Task I LTPS. The body shell, with the exception of the avionics/equipment ring, is a graphite epoxy sandwich. Tanks are constructed of 2219 aluminum and are cantilevered from the body shell via bipod strut mounting trusses. The struts used in the LH<sub>2</sub> mounting truss are glass epoxy and the struts in the LO<sub>2</sub> truss are graphite epoxy. Strut material selection was based on an optimization study that considered the strength, heat conduction characteristics and mass of the struts.

Electrical power is supplied by modified STS Orbiter fuel cells. A 7.8 m<sup>2</sup> radiator is located around the periphery of the LTPS body shell to control fuel cell temperature. All

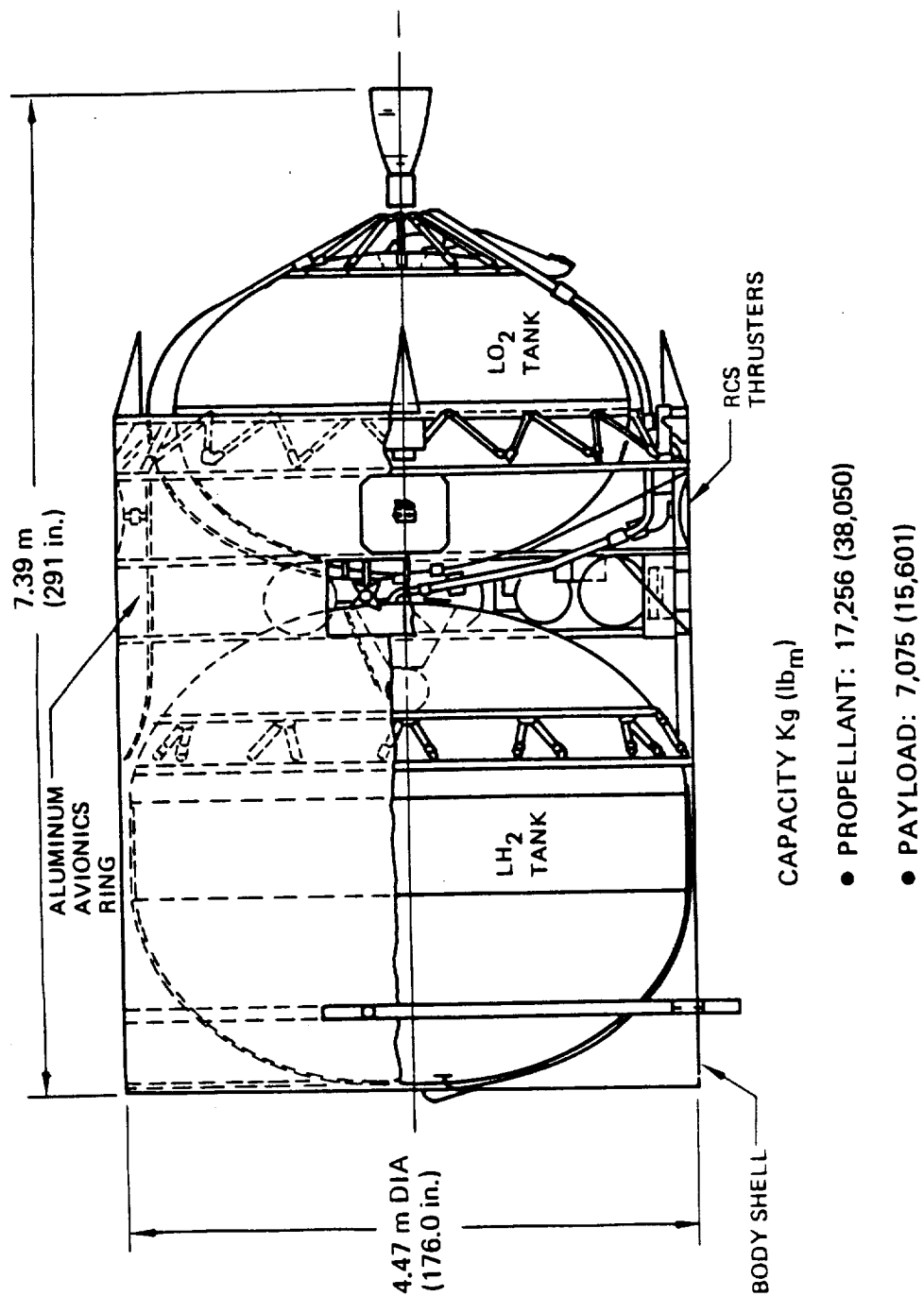


Figure 3-6: Task 1 Baseline LTPS Design

Graphite/epoxy body shell
2219 Aluminum LH <sub>2</sub> and LO <sub>2</sub> tanks
IUS avionics components
Passive thermal management of avionics
Modified orbiter O <sub>2</sub> -H <sub>2</sub> fuel cells
IUS power distribution electronics
2224 N thrust main impulse engine
Autogenous main tank pressurization
IUS hydrazine attitude control system
Triple inhibit against hazardous fluid leakage
Bipod strut tank support systems
• Glass/epoxy struts for LH <sub>2</sub> supports
• Graphite/epoxy struts for LO <sub>2</sub> supports
5% Weight margin for existing hardware
15% Weight margin on new hardware

*Table 3-5: Task I LTPS Design Features*

other equipment cooling is accomplished passively by radiation from the aluminum girth ring.

A mass statement for the Task I LTPS is presented in Table 3-6. Total launch weight, including payload and the fully loaded LTPS is 27100 kg. The airborne support equipment (ASE), including the structure for securing and deploying the LTPS and payload, has a total mass of 2554 kg. Thus, the total mass loaded in the Orbiter cargo bay for an LTPS/payload launch would be 29654 kg.

### 3.5 TASK II LTPS CONCEPTUAL DESIGNS

This section describes the 3 LTPS conceptual designs developed for the Task II insulation optimization studies. The designs define the general configuration, subsystem arrangement, mass, dimensions and materials for each LTPS. The purpose of developing these point designs, as stated in section 3.0, was to:

- a. Develop parametric design data for determining the impact of insulation design on LTPS and payload mass and size.
- b. Define configurations, dimensions, masses and materials for propellant tank thermal analysis models.
- c. Determine the masses and sizes of major LTPS subsystems for input to the payload prediction computer programs used to optimize tank insulation designs.

Figures 3-7, 3-8 and 3-9 show the general configuration, subsystem arrangement and overall dimensions of the three LTPS point designs developed at the beginning of Task II. Major differences between the three LTPS designs are evident in the size and shape of the propellant tanks. As the payload packaging density was decreased, larger and larger payload lengths were possible until, at about  $40 \text{ kg/m}^3$ , the Orbiter payload volume limit was reached. At this point, the total length of the combined LTPS, payload and ASE equaled the available Orbiter cargo bay payload volume length of 16.95 m. Between payload densities of  $56 \text{ kg/m}^3$  and  $40 \text{ kg/m}^3$ , the payload mass and LTPS size and mass remained constant. At payload densities below  $40 \text{ kg/m}^3$ , the payload was sized to fill the available Orbiter cargo bay volume. For these cases, the payload mass and the mass and size of the LTPS decreased with decreasing payload density. The use of torroidal  $\text{LO}_2$  tanks shortened the LTPS and resulted in increased payload length and mass. The LTPS for the  $56 \text{ kg/m}^3$  payload density shown in Figure 3-7 is essentially identical to the Task I design described in section 3.4. The primary difference is the Task II version has less predicted payload capacity. This reduction in payload resulted from Task I thermal analyses which showed the initial predictions for propellant tank heat leak were optimistic. The larger values of heat leak resulted in a greater propellant vent loss (376 kg over the mission) which reduced the payload mass of the Task II design.

The initial mass of the LTPS designed for a  $40 \text{ kg/m}^3$  payload density (Figure 3-8) is almost identical to the initial mass of the LTPS designed for a  $56 \text{ kg/m}^3$  payload density (Figure 3-7). However, the LTPS designed for the lower density payload is shown to have a torroidal  $\text{LO}_2$  tank. The torroidal tank was selected because the  $40 \text{ kg/m}^3$  payload density was found to be on the border between being a mass-limited or volume-limited case. Hence, the shorter torroidal tank was selected to maximize payload length, the primary objective for LMSS-type payloads. The torroidal tank LTPS was found to be slightly heavier than the ellipsoidal version because the torroidal tank is inherently heavier and tank and engine supports also weigh more.

	Kg (lb <sub>m</sub> )
<b>SUBSYSTEMS</b>	
ENGINE .....	38.6 (85.1)
AVIONICS .....	294.0 (648.2)
POWER SUPPLY AND DISTRIBUTION .....	288.0 (634.9)
ATTITUDE CONTROL .....	62.6 (138.0)
FUEL CELL REACTANTS .....	39.9 (88.0)
THERMAL MANAGEMENT .....	81.6 (179.9)
TOTAL SUBSYSTEM MASS .....	804.7 (1774.0)
STRUCTURAL HARDWARE .....	821.0 (1810.0)
INSULATION .....	53.5 (117.9)
BODY SHELL .....	177.8 (392.0)
TANKS .....	370.6 (817.0)
RESIDUAL PROPELLANTS .....	165.6 (365.1)
TOTAL BURNOUT MASS .....	2393.2 (5276.0)
MAIN IMPULSE PROPELLANTS .....	17256.4 (38050.1)
LOSSES .....	375.7 (828.3)
TOTAL EXPENDED MASS .....	17632.1 (38872.0)
TOTAL INITIAL MASS .....	20025.3 (44148.0)
PAYLOAD MASS .....	7075.0 (15601.0)
ASE .....	2554.0 (5630.5)
TOTAL LIFTOFF MASS .....	29654.3 (65379.5)

*Table 3-6: Task 1 LTPS Mass Summary*

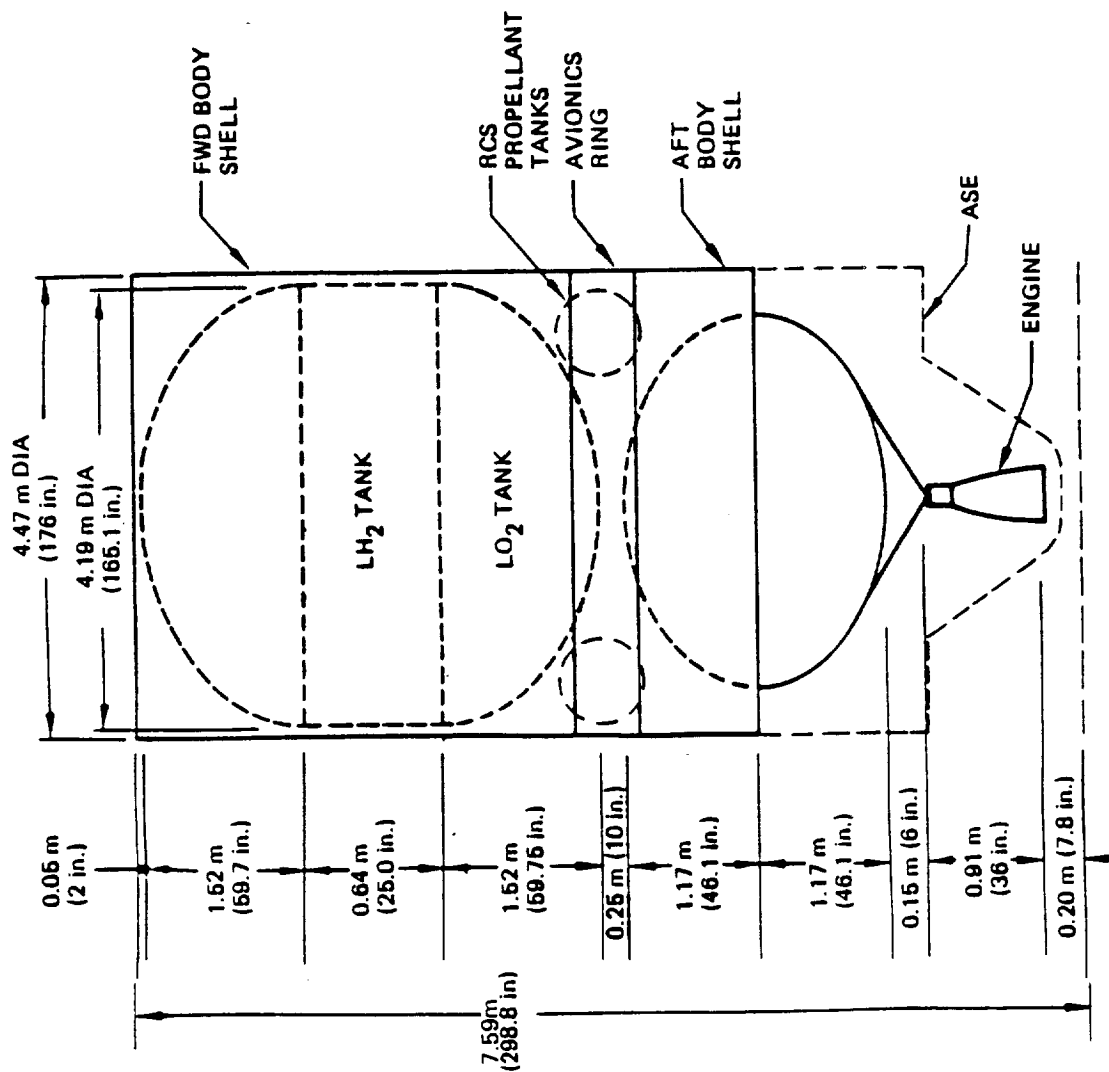
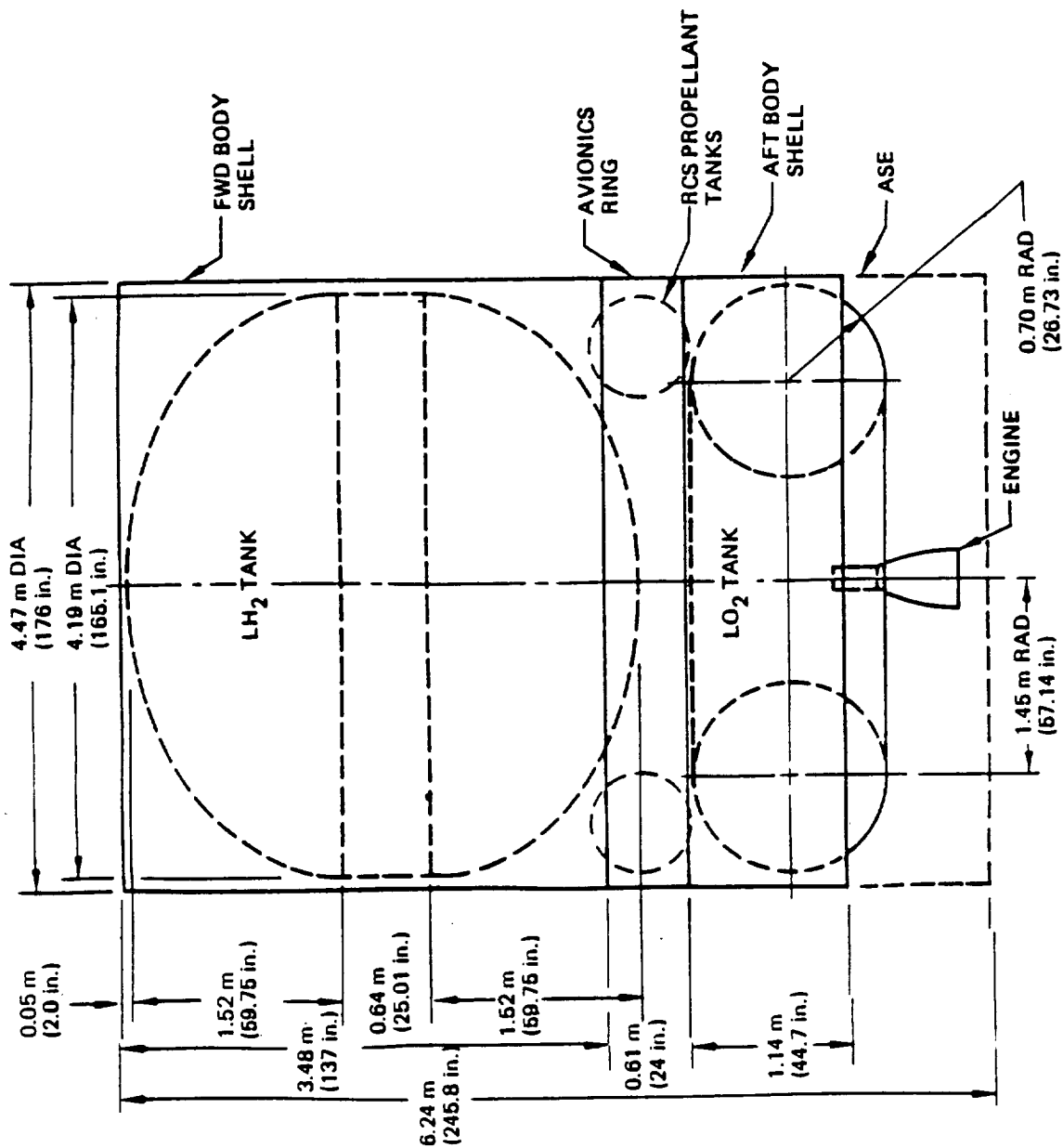


Figure 3-7: LTPS for 56 Kg/m<sup>3</sup> (3.5 lb<sub>m</sub>/ft<sup>3</sup>) Payload Density

<u>MASS SUMMARY</u> Kg (lb <sub>m</sub> )	
START MISSION	26939 (59390)
USEABLE PROPELLANT	17336 (38218)
BURNOUT MASS	2393 (5276)
<u>PAYLOAD CAPABILITY</u>	
TANK VOLUME m <sup>3</sup> (ft <sup>3</sup> )	6835 (15068)
LH <sub>2</sub> TANK	38.5 (1357.6)
• LO <sub>2</sub> TANK	13.7 (483.5)
<u>PAYLOAD LENGTH</u> m (ft)	8.1 (26.4)



MASS SUMMARY Kg (lb <sub>m</sub> )	
• START MISSION	26909 (59323)
• USEABLE PROPELLANT	17341 (38229)
• BURNOUT MASS	2554 (5631)
PAYLOAD CAPABILITY	6706 (14785)
TANK VOLUME m <sup>3</sup> (ft <sup>3</sup> )	
• LH <sub>2</sub> TANK	38.5 (1358.6)
• LO <sub>2</sub> TANK	13.8 (488.6)
PAYLOAD LENGTH m (ft)	10.7 (35.1)

Figure 3-8: LTPS for 40 Kg/m<sup>3</sup> (2.5 lb<sub>m</sub>/ft<sup>3</sup>) Payload Density

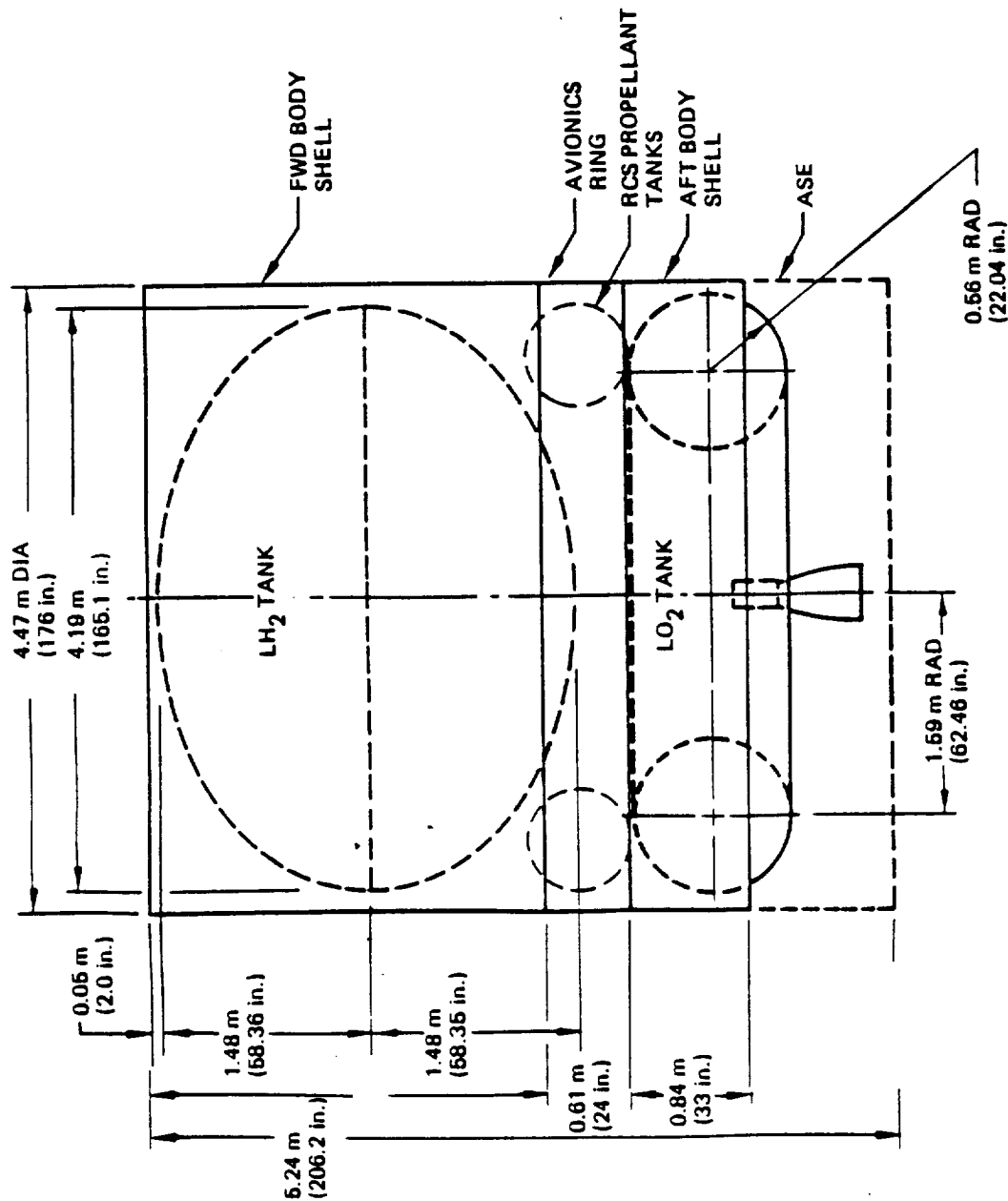


Figure 3-9: LTPS for 24 Kg/m<sup>3</sup> (1.5 lb<sub>m</sub>/ft<sup>3</sup>) Payload Density

MASS SUMMARY Kg (lb <sub>m</sub> )	
• START MISSION	19113 (42135)
• USEABLE PROPELLANT	12298 (27113)
• BURNOUT MASS	2236 (4930)
PAYLOAD CAPABILITY	4414 (9731)
TANK VOLUME m <sup>3</sup> (ft <sup>3</sup> )	
• LH <sub>2</sub> TANK	27.3 (964.0)
• LO <sub>2</sub> TANK	9.8 (346.7)
PAYLOAD LENGTH m (ft)	11.7 (38.4)



Table 3-7 summarizes the mass of each LTPS, including inerts and expendables. Subsystem masses which were assumed to be identical to those of the Task I LTPS were:

Engine	38.6 kg
Avionics	294. kg
Power supply and distribution	288. kg
Attitude control	62.6 kg
Fuel cell reactants	39.9 kg
Thermal management	81.6 kg

Propellant vent losses during; 1) ground-hold, 2) before LTPS engine ignition and 3) during orbit transfer, are based on the thermal model predictions described in section 4. The tank insulation for the three baseline LTPS designs was helium-purged MLI. Heat leaks through struts and MLI penetrations caused more than 95% of the propellant vent loss during the mission. Tank support struts were optimized to maximize payload mass. The optimization involved a trade between strut mass and propellant boil-off mass and their combined affect on LTPS payload mass. The primary constraint for the optimization was the structural performance of the struts. That is, all strut designs were required to satisfy structural load carrying criteria. It was assumed all designs used the same number of struts for each tank support system; 24 struts for the LH<sub>2</sub> tank and 32 struts for the LO<sub>2</sub> tank. Appendix B summarizes the tank support strut optimization study. The resulting strut designs for the three LTPS propellant tanks are described in Table 3-8.

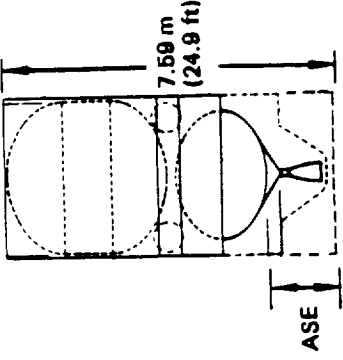
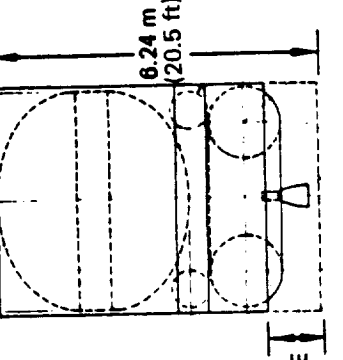
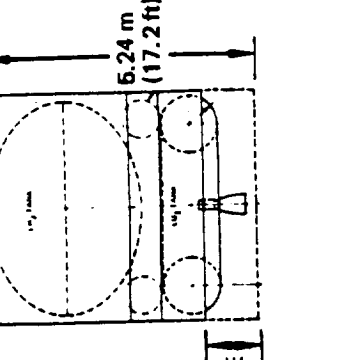
LTPS Configuration	Packaged Payload Density		
	56 Kg/m <sup>3</sup> (3.5 lb <sub>m</sub> /ft <sup>3</sup> )	40 Kg/m <sup>3</sup> (2.5 lb <sub>m</sub> /ft <sup>3</sup> )	24 Kg/m <sup>3</sup> (1.5 lb <sub>m</sub> /ft <sup>3</sup> )
LTPS Mass Summary Kg (lb <sub>m</sub> )			
	804.70 (1,774)	804.70 (1,774)	804.70 (1,774)
Fixed mass			
• Engine	821.00 (1,810)	990.70 (2,184)	927.20 (2,044)
• Avionics	53.52 (118)	60.78 (134)	50.80 (112)
• Thermal management	177.80 (392)	181.00 (398)	141.50 (312)
• Power supply and dist.	370.60 (817)	371.50 (819)	309.80 (683)
• Attitude control	67.13 (148)	45.36 (100)	45.36 (100)
• Fuel cell reactants	87.54 (193)	87.54 (193)	61.69 (136)
Structural hardware	10.89 (24)	12.70 (28)	10.43 (23)
Insulation	2393.00 (5,278)	2554.00 (5,631)	2236.00 (4,930)
Body shell	17338.00 (38,218)	17341.00 (38,229)	12298.00 (27,113)
Tanks	9.879 (22)	12.25 (27)	10.43 (23)
Residual propellants	178.20 (395)	131.50 (290)	133.80 (295)
Propellant loading uncertainty	84.37 (186)	61.69 (136)	62.60 (138)
Propellant 5 min. hold boil-off	33.11 (73)	33.11 (73)	33.11 (73)
Total burnout mass	68.95 (152)	68.95 (152)	68.95 (152)
Main impulse propellants	17711.00 (39,046)	17648.00 (38,907)	12556.00 (27,681)
Vent loss before launch	6835.00 (15,068)	6706.00 (14,785)	4414.00 (9,731)
Vent loss before first burn	2554.00 (5,631)	2546.00 (5,612)	2546.00 (5,612)
Vent loss after first burn	29473.00 (65,039)	29454.00 (64,935)	21858.00 (47,748)
Start stop losses			
RCS propellants			
Total expended mass			
Payload			
ASE			
Total mass			

Table 3-7: Task II LTPS Mass Summaries

TANK TYPE	STRUT MATERIAL	STRUT CONDUCTIVITY – TEMPERATURE DEPENDENCE W/m - K (BTU/hr-ft-°F)	NO. STRUTS	STOWED PAYLOAD DENSITY, kg/m <sup>3</sup> (lb <sub>m</sub> /ft <sup>3</sup> )					
				56 (3.5)		40 (2.5)		24 (1.5)	
				AREA, ° cm <sup>2</sup> (in <sup>2</sup> )	LENGTH, cm (in)	AREA, ° cm <sup>2</sup> (in <sup>2</sup> )	LENGTH, cm (in)	AREA, ° cm <sup>2</sup> (in <sup>2</sup> )	LENGTH, cm (in)
HYDROGEN	FIBERGLASS/ EPOXY	$0.086 + 1.98 \times 10^{-3} T$ $(0.342 + 6.35 \times 10^{-4} T)$	24	44.6 (6.9)	12.4 (4.9)	44.6 (6.9)	12.4 (4.9)	27.0 (4.2)	41.7 (16.4)
OXYGEN	GRAPHITE/ EPOXY	$0.138 + 0.146 T$ $(21.7 + 0.047 T)$	32	310 (48.1)	143 (56.4)	70.7 (11.0)	52.6 (20.7)	50.3 (7.8)	35.1 (13.8)

\*Cross-section area of all support struts

Note: T is in °F

Table 3-8: Tank Support Strut Data



## **4.0 PREDICTED PROPELLANT THERMAL LOADS**

Propellant thermal loads (i.e., total heat leak into the tanks) have a significant impact on LTPS payload delivery capability and therefore are a major consideration in tank insulation design. Propellant heat leak depends not only on the tank design and mission phase, but also on the amount and type of insulation. Moreover, the impact of insulation performance on payload mass is very sensitive to ground-hold environments. The influence of tank configuration, mission phase and insulation type and thickness on the propellant thermal load were predicted in this study, and parametric correlations were developed to aid in the comparison of LTPS tank insulation designs.

Section 4.1 presents the approach used to predict the heat transfer rate to the propellants. Propellant thermal loads attributed to tank insulation, penetrations, and support system are discussed in sections 4.2, 4.3, and 4.4 respectively.

### **4.1 THERMAL MODELING APPROACH**

Heat transfer between the LTPS propellant tank(s) surfaces and the external environment depends on the mission phase. During the ground-hold part of the mission the Orbiter cargo bay defines the external environment seen by the LTPS. In this study, a steady-state condition was assumed to exist. Important heat transfer mechanisms during ground hold include radiation, conduction, and convection. Following lift-off, the Orbiter bay, LTPS purge enclosures, and MLI are vented to space, eliminating the convection heat transfer mechanism. After attaining LEO, the Orbiter bay doors are opened. This adds to the complexity of the LTPS-environment interchange by:

- a. Exposing the LTPS external surfaces to direct solar, albedo, and earth long-wave radiation sources, and
- b. Providing the LTPS with a heat sink to deep space.

Upon LTPS/LSS separation from the Orbiter, the cargo bay thermal interaction with the LTPS ceases.

A Thermal Math Model (TMM) of the Task I LTPS baseline configuration was initially developed to determine the time-varying nature of the propellant thermal load. The model accounted for variations in environmental heat sources and heat transfer mechanisms. It also included the effects of LTPS heat capacitance, and natural-convection during the ground-hold mission phase. The model was designed to allow a wide range of insulation thicknesses and types (either helium-purged MLI or nitrogen-purged MLI with a foam substrate) to be evaluated. TMMs of the Task II LTPS design were subsequently developed from the Task I model. They accounted for differences in tank configuration and LTPS dimensions.

Thermal models considered two extreme ground-hold purge enclosure environments. In one extreme, minimum convective coupling between the Orbiter bay and the MLI was assumed to exist. This condition yielded relatively cold tank insulation temperatures. In the other extreme, forced convection in the purge enclosure was assumed. This condition was simulated by setting the MLI outer surface temperature to equal 294°K (70°F) during the ground-hold and initial-ascent mission phases. Physically this extreme could be achieved by either:

- a. Introducing enough warm gas into the purge enclosure to ensure a warm MLI surface temperature, or
- b. Altering the LTPS design to allow greater thermal contact between the Orbiter bay and the MLI surface.

This ground-hold environment will be referred to as enhanced or forced-convection, and it serves to contrast results obtained for the natural-convection environment which would be difficult, if not impossible to achieve. The natural-convection condition however, was considered because it represents a lower bound for the ground-hold heat transport mechanism.

Subsection 4.1.1 describes the LTPS external environments that were used for thermal modeling. Subsection 4.1.2 discusses the LTPS thermal models that were developed.

#### **4.1.1 LTPS Environments**

During the ground-hold and the ascent-to-LEO mission phases, the LTPS environment is controlled by the Orbiter cargo bay. In developing the LTPS thermal models, the cargo bay temperatures were assumed to be independent of their surroundings. The Reference 6 cargo bay temperatures were used, and their location-time relationships are depicted in Figure 4-1.

Radiation and convection heat transfer mechanisms thermally couple the cargo bay with the LTPS external surfaces prior to launch and during the first few minutes after STS liftoff. Radiation exchange between LTPS and cargo bay surfaces was determined with the aid of the Monte-Carlo thermal code RADSIM (Appendix B describes RADSIM). This code was used to determine the radiation interchange factors between different portions of the cargo bay and the LTPS exterior surfaces. RADSIM modeling assumed blackbody behavior for the Orbiter cargo bay. Radiation surface properties of LTPS external surfaces are given in Table 4-1.

During ground-hold energy is transferred to the LTPS external surfaces by convection as well as radiation. Prior to launch the Orbiter bay is purged with nitrogen gas. Natural convection by the purge gas was estimated by standard Grashof-Prandtl number (or Rayleigh number) correlations. Furthermore, the correlations were chosen to reflect the geometric relationship between the LTPS surfaces and the Orbiter. For example, convection between the cargo bay and the LTPS body shell-avionics ring surfaces was determined by using a correlation for concentric cylinders. The fore and aft LTPS closeouts were modeled as cool discs facing upward and downward, respectively. The correlations were then incorporated into the thermal math models. To a good approximation, a temperature of 294°K was found to be typical for the external LTPS surfaces prior to launch.

Heat transfer to the LTPS external surfaces by natural-convection will continue for several minutes after launch. Figure 4-2 shows the cargo bay pressure-time curve as determined from the STS III launch data (data was furnished to Boeing by the NASA LeRC program manager). The pressure profile for a Saturn V launch is also shown for comparison. It is seen that when the gas pressure became lower than 10 torr, the pressure decay rate was significantly lessened. At this pressure level, gas transport characteristics begin to change, and the transition between continuum and free-molecular flow regimes occurs. This may decrease pressure decay rate because of:

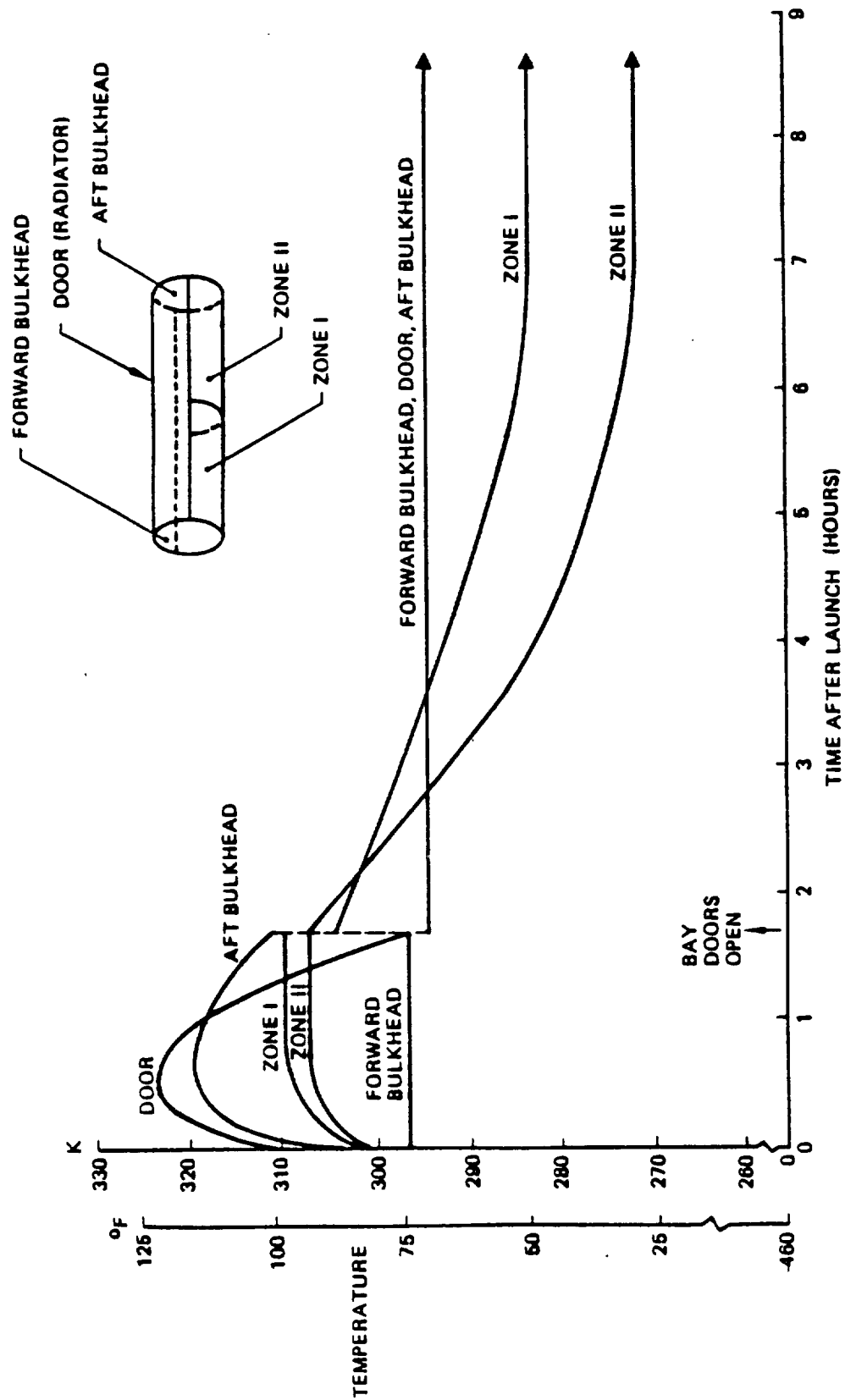


Figure 4-1: Orbiter Bay Temperature History (Reference 6)

	Material	$\alpha_s/\epsilon_{IR}$
Fore and Aft Purge Closeouts	Kapton	0.14/0.08
Fore and Aft Body Shell Coating	White-Tedlar <sup>1.</sup>	0.37/0.77
Avionics Ring and Fuel Cell Radiator	FOSR <sup>2.</sup>	0.014/0.750

1. Tedlar is manufactured by Dupont. Its optical properties are achieved by adding titanium dioxide.
2. Flexible Optical Solar Reflector (FOSR): Sheldahl P/N G409750, a silvered Teflon film coated with an tin oxide to facilitate electrical grounding.

*Table 4-1: Radiative Properties of the LTPS External Surfaces*



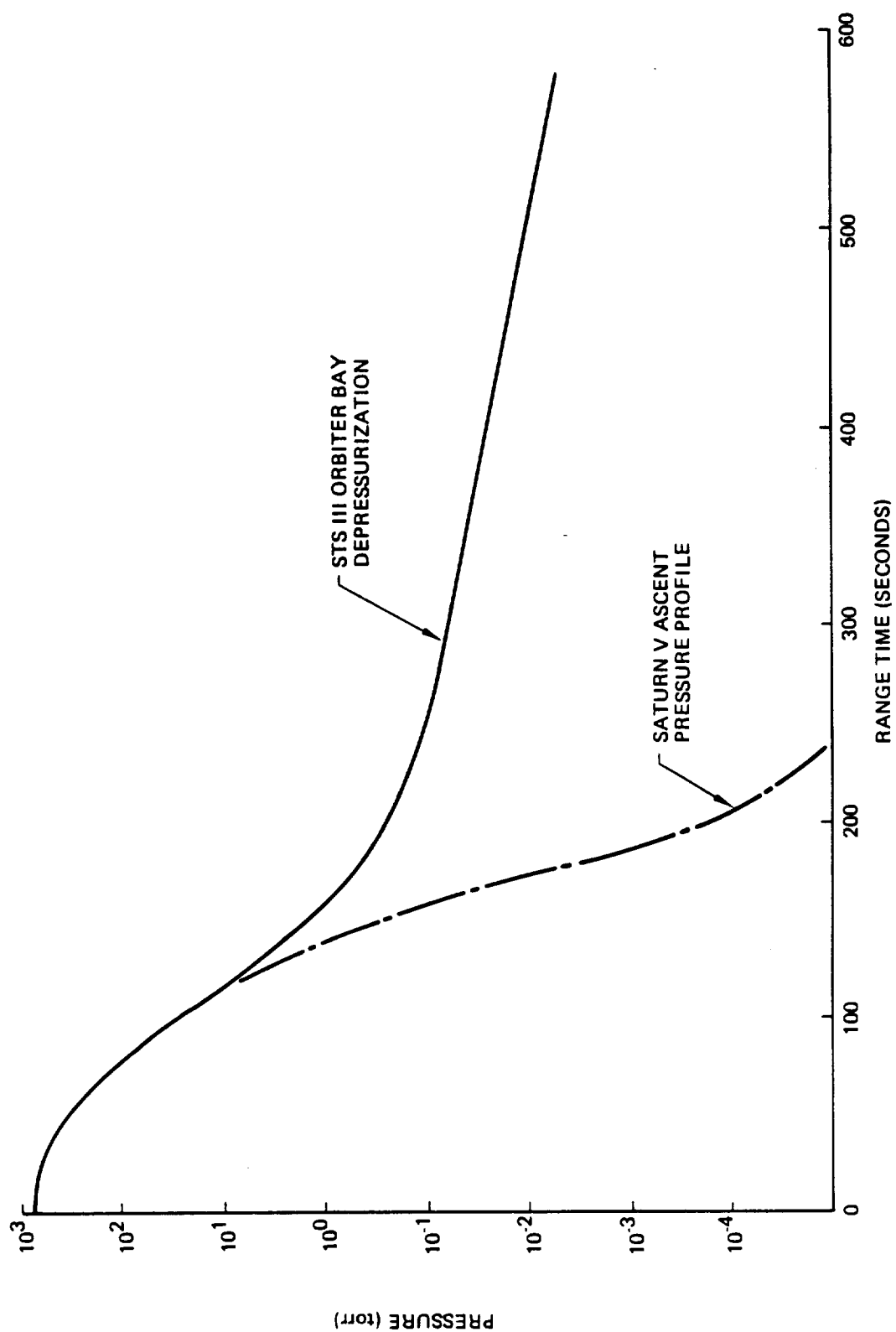


Figure 4-2: Cargo Bay Pressure History

- a. Choked flow through the cargo bay external surfaces, and/or
- b. Trapping of residual purge gas within the Orbiter bay cavities.

At the onset of the transition gas dynamic regime (a Knudsen number of 10 was used to define this point) the natural-convection model was replaced by a rarified gas heat-transport model. Knudsen number is defined as the ratio of gas molecular mean free path to characteristic distance (the distance between the LTPS body shell and Orbiter cargo bay, for example). Convection coupling through the slip-flow, transition, and free-molecular flow regimes continued until the gas pressure reached a level of  $10^{-5}$  torr, at approximately 25 minutes after launch. The amount of time required for the Orbiter bay pressure to reach  $10^{-5}$  torr was estimated by extrapolating the ascent depressurization curve in Figure 4-2. References 9 and 10 may be consulted for further information concerning rarified gas thermal transport. For the remainder of the mission, only the radiation heat transfer mode connected the external surfaces of the LTPS with the environment.

After the Orbiter cargo doors are opened at LEO, radiant energy transfer between the LTPS and its environment changes continually. Figures 4-3, 4-4, and 4-5 depict the geometric models that were used in the RADSIM computer program to determine the radiation interchange factors. Environmental thermal loads on the LTPS external surfaces were calculated with the thermal code OPERA (Appendix A provides a short description of both RADSIM and OPERA). The effects of LSS shadowing and reflection were taken into account. The LSS antenna disk was made of gold-plated molybdenum wire mesh. Depending on the mission phase, OPERA defined direct and reflected radiative thermal loads due to solar and earth energy sources. Environmental thermal loads were calculated for a number of orbit positions to account for the effect of earth shadowing and a changing LTPS/LSS orientation with respect to the sun and earth.

RADSIM and OPERA were used to define thermal environments and radiation interchange factors during LTPS/LSS deployment and checkout, LEO to GEO transfer, and LTPS removal to disposal orbit.

#### **4.1.2 LTPS Thermal Models**

Thermal Math Models (TMMs) for the tandem ellipsoidal tank and the ellipsoidal hydrogen/toroidal oxygen tank baseline LTPS conceptual designs were developed. The previously described thermal environment heat fluxes were included in them. The resulting thermal networks were solved by the NASA-standard code SINDA.

##### **4.1.2.1 Thermal Model Description**

Figure 4-6 depicts the TMM that was developed for the tandem-ellipsoidal tank LTPS baseline design. The thermal model for the ellipsoidal/toroidal tank LTPS is shown in Figure 4-7.

The axi-symmetric LTPS cylindrical shape permitted the use of a two-dimensional geometry for the TMM thermal network. Layouts of thermal model network nodes are shown in Figures 4-6 and 4-7 along with important LTPS features. Three-dimensional radiation interchange between the LTPS and its environment was determined with RADSIM and OPERA. Circumferential variations in radiation interchange factors were then area-totaled for each external surface node. For radiation interchange with the Orbiter and payload, this procedure consisted of multiplying the interchange factors between all LTPS surface nodes and each Orbiter or payload surface node by the appropriate LTPS surface node area and summing the products. In the case of solar, earth

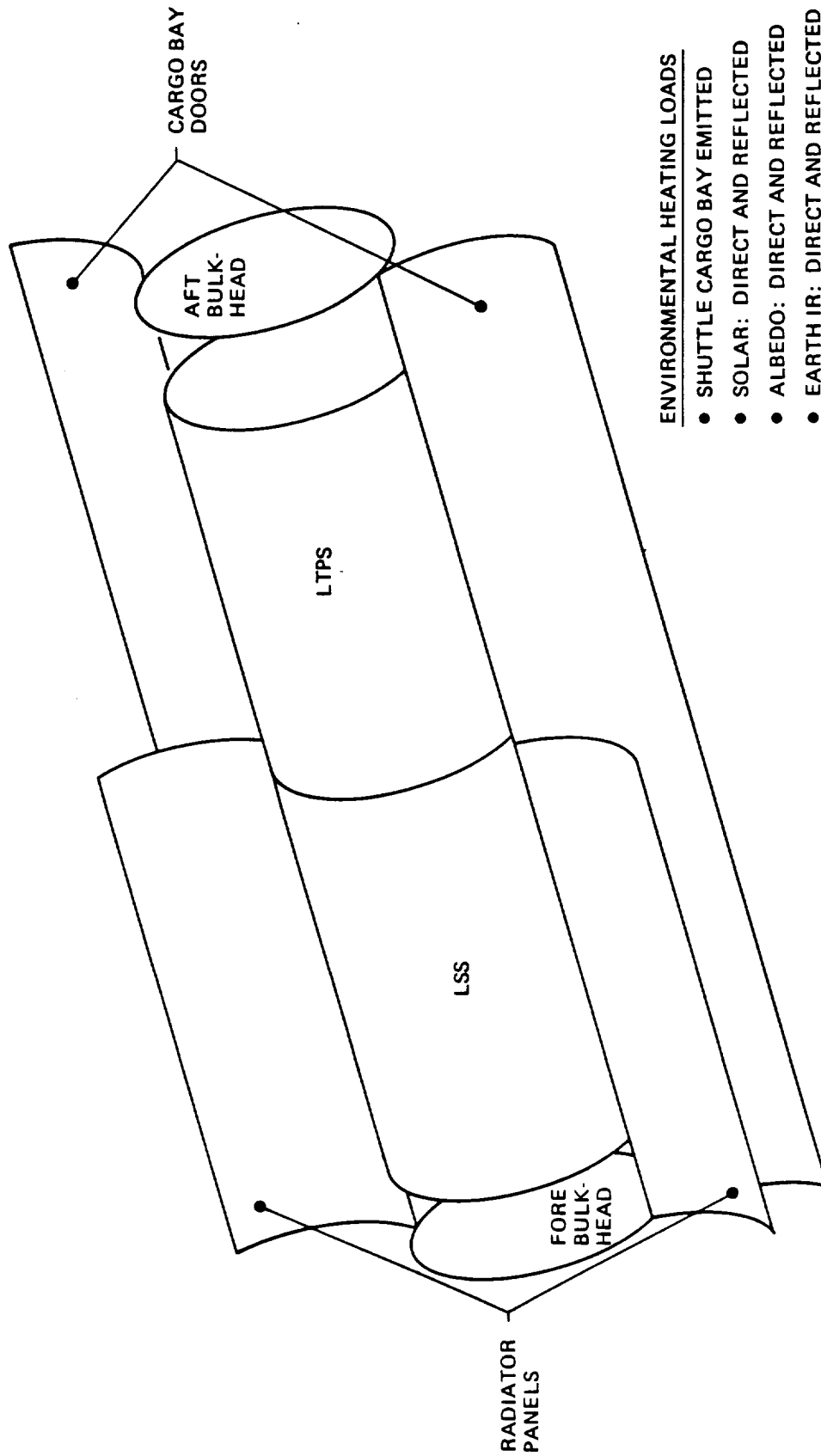


*Figure 4-3: Geometric Model of Orbiter Cargo Bay and Stowed LSS/LTPS Used for Radiation Heat Transfer Analysis*

# ENVIRONMENTAL HEATING LOADS

- SHUTTLE CARGO BAY EMITTED
- SOLAR: DIRECT AND REFLECTED
- ALBEDO: DIRECT AND REFLECTED
- EARTH IR: DIRECT AND REFLECTED

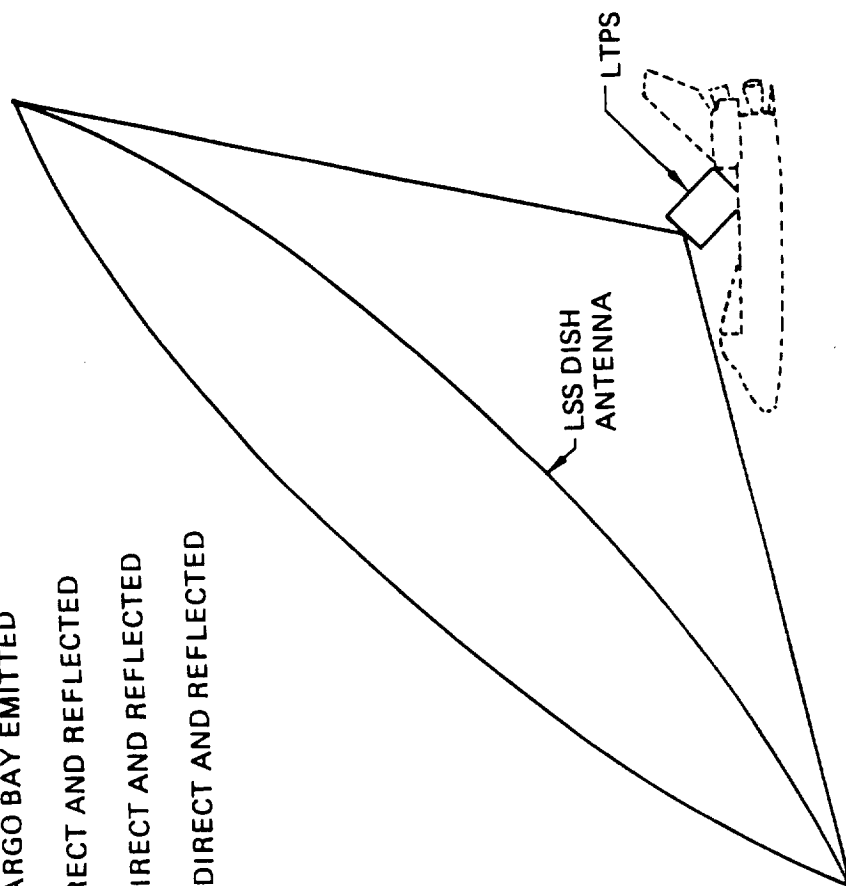
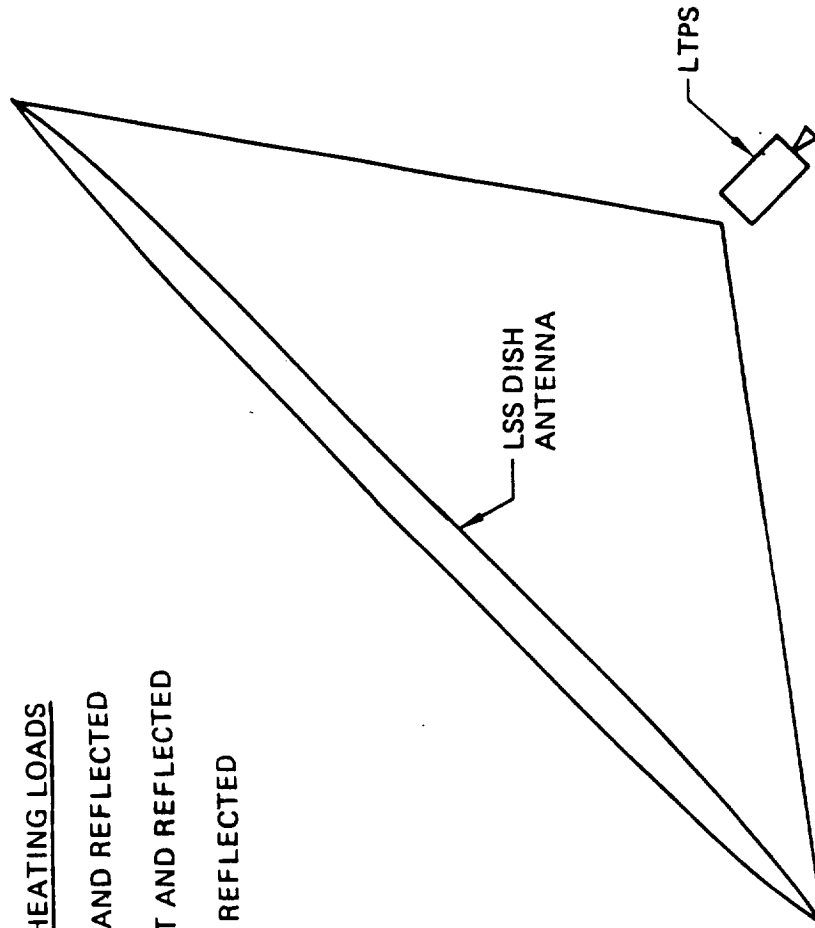


Figure 4-4: Geometric Model of LSS/L TPS Erected in Orbiter Cargo Bay

ENVIRONMENTAL HEATING LOADS

- SOLAR: DIRECT AND REFLECTED
- ALBEDO: DIRECT AND REFLECTED
- IR: DIRECT AND REFLECTED



*Figure 4-5: Geometric Model of LSS/L TPS in Free Flight*

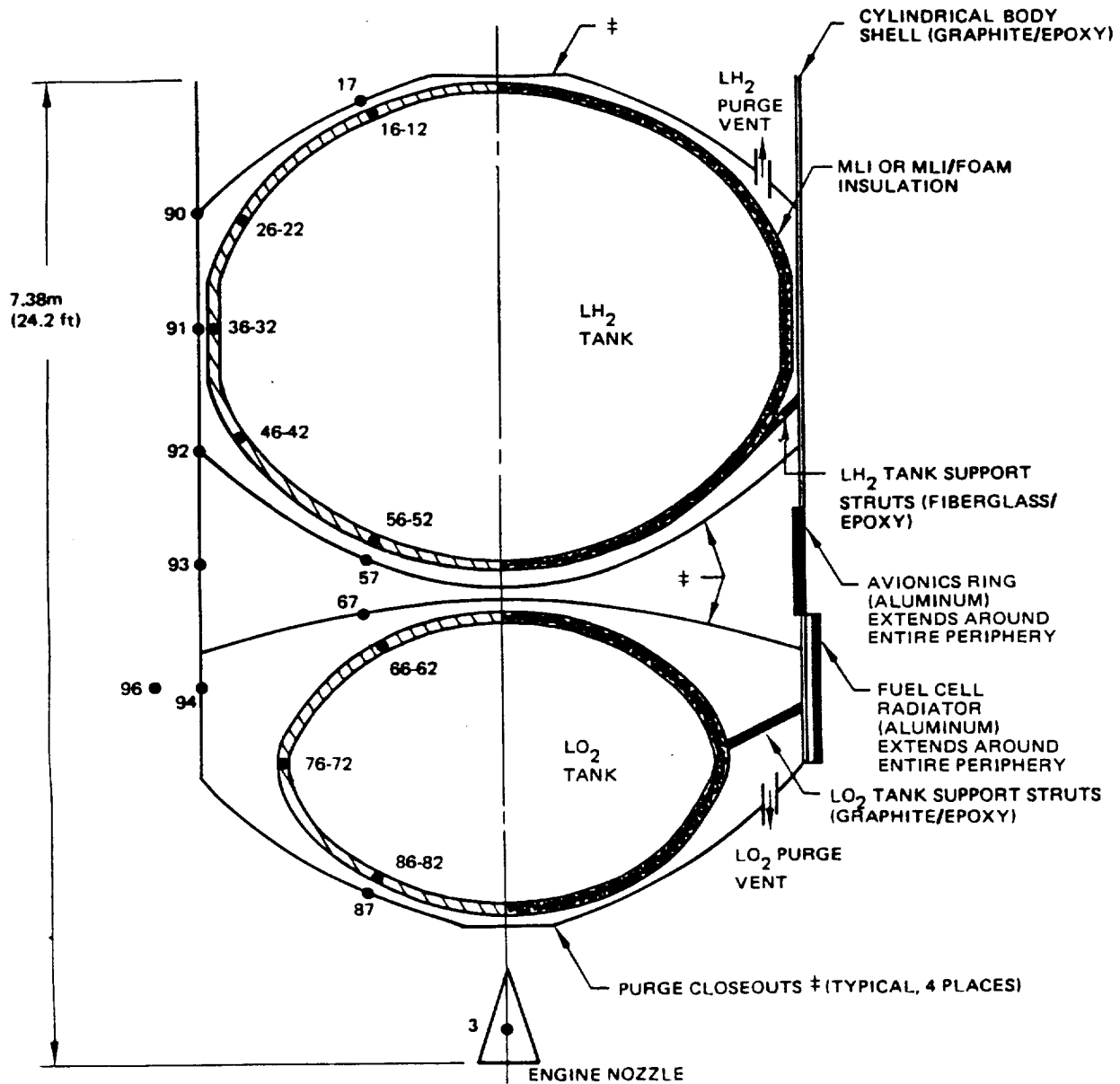


Figure 4-6: Nodal Map of Thermal Model for 56 Kg/m<sup>3</sup> (3.5 lbm/ft<sup>3</sup>) Payload Density LTPS

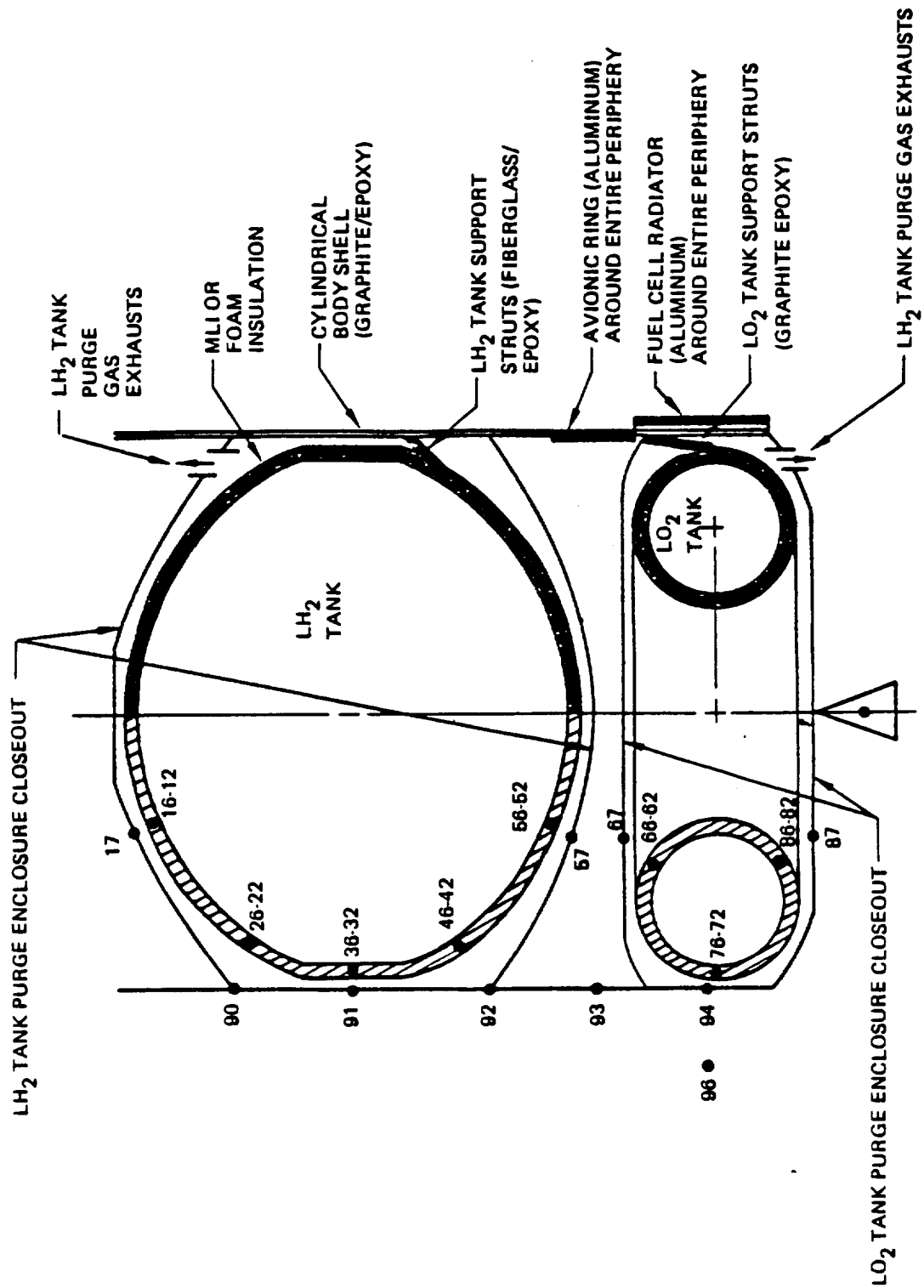


Figure 4-7: Nodal Map of Thermal Model for  $40 \text{ Kg/m}^3$  ( $2.5 \text{ lb}_m/\text{ft}^3$ ) and  $24 \text{ Kg/m}^3$  ( $1.5 \text{ lb}_m/\text{ft}^3$ ) Payload Density

IR and albedo heat flux, the procedure consisted of multiplying the particular flux (e.g. solar) predicted for each LTPS surface node by its proper area and summing the products to arrive at the total solar radiative flux on a particular segment of body shell.

Several heat sources in addition to the environmental thermal loads were included in the TMM. These heat sources were:

- a. Radiation from the engine nozzle to the aft closeout thermal insulation blanket covering the base of the LTPS.
- b. Thermal soak from the fuel cell radiator to the LTPS body shell.
- c. Electrical dissipation by equipment in the avionics bay located between the fuel and oxidizer tanks.

A brief discussion of each heat source is presented in the following paragraphs.

During orbit transfer, the engine operates for approximately 3000 to 3700 sec for each perigee burn. Radiation from the hot engine nozzle is incident on the thermal insulation blanket covering the base of the LTPS. Some of the thermal energy is absorbed by the blanket and is reradiated to the outer surface of the LO<sub>2</sub> tank insulation. In the thermal model, the engine nozzle was treated as a blackbody emitter at a temperature of 1110°K. The radiation interchange factor between the nozzle and closeout insulation blanket was calculated by RADSIM. Thermal coupling between the nozzle and aft closeout was represented by a radiation conductor in the thermal math model.

Thermal soak from the fuel cell radiator to the LTPS body shell was assumed to occur through the MLI blanket located between the radiator and body shell, and through the insulating standoffs that served as structural mounts for the radiator. The fuel cell radiator was sized to reject 1958W of waste heat during orbit transfer. It was 20.47 cm wide and extended circumferentially around the vehicle exterior. In the thermal model the radiator was thermally coupled to the vehicle exterior nodes by conduction paths representing the insulating standoffs and by radiation and conduction paths representing the MLI blanket.

Electrical power dissipation by equipment in the avionics bay was assumed to be 756W. This value was based on the OTV avionics power levels described in Reference 1. The electrical dissipation was assumed to be uniformly distributed around the inner circumference of the avionics ring which formed a segment of the vehicle body shell. As shown in Figures 4-6 and 4-7, this ring is a cylindrical aluminum shell located between the fuel and oxidizer tanks. Most of the avionics equipment is mounted directly to the avionics ring. The avionics electrical dissipation was treated as a heat source to node 93 which represented the entire ring.

The LTPS external surfaces consist of the body shell, the fore and aft purge closeouts, the fuel cell radiator and an avionics ring located between the fore and aft body shell sections. The body shell is composed of a Nomex core sandwiched between two graphite-epoxy face sheets. The internal and external face sheets are thermally connected by conduction and radiation through the Nomex core. Resistance to heat flow through the body shell core was conservatively assumed to be negligible in the thermal models, and



the two face sheets were therefore at the same temperature. The mass-averaged capacitance of the body shell was estimated at  $0.96 \text{ J/g-}^{\circ}\text{K}$ . Due to differences in layup, the fore and aft body-shell sections had a mass per unit length of 39.2 and 50.8 kg/m, respectively. Consequently, the thermal capacitance of the body shell per unit length differed between the fore and aft section.

The TMM also included a node for the 58.1 kg aluminum avionics ring. Conduction through the fore and aft purge volume closeouts was assumed to be infinite. Closeouts were 4 mil aluminized Kapton sandwiched between scrim net for reinforcement. Due to the thin gage of material used in the closeouts, and the relatively low heat flux levels through them, the assumption of infinite conduction was reasonable. Heat capacitance of the closeouts was assumed to be negligible.

Vehicle external surfaces, including the body shell, avionics ring and purge enclosure closeouts, were thermally connected to the propellant tanks in the LTPS thermal model networks. Three heat transfer nodes between tanks and external surfaces were included in the models. These nodes were conduction, convection and radiation.

The structural support system was the principal conduction heat flow path between the body shell and the tanks. The support system was a bipod strut truss based on the OTV tank support design described in Reference 1.  $\text{LH}_2$  tank support struts were constructed of fiberglass epoxy and the  $\text{LO}_2$  tank support struts were graphite epoxy. Table 3-8 summarizes the physical and thermal characteristics of the tank support struts.

Radiative interchange factors between the tank MLI outer surfaces and the interior surfaces of the body shell, avionics ring and purge closeouts were calculated with the RADSIM program. Radiative properties of the LTPS internal surfaces are summarized in Table 4-2. The predicted radiation interchange factors were used to calculate radiation coupling between the propellant tank MLI blankets and the internal surfaces of the vehicle body shell and purge closeouts.

In addition to conductive and radiative coupling, the LTPS thermal math models also included connective heat transfer between the tank insulation and interior surfaces of the vehicle body shell and purge closeouts. Convective heat transfer occurs during ground hold operation, after chilldown and fill of the tank, and continues until the purge enclosure is evacuated during Orbiter ascent.

Two modes of convective heat transfer were modeled. The first was natural convection. This mode would occur if gas velocities in the purge volume were very small. In order to calculate the natural convection conductances between purge volume surface nodes, the characteristic nodal surface area-to-length ratios were first calculated for each nodal pair. Then the effective convective conductance between surface nodes was calculated by multiplying the characteristic area to length ratio by the purge gas conductivity and the free-convection Nusselt number. The Nusselt numbers were determined by standard Rayleigh number correlations for enclosed gas volumes. The particular correlation used for each nodal pair was selected on the basis of geometric similarity with the portion of the vehicle purge volume under consideration. Free-convection conductances were dependent on the temperature difference between enclosure surfaces. Under laminar flow conditions, the conductance was proportional to the temperature difference raised to the  $1/4$  power. For turbulent conditions the conductance was proportional to the temperature difference raised to the  $1/3$  power.

	Material	$\epsilon_{IR}$
Purge Closeouts	DAK <sup>1</sup>	0.03
Body Shell	Graphite	0.90
Avionics Ring	Aluminum	1.00 <sup>2</sup>
MLI	DAK	0.03

1 Double aluminized Kapton

2 Blackbody properties were conservatively assumed because of cavities between adjacent avionics ring equipment.

*Table 4-2: Radiative Properties of LTPS Internal Surfaces*

Gas pressure in the purge volume during ascent was assumed to follow the Orbiter III cargo bay pressure cargo bay pressure profile shown in Figure 4-2. Variation of effective gas conductance with pressure was included in the thermal network model of the purge enclosure. Thermal transport by rarefied gases was modeled by the methods described in References 9 and 10.

Figure 4-8 shows the typical one-dimensional (4-node) network used to predict insulation thermal performance. The foam thermal resistance was modeled with two conductors, linked in series, and separated by a centrally located node. The foam capacitance was lumped into this central node. Also shown in Figure 4-8, is the thermal network for the MLI. As with the foam network, heat transfer was assumed to be in a direction normal to the propellant tank surface. Thermal energy transport through the MLI was divided into two components: (1) the basic component which included transport through the radiation shields and (2) the degrade component which included transport through seams, purge pins, positioning pins, etc.

A short discussion of each MLI heat transport component follows:

#### Basic MLI

Heat transfer mechanisms through the basic MLI include:

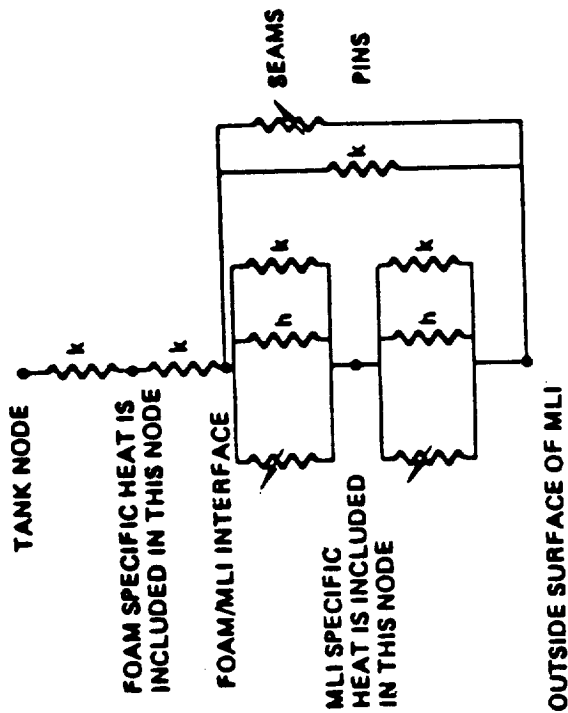
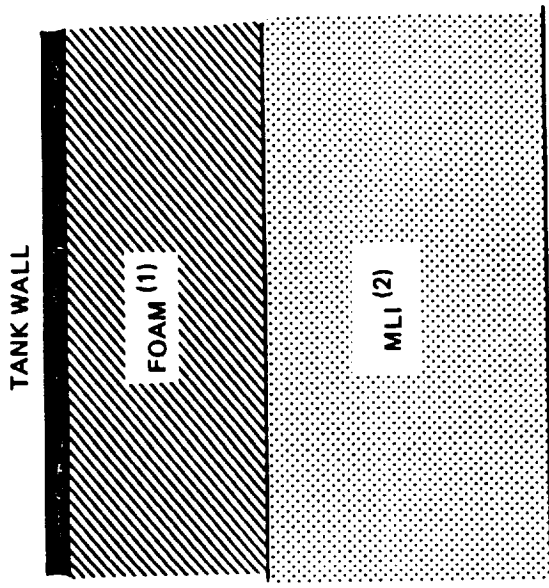
- a. Interlayer radiation between adjacent shields of the MLI blanket,
- b. Solid conduction through the shield spacers, and
- c. Purge gas conduction during the initial mission phases.

The thermal conductance of the thin radiation shields, which had a nominal thickness on the order of 0.0076 mm, was assumed to have a negligible effect on the overall MLI thermal conductance. Furthermore it was assumed that the MLI had a constant thickness throughout the mission, and that MLI billowing during ascent depressurization was minimal.

Reference 11 presents a combined analytical and experimental study that developed prediction models for basic MLI performance. Other experimental investigations (e.g. References 12 and 13) have found good agreement between measurement and Reference 11 predictions. The Reference 11 MLI performance prediction models were developed for double-aluminized Mylar blankets with silk net spacers. However, they were used in this study to evaluate MLI performance for DAK blankets with Dacron net spacers because the thermal conductivity of the radiation shields and spacer has little effect on MLI performance. Figure 4-9 presents the equations used to predict basic MLI thermal performance. A volumetric thermal capacitance of  $36.43 \text{ KJ/m}^3\text{-}^\circ\text{K}$  was assumed for all MLI blankets.

The radiation and solid conduction heat transfer mechanisms were assumed to be present during all mission phases. Purge gas convection within the MLI was treated as a gas conduction problem, and it was assumed that the gas temperature leaving the MLI was the same as that entering the MLI. The MLI pressure decay during launch was assumed to follow the cargo bay pressure history given by Figure 4-2. The interstitial pressure time dependency was investigated to substantiate this assumption.

A comparison of Boeing-predicted blanket depressurization with experimental data was presented in Figure 2-7. The predicted blanket pressure differential, defined as the



NOMENCLATURE:



- (1) TYPE FOAM:
- ROHACELL 31 (BASELINE)
  - BX250A (ALTERNATE)
- (2) MLI:
- DAK (DOUBLE ALUMINIZED KAPTON)
  - DACRON NET SPACERS
  - 24 SHIELDS/cm (61 SHIELDS/in.)

Figure 4-8: Insulation Thermal Model Details

Basic MLI: Double aluminized Kapton with net spacers

$$\dot{q}''_{\text{MLI}} = \dot{q}''_{\text{MLI, solid conduction}} + \dot{q}''_{\text{MLI, radiation}} + \dot{q}''_{\text{MLI, gas}}$$

$$\dot{q}'' \left( \frac{\text{W}}{\text{m}^2} \right) = C_s \frac{\bar{N} 2.56 \left( \frac{T_{\text{Hot}} + T_{\text{Cold}}}{2} \right) \left( T_{\text{Hot}} - T_{\text{Cold}} \right)}{N_s} + \frac{C_r \epsilon \text{TR} \left( \frac{4.67}{T_{\text{Hot}}} - \frac{4.67}{T_{\text{Cold}}} \right)}{N_s \cdot 1} + K_{\text{gas}} \frac{(T_{\text{Hot}} - T_{\text{Cold}})}{\delta_{\text{MLI}}}$$

Degraded MLI: (References 13, 14, 15, & 16)

$$\dot{q}''_{\text{MLI, degraded}} = \dot{q}''_{\text{pins}} + \dot{q}''_{\text{seams}}$$

$$\dot{q}'' \left( \frac{\text{W}}{\text{m}^2} \right) = K_{\text{pins}} \left( \frac{T_{\text{Hot}} - T_{\text{Cold}}}{\delta_{\text{MLI}}} \right) + 0.63 \times 10^{-4} \left( T_{\text{Hot}}^4 - T_{\text{Cold}}^4 \right)$$

$\bar{N}$  : no. of layers/cm

$N_s$  : no. of layers

$\delta_{\text{MLI}}$  : MLI thickness (m)

Temperature in Kelvin

$K_{\text{gas}}$  : purge gas effective thermal conductivity (W/m · K)

$$C_s = 8.95 \times 10^{-8}$$

$$C_r = 5.39 \times 10^{-10}$$

$$\epsilon \text{TR} = 0.031$$

$$\sigma = 5.7 \times 10^{-8} \text{ W/m}^2 \cdot \text{K}^4$$

$$K_{\text{pins}} = 1.5 \times 10^{-5} \text{ W/m} \cdot \text{K}$$

Figure 4-9: Equations Used to Predict MLI Heat Leak

difference between the MLI boundary pressure and the maximum interstitial pressure, was in good agreement with the data. The pressure decay model used to predict the Figure 2-7 MLI venting characteristics was modified to include Orbiter bay depressurization history, as given by Reference 5. The subsequent predicted interstitial pressure decay was found to closely match the assumed boundary pressure, as shown in Figure 4-10. Consequently, it was decided to use the Orbiter III depressurization history for the MLI interstitial pressure decay in calculating the gas conductance component of the MLI overall thermal performance. A uniform pressure throughout the blanket was assumed.

Interstitial gas heat transfer during the launch phase of the mission was predicted with information given in Reference 12. Figure 2-6 shows that heat transfer by rarified gases becomes negligible at pressures on the order of  $10^{-5}$  torr. This pressure level would be reached at approximately 25 minutes after launch based on extrapolation of available Orbiter III flight data (see Figure 4-2).

The foregoing discussion has tacitly assumed that the MLI has been suitably preconditioned so that water vapor outgassing is unimportant. Although outgassing effects may last for days, it was outside this study's scope to evaluate the trade of MLI blanket preconditioning versus outgassing effects.

### Degraded MLI

Degraded MLI performance results from installation of the blankets on the propellant tanks. Seams between adjacent blanket panels allow thermal radiation to pass through the MLI system. Additional degradation is caused by positioning and purge pins that provide a conduction path which short-circuits the MLI insulation. Prediction of the thermal load caused by MLI seams and pins is very dependent on the type of installation procedures used. In this study, the radiation thermal load due to seams was based on the experimental information for a small-scale test tank described in Reference 13. Since the small tank described in Reference 13 had more seams per unit tank surface area than the larger LTPS-type tanks, the seam thermal loads predicted in this study are therefore conservatively high. Pin conduction was approximated from information found in References 13, 14, 15, and 16. Figure 4-9 summarizes the equations used to predict degraded MLI performance.

#### **4.1.2.2 Typical Thermal Math Model Results**

Figure 4-11 shows typical post-launch heat flux predictions for helium-purged MLI insulated LH<sub>2</sub> and LO<sub>2</sub> tanks. Prior to launch, assuming natural convection within the helium purge enclosure, the insulation heat fluxes were approximately 440 W/m<sup>2</sup> (140 Btu/hr-ft<sup>2</sup>) for the hydrogen tank and 285 W/m<sup>2</sup> (90 Btu/hr-ft<sup>2</sup>) for the ellipsoidal oxygen tank. Actual experience (Reference 13) with helium-purged MLI systems indicates the prelaunch fluxes may be as high as approximately 780 to 620 W/m<sup>2</sup> for the LH<sub>2</sub> and LO<sub>2</sub> tanks respectively. The larger observed fluxes may be due to greater convective heat transfer coupling in the purge enclosure. Analyses have indicated that the ground-hold heat flux would be approximately doubled by assuming enhanced (forced) convection rather than natural-convection in the purge enclosures. Hence, if the test insulation were subjected to an enhanced convection environment, heat fluxes would be about 880 W/m<sup>2</sup> and 700 W/m<sup>2</sup> for LH<sub>2</sub> and LO<sub>2</sub> tanks, respectively, rather than 440 W/m<sup>2</sup> and 285 W/m<sup>2</sup> as predicted for natural convection.

As can be seen in Figure 4-11, the heat leak rapidly decreased by more than two orders of magnitude as the MLI evacuated following lift-off. Before the Orbiter bay doors opened at LEO, the initial heating trend shown for both tanks was caused by aerodynamic heating

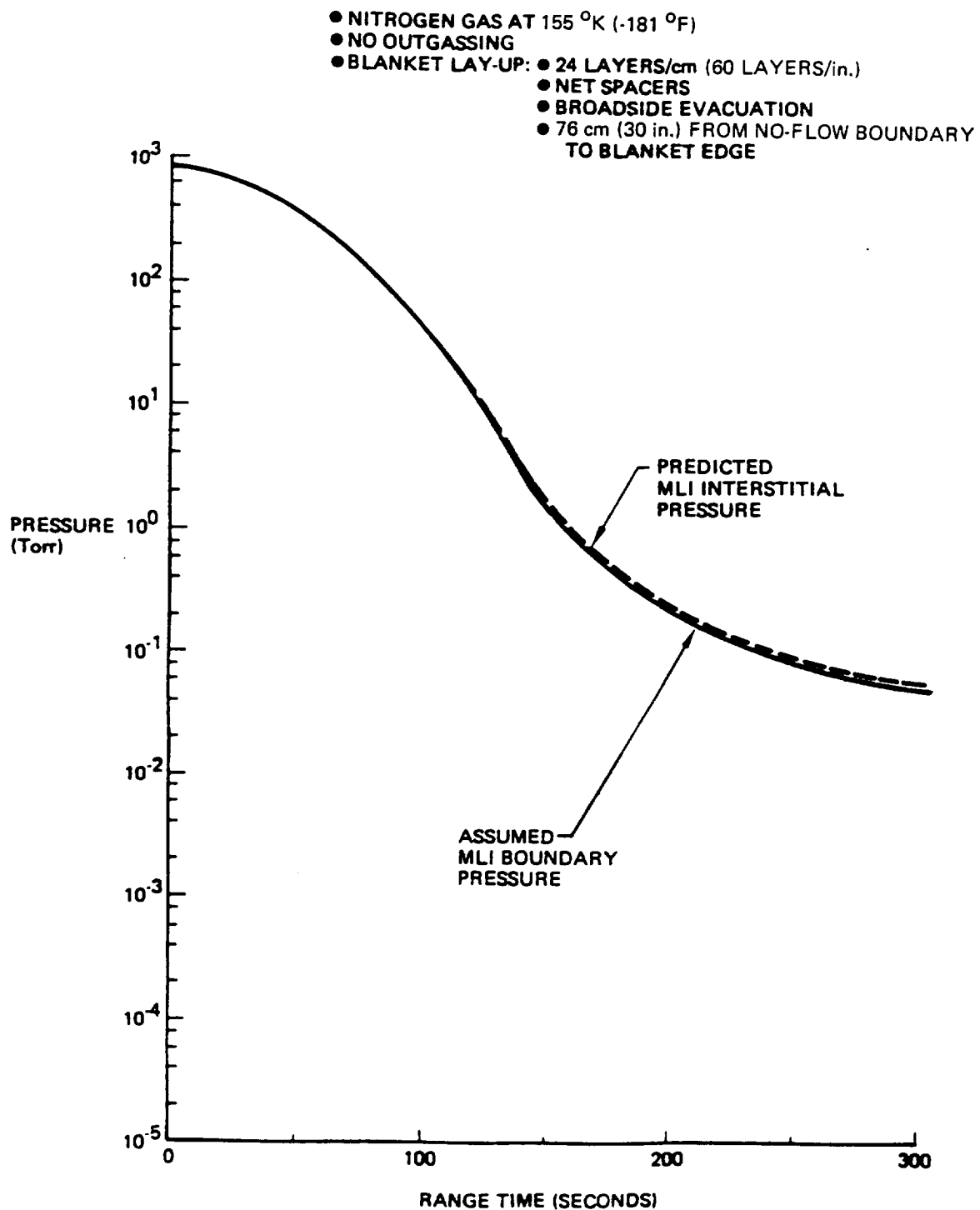


Figure 4-10: Comparison of Predicted MLI Interstitial Pressure with the Assumed External Boundary (Orbiter Cargo Bay) Pressure History as a Function of Time After Launch

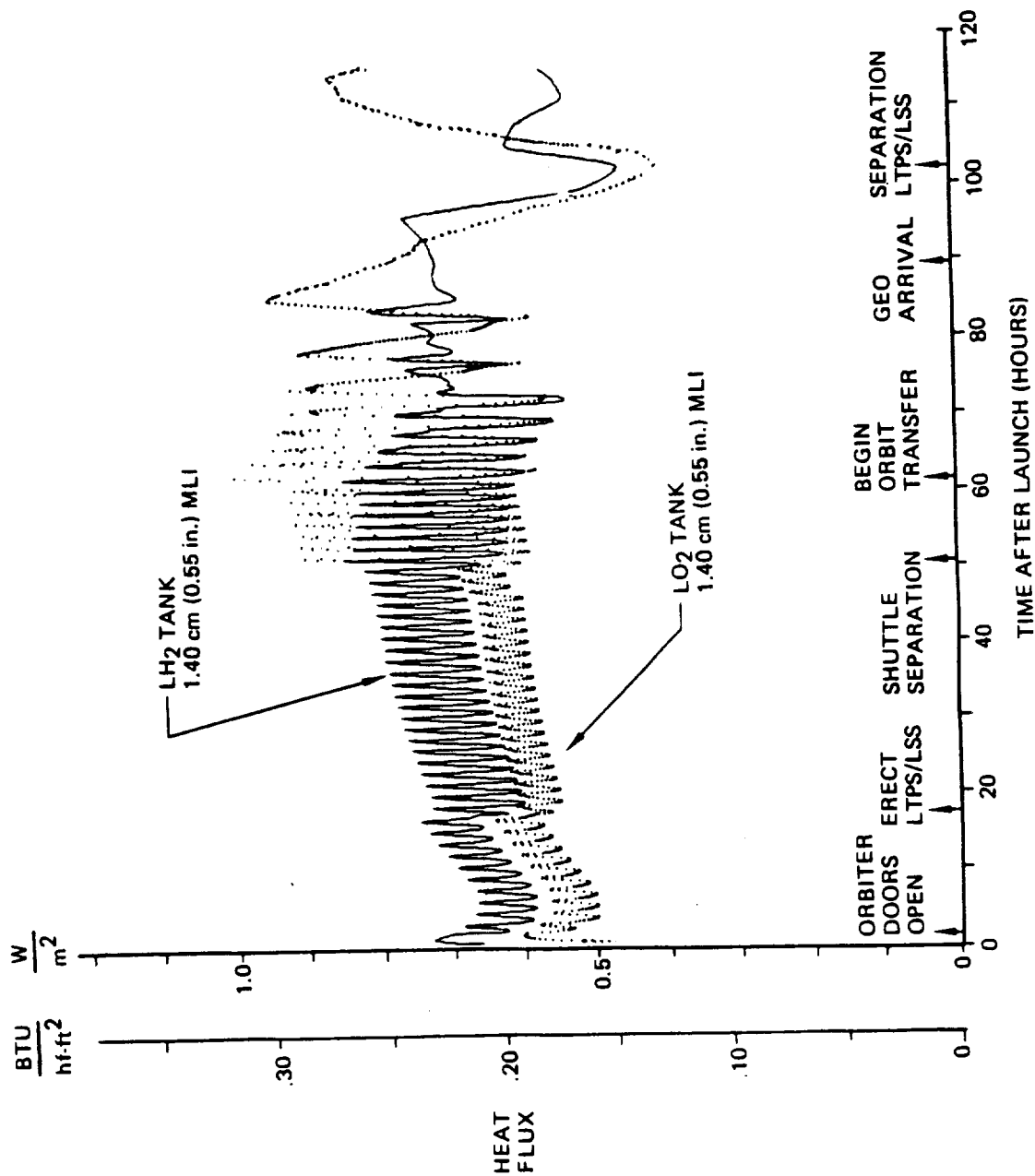


Figure 4-11: Predicted Heat Leak for a He-Purged MLI System with a Natural Convection Ground-Hold Environment



during launch. As the Orbiter bay cooled after leaving the earth's atmosphere, this trend was reversed. Further cooling occurred after the bay doors were opened at 100 minutes after launch. Figure 4-12 shows the heat flux history for the LH<sub>2</sub> and LO<sub>2</sub> tank insulations on an expanded time scale for the first 20 hours of the mission.

After the bay doors were opened, cyclic thermal loads occurred because of earth shadowing and a changing vehicle orientation with respect to environmental heat sources. Moreover, the average insulation heat flux is shown to increase between consecutive orbit periods. This slow increase can be attributed to increasing body shell temperatures due to environmental heating from earth albedo and earth IR. The poor thermal connection between the MLI and the Orbiter bay environment caused insulation heat fluxes to rise slowly.

The LTPS and LSS were erected from the cargo bay at 17 hours following lift-off. This event caused the LTPS external surfaces to cool due to the increased radiation view-factor to deep space. A corresponding decrease in the insulation heat flux was predicted, and the MLI heating rate was also reduced. Since the LTPS exposure to the environment was increased from the previous mission phase, the magnitude of the orbital variations became larger. Four hours before LTPS/LSS separation from the shuttle, at 46 hours after launch, the LTPS fuel cells and avionics gear were assumed to be turned on for checkout. An associated increase in heat leak to the oxygen tank resulted from this event.

The LTPS and LSS were deployed from the Orbiter at 50 hours after launch. Further increases in magnitude of the cyclic thermal loads are seen to occur in Figure 4-11. Moreover, the heat flux peaks for the oxygen tank become larger than those for the hydrogen tank. Reasons for this behavior are:

- a. A larger environmental load on the aft section of the LTPS, and
- b. Frontal shadowing of environmental loads on the LH<sub>2</sub> tank by LSS.

LEO to GEO transfer was initiated at 61 hours after launch. Although cyclic heat flux variations continued, the periods became longer as the orbit period increased. Furthermore, the curve shapes between consecutive cycles in Figure 4-11 are seen to be different. These alterations are caused by a changing orbit trajectory.

Figures 4-13 and 4-14 show the typical predicted heat fluxes for MLI/foam insulations. The data in Figure 4-14 is identical to that in Figure 4-13 but the time scale for the first 20 hours has been expanded to show the initial decrease in heat flux as the MLI is evacuated. Due to better ground-hold insulation performance, the initial heat flux is substantially reduced from the MLI-only case. The predicted prelaunch heat fluxes to the hydrogen and ellipsoidal-oxygen tanks were of 75 W/m<sup>2</sup> (23.9 Btu/hr-ft<sup>2</sup>) and 44.0 W/m<sup>2</sup> (14.0 Btu/hr-ft<sup>2</sup>), respectively. The primary difference between the post-launch heat flux histories for MLI only and MLI/foam insulations occurs before LTPS/LSS separation from the shuttle, as seen by comparing Figure 4-11 with Figure 4-13.

In Figure 4-11, which shows predicted tank heat flux for helium-purged MLI insulations, the heat flux increases slowly following the opening of the Orbiter cargo bay doors and continues to increase after LTPS/LSS erection. In Figure 4-13 however, the heat flux for MLI/foam insulated tanks decreases following cargo bay door opening. The principal reason for this difference in heat flux profiles is the difference in vehicle body shell temperatures prior to launch. In the case of helium-purged MLI insulated tanks, the

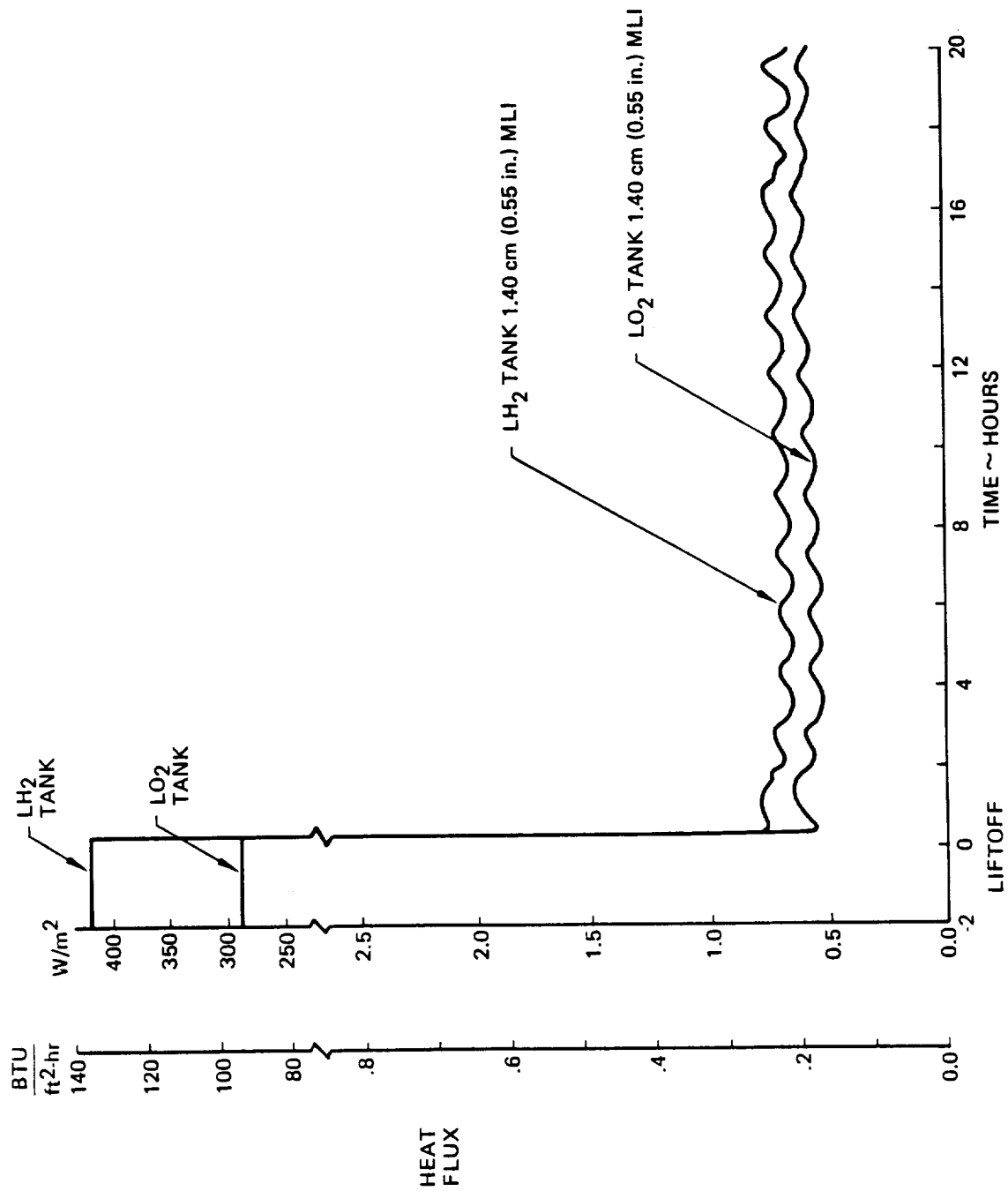


Figure 4-12: Predicted Heat Leak for a He-Purged MLI System With a Natural-Convection Ground-Hold Environment; First 20 Hours of Mission

- MLI/FOAM INSULATION, NATURAL CONVECTION  
GROUND-HOLD ENVIRONMENT

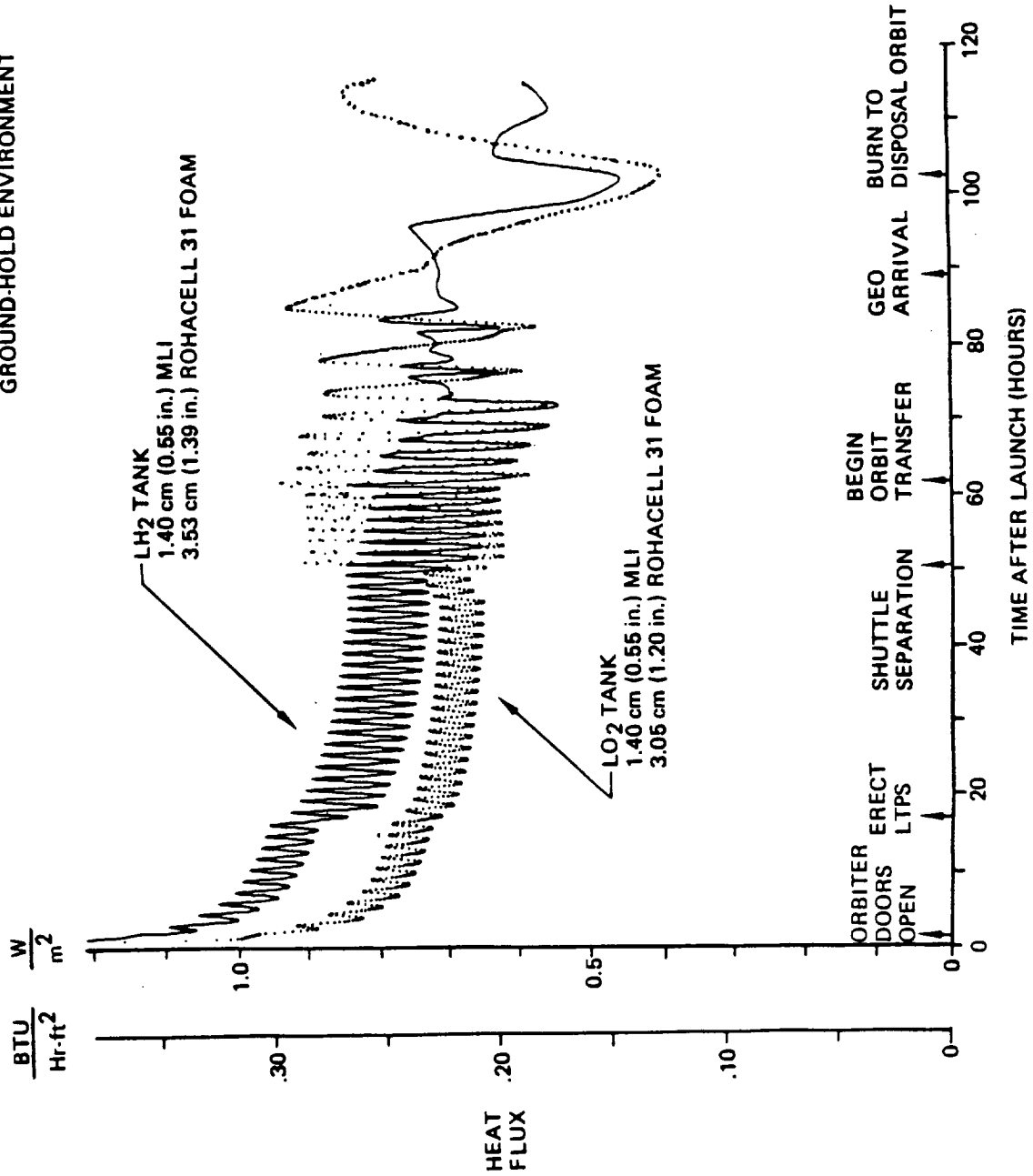


Figure 4-13: Predicted Heat Leak for a  $N_2$ -Purged MLI/Foam System with a Natural-Convection Ground-Hold Environment

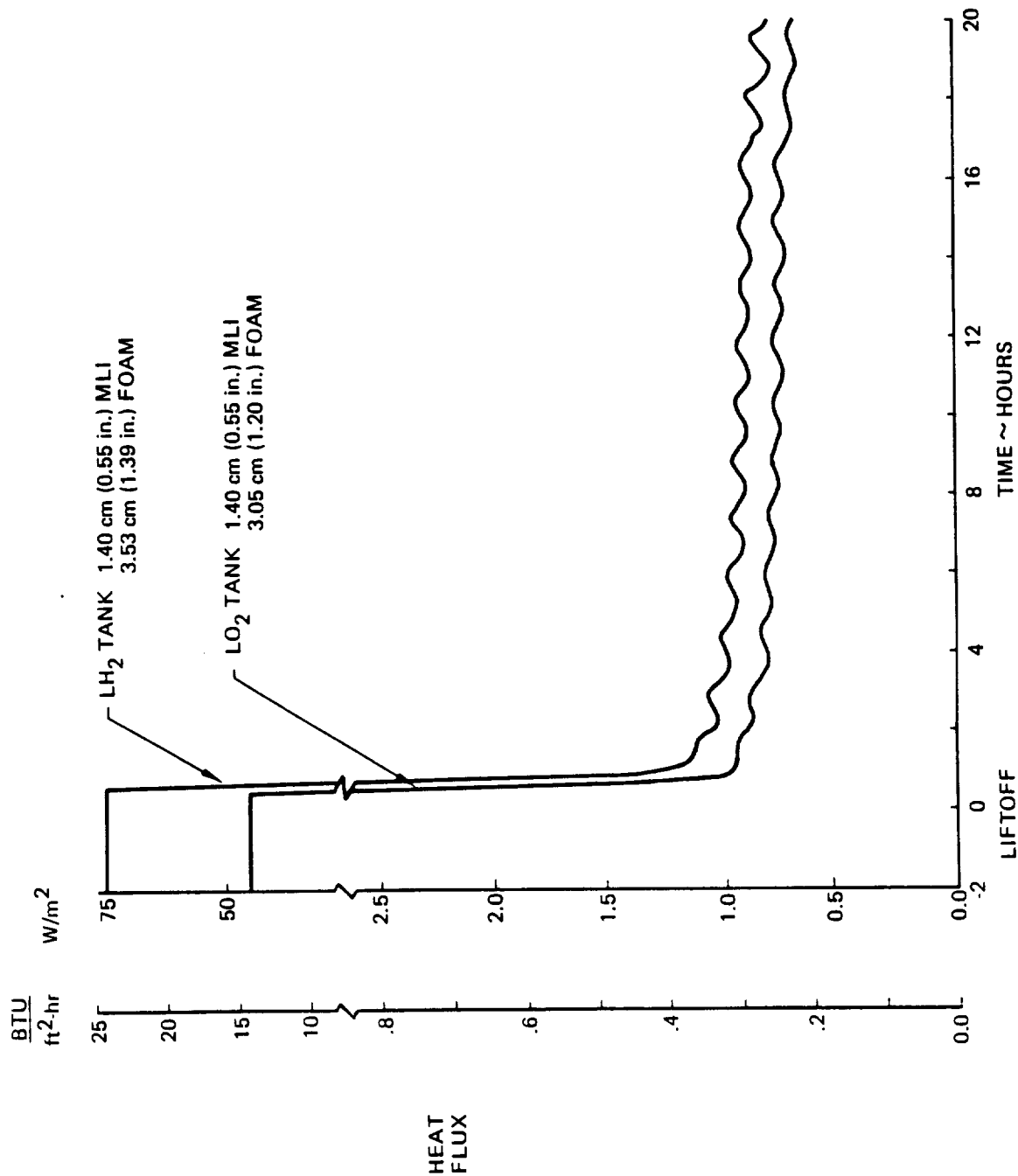


Figure 4-14: Predicted Heat Leak for a N<sub>2</sub>-Purged MLI/Foam System With a Natural-Convection Ground-Hold Environment; First 20-Hours of Mission

overall effective thermal conductance between the cold tank wall and vehicle body shell is relatively high due to the conductivity of helium in the MLI and purge enclosure. Therefore, the body shell temperature during groundhold was lower than its equilibrium temperature in the Orbiter cargo bay with the doors open in low earth orbit. Hence, following launch, the vehicle body shell temperature began to rise causing the purge enclosure environment to warm and consequently heat flux through the tank insulation increased.

In the case of the nitrogen-purged MLI/foam-insulated tanks, the net thermal coupling between vehicle body shell and tanks was considerably less than that of the helium-purged MLI designs. Therefore, the body shell and MLI temperatures were closer to the assumed Orbiter bay background temperature of 297°K during ground-hold. Following launch, the average vehicle body shell temperature, in this case, slowly decreases toward the equilibrium value for the open-door Orbiter bay environment. Hence the LTPS purge volume cools and heat flux through insulation slowly drops off.

Since the fore and aft purge volume close-outs were assumed to have no thermal mass, they respond instantaneously to environmental changes. This response causes the one orbit period fluctuations superimposed on the long time-constant changes in insulation heat fluxes shown in Figures 4-11 and 4-13.

Predicted tank MLI outer surface temperatures are presented in Figures 4-15 through 4-18 for the LTPS mission. This data is from the computer analysis that generated the heat flux histories in Figures 4-11 through 4-14.

Figures 4-15 and 4-16 show the He-purged MLI outer layer temperatures for the LH<sub>2</sub> and LO<sub>2</sub> tanks under a natural-convection ground-hold environment. During prelaunch conditions, the MLI outer layer temperature stabilized at about 200°K for both tanks. In contrast, referring to Figures 4-17 and 4-18, the MLI outer layer temperature for N<sub>2</sub>-purged MLI/foam insulation is about 256°K for both tanks.

During launch the effect of ascent heating on the Orbiter cargo bay caused MLI surface temperatures to rise. When the cargo bay doors opened at about 100 minutes the temperature dropped. Cyclic variations in temperatures are due to variations in the orbital thermal environment. As the LTPS reached geosynchronous altitudes, the frequency of these variations can be seen to decrease. The drop in temperatures at about 100 hours were caused by orientation of the LTPS away from the sun during maneuvers prior to burn to disposal orbit.

#### **4.1.2.3 Enhanced-Convection Thermal Modeling**

Thermal modeling of forced, or enhanced, convection in the LTPS purge enclosure was based on the assumption that the warm purge gas held the MLI outer surface temperature at 294°K. This enabled a closed-form prediction of propellant thermal loads during ground-hold to be obtained. The thermal math models were used to estimate insulation performance during the transition from ground-hold to on-orbit conditions, and for orbit transfer. A qualitative description of the approach which was used is given in the following discussion.

Insulation heat flux prior to launch was determined by dividing the temperature difference across the insulation (274°K for the hydrogen tank and 200°K for the oxygen tank) by the sum of the foam and MLI thermal resistances. Resistance is defined by the thickness divided by the temperature-averaged thermal conductivity. Prelaunch heat fluxes were

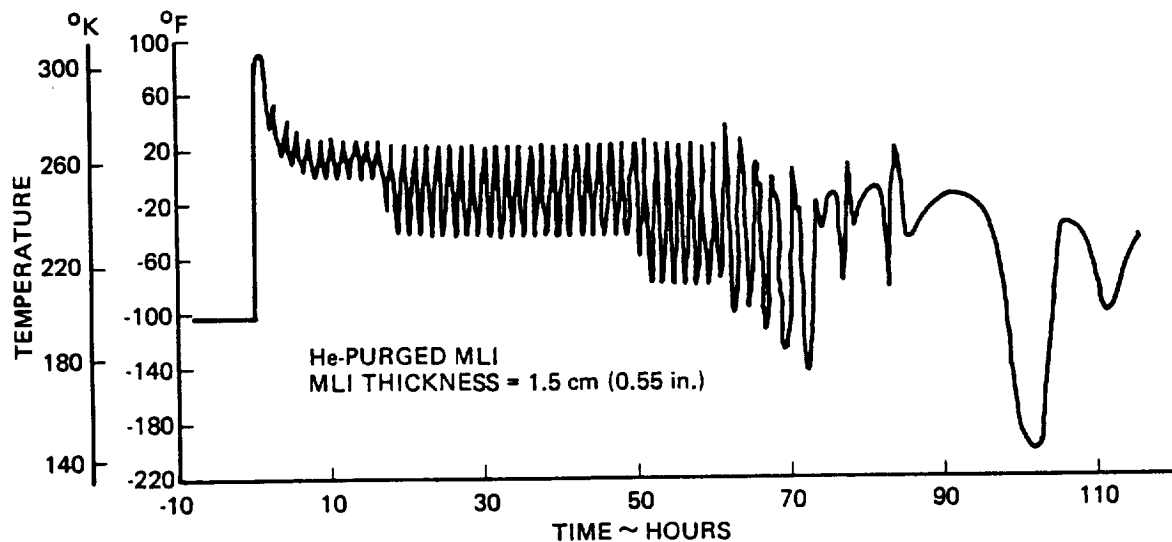


Figure 4-15: Typical LH<sub>2</sub> Tank MLI Outer Layer Temperature History Natural-Convection Ground-Hold Environment, He-Purged MLI

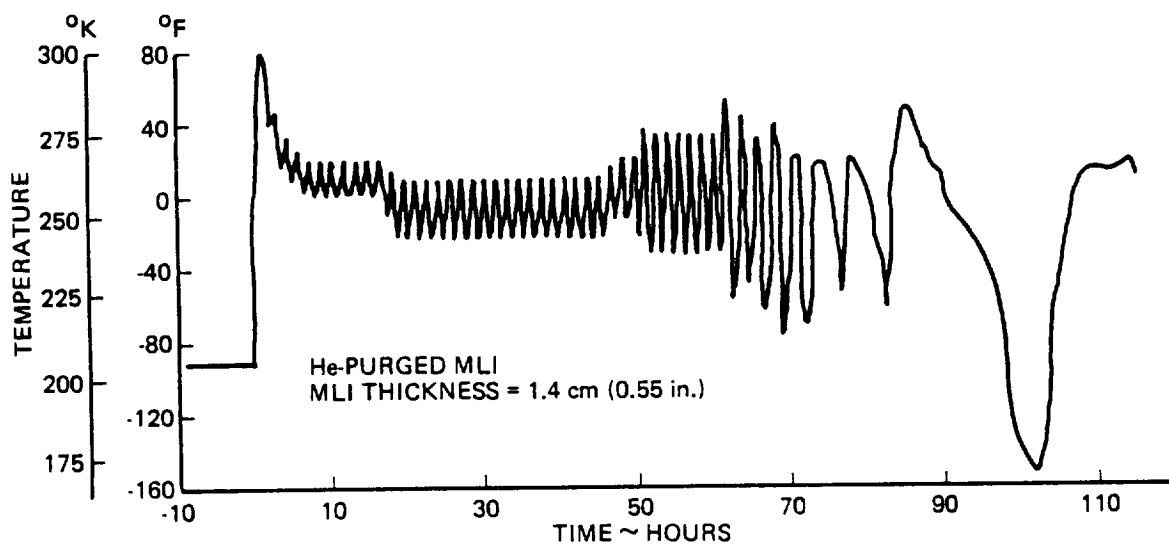


Figure 4-16: Typical LO<sub>2</sub> Tank MLI Outer Layer Temperature History, Natural-Convection Ground-Hold Environment, He-Purged MLI

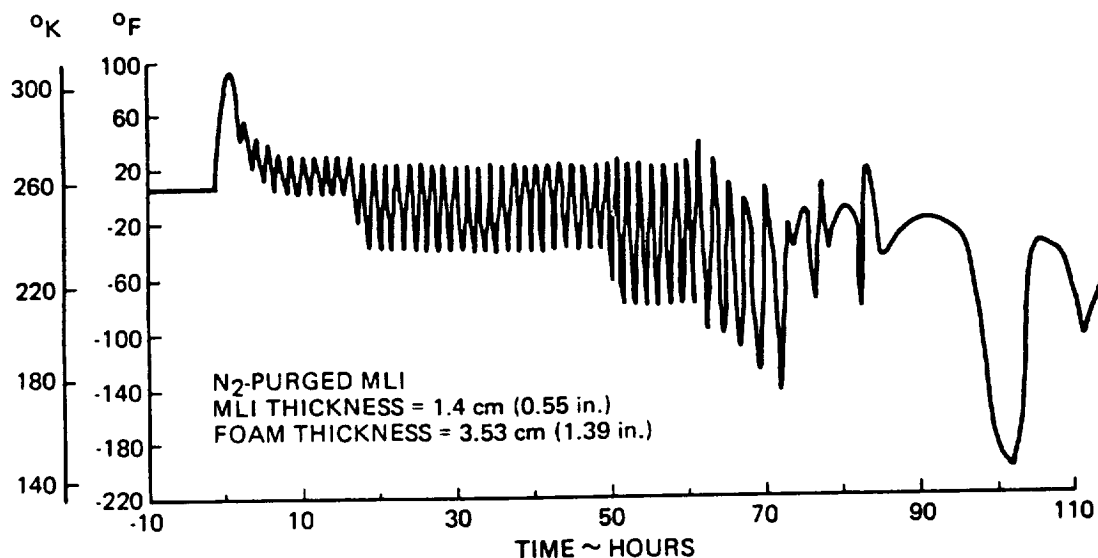


Figure 4-17: Typical LH<sub>2</sub> MLI Outer Layer Temperature History, Natural-Convection Ground-Hold Environment, N<sub>2</sub>-Purged MLI/Foam

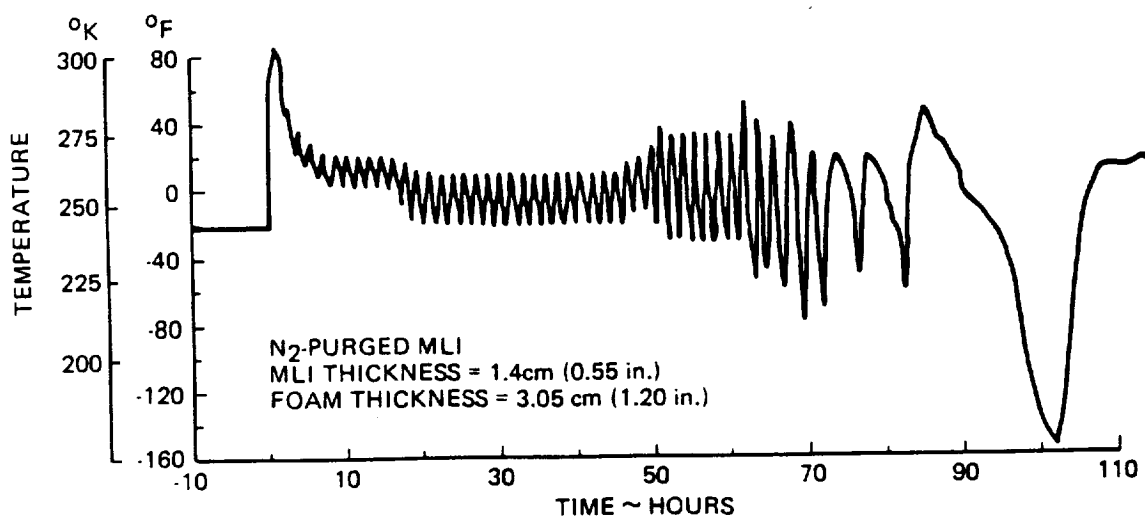


Figure 4-18: Typical LO<sub>2</sub> MLI Outer Layer Temperature History, Natural-Convection Ground-Hold Environment, N<sub>2</sub>-Purged MLI/Foam

assumed to continue until about three minutes after launch, when depressurization started to effect MLI gas conduction.

Ground-hold heat fluxes for the enhanced convection purge enclosure environment were typically in the range of  $473 \text{ W/m}^2$  ( $150 \text{ BTU/ft}^2\text{-Hr}$ ) for  $\text{LH}_2$  tanks and  $350 \text{ W/m}^2$  ( $111 \text{ BTU/ft}^2\text{-Hr}$ ) for  $\text{LO}_2$  tanks insulated with helium-purged MLI. These fluxes were approximately double the values that would be predicted from MLI systems of identical thickness under natural convection conditions. In the case of MLI/foam systems, predicted heat fluxes for enhanced-convection ground-hold conditions were about  $221 \text{ W/m}^2$  ( $70 \text{ BTU/ft}^2\text{-Hr}$ ) for both the  $\text{LH}_2$  and  $\text{LO}_2$  tanks. Identical insulations subjected to a natural convection environment would allow a heat flux of approximately  $126 \text{ W/m}^2$  ( $40 \text{ BTU/ft}^2\text{-Hr}$ ) to enter the tanks during ground hold operations.

Section 4.1.2.2 showed that ground-hold conditions influenced the propellant thermal loads until 50 hours after launch. The transition period from ground-hold to on-orbit conditions was therefore defined by the time interval from approximately three minutes to 50 hours after launch.

MLI heat flux for the transition period depended on the amount of MLI and the MLI temperature prior to gas evacuation. For both the MLI and the MLI/foam insulation concepts exposed to the pre-launch enhanced-convection environment, the MLI temperatures are relatively warm when compared to the on-orbit MLI temperatures. It follows that the MLI must cool to attain on-orbit conditions. This situation is similar to the TMM predictions for the MLI/foam insulations that are exposed to the natural-convection environments. TMM heat flux predictions were correlated to include the effects of MLI thickness and prelaunch MLI temperatures on average heat flux. These correlations were then used to estimate the time-averaged heat flux for all insulation concepts exposed to the enhanced-convection prelaunch environment. Foam cooling was included in the time-averaged heat flux to define the insulation performance for the transition period.

For the remainder of the mission, from 50 to 115 hours after lift-off, TMM predictions were used to define the insulation heat flux.

## 4.2 PREDICTED INSULATION PERFORMANCE

As stated in the introduction to this chapter, the objective of the thermal analysis task was to predict propellant tank heat leaks for the LTPS mission. These heat leak predictions were needed to calculate propellant boiloff losses for tank insulation optimization based on system payload capacity. It was therefore necessary to generate heat leak predictions for a wide range of insulation thicknesses for each basic design (i.e. helium-purged MLI and nitrogen-purged MLI/foam) to ensure that data were available in the region of optimum thickness. This was accomplished by selecting maximum and minimum insulation thicknesses along with intermediate values and generating heat flux predictions for these point designs with the thermal math models.

The predicted insulation fluxes are presented in this section. They are based on the thermal modeling described in section 4.1.

Insulation heat flux was predicted for two of the three baseline LTPS conceptual designs. The designs chosen had packaged LSS densities of  $56$  and  $40 \text{ kg/m}^3$ . Predicted heat fluxes for the LTPS design with a  $24 \text{ kg/m}^3$  packaged LSS density, and a smaller toroidal tank, were assumed to be identical to those for the  $40 \text{ kg/m}^3$  packaged LSS density LTPS because there was little difference in the predicted MLI performance between the



tandem-ellipsoidal and an ellipsoidal/toroidal propellant tank configuration LTPS designs when the insulation was evacuated. It was therefore deemed reasonable to neglect minor configuration differences between LTPS designs, with different-sized toroidal and ellipsoidal tanks, for prediction of on-orbit MLI performance.

For the prelaunch portion of the mission, heat flux predictions were not of sufficient accuracy to account for differences due to moderate variations in tank size. The enhanced convection environment was bounded by assuming a 294°K MLI outer-surface temperature. As such, there is no difference between the hydrogen tanks, or the oxygen tanks, for the three LTPS conceptual designs. Hence, the insulation pre-launch heat fluxes that were predicted for the 40 kg/m<sup>3</sup> packaged LSS density LTPS were also used for the LTPS with a 24 kg/m<sup>3</sup> one.

For most of the LTPS mission, the insulation heat flux was time-dependent. The fluxes were integrated with respect to time, and an average flux for several mission subintervals was defined. Three subintervals were selected to correspond with the sequential mission phases of:

- a. Ground-hold and Initial Launch Phase,
- b. Initial Launch Phase to Orbiter Separation, and
- c. LTPS Free-Flight.

Insulation designs were varied to develop parametric correlations for each mission subinterval. The resulting correlations for predicting insulation thermal performance are presented in the following subsections.

#### **4.2.1 Ground-Hold and Initial Launch Phases**

Thermal math model predictions showed that the steady-state prelaunch heat fluxes were not significantly altered until several minutes after launch: 2.5 minutes for helium-purged MLI, and 2.8 minutes for nitrogen-purged MLI. These times correspond to the points at which heat transfer by gas conduction is reduced, due to depressurization, and they were taken to represent the end of the initial launch phase. Prelaunch thermal conditions were therefore assumed to persist over the first 2.5 to 2.8 minutes of the mission.

Before insulation heat flux could be predicted as a function of thickness, it was necessary to determine reasonable ranges of thicknesses that would bound the optimum values. In the case of helium-purged MLI, this determination is relatively simple. Based on published tank insulation design information, a thickness range of 0.5 to 10 cm was selected for helium-purged MLI.

For nitrogen-purged MLI/foam insulations however, determination of the proper thickness range was more complicated. The complication arose from the fact that MLI-foam interface temperatures were specified, and the thicknesses of foam and MLI that gave the desired interface temperature were dependent on the outer surface temperature of the MLI during ground-hold conditions. The MLI outer surface temperature was, in turn, dependent on the heat transfer conditions between the environment and the MLI surface, as well as the total insulation system thickness.

The following text describes how the analysis of pre-launch thermal conditions was used to determine the appropriate range of thicknesses for MLI/foam insulation thicknesses. Following this description, insulation heat flux predictions for the prelaunch phase of the LTPS mission are presented.

#### MLI/Foam Sizing

Nitrogen-purged insulations were designed to enable a specified MLI/foam interface temperature to be obtained. Three interface temperatures were considered; 144, 200, or 244°K. For a given MLI surface temperature, the total temperature drop across the insulation system was fixed. The temperature difference across the foam sublayer was determined by multiplying the total temperature drop by the ratio of the MLI and foam combination thermal conductance to foam thermal conductance (conductance is defined as the effective thermal conductivity divided by thickness). The temperature differential across the foam was added to the tank temperature to determine the interface temperature for a given MLI surface temperature.

Unlike the enhanced-convection environment, for which the outside surface temperature of the MLI was equal to 294°K, MLI surface temperatures predicted for natural-convection environment varied with the type and the amount of insulation. Furthermore, MLI surface temperatures exhibited a spatial dependency. Colder insulation temperatures were predicted for the top and bottom of the hydrogen tank and the top of the oxygen tank.

Figure 4-19 shows MLI exterior surface temperature dependency on overall MLI/foam insulation conductance. These predicted surface temperatures were used to select MLI and foam thicknesses for the natural-convection prelaunch environments.

Figure 4-20 illustrates the relationship between MLI and foam thicknesses for different interface temperatures on the hydrogen tanks. It also shows the importance of the environmental conditions in selecting insulation thicknesses. For example, with natural-convection and a 244°K minimum interface temperature, the minimum allowed foam thickness is about 11 cm. This foam thickness corresponds to a zero MLI thickness. Increasing the foam thickness to 13 cm requires nearly 1 cm of MLI to be added to maintain the MLI/foam interface temperature at 244°K. Enhanced-convection prelaunch environments yield similar relationships between MLI and foam thicknesses (as shown by the dashed lines in Figure 4-20), but much less foam is needed to obtain a given interface temperature.

Figures 4-21 and 4-22 show similar MLI/foam sizing results for the toroidal and ellipsoidal oxygen tanks.

#### Heat Flux Correlations

Figure 4-23 shows the predicted ground-hold thermal fluxes for helium-purged MLI. This figure shows the effect of environmental conditions on insulation heat flux. Enhanced-convection modeling assumed that the temperature drop across the insulation did not change with insulation thickness. In this case, the heat flux is therefore inversely proportional to the MLI thickness. This relationship is the reason for the linear dependence of heat flux on insulation thickness shown in Figure 4-23 for the enhanced convection environment. Natural-convection modeling yielded a decreasing MLI surface temperature with a decreasing MLI thickness. As shown in Figure 4-23, the heat flux for the natural-convection environment was always less than that for the enhanced-

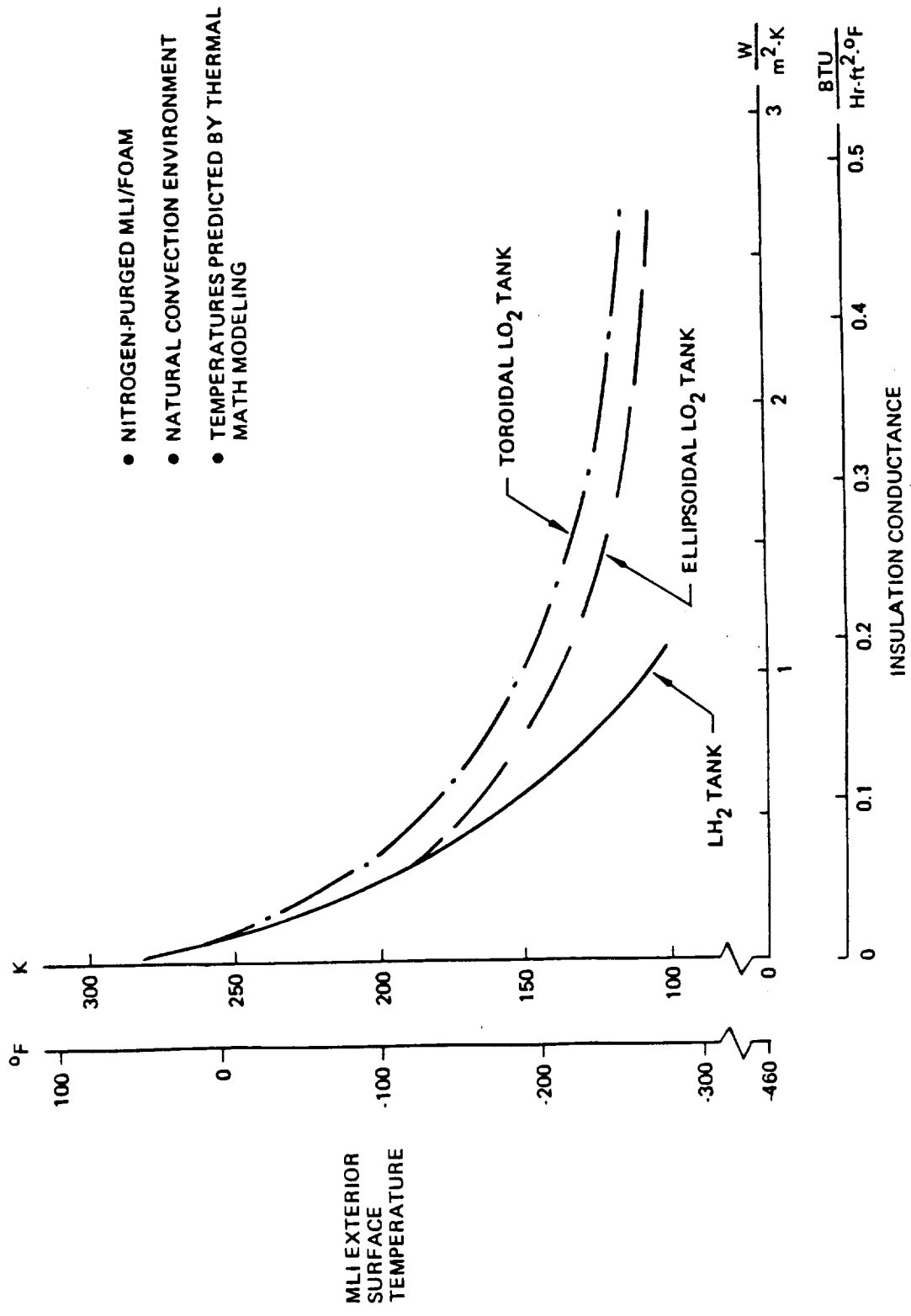


Figure 4-19: Minimum MLI Exterior Surface Temperatures for Ground-Hold in a Natural Convection Purge Enclosure Environment

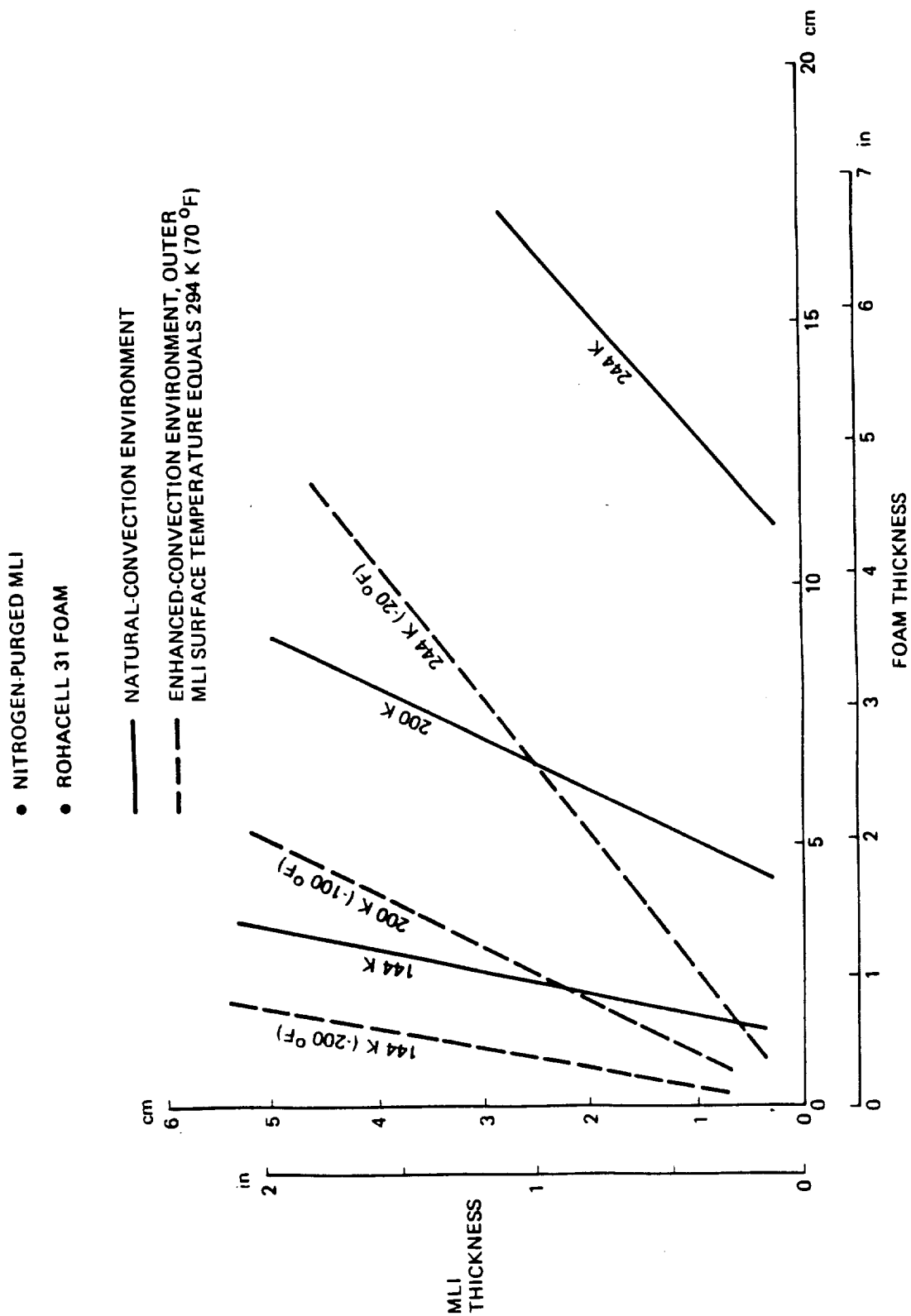


Figure 4-20: LH<sub>2</sub> Tank Insulation Thicknesses for Various MLI/Foam Interface Temperatures

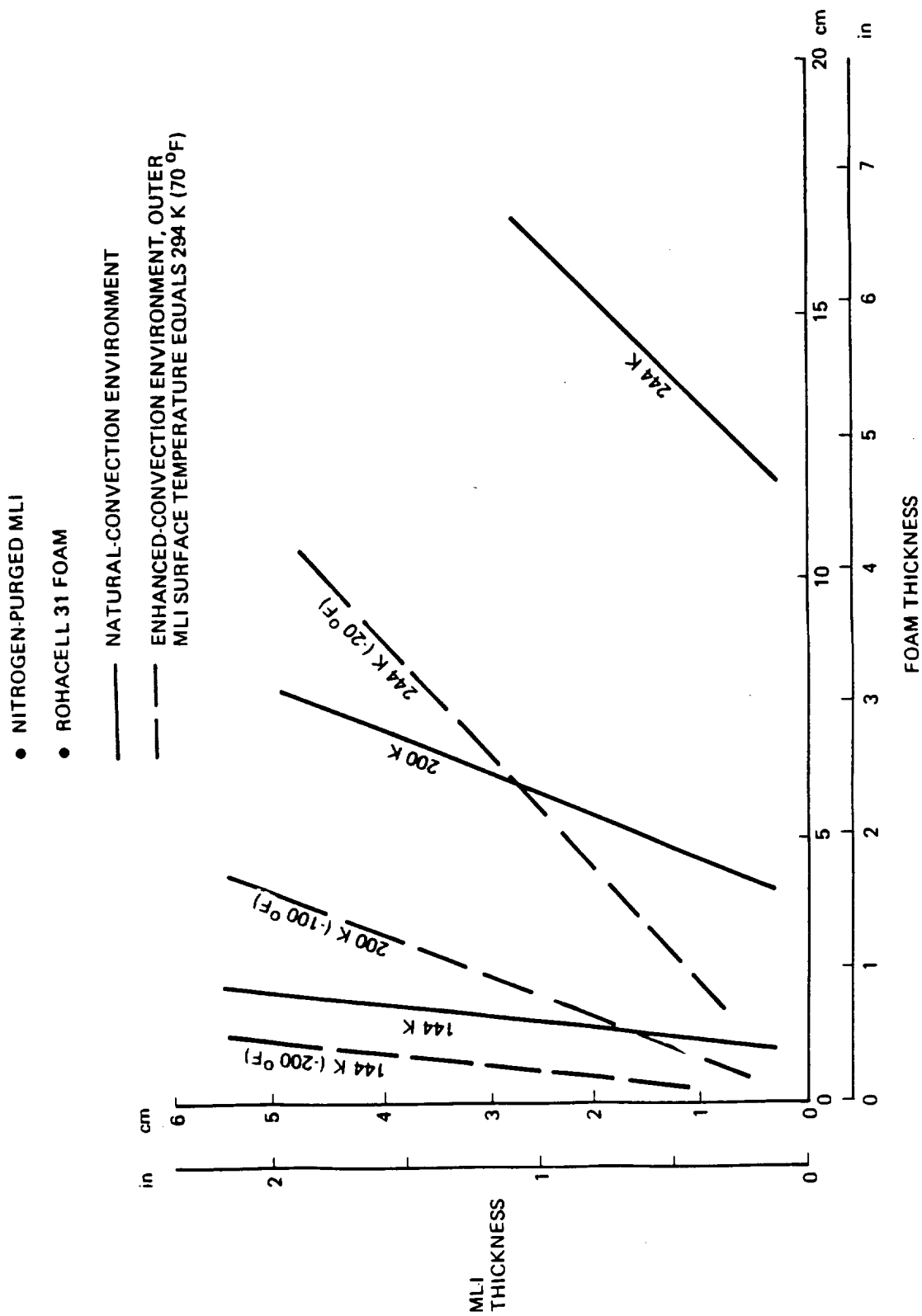


Figure 4-21: Toroidal LO<sub>2</sub> Tank Insulation Thicknesses for Various MLI/Foam Interface Temperatures

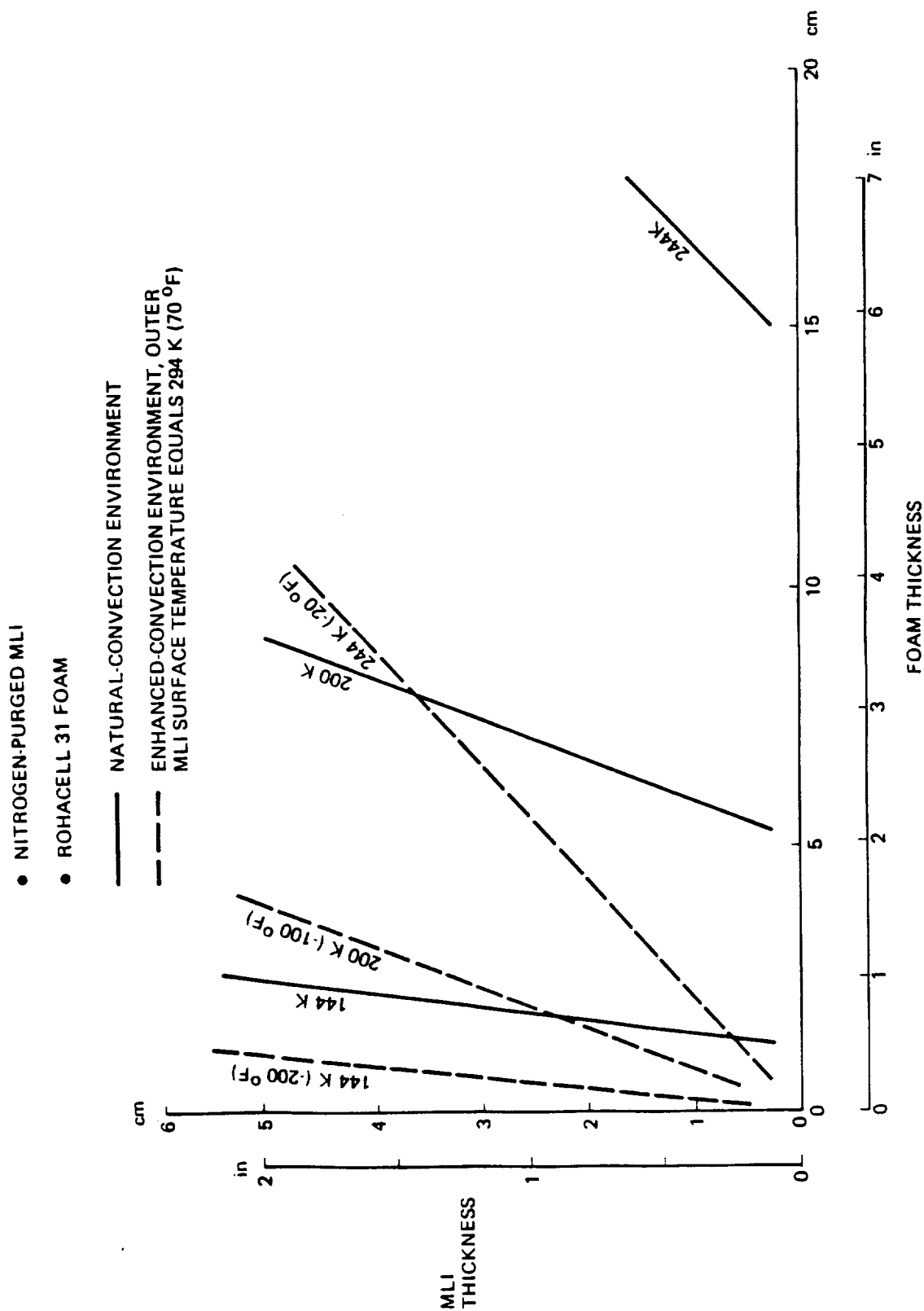


Figure 4-22: Ellipsoidal  $LO_2$  Tank Insulation Thicknesses for Various MLI/Foam Interface Temperatures

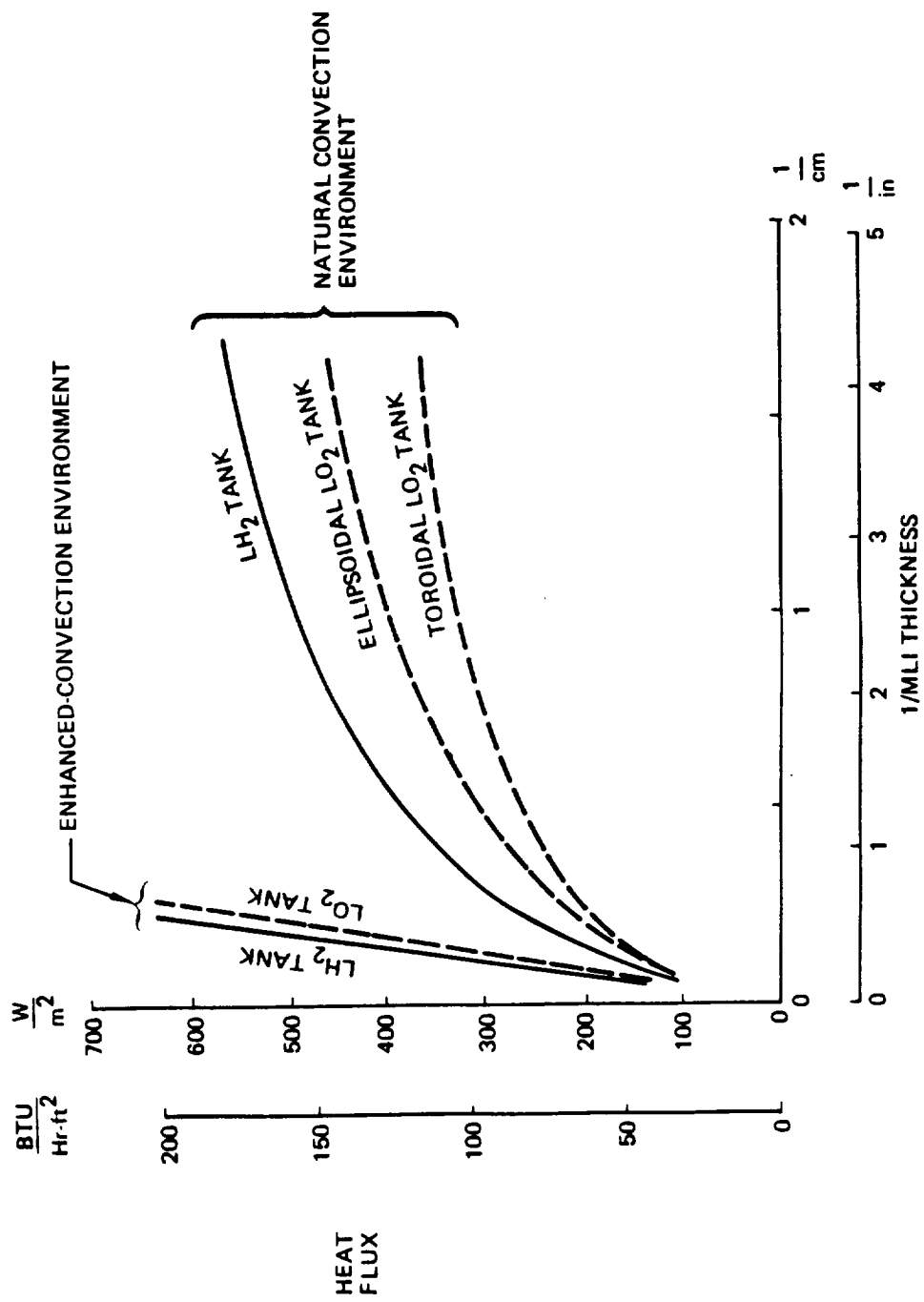


Figure 4-23: Predicted Heat Flux Through Helium-Purged MLI During the Ground-Hold Mission Phase

convection environment. Furthermore, at larger MLI thicknesses (small values of inverse thickness) the surface temperature approached the 294°K temperature used for the enhanced-convection case and the heat flux predictions for the two environments became identical.

Figure 4-24 shows similar predictions for the ground hold heat leak through MLI/foam insulations. Insulation conductance, rather than thickness, was used to correlate the heat flux for these concepts. The insulation conductance was determined by dividing the product of MLI and foam conductance by their sum.

#### **4.2.2 Initial-Launch Phase to Orbiter Separation**

Figures 4-11 and 4-13 showed that ground-hold environments effected MLI performance until the LTPS and LSS were separated from the Orbiter. During the initial phase of this transition period, the foam sublayer cooled to within several degrees of the propellant temperature. After the MLI was evacuated, it also underwent a temperature change from the ground-hold and initial-launch mission phases.

Propellant heating rates, generated by the TMM(s), were integrated with respect to time. The thermal load attributed to foam cooling, if any, was subtracted from the total integrated heat flux to define the heat leak through the insulation. Dividing by the tank area and the duration of the transition period ( $\approx 50$  hours) yielded a time-averaged insulation heat flux. As such, this heat flux included the effects of purge gas depressurization, changing LTPS environmental heat sources, and MLI capacitance. Figure 4-25 shows the predicted insulation heat flux for helium-purged MLI designs.

Figure 4-26 shows the insulation fluxes predicted for the MLI/foam insulation. Correlation of TMM predictions for the MLI/foam insulations was relatively difficult, due to a wide range of prelaunch thermal conditions. It was found by trial and error that the average heat flux could be satisfactorily correlated against itself when divided by the product of the MLI thickness and a maximum temperature potential. This correlation proved satisfactory for the MLI/foam insulations subjected to either a natural-convection ground-hold environment or an enhanced-convection environment.

#### **4.2.3 LTPS Free-Flight**

Prelaunch conditions had no effect on predicted insulation heat flux histories after LTPS/LSS separation from the Orbiter. Furthermore, no differences in predicted fluxes were observed between foam and no-foam concepts with an equivalent MLI thickness. Figure 4-27 illustrates the time-averaged heat fluxes for the LTPS free-flight mission phases.

For the 11 hour hold on LEO, there was no significant difference between the hydrogen and oxygen tank heat fluxes. After initiation of orbit transfer, the average heat flux became smaller because of reduced albedo and earth-infrared thermal loads. The heat flux for the hydrogen tank is also seen to be less than that for an oxygen tank with an equivalent MLI thickness. This relative ordering was caused by the LSS shadowing of the LTPS.

### **4.3 PREDICTED TANK PENETRATION HEAT LEAK**

Penetration heat leak is attributed to fill, pressurization, vent, and propellant-feed plumbing lines. Additional penetrations include cables for instrumentation to determine



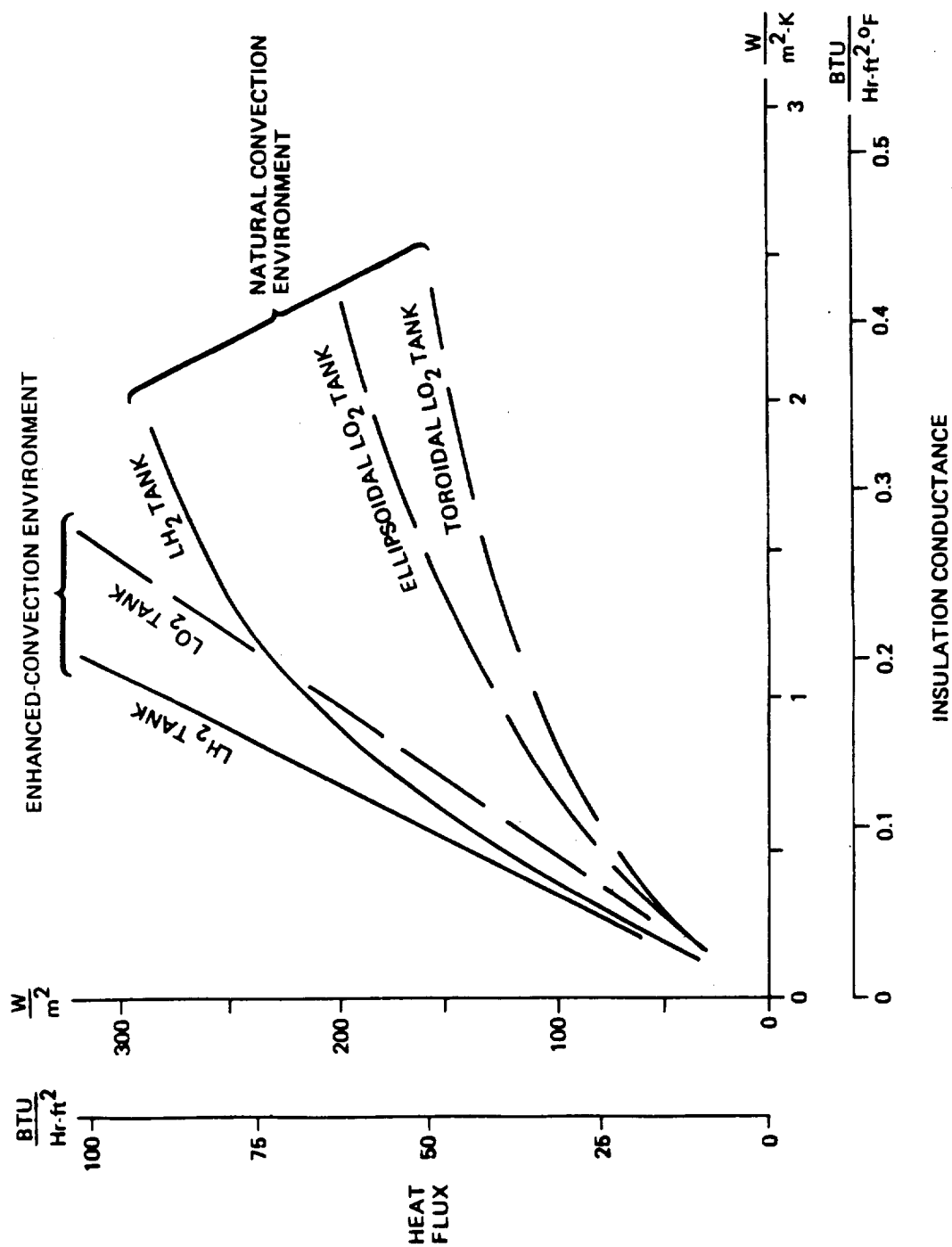


Figure 4-24: Predicted Heat Flux Through Nitrogen-Purged MLI/Foam Insulation During the Ground-Hold Mission Phase

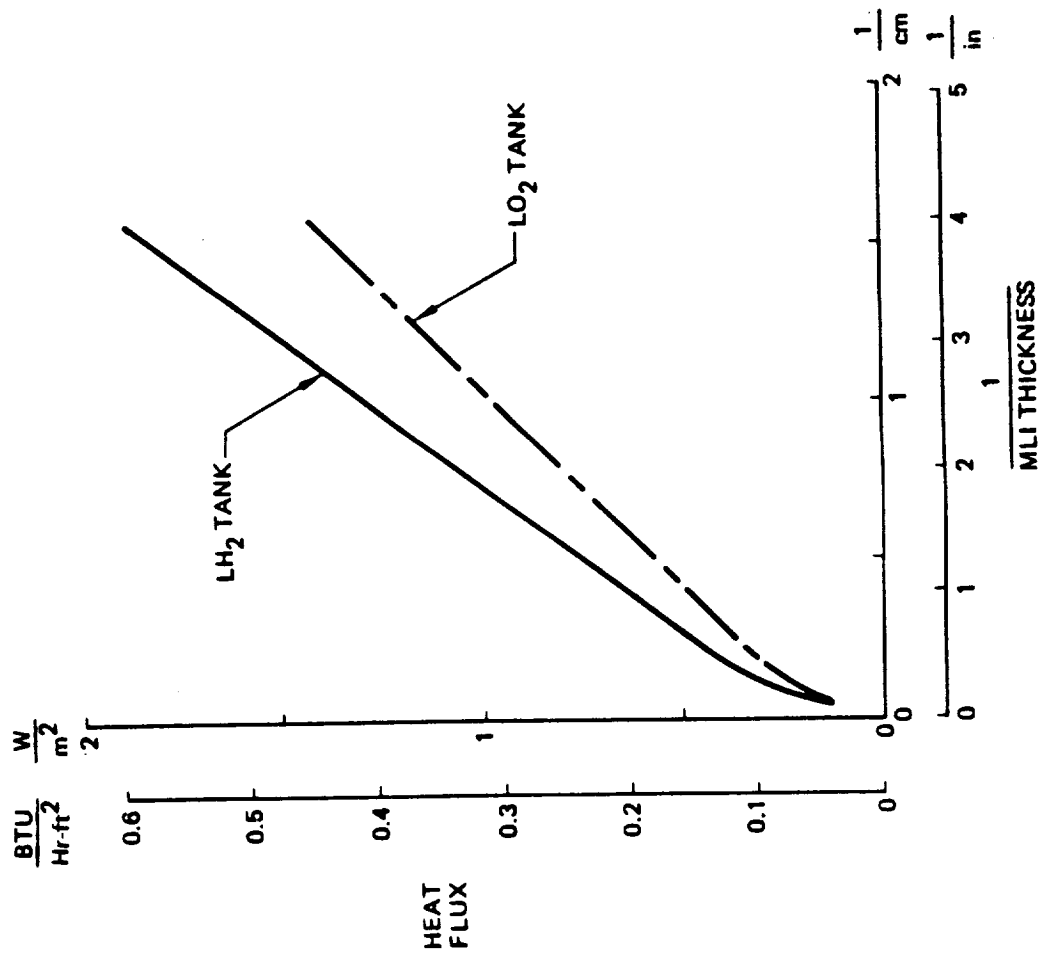


Figure 4-25: Time-Averaged Heat Flux Through Helium-Purged MLI for Mission Phase Extending From Insulation Evacuation Through LMSS/L TPS Separation From the Orbiter

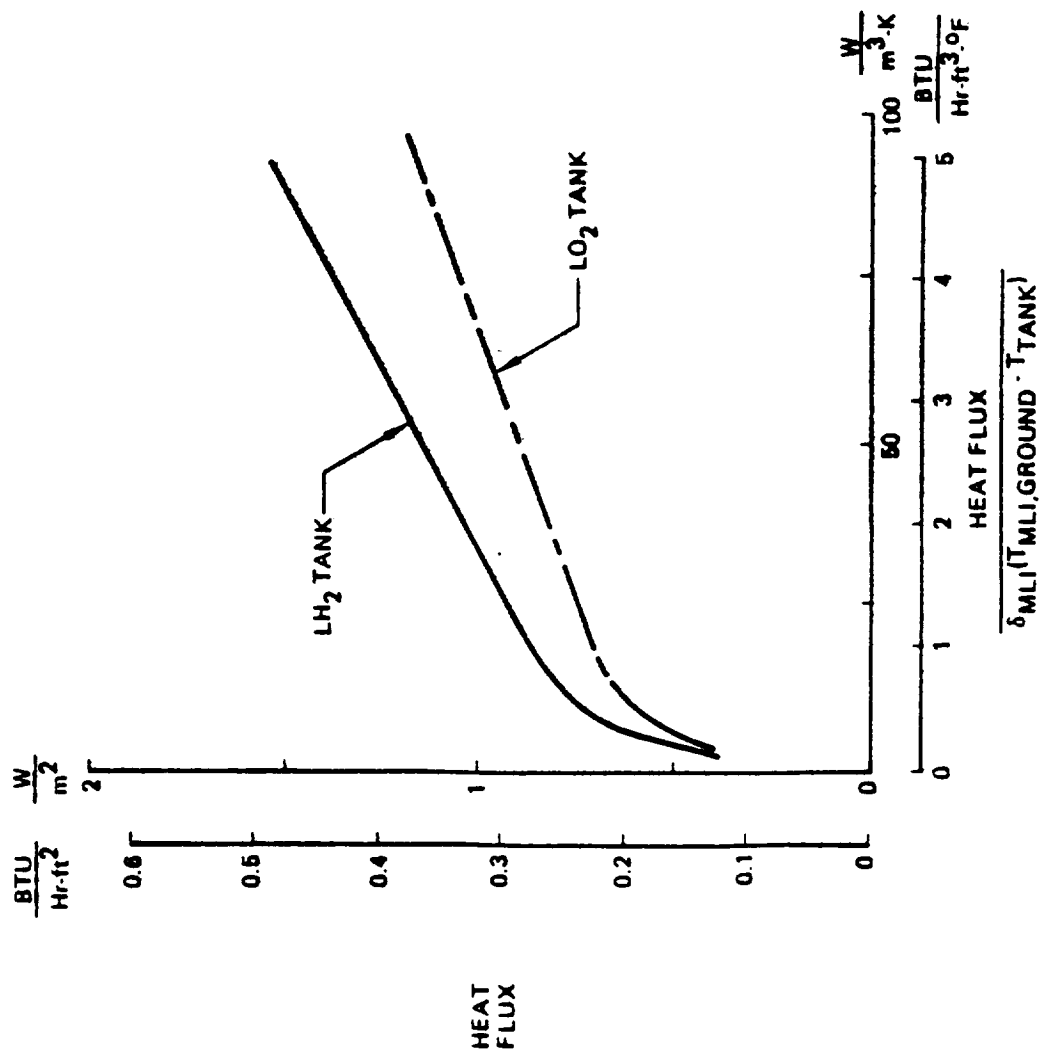


Figure 4-26: Time-Averaged Heat Flux Through Nitrogen-Purged MLI/Foam Insulations for Mission Phase Extending From Insulation Evacuation Through LMSS/LTPS Separation From the Orbiter

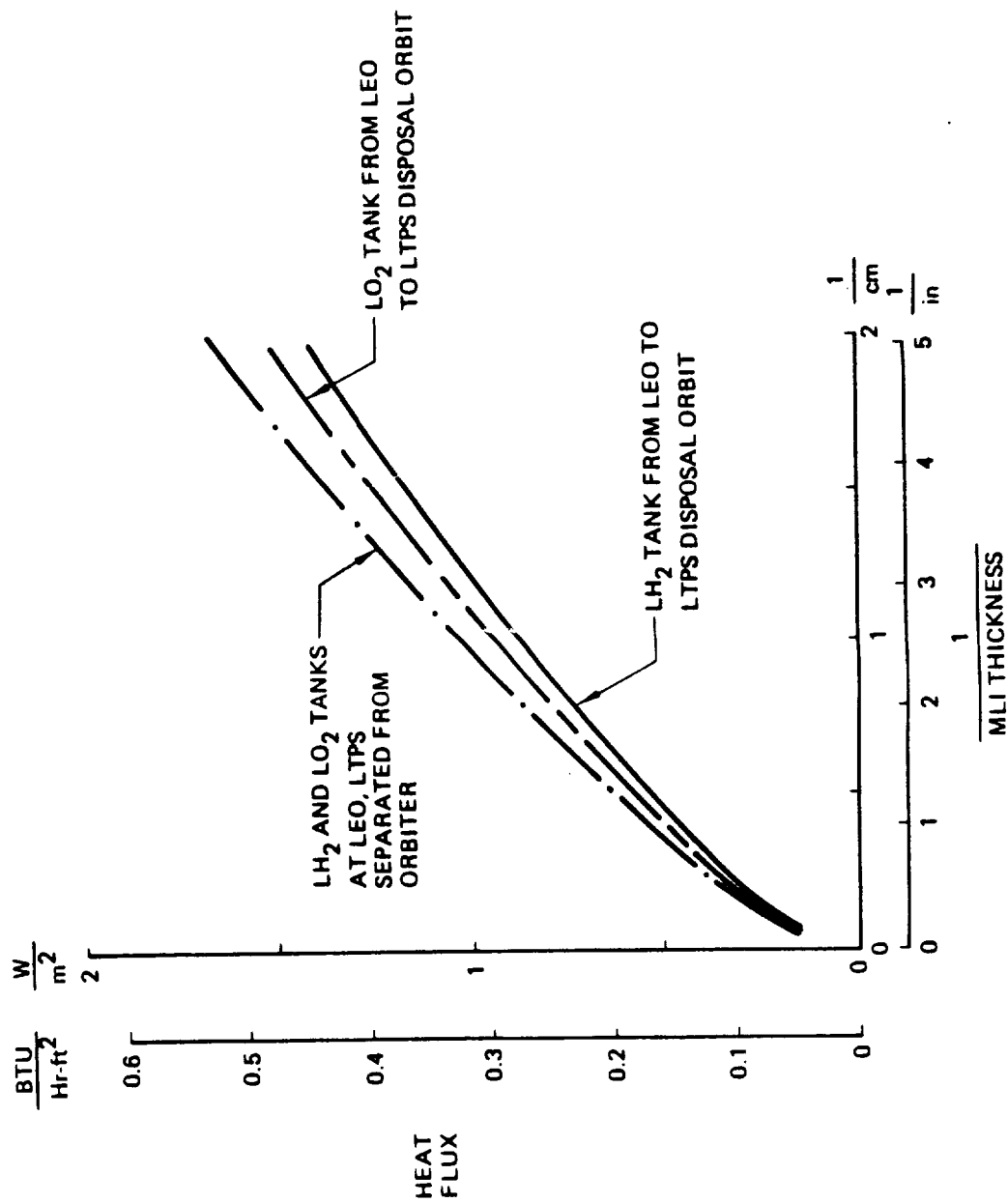


Figure 4-27: Time-Averaged Heat Flux Through Propellant Tank Insulations for Mission Phase Extending From LMSS/LTPS Separation From the Orbiter Through Insertion of the LTPS in Disposal Orbit

the liquid propellant(s) height during the prelaunch mission phase. In this study negligible heat soak back, through the propellant supply lines, from the LTPS engine was assumed. This assumption was based on conversations with Pratt and Whitney.

Heat leak through tank penetrations is very dependent on penetration design. For example, heat leak through the fill line could be greatly reduced if a concentric vent line could be used. Rather than perform a detailed thermal analysis for the penetrations, constant heat leaks of 29W and 22W were used for the hydrogen and oxygen tank penetrations respectively.

#### **4.4 PREDICTED TANK SUPPORT HEAT LEAK**

Time-averaged predictions for support strut heat leaks are given in Table 4-3. Table 3-8 of this report summarizes support strut design information.

For each LTPS conceptual design, with the natural convection prelaunch environment, the prelaunch support strut heat leak for MLI/foam insulated-tanks was larger than that for tanks insulated with MLI only. This was due to warmer body shell temperatures that occurred for MLI/foam insulated tanks. Since the strut heat leak is proportional to the difference between tank wall temperature and body shell temperature, a higher body shell temperature therefore resulted in greater strut heat leak. The body shell temperatures for MLI/foam insulated tanks were greater than those for MLI-only insulated tanks because the lower thermal conductance of N<sub>2</sub>-purged MLI/foam reduced the influence of the cold tank on the equilibrium body shell temperature prior to launch. For the remainder of the mission, little difference between the predicted strut heat leaks for various insulation concepts was predicted.

For the enhanced-convection pre-launch environment, the LTPS body shell temperature was fixed at 294°K. Predictions of strut heat leak for the enhanced-convection cases were found to approximately equal those of the MLI/foam insulated tanks in a natural convection environment.

HEAT LEAK, WATTS (BTU/hr)					
LTPS PACKAGED LSS DENSITY, Kg/m <sup>3</sup> (Lb <sub>m</sub> /ft <sup>3</sup> )	TYPE TANK	MISSION PHASE TYPE INSULATION	GROUND-HOLD TO INITIAL ASCENT (T + 4 MINUTES TO T + 3 MINUTES)	INITIAL ASCENT TO ORBITER SEPARATION (T + 3 MINUTES TO T + 50 HOURS)	ORBITER SEPARATION TO DISPOSAL ORBIT (T + 50 HOURS TO T + 115 HOURS)
56 (3.5)	LH <sub>2</sub>	MLI MLI/FOAM	2.2 (7.5) 3.7 (12.6)	3.2 (10.9) 3.2 (10.9)	2.6 (8.9) 2.6 (8.9)
	LO <sub>2</sub>	MLI MLI/FOAM	95 (324) 123 (420)	97 (331) 98 (334)	85 (290) 85 (290)
40 (2.5)	LH <sub>2</sub>	MLI MLI/FOAM	2.2 (7.5) 3.8 (13)	3.2 (10.9) 3.2 (10.9)	2.6 (8.9) 2.6 (8.9)
	LO <sub>2</sub>	MLI MLI/FOAM	47 (160) 72 (246)	59 (201) 60 (205)	54 (184) 54 (184)
24 * (1.5)	LH <sub>2</sub>	MLI MLI/FOAM	2.3 (7.8) 4.0 (13.7)	3.4 (11.6) 3.4 (11.6)	2.8 (9.6) 2.8 (9.6)
	LO <sub>2</sub>	MLI MLI/FOAM	50 (171) 77 (263)	63 (215) 64 (218)	57 (195) 57 (195)

\* Heat leaks for this LTPS design were scaled by a conductance ratio from the 40 Kg/m<sup>3</sup> (2.5 lb<sub>m</sub>/ft<sup>3</sup>) packaged LSS conceptual design.

Table 4-3: Tank Support System Heat Leak

## 5.0 OPTIMIZATION

This section describes the analytical study of optimum LTPS propellant tank insulation design and summarizes study results. The objective of this study was to identify the insulation types and thicknesses that maximize LTPS payload delivery capability for package payload densities of  $56 \text{ kg/m}^3$ ,  $40 \text{ kg/m}^3$  and  $24 \text{ kg/m}^3$ . Optimum insulation designs were calculated for each of the 13 design conditions indicated in Table 2-3. Five insulation concepts were studied. Helium-purged MLI was selected as the state-of-the-art baseline. The other 4 insulations investigated were foam/MLI combinations purged with nitrogen. Three of the combination insulations consisted of Rohacell 31 foam and MLI. Foam-thickness-to-MLI-thickness ratios were selected to give foam-MLI interface temperature of  $244^\circ\text{K}$ ,  $200^\circ\text{K}$  and  $144^\circ\text{K}$  during ground hold purging. The fifth insulation consisted of BX250A foam and MLI with an interface temperature of  $200^\circ\text{K}$ .

Two ground hold conditions were studied because it was determined that the assumed convective environment within the purge enclosure had a significant influence on insulation thickness and payload mass.

The conditions studied represent the two convective heat transfer extremes that could occur between the MLI outer layer and the purge enclosure inner surface. In this study the purge enclosure outer surface was assumed to be held at  $294^\circ\text{K}$  during ground hold operations. For the minimum thermal coupling case, natural convection heat transfer, it was assumed that the gas in the purge enclosure was stagnant and heat was transferred from the purge enclosure outer surface to the MLI by radiation and free convection. For the maximum thermal coupling case, enhanced convection heat transfer, it was assumed that warm purge gas was circulated in the enclosure and the convective heat transfer coefficient was large enough to cause the MLI surface temperature to be at  $294^\circ\text{K}$ .

An iterative procedure was used to identify the insulation thickness that maximized LTPS payload delivery capability. The procedure consisted of the 4 following steps which were repeated until the maximum payload case was found.

- a. Estimate a new insulation thickness by incrementally changing the current value.
- b. Calculate propellant tank heat leak over the entire mission.
- c. Calculate new values of propellant tank volume and wall thickness.
- d. Calculate new values of LTPS mass and length and payload mass and length.

The 3 baseline LTPS conceptual designs described in section 3.5 were used as starting points for the optimization procedure. A computer program was developed to perform the LTPS and payload sizing calculations thereby greatly reducing the computational time required to find the optimum insulation thicknesses. The program was run interactively with the user estimating new values of insulation thickness and the program responding with predicted payload mass. For the highest density payload case ( $56 \text{ kg/m}^3$ ), the optimization of LTPS payload essentially involved a trade between insulation mass and the combined masses of vented propellant and tankage. In this case, orbiter payload launch mass was the prime constraint. For lower density payloads, the principal constraint was orbiter cargo bay length, and the LTPS payload capability was influenced primarily by insulation thickness and tank length.

The insulation optimization study lead to the following significant results:

- a. LTPS payload mass was increased by as much as 184 kg (406 lbm) by replacing He-purged MLI with N<sub>2</sub>-purged MLI/foam combinations when enhanced convection was maintained in the purge enclosure.
- b. For He-purged MLI cases, the natural-convection purge enclosure environment resulted in the largest LTPS payload masses.
- c. For N<sub>2</sub>-purged MLI/foam combinations, the warm-gas, forced convection condition in the purge enclosure during ground hold resulted in the largest LTPS payload masses.
- d. From the standpoint of maximum payload capability, the best foam/MLI interface temperature was 144°K. However, the loss in payload mass in going from 144°K to 244°K was only a maximum of 42 kg (93 lbm).

The following sections describe the details of the insulation optimization study. Groundrules and assumptions adopted to simplify the LTPS payload sizing calculations and focus the scope of the study are summarized. The general optimization approach is described and the computer program used to predict size and mass characteristics of LTPS and payload combinations is discussed. Parametric LTPS design data and algorithms contained in the program are described in detail. In the final section optimization study results are presented and discussed.

## 5.1 OPTIMIZATION GROUND RULES AND ASSUMPTIONS

Groundrules and assumptions were established at the beginning of the LTPS insulation optimization study to define the scope of the effort and simplify the problem to a tractable form. The following groundrules were established to define the optimization study:

- a. The mission timeline presented in Table 3-3 applied to all LTPS vehicles.
- b. Shuttle payload mass capability was 29,478 kg (65,000 lbm) at liftoff for all missions.
- c. Shuttle cargo bay length available for the combined LTPS/ASC/payload was 16.95m (55.6 ft) for all missions.
- d. Propellant oxidizer-to-fuel ratio was 6:1 with a specific impulse of 4560 N-sec/kg (465 sec). Engine thrust level was 2224N (500 lbf) for all vehicles.
- e. Three LTPS packaged payload densities were considered: 56 kg/m<sup>3</sup>, 40 kg/m<sup>3</sup> and 24 kg/m<sup>3</sup>.
- f. Two insulation types were investigated. These were, He-purged MLI and N<sub>2</sub>-purged MLI/foam.
- g. For MLI/foam combinations, three MLI-foam interface temperatures during ground-hold purging were considered; 244°K, 200°K and 144°K.



- h. Two foam materials, Rohacell 31 and BX250A were investigated with Rohacell 31 being the baseline material for which the majority of the designs were developed. BX250A was used in one design for the purpose of comparison with the payload performance derived with Rohacell 31.
- i. Two thermal environments in the purge enclosure during ground-hold operations were considered. These environments were:
  - 1. Natural convection, and
  - 2. Enhanced convection in which the outer layer of the MLI was maintained at 294°K.

A number of simplifying assumptions were made to reduce the complexity of the insulation optimization problem. These assumptions dealt with second and third order effects which, it was felt, would not significantly impact the results of the analysis, either in terms of insulation thicknesses or the relative ranking of insulation concepts.

The following assumptions were made in the development of the insulation parametric data and the computerized LTPS sizing models:

- a. Heat flux through a given thickness of tank insulation was dependent only upon mission time and the basic LTPS shape. Therefore, the fluxes calculated for each of the baseline LTPS vehicles were assumed to be independent of LTPS tank size perturbations on these basic designs.
- b. Tank heat leak through support struts and insulation penetrations (fill lines, vent lines, drain lines, etc.) was independent of tank size and mass perturbations. These heat leaks were assumed to be equal to the values discussed in section 4.4 of this report for the baseline LTPS vehicles.
- c. All heat leak was absorbed by liquid boiling. Except for tank lock-up during STS ascent, all vapor generated by boiling was vented directly overboard.
- d. The effect of propellant conditioning and pressurization on the mass of vented propellant was assumed to be identical for all LTPS designs analyzed. Hence the pressurization system was not modeled.
- e. For a given LTPS, the optimum LH<sub>2</sub> and LO<sub>2</sub> tank insulation designs were assumed to be independent. Hence the two tank insulations were optimized separately for maximum LTPS payload.
- f. Auxiliary propellant consumption was assumed to be equal to the baseline LTPS values for all vehicle size perturbations about the baseline.
- g. All LTPS vehicles were assumed to have the same  $V$  requirement for LEO to GEO transfer and for GEO to disposal orbit. Orbit transfer parameters summarized in Table 3-4 were used to calculate mass ratios which were assumed to be the same for all vehicles.
- h. ASE mass did not change with perturbations in baseline LTPS size and mass.
- i. Insulation mass per unit volume was assumed to be constant for all vehicle configurations.

- j. The mass of propellant conditioning, acquisition and servicing (fill and drain) hardware was assumed to be constant for all vehicle size perturbations about the baseline LTPS designs.
- k. The total tank heat leaks over the LTPS mission were assumed to be constant over three phases of the mission: 1) ground hold and initial ascent, 2) initial ascent through separation from the orbiter and 3) free flight to disposal orbit insertion. These average heat leaks were calculated for each tank shape (cylindrical, ellipsoidal and toroidal) from LTPS thermal math model predictions.
- l. No accounting was made for the effect of tank pressurant on propellant boil-off.
- m. A propellant loading uncertainty penalty of 0.5% was assumed for both LH<sub>2</sub> and LO<sub>2</sub> tanks.
- n. Propellant tank self-pressurization during the 90 second lock-up period following liftoff was based on Centaur tank pressurization measurements (see Appendix E).
- o. Propellant losses due to engine starting and stopping were constant for all cases studied.
- p. Tank volume occupied by baffles, acquisition systems, pressurant systems etc., was assumed to be zero.

## 5.2 OPTIMIZATION APPROACH

This section describes the approach that was taken to identify the best insulation concepts for LTPS vehicles designed for the 3 packaged payload densities. Delivered payload mass to GEO was selected as the quantitative measure for comparing the benefit of each insulation candidate considered.

The principal independent variables for each insulation type (He - purged MLI, N<sub>2</sub>-purged MLI/Rohacell 31 foam and N<sub>2</sub>-purged MLI/BX250A foam) investigated, were insulation thickness and tank percent ullage volume. In the case of MLI/foam combinations, foam thickness rather than combined MLI/foam thickness, was used as the independent variable. The reason for this approach, as will be shown in section 5.7 was that for each MLI/foam interface temperature selected, a large range of combinations of foam and MLI thicknesses were possible.

A sizing model was developed to predict the mass and length of LTPS vehicles and to calculate payload mass. This model, which was computerized to minimize computation time, used the three baseline LTPS vehicles described in section 3.5 as starting points for vehicle sizing. The model contained parametric information and equations relating insulation thickness to insulation mass and to tank heat leak for all mission phases. It also contained information relating insulation thickness and tank percent ullage volume to tank mass and effective liquid propellant density. Details of the parametric LTPS sizing data developed for the model are described in section 5.4.

Inputs to the interactive computerized vehicle sizing model included: 1) payload packaged density, type of purge gas, type of foam insulation, insulation thickness (either MLI, or foam if the MLI was N<sub>2</sub>-purged), MLI/foam interface temperature, and propellant tank percent ullage volume. The model interactively sized a new LTPS, starting with the appropriate baseline design (as determined by payload packaged density). Payload mass

was calculated and printed out at a user keyboard terminal. The user then was given the option of either changing insulation thickness or percent ullage volume, or inputting a completely new set of variables.

A procedure was developed to rapidly converge on the optimal value of insulation thickness and percent ullage volume. Starting with the appropriate baseline LTPS, an incremental change in the independent variables (IV), either insulation thickness or percent ullage volume, was made and the sign of the partial derivative of MPL/IV was determined by predicting a new payload mass, MPL. Once the sign of the partial derivative was established, new values of the independent variable could be selected to increase payload mass. The value of the independent variable was incrementally changed until the new value of payload mass was less than the previously calculated value. This condition identified the general location of the optimum LTPS design. A prediction-correction technique was then used to converge on the optimum design.

### 5.3 LTPS SIZING MODEL

The computer programs developed to size LTPS/payload combinations are described in this section. The programs were used to identify the insulation designs that maximized LTPS payload delivery capability. Principal program inputs were insulation thickness, insulation type (He-purged MLI or N<sub>2</sub>-purged MLI/foam combinations) and tank percent ullage volume. The programs calculated LTPS and payload length and mass.

Two versions of the program were written (Appendix C). In one, entitled TRADE, it was assumed natural convection occurred in the purge enclosure during ground hold operation. In the other program, TRADE2, it was assumed that enhanced convection of warm purge gas in the purge enclosure maintained the outer layer of MLI at 294°K.

The following subsections describe the computer models. The description is presented in three parts. First, the primary independent and dependent variables of the models are described. Program logic flow is briefly summarized in the second subsection. Finally, computational algorithms and parametric design data used in the programs are described.

#### 5.3.1 Model Variables

Model variables consisted of: 1) the independent variables which were computer program inputs, 2) assigned values which were assumed to be invariant for the range of independent variables considered; and 3) dependent variables, which were calculated by program algorithms, as either final output or values used internally in intermediate computational steps.

Independent variables assigned by the user were the following:

<u>Independent Variable Name</u>	<u>Variable Description</u>
PLDEN	Payload density, either 56, 40, or 24 kg/m <sup>3</sup> .
TYPET	Type of tank for which the insulation is to be sized. Either LH <sub>2</sub> or LO <sub>2</sub> is specified.

TYPEG	MLI purge gas. Either helium or nitrogen is specified. If helium is specified, the insulation type is MLI only. If nitrogen is specified, the insulation type is an MLI/foam combination.
DELM	MLI thickness for helium purged insulation cases.
TYPEF	Foam material. Either Rohacell 31 or BX 250A is specified.
DELF	Foam thickness for those cases which nitrogen purged MLI is specified.
TIM	Interface temperature between foam and MLI during MLI purging. Used only when nitrogen-purged MLI is specified.
S4	Percent ullage volume at T-4 minutes (4 minutes before tank lock-up and launch).

These 8 independent variables provided the information needed by the computer program to size each LTPS and determine its maximum payload mass and length.

LTPS sizing variables which were determined to have a weak influence on the optimum insulation thickness, were assigned nominal values. These values were held constant for all stage and payload sizing calculations. The following summary lists the variables that were held constant and gives the assigned value of each.

<u>Variable Name</u>	<u>Assigned</u>
1) BX250A foam density	36.85 kg/m <sup>3</sup> (2.3 lbm/ft <sup>3</sup> )
2) Rohacell 31 foam density	30.44 kg/m <sup>3</sup> (1.9 lbm/ft <sup>3</sup> )
3) Heat leak to hydrogen tanks through insulation penetrations (excluding support struts)	29W (100 BTU/hr)
4) Heat leak to oxygen tanks through insulation penetrations (excluding support struts).	22W (74 BTU/hr)
5) Density of liquid hydrogen	70 kg/m <sup>3</sup> (4.3693 lbm/ft <sup>3</sup> )
6) Density of hydrogen vapor	1.61 kg/m <sup>3</sup> (0.1004 lbm/ft <sup>3</sup> )
7) Density of liquid oxygen	1131.5 kg/m <sup>3</sup> (70.633 lbm/ft <sup>3</sup> )
8) Density of oxygen vapor	5.39 kg/m <sup>3</sup> (0.3365 lbm/ft <sup>3</sup> )
9) Heat of vaporization of liquid hydrogen	435.0 KJ/kg (187 BTU/lbm)
10) Heat of vaporization of liquid oxygen	209.4 KJ/kg (90 BTU/lbm)
11) Density of MLI	35.08 kg/m <sup>3</sup> (2.19 lbm/ft <sup>3</sup> )
12) Mass of hydrogen lost due to engine starting and stopping over the 8 perigee burn mission, and orbit circularization	4.55 kg (10.0 lbm)
13) Mass of oxygen lost due to engine starting and stopping over mission	28.64 kg (63.0 lbm)
14) LTPS body shell weight per foot of length	39.2 kg/m (26.3 lbm/ft)
15) Maximum payload packaged diameter	4.48m (14.7 ft)

16)	Maximum length of the LTPS, ASE and packaged payload	16.95m (55.6 ft)
17)	Space shuttle maximum payload mass, including ASE, LTPS and payload.	29,478 kg (65,000 lbm)
18)	Weight of auxillary propellants (RCS)	51.36 kg (113 lbm)

Dependent variables calculated by the program, and accessible to the user through program output, are summarized in Table 5-1. The two principal dependent variables for MLI and MLI/foam insulation optimization are 1) payload mass and; 2) payload length. The other dependent variables are used in LTPS sizing calculations to determine LTPS mass and overall length.

These assumptions simplified the sizing model and reduced computation time and cost. In some instances assumptions were adopted to bound the solution when exact design information was unavailable. This was the case in the definition of the ground-hold purge enclosure environment. In other cases, simplifying assumptions were made to eliminate from consideration design variables that had minimal influence on LTPS and payload sizing. The elimination of second and third order effects was justified by the lack of detailed design information available for the baseline LTPS configuration.

### 5.3.2 Computer Model Logic Flow

The computer program developed to identify the MLI/foam and MLI-only insulation systems that optimized LTPS payload mass consisted of a main routine and 11 subroutines. The program was written to operate interactively, prompting the user for input data and writing out intermediate and final results to assist the user in making input decisions.

A logic flow diagram of the main routine is shown in Figure 5-1. Input information is provided to the routine through 5 sets of data. Payload density (either 56, 40, or 24 kg/m<sup>3</sup>) is specified by the user, as are the tank type, ullage volume and purge gas type (He or N<sub>2</sub>). If N<sub>2</sub> is specified, the routine requests values for MLI/foam interface temperature, foam type and foam thickness. If He is specified as the purge gas, the routine requests a value for MLI thickness. For N<sub>2</sub>-purged MLI/foam combinations, the routine calculates the thickness of MLI required to maintain the specified MLI/foam interface temperature during ground hold. Once the insulation thicknesses are established, the routine calls subroutines GRFLX, TRFLX and SPFLX. These subroutines calculate the average heat leak through the tank insulation during ground hold operations and initial ascent (GRFLX), initial ascent through LTPS/orbiter separation (TRFLX), and orbiter separation through disposal orbit insertion (SPFLX).

After calculating heat fluxes, the main routine then iteratively sizes an LTPS for the given input conditions and calculates its payload capacity. The starting point for all LTPS sizing is one of the three baseline conceptual designs described in section 3.5 for packaged payload densities of 56, 40 and 24 kg/m<sup>3</sup>. Mass property data, tank sizes, payload mass and stage length (including ASE) are stored for each of these designs. These values are used by the routine as the first guess at LTPS mass, size and payload characteristics.

Details of the LTPS sizing routine are shown in the Figure 5-2 flow chart. Heat leaks for the particular insulation design under consideration are used to calculate new values for vent losses and propellant loading density. Tanks are then resized and weighed and new values calculated for propellant mass, insulation mass and body shell mass. Once new estimates of LTPS mass and length are calculated, the routine then predicts payload mass.

Dependent Variable Name	Dependent Variable Description
DELM	MLI thickness for N <sub>2</sub> -purged cases
GFLX	Heat flux through insulation during ground hold
TFLX	Average heat flux through insulation from launch to orbiter separation
SFLXOT	Heat flux through insulation from orbiter separation to LTPS disposal
QSTRH1 & QSTRO1	Heat leak through hydrogen and oxygen tank support struts respectively during ground hold
QSTRH2 & QSTRO2	Heat leak through hydrogen and oxygen tank support struts respectively from ascent to orbiter separation
QSTRH3 & QSTRO3	Heat leak through hydrogen and oxygen tank support struts respectively from orbiter separation to LTPS disposal
WHPN & WOPN	Hydrogen and oxygen loading (liquid) at T-4 minutes
WH4N & WO4N	Hydrogen and oxygen boil-off from T-4 to T=0 minutes
WH5N & WO5N	Additional LH <sub>2</sub> and LO <sub>2</sub> boiled off during 5 minute contingency hold between T-4 and T=0 minutes
WHBI & WOBI	LH <sub>2</sub> and LO <sub>2</sub> vented prior to first LTPS motor burn
WHIMP & WOIMP	LH <sub>2</sub> and LO <sub>2</sub> burned during transfer and disposal
WHAI & WOAI	LH <sub>2</sub> and LO <sub>2</sub> vented during transfer
WHRES & WORES	LH <sub>2</sub> and LO <sub>2</sub> residuals
WHLU & WOLU	LH <sub>2</sub> and LO <sub>2</sub> loading uncertainty
VHTN & VOTN	LH <sub>2</sub> and LO <sub>2</sub> tank volumes
THINS & TONIS	LH <sub>2</sub> and LO <sub>2</sub> tank insulation thicknesses
AHTM & AOTN	LH <sub>2</sub> and LO <sub>2</sub> tank surface areas
HHTN & HOTN	LH <sub>2</sub> and LO <sub>2</sub> tank lengths
PLMASS	Payload mass
MASE	ASE mass
WBO	LTPS burnout mass
WBOP	LTPS inert mass exclusive of tanks, insulation, and body shell
WINS	Tank insulation mass
WBS	LTPS body shell mass
HTW & OTW	LH <sub>2</sub> and LO <sub>2</sub> tank mass
PVOL	Payload volume
SLN	Orbiter cargo bay length required for LTPS and ASE

Table 5-1: LTPS Sizing Model Dependent Variables

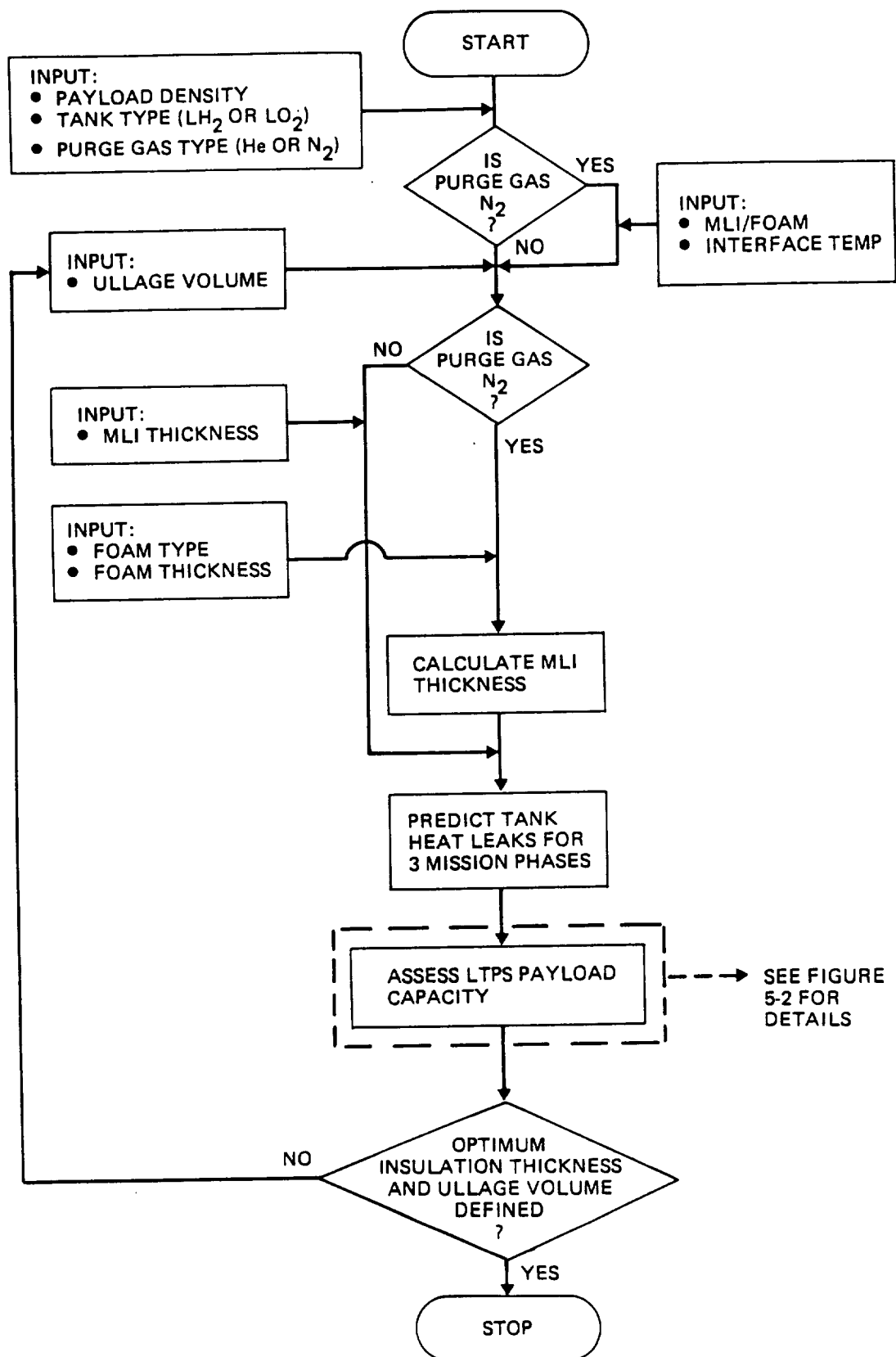


Figure 5-1: Insulation Optimization Model Logic Flow





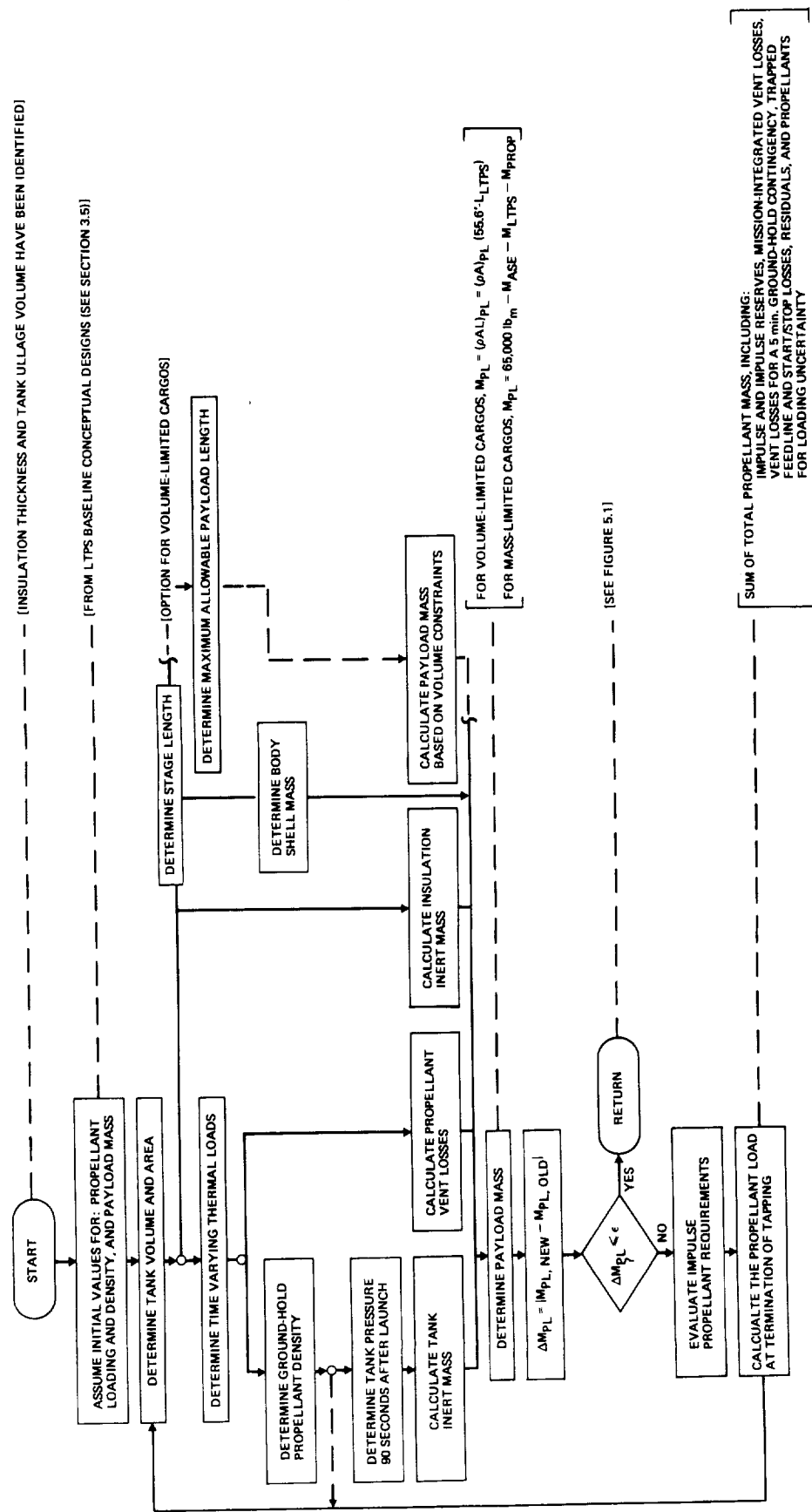


Figure 5-2: LTPS Payload Calculation Logic Flow



A convergence check, comparing currently predicted payload mass with the value calculated in the previous iteration, is made. If the convergence criterion is not satisfied, a new iteration is entered.

Listings of two versions of the LTPS sizing model are provided in Appendix F. The first version, TRADE, was developed with the assumption that a natural convection thermal environment existed in the purge enclosure during ground hold conditions. In the second version, TRADE2, it was assumed that enhanced convection existed in the purge enclosure and the MLI outer layer was maintained at 294°K (70°F) during insulation purge.

### 5.3.3 Algorithms and Calculation Details

LTPS parametric design and thermal performance data was incorporated into the TRADE and TRADE2 sizing programs. The following table shows where each set of parametric data resides in the programs and refers to the figure number in this report where the data is presented graphically. The parametric design data is discussed in section 5.4.

<u>Data Description</u>	<u>Subroutine Name</u>	<u>Reference Figure No.</u>
MLI thickness as a function of foam thickness for MLI/foam interface temperatures of 244°K (-20°F), 200°K (-100°F) and 144°K (-200°F).	THMIN	4-20, 4-21 and 4-22
Heat flux through He-purged MLI during ground hold as a function of inverse MLI thickness.	GRFLX	4-23
Heat flux through N <sub>2</sub> -purged MIL during ground hold as a function of effective conductance through MLI and foam.	GRFLX	4-24
Time-averaged heat flux through helium purged MLI from ascent through Orbiter/LTPS separation as a function of inverse MLI thickness.	TRFLX	4-25
Time-averaged heat flux through N <sub>2</sub> -purged MLI/foam from ascent through Orbiter/LTPS separation as a function of effective insulation conductance per unit thickness of MLI.	TRFLX	4-26
Time-averaged heat flux through He-purged MLI and N <sub>2</sub> -purged MLI/foam from Orbiter/LTPS separation through disposal orbit insertion as a function of inverse MLI thickness.	SPFLX	4-27
Tank mass as a function of tank volume.	WTANK	5-4
Tank mass as a function of tank pressure.	WTANK	5-3

Propellant effective liquid density as a function of percent ullage volume and tank heat leak during ground hold.

REDDEN

5-5 & 5-6

Tank pressure after 90 second lockup as a function of heat leak and percent ullage volume.

ROUTINE IN  
MAIN PROGRAM

5-7 & 5-8

Mass ratios for the 8-burn LEO to GEO orbit transfer described in Section 3.2 and for the insertion of the LTPS into disposal orbit were assumed to be constants for all LTPS designs analyzed by TRADE and TRADE2. The following mass ratio values were used in the programs:

$$\frac{\text{Mass of LTPS \& Payload prior to first engine burn}}{\text{Mass of LTPS \& Payload after circularization burn}} = 2.823$$

$$\frac{\text{Mass of LTPS prior to transfer to disposal orbit}}{\text{Mass of LTPS after insertion into disposal orbit}} = 1.0229$$

These ratios were based on the results of vehicle performance calculations for a specific impulse of 4560 N-sec/kg.

The TRADE and TRADE2 programs employed the following expressions to calculate LTPS and payload mass.

$$\text{LTPS PAYLOAD MASS 1} = \text{ORBITER PAYLOAD MASS LIMIT} - \text{ASE MASS} - \text{LIFT-OFF PROPELLANT MASS} - \text{INERT MASS}$$

$$\text{LTPS PAYLOAD MASS 2} = \text{PAYLOAD DENSITY} \times \left( \text{AVAILABLE ORBITER CARGO BAY VOLUME} - \text{LTPS VOLUME} \right)$$

where:

$$\text{ORBITER PAYLOAD MASS} = 29478 \text{ kg (65,000 lbm)}$$

$$\text{ASE MASS} = 2536 \text{ kg (5592 lbm) for tandem ellipsoidal tank LTPS and } 2548 \text{ kg (5618 lbm) for toroidal LO}_2 \text{ tank LTPS}$$

$$\text{LIFT-OFF PROPELLANT MASS} = \text{MAIN IMPULSE PROPELLANTS} + \text{START/STOP LOSSES} + \text{VENT LOSSES} + \text{PROPELLANT LOADING UNCERTAINTY PENALTY} + \text{5-MINUTE CONTINGENCY GROUND HOLD PENALTY}$$

$$\text{INERT MASS} = \text{TANK MASS} + \text{INSULATION MASS} + \text{BODY SHELL MASS} + \text{MISC STRUCTURE \& EQUIPMENT MASS}$$

$$\text{AVAILABLE} = 16.9 \text{ m (55.6 ft)}$$

ORBITER  
CARGO BAY  
LENGTH

$$\text{LTPS LENGTH} = \frac{\text{LH}_2 \text{ TANK}}{\text{LENGTH}} + \frac{\text{LO}_2 \text{ TANK}}{\text{LENGTH}} + \frac{2 \times \text{LH}_2 \text{ TANK}}{\text{INSULATION THICKNESS}} + \frac{2 \times \text{LO}_2 \text{ TANK}}{\text{INSULATION THICKNESS}} + \text{FIXED REFERENCE LENGTH}$$

The programs compared the two values of payload mass and selected the smaller of the two as the correct value. If:

$$\text{LTPS PAYLOAD MASS 1} < \text{LTPS PAYLOAD MASS 2}$$

then the LTPS payload mass was limited by the Orbiter payload mass capability. On the other hand, if:

$$\text{LTPS PAYLOAD MASS 2} < \text{LTPS PAYLOAD MASS 1}$$

then the LTPS payload mass was limited by the length of the Orbiter cargo bay available volume.

#### 5.4 LTPS DESIGN PARAMETRICS

Insulation design was found to affect LTPS mass and length (and therefore payload mass) in the following manner:

- a. Insulation design influences the heat leak into propellant tanks and therefore impacts:
  1. propellant vent loss,
  2. effective liquid density of the propellant due to vapor bubbles,
  3. peak tank pressure due to self pressurization during vent valve lock-up,
  4. tank volume (and length for maximum diameter tanks) and tank mass.
- b. Insulation design impacts the inert mass of the LTPS. The greater the insulation thickness and density, the greater the inert mass.
- c. Insulation thickness affects the LTPS overall length, and therefore impacts payload mass for volume-limited cargos.
- d. Insulation thickness affects LTPS body shell mass directly by influencing insulated tank overall length and indirectly by influencing tank pressure shell length due to the effect of heat leak on tank volume.

The relationship between insulation design and the variables affecting LTPS mass and length were developed and expressed in mathematical terms. These mathematical relationships provided the parametric data that was used to predict the influence of insulation design variables on LTPS payload mass and identifying optimum insulation concepts.

This section describes the parametric design data that was developed for the LTPS sizing model. The model itself is described in the previous section (5.3 LTPS Sizing Model). The following specific sets of parametric information are discussed:

- a. Insulation parametrics including;
  1. the relationship between foam thickness and MLI thickness for constant values of MLI/foam interface temperature,
  2. the relationship between insulation design and heat leak through the insulation, and
  3. insulation mass as a function of thickness and insulation type.
- b. Propellant tank parametrics, including the effect of volume on tank mass and the effect of peak pressure differential (between the inside of the tank and outside) on tank mass.
- c. The influence of heat leak on effective liquid density during ground hold conditions.
- d. The effect of ullage volume and heat leak on tank peak pressure due to self-pressurization during vent valve lock-up.
- e. The effect of tank length and insulation thickness on structural mass.

#### **5.4.1 Insulation Parametrics**

For the case of MLI/foam insulations, an infinite number of foam thicknesses are possible for each interface temperature. However, for any value of foam thickness, there exists only one corresponding value of MLI thickness that will give a selected interface temperature.

The assumed heat transfer environment between the outer layer of MLI and the outside of the purge enclosure (the LTPS body shell in this case) affects the relationship between MLI and foam thickness. For a given value of foam thickness, the greater the thermal coupling between MLI and LTPS body shell, the greater the MLI thickness required to maintain a specified interface temperature. The relationships between MLI thickness and foam thickness were determined by mathematically modeling the heat transport through MLI/foam insulations as described in section 4.3 of this report. The result of this analytical effort was a set of linear functions relating MLI thickness and foam thickness. These relationships are shown graphically in Figures 4-20, 4-21 and 4-22. The solid lines denote a natural convection environment within the purge enclosure and the dashed lines represent an enhanced convection environment in which the MLI outer layer was assumed to be maintained at 294°K. The data in these charts were used in the LTPS sizing model to calculate MLI thickness for specified values of foam thickness and interface temperature.

One of the primary results of the initial LTPS thermal analysis, performed under Task I, was the fact that insulation heat leak during all mission phases (ground-hold as well as in-space) played a major role in sizing the LTPS.

Insulation heat leak affected payload mass through its effect on: 1) propellant vent loss, 2) tank volume, wall thickness and mass, and 3) effective liquid density at the conclusion of tank fill. Since there were to be a large number of LTPS conceptual designs to be analyzed in the evaluation of optimum insulation combinations, it was necessary to develop parametric data relating insulation characteristics to heat leak. This parametric data was required because the cost of performing a full mission thermal analysis for each LTPS design considered in the insulation optimization process, would have been prohibitive.

Parametric insulation performance data was developed from the thermal analyses performed on the 3 baseline LTPS vehicles as discussed in section 4.4. These analyses predicted the LH<sub>2</sub> and LO<sub>2</sub> heat leaks from beginning of mission (ground-hold operations) through LTPS injection into disposal orbit for a range of insulation thicknesses. Time-averaged tank insulation heat fluxes were calculated from predicted heat leak timelines (see Figures 4-11 and 4-13).

This calculation was accomplished by first subtracting strut and penetration heat leaks from the total tank heat leak to obtain the heat leak attributable to the insulation system. The insulation heat leak was then time-averaged over 3 mission phases and the average values divided by tank surface area to arrive at average fluxes. The 3 mission phases over which average heat flux values were calculated were as follows:

- a. Ground hold through MLI evacuation
- b. MLI evacuation through LTPS/Orbiter separation
- c. LTPS/Orbiter separation through disposal orbit injection.

Time-average tank insulation heat fluxes for the baseline LTPS vehicles were converted into parametric insulation performance data by correlating the predicted average heat fluxes with insulation conductance parameters. Figures 4-23 through 4-27 summarize the insulation performance curves that were developed for the LTPS sizing model. Figure 4-23 shows the relationship between insulation heat leak during ground-hold MLI purging and the reciprocal of MLI thickness for He-purged MLI. The reciprocal of MLI thickness is proportional to the effective conductance of purged MLI ( $K_{MLI}$ ). That is,

$$\frac{1}{S_{MLI}} = K_{MLI} \left( \frac{1}{k_{cond} + k_{rad}} \right)$$

where

- |                  |  |
|------------------|--|
| $K_{MLI}$ =      | effective thermal conductance per unit area of MLI – W/cm <sup>2</sup> -°K             |
| $\delta_{MLI}$ = | thickness of MLI – cm  |
| $k_{cond}$ =     | effective thermal conductivity of purged MLI due to conduction heat transfer – W/cm-°K |
| $k_{rad}$ =      | effective radiation conductivity of purged MLI – W/cm-°K                               |

In the case of the natural convection boundary condition at the outer surface of the MLI, the heat leak is dependent on tank shape as well as tank type (i.e., LH<sub>2</sub> or LO<sub>2</sub>). This

dependency on tank shape is due to the fact that the magnitude of the natural convection heat transfer coefficient at the MLI outer surface is dependent on the orientation of the surface (i.e., vertical, downward-facing or upward-facing). For the enhanced convection environment condition, this dependency did not exist since it was assumed that the MLI outer layer was uniformly maintained at 294°K. Heat leak fluxes ranged from 100 to 600 W/m<sup>2</sup> for the He-purged MLI designs considered in the subject analysis.

Figure 4-24 shows the relationship between insulation heat flux and the overall effective insulation conductance for N<sub>2</sub>-purged MLI/foam combinations. Heat leak fluxes ranged from 50 to 300 W/m<sup>2</sup>. The fact that heat leak fluxes through MLI/foam combinations were generally less than half that of MLI-only, for equal insulation thicknesses, was due almost entirely to the fact that the thermal conductivity of N<sub>2</sub> is less than one-fifth that of He.

Figures 4-25 and 4-26 show predicted insulation heat leak flux during the mission phase extending from MLI evacuation through LTPS Orbiter separation. For the case of He-purged MLI systems it was found that predicted time-averaged heat fluxes correlated with the reciprocal of MLI thickness. However, for MLI/foam combinations, it was found that the stored thermal energy of the MLI and foam (as typified by the temperature gradients through each) prior to launch, played a significant role in the insulation heat leak flux during this transition period. Hence, as shown in Figure 4-26, it was found that predicted heat fluxes through N<sub>2</sub>-purged MLI/foam insulation could best be correlated by the nonexplicit expression:

$$\text{Heat flux} = \frac{f(\text{Heat flux})}{\delta_{\text{MLI}}(T_{\text{External MLI}} - T_{\text{Tank}})}$$

In order to calculate insulation heat flux from the curves in Figure 4-26, it was necessary to solve iteratively by trial and error.

During the third mission phase, there was little change in the predicted thermal gradients through either the MLI or MLI/foam insulation. In this phase, from LTPS/Orbiter separation through disposal orbit injection, the heat leak was controlled almost totally by the MLI performance. This predominance of the MLI was due to the fact that the thermal resistance through evacuated MLI was much greater than the resistance through a comparable thickness of foam. Therefore, as shown in Figure 4-27, it was found that for both MLI-only and MLI/foam insulations, heat leaks correlated with the reciprocal of MLI thickness.

The relationship between insulation mass and insulation thickness was assumed to be expressed as:

$$\text{Insulation Mass} = \text{Tank Surface Area} \times (\text{foam thickness} \times \text{foam density} + \text{MLI thickness} \times \text{MLI density})$$

This expression ignores the fact that insulation surface area increases with thickness. However, for the range of insulation thickness considered (0 to 12 cm) this simplification introduced a negligible error into the mass calculation.



### 5.4.2 Propellant Tank Parametrics

A parametric study was conducted to determine the dependence of cryogenic tank weight upon design internal pressures. Such weights were required for their contributions to mass-limited payload determination and for pressure-volume trades needed to optimize tank sizing for tank locsidered (0 to 12 cm) this simplification-up pressure rises.

The OTV (Reference 1) LH<sub>2</sub> and LO<sub>2</sub> tank designs were used as baselines in the development of weight-pressure relationships. The reference identified weights of the tank membranes, weld lands and tolerances, manhole and local beef-ups and support structure. The support structure weights were further broken down to the contributions from the main support ring, struts, strut brackets and pins, and the thrust ring for the LO<sub>2</sub> tank. For the purpose of parametric pressure sizing, two basic groundrules were adopted:

- a. Weight versus pressure is linear for tank membranes, weld lands, manhole, and local beef-up components.
- b. Weight of the support structure varies linearly with the change in the total loaded tank weight, as influenced by variation from (a) above.

The results of the parametric tank weight versus pressure study are shown in Figure 5-3.

This figure shows that the mass of both LO<sub>2</sub> and LH<sub>2</sub> tanks are independent of pressure until the wall thickness required for strength exceeds minimum gage. Beyond the transition region, mass increases linearly with pressure.

Figure 5-4 shows the relationship between tank mass and volume that was used in the TRADE and TRADE 2 LTPS sizing programs. Values of mass and volume for the reference LO<sub>2</sub> and LH<sub>2</sub> tanks are given. Note that the dashed line represents both toroidal and ellipsoidal LO<sub>2</sub> tanks.

### 5.4.3 Propellant Density

The effective density of the loaded propellant during ground hold operation is dependent on the heat flux through the tank walls. The presence of vapor bubbles at the tank walls, as well as those rising through the liquid, in effect decrease the density of the propellant in the tank. As the heat flux to the tank increases, the total volume of bubbles formed at the wall, and rising through the liquid, increases. Therefore, the effective density of the tanked liquid propellant, which decreases with increasing heat flux, can be expressed as:

$$\text{Effective liquid density} = \frac{(\text{vapor bubble volume} \times \text{vapor density} + \text{liquid volume} \times \text{liquid density})}{\text{total volume}}$$

The impact of decreased effective density on LTPS mass and size is to increase tank volume (and length and mass) for a given liquid propellant mass loading requirement.

In calculating the effect of ground hold heat leak (through insulation, tank support struts and other insulation penetrations) on propellant effective liquid density, it was assumed that the liquid and vapor phases were in thermodynamic equilibrium at saturation conditions. Hence all the heat leak through the tank walls was assumed to vaporize liquid.

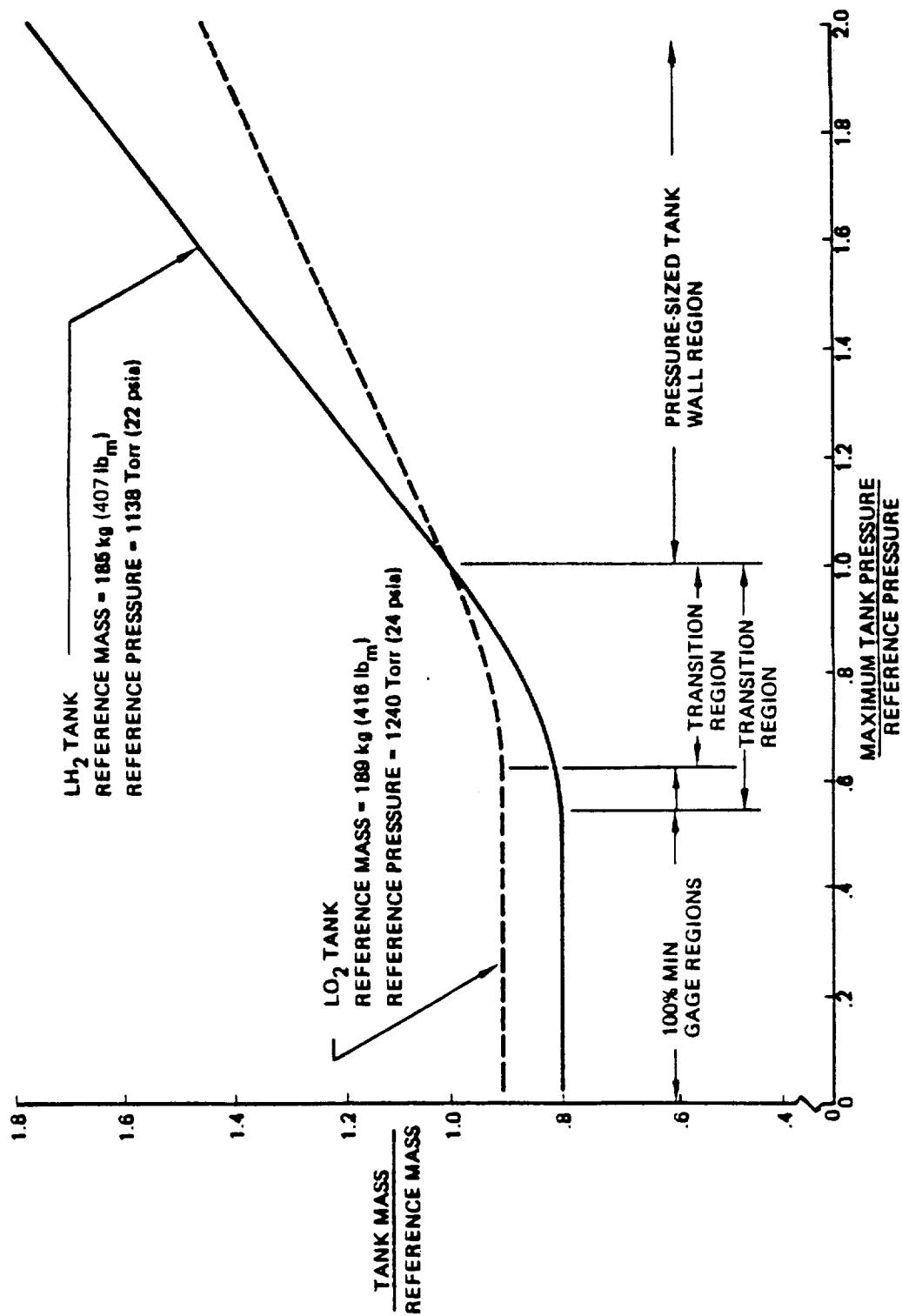


Figure 5-3: Tank Mass Dependency on Internal Pressures

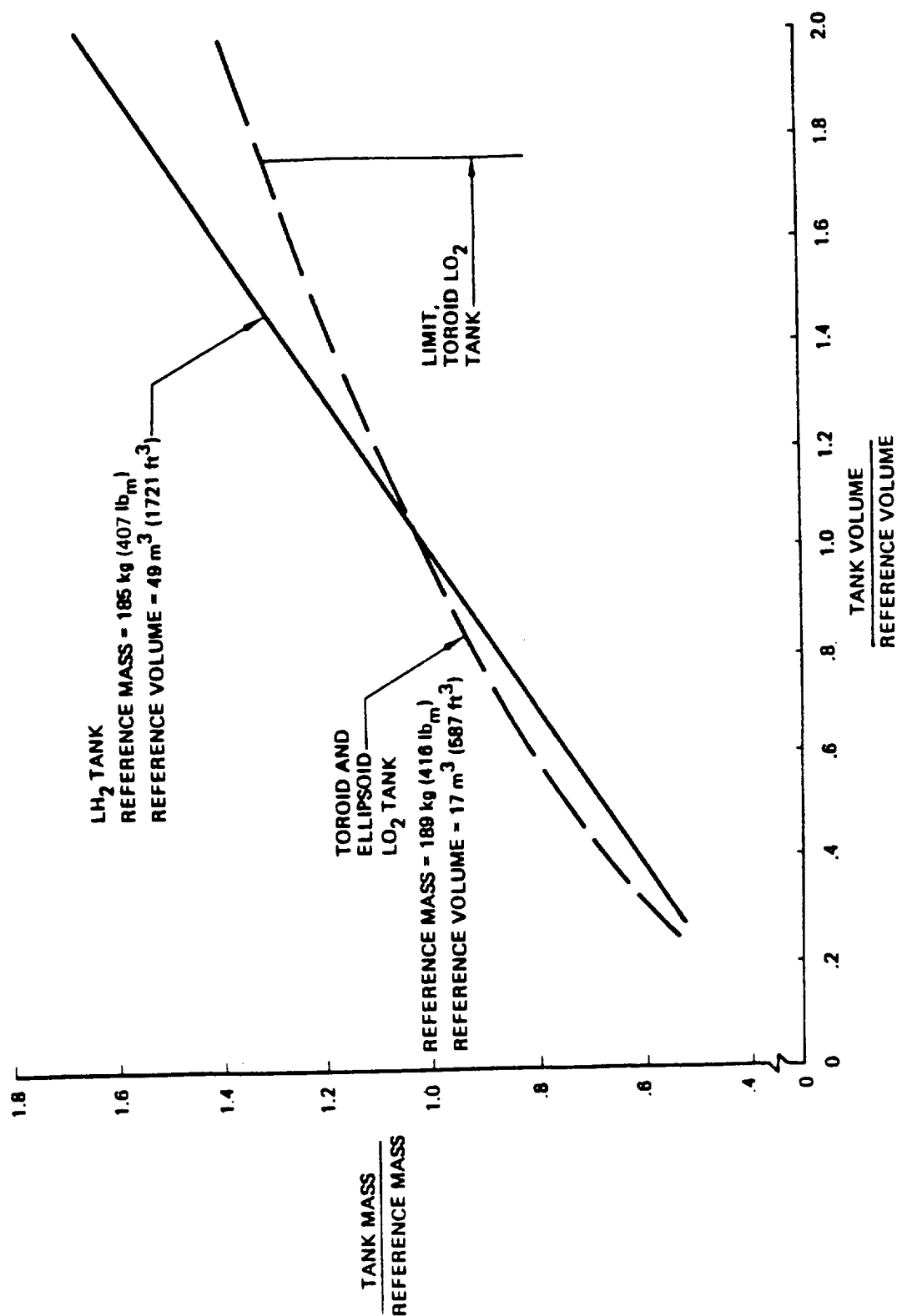


Figure 5-4: Tank Mass Dependency on Tank Volume

Vapor bubble size and terminal velocity in the liquid were calculated by the methods described in Appendix D. Terminal velocity and average rise distance were used to calculate average residence time of vapor bubbles in the propellant liquid phase for the 3 baseline LTPS tank designs described in section 3.5 of this report. Rise distance was dependent on tank shape and ullage volume. Therefore, the rise distance in the shorter toroidal tanks was less than the rise distance in ellipsoidal dome tanks of equal volume. For a given tank configuration, rise distance decreased with increasing ullage volume. Since bubble residence time was directly proportional to rise distance, the effective propellant density, for a given heat leak value, was greater in short tanks than in long tanks and increased with increasing ullage volume.

Figures 5-5 and 5-6 show typical sets of parametric data that were developed to relate effective propellant density to ground hold heat flux and percent ullage volume. These charts are for the ellipsoidal dome LH<sub>2</sub> and LO<sub>2</sub> tanks of the baseline Task II LTPS shown in Figure 3-7. The heat flux in these charts is the total ground-hold heat leak to the propellant, including contribution of the insulation, struts and other insulation penetrations, divided by the total surface area of the tank.

#### **5.4.4 Self Pressurization**

As described in the section 3.2.3 discussion of the selected mission timeline, it was assumed the LTPS propellant tanks were not allowed to vent during the first 90 seconds of launch. This restriction would be imposed for safety reasons. After 90 seconds it was assumed that sufficient altitudes would be reached that venting overboard could be resumed. During the period of no venting the pressure in the propellant tanks would rise.

This tank self-pressurization is caused by continued boiling of the propellant after vent-valve lock-up at launch. The resultant pressure rise can, under certain circumstances, determine the peak design pressure of the tank. This circumstance occurs if the pressure at the end of lock-up exceeds the normal vent valve opening pressure.

The pressure rise during lock-up depends upon the magnitude of the heat leak into the tank, the mass of liquid in the tank, the percent ullage volume and the thermodynamic state of the liquid and vapor phases.

A simplified approach was taken in relating tank pressure rise to heat leak and percent ullage volume. The details of the analysis are described in Appendix E. In essence, for the purpose of sizing tank wall thickness, it was assumed that the correlations between pressure rise rate and percent ullage volume and heat leak described in References 17 and 18 were valid for the LTPS. Centaur tank self pressurization measurements made during actual launches were used to determine the correlation constant.

Figures 5-7 and 5-8 show typical parametric data that were developed to relate tank peak pressure to heat leak during the first 90 seconds after launch and percent ullage volume. These charts are for the LH<sub>2</sub> and LO<sub>2</sub> tanks of the baseline LTPS shown in Figure 3-7. Similar sets of data were developed for the other two baseline LTPS vehicles.

#### **5.4.5 Structural Mass**

Structural mass (i.e., the LTPS body shell and other load carrying structure) is dependent on tank volume and insulation thickness. As the insulation thickness increases and the tank volumes increase (in the case of maximum diameter tanks) the LTPS structure must increase in length accordingly. For the purpose of developing parametric structure mass

- HYDROGEN TANK
- TANK VOLUME =  $27.3 \text{ m}^3$  (964  $\text{ft}^3$ )
- SATURATED LIQUID DENSITY =  $70.00 \text{ kg/m}^3$  (4.369  $\text{lb}_m/\text{ft}^3$ )

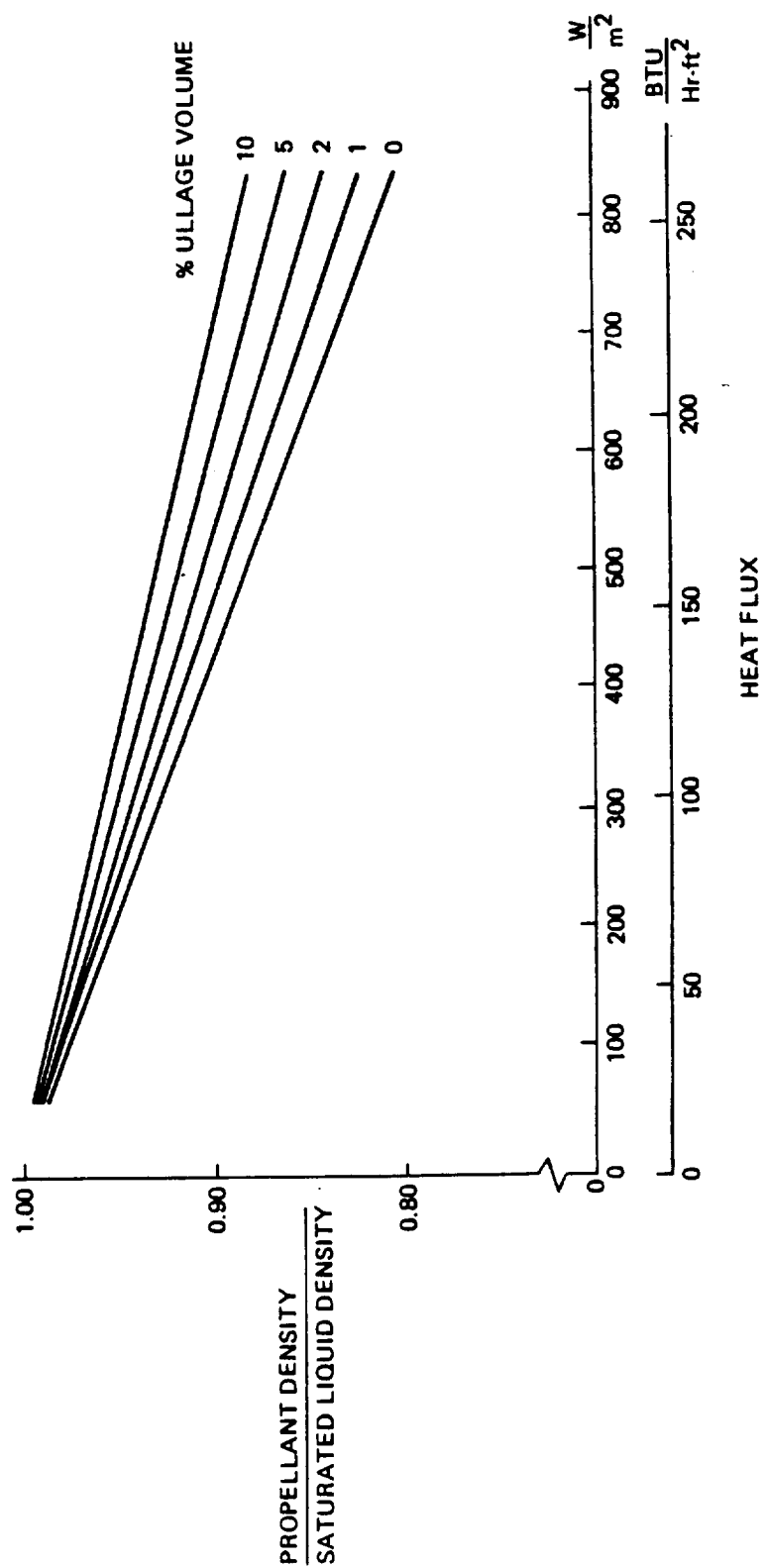


Figure 5-5: Effect of Heat Flux on Density of Tanked  $\text{LH}_2$

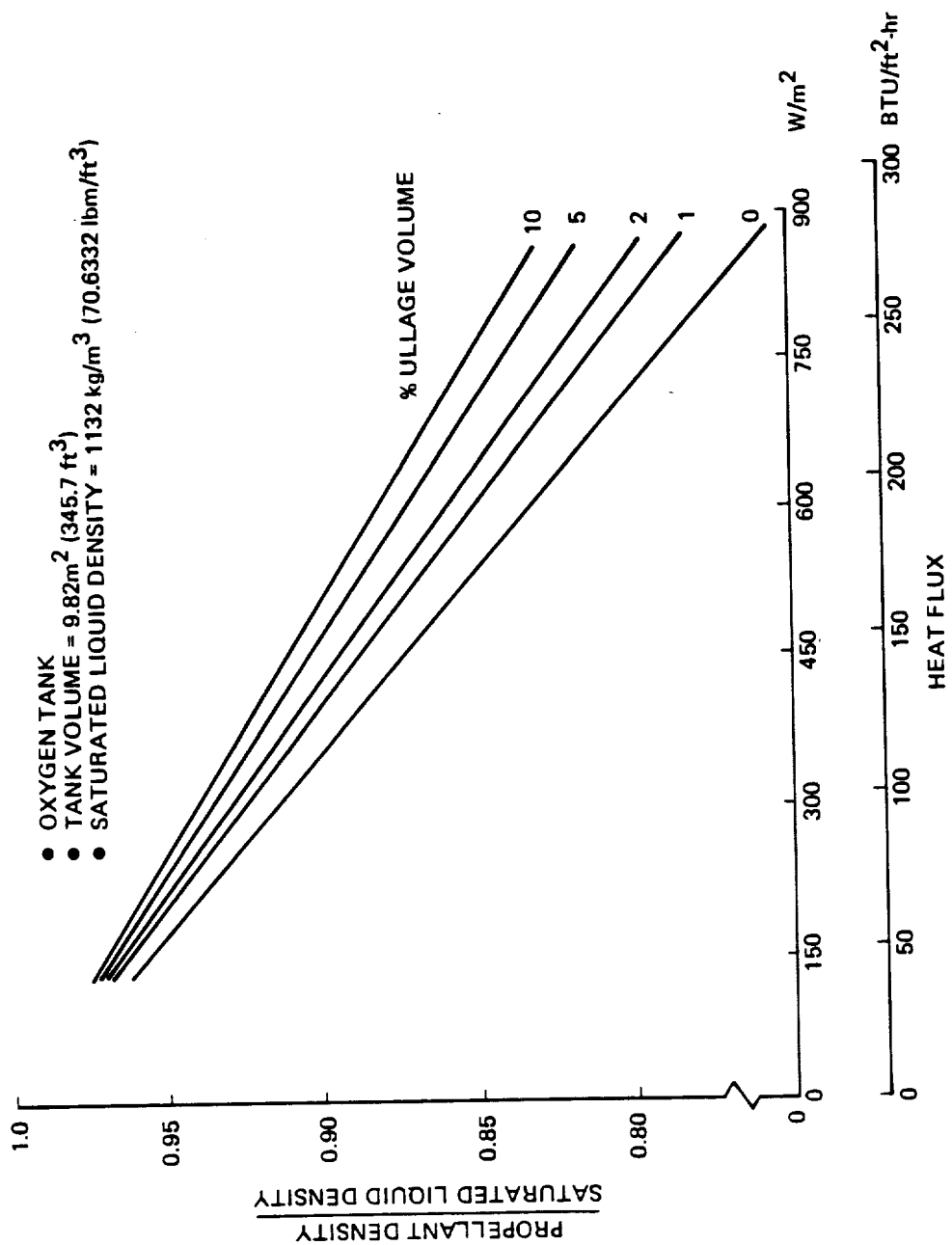


Figure 5-6: Effect of Heat Flux on Density of Tanked LO<sub>2</sub>

- HYDROGEN TANK
- TANK VOLUME =  $27.3 \text{ m}^3$  (964  $\text{ft}^3$ )
- INITIAL TANK PRESSURE = 1.2 ATM (18 psia)

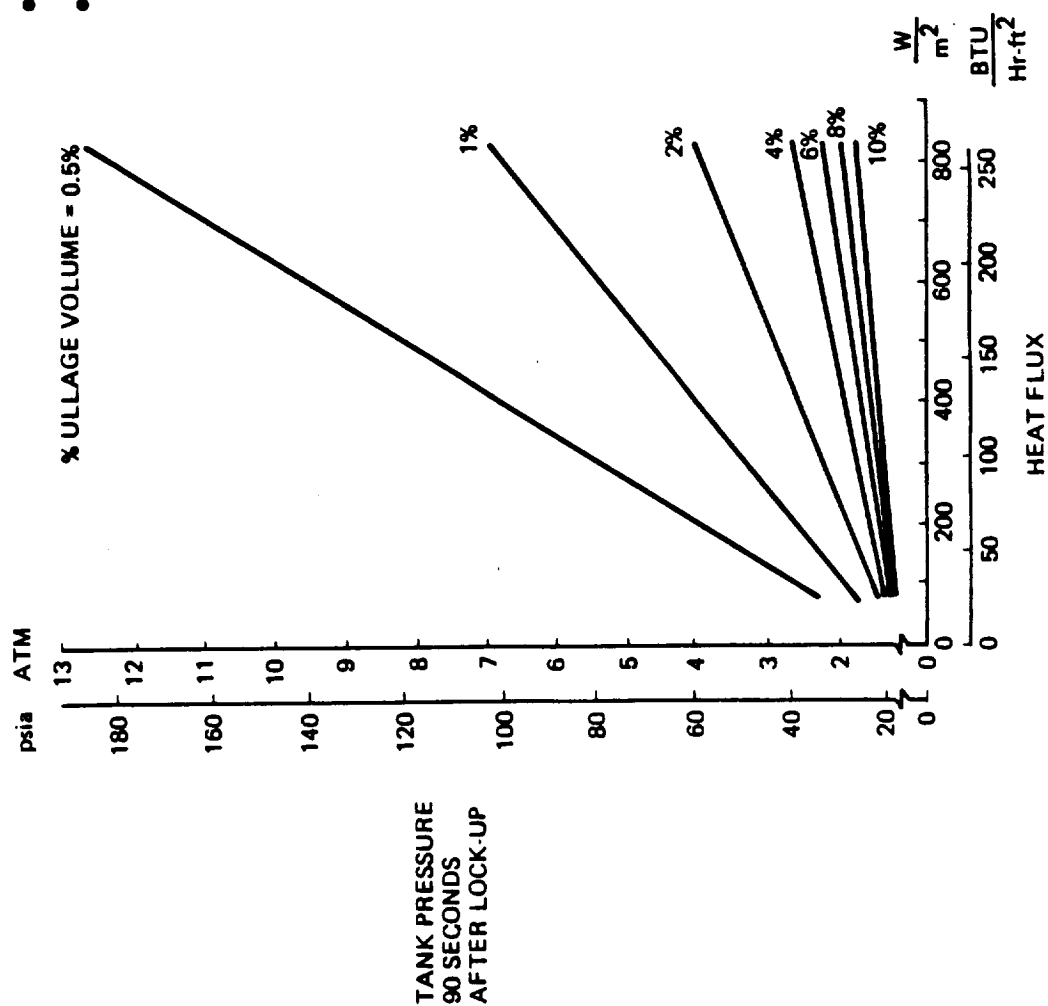


Figure 5-7: Effect of Heat Flux on  $\text{LH}_2$  Tank Self-Pressurization

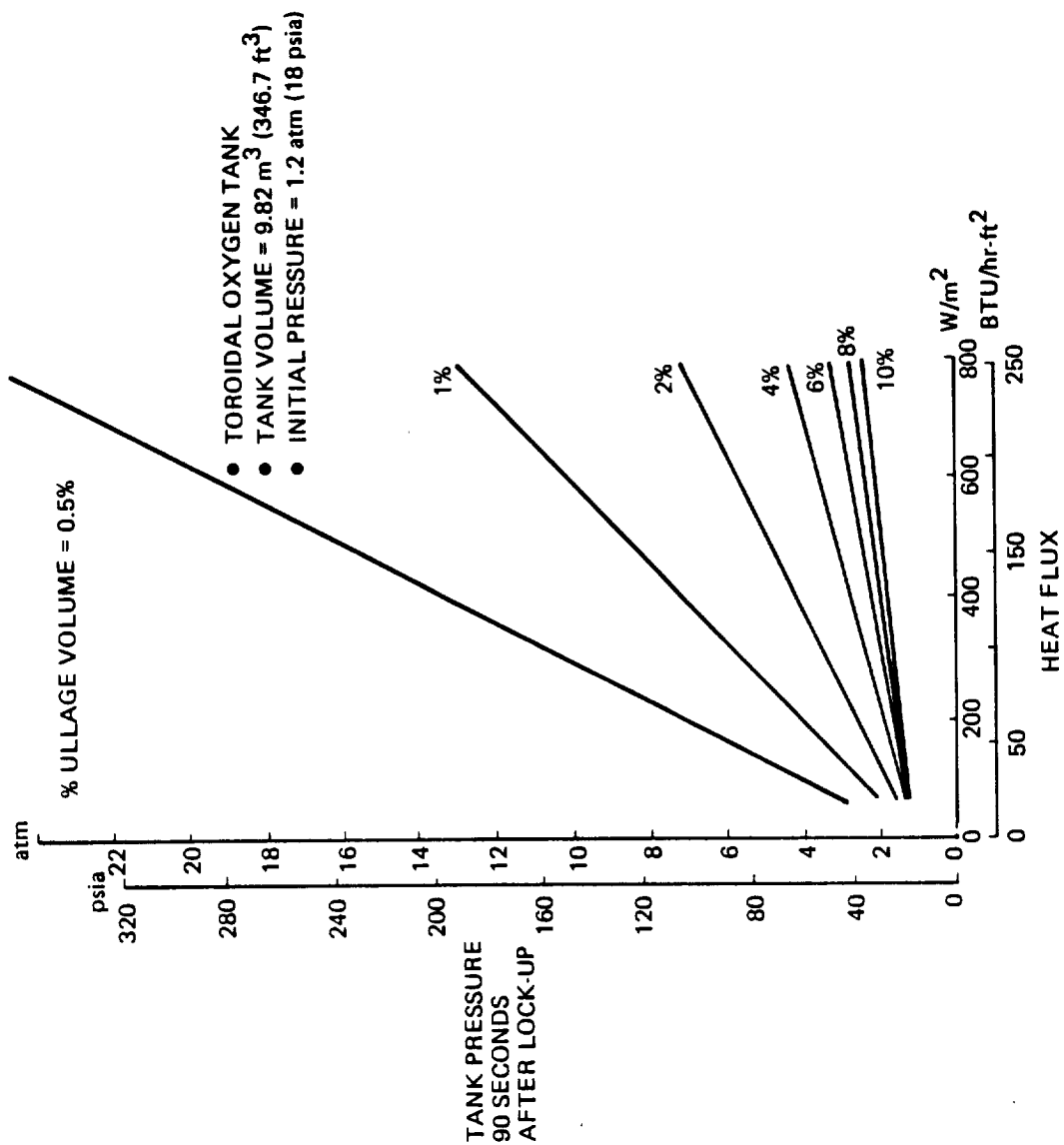


Figure 5-8: Effect of Heat Flux on LO<sub>2</sub> Tank Self-Pressurization



data, it was assumed that each LTPS baseline vehicle had a characteristic length that was invariant as the tank volume and insulation thickness changed. This characteristic length included the following elements:

- a. Clearance between the LH<sub>2</sub> tank forward dome and the payload interface ring.
- b. Clearance between the LH<sub>2</sub> tank aft dome and the LO<sub>2</sub> tank.
- c. Engine and thrust structure between the engine gimbal and LO<sub>2</sub> tank aft dome (for the tandem ellipsoidal tank LTPS shown in Figure 3-7). For the toroidal LO<sub>2</sub> tank baseline LTPS vehicles (Figures 3-8 and 3-9) this length element consisted of a standard distance between the exit plane of the engine nozzle and the aft surface of the toroidal tank.
- d. Clearance between the nozzle exit plane and the aft bulkhead of the Orbiter cargo bay.

The assumed invariant characteristic lengths for the baseline vehicles and all size perturbations about them were as follows:

LTPS PAYLOAD PACKAGED DENSITY	ASSUMED INVARIANT LTPS LENGTH ELEMENT
56 (kg/m <sup>3</sup> )	154.7 cm
40 (kg/m <sup>3</sup> )	184.4 cm
24 (kg/m <sup>3</sup> )	168.4 cm

In addition to the above invariant dimensions, the LTPS overall length included the axial dimensions of each tank and twice the insulation thickness on each tank. Thus the overall stage length was expressed as:

$$\begin{array}{lcl} \text{Overall} & & \\ \text{LTPS} & = & \text{Invariant} \\ \text{Length} & & \text{Length} \\ & & \text{Including} \\ & & \text{Engines, etc} \end{array} + \begin{array}{l} \text{LH}_2 \\ \text{Tank} \\ \text{Length} \end{array} + \begin{array}{l} \text{LO}_2 \\ \text{Tank} \\ \text{Length} \end{array} + 2 \times \begin{array}{l} \text{LH}_2 \text{ Tank} \\ \text{Insulation} \\ \text{Thickness} \end{array} + 2 \times \begin{array}{l} \text{LO}_2 \text{ Tank} \\ \text{Insulation} \\ \text{Thickness} \end{array}$$

Structural mass was related to changes in LTPS overall length caused by dimensional changes in the tanks and insulation. The governing expression that was developed for this relationship was

$$\begin{array}{l} \text{Structural Mass} = \\ \text{(not including tanks)} \end{array} M_{INV} + A \times (L_{H_2} + L_{O_2} + 2 \times (I_{H_2} + I_{O_2}))$$

where

$$\begin{array}{ll} M_{INV} & = \text{The portion of the total structural mass that is assumed} \\ & \text{invariant with changes in tank length and insulation thickness} \\ A & = \text{Structural mass per unit length of LTPS body shell (excluding} \\ & \text{avionics ring, payload interface ring, fuel cell radial tank} \end{array}$$

support rings, etc. which were included in  $M_{INV}$ ). The value of  $A$  was calculated to be 39.2 kg/m.

$L_{H_2} \& L_{O_2} =$  Overall length of hydrogen and oxygen tanks respectively.

$I_{H_2} \& I_{O_2} =$  Thickness of  $H_2$  and  $O_2$  tank insulation.

The above expression was used to develop data which related structural mass to LTPS tank and insulation combined length for each of the 3 baseline vehicles. It was included in the LTPS sizing model as part of the payload mass calculation algorithm.

## 5.5 INSULATION OPTIMIZATION RESULTS

Twenty-six LTPS vehicles were sized for He-purged MLI and  $N_2$ -purged MLI/foam insulation systems. In each case, the optimum insulation thickness for maximum payload delivery to GEO was found with the aid of two computer programs TRADE and TRADE2. The search for optimum insulation thickness was conducted by using these computer programs to predict LTPS payload mass for a range of insulation thickness. Once the optimum value was bounded, a process of estimation and correction was used to converge on the value of insulation thickness that maximized payload mass. Optimum insulation thickness for the  $LO_2$  and  $LH_2$  tanks were calculated separately. It was assumed that the optimized insulation thicknesses for the  $LH_2$  and  $LO_2$  tanks were independent. Therefore the LTPS design that incorporated the independently-optimized  $LH_2$  and  $LO_2$  tank insulation designs was assumed to have the maximum payload placement capability.

Table 5-2 identifies the 13 LTPS optimum insulation designs that were analyzed for each of the 2 purge enclosure thermal conditions (natural convection and enhanced convection) assumed to exist during ground hold operations. Key results of these calculations were:

- a. The assumed heat transfer environment in the MLI purge enclosure had a major impact on predicted LTPS payload placement capability. For He-purged MLI insulated tanks, the natural convection purge enclosure environment resulted in the greatest LTPS payload placement capability. However, for  $N_2$ -purged MLI/foam insulations, payload placement capability was greatest for the enhanced convection environment. It was found that for He-purged MLI designs, the natural convection purge enclosure environment assumption lead to LTPS payload placement capability 54 to 208 kg (119 to 459 lbm) greater than the payload placement capability predicted for the enhanced convections environment. In the case of MLI/foam combinations, the natural convection environment assumption lead to payload placement capability as much as 431 kg (950 lbm) below the values predicted for enhanced convection.
- b. The application of enhanced-convection  $N_2$ -purged MLI/foam insulation in place of natural-convection He-purged MLI either improved LTPS payload placement capability by up to 26 kg (57lbm) for the highest payload packaging density or decreased it by as much as 56 kg (123 lbm) in the case of the intermediate packaging densities.
- c. Propellant vent losses and insulation mass were the two elements of the LTPS that were most sensitive to changes in insulation thickness. LTPS payload placement capability was therefore optimized at approximately the point at which the sum of insulation mass and propellant vent loss mass were minimized.

NATURAL-CONVECTION AND ENHANCED CONVECTION GROUND-HOLD ENVIRONMENT						
PAYLOAD DENSITY kg/m <sup>3</sup> (lb <sub>m</sub> /ft <sup>3</sup> )	HYDROGEN-OXYGEN TANK CONFIGURATION	MLI – HELIUM PURGE (CHOSEN AS BASELINE)	MLI/FOAM – NITROGEN PURGE			
			TYPE FOAM			
			MINIMUM PURGE GAS TEMPERATURE, K (°F)			
			ROHACELL 31 244 (-20)	ROHACELL 31 200 (-100)	ROHACELL 31 144 (-200)	BX250A 200 (-100)
56 (3.6)	TANDEM ELLIPSOIDAL	X	X	X	X	
40 (2.6)	ELLIPSOIDAL H <sub>2</sub> – TOROIDAL O <sub>2</sub>	X	X	X	X	X
24 (1.5)	ELLIPSOIDAL H <sub>2</sub> – TOROIDAL O <sub>2</sub>	X	X	X	X	

Table 5-2: Insulation Designs Optimized in Task II

- d. LTPS payload mass was relatively insensitive to the percent ullage volume selected for the propellant tanks. The optimum percent ullage volumes ranged from approximately 10% for the highest payload packaging density to about 0.5% for the lowest payload packaging density.
- e. From the standpoint of LTPS payload placement capability, Rohacelle 31 foam was preferable to BX250A.

The following text describes the details of the insulation optimization analysis and presents the results in graphical and tabular format.

Figure 5-9 presents a typical LTPS/payload mass summary generated from the TRADE and TRADE2 computer program calculations. The solid curves are the results for a natural-convection purge enclosure environment, and the dashed curves represent the results for an enhanced convection environment. Payload packaged density was  $56 \text{ kg/m}^3$  for both cases and the MLI/foam interface temperature was  $144^\circ\text{K}$ . As can be seen, the optimum  $\text{LH}_2$  tank foam thickness for the enhanced convection purge environment is only about 0.56 cm as compared with 1.78 cm for the natural convection environment. This difference is caused by the fact that the low natural convection conductance between the LTPS body shell and the tank MLI required additional foam to maintain the selected MLI/foam interface temperature.

Insulation mass (foam + MLI) increases linearly with increasing foam thickness (MLI thickness was linearly proportional to foam thickness as shown in Figures 4-20 through 4-22). Propellant vent losses are seen to initially drop off rapidly with increasing foam thickness and then decrease slowly as larger values of foam thickness are reached. This phenomenon is caused by the fact that at low values of foam thickness the MLI thickness is also low (see Figures 4-20 through 4-22) and heat leaks during all mission phases are high. As the foam thickness is increased, the MLI thickness must also be increased to maintain the desired interface temperature and the heat leak through the insulation to the propellant is reduced. However, the heat leak through tank support struts and insulation penetrations is independent of insulation thickness and remains constant as foam thickness is increased. Hence at large values of foam thickness the total heat leak (and propellant vent loss) approaches a constant value determined by the strut and penetration heat leaks.

A typical set of results for the optimization of an LTPS with He-purged MLI-covered tanks is shown in Figure 5-10. This chart shows the predicted influence of MLI thickness on LTPS and payload length for the case in which packaged payload density is  $24 \text{ kg/m}^3$  (volume-limited cargo). The dashed lines represent TRADE2-predicted results for the enhanced convection purge enclosure environment and the solid lines represent the results predicted by TRADE for the natural-convection environment.

It can be seen that the LTPS optimum payload length and mass for the natural-convection He-purged environment condition occurs at a much lower value of MLI thickness than the optimum thickness for the enhanced convection condition. In addition, the optimum payload length and mass for the natural convection case are greater than the optimized length and mass predicted for the enhanced convection case. The primary impact of the assumed purge enclosure environment on payload length and mass occurred through the effect on tank length. For a fixed value of He-purged MLI thickness, the enhanced convection environment resulted in greater heat leaks during ground-hold. Hence tank volumes were larger to account for lower effective liquid density (due to boiling) and greater vent losses after tank topoff.

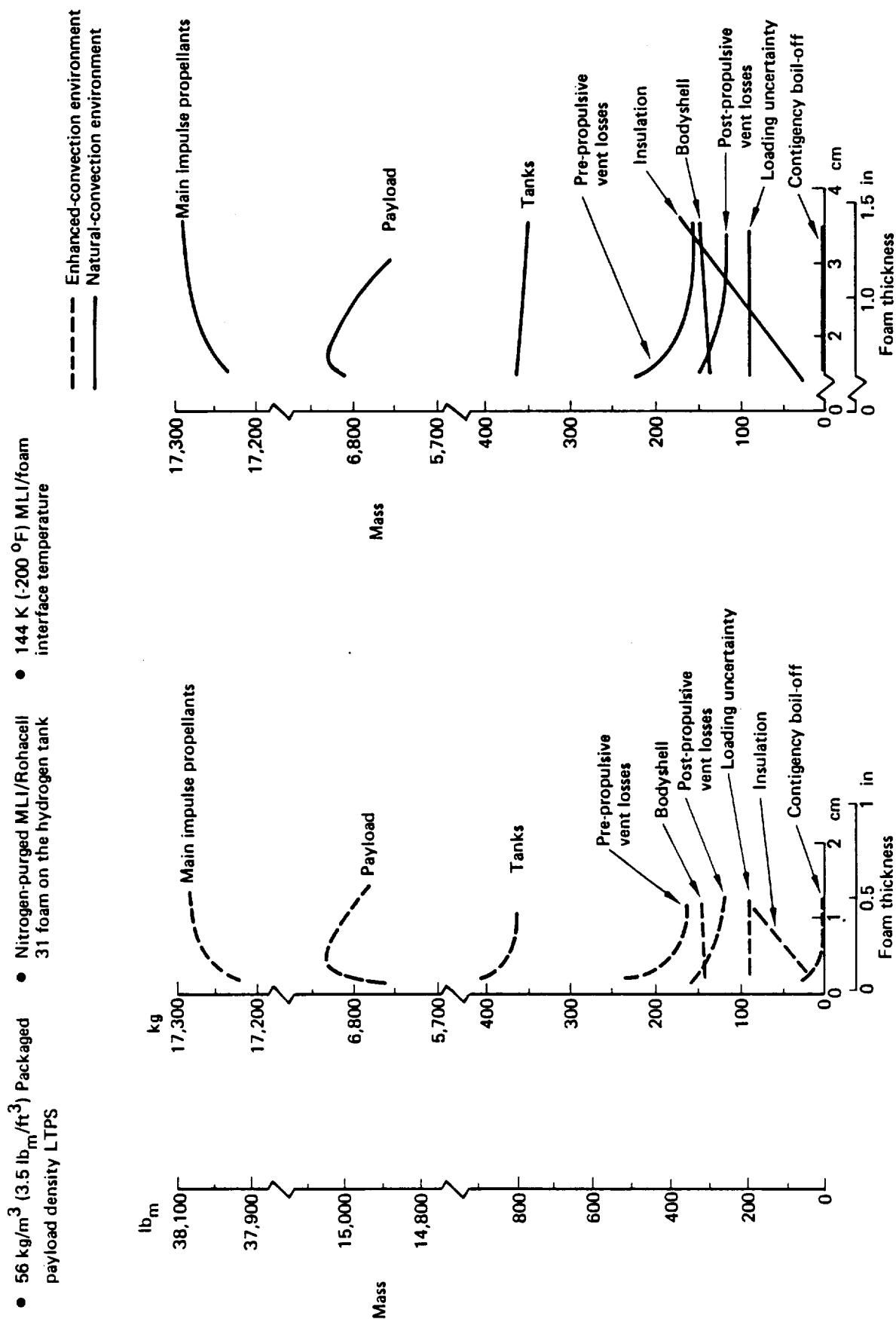


Figure 5-9: Effect of Foam Thickness on Payload and LTPS Subsystem Mass

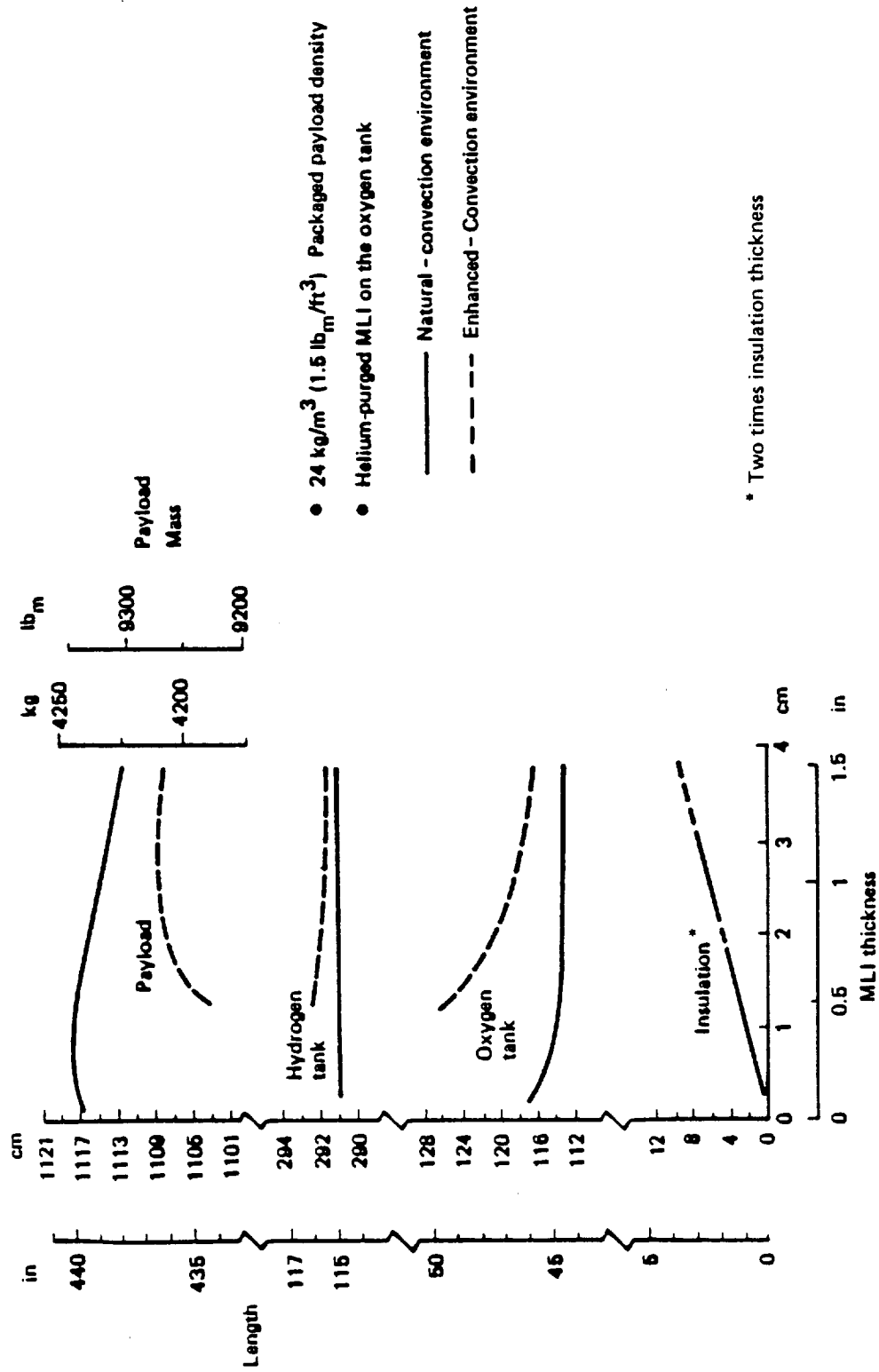


Figure 5-10 : Effect of MLI Thickness on Payload And LTPS Length for  
Volume-Limited Payloads

Typical LTPS payload optimization results for He-purged MLI and N<sub>2</sub>-purged MLI/foam insulation designs are presented in Figures 5-11, 5-12 and 5-13. These charts show the influence of insulation thickness and percent ullage volume on LTPS payload mass. Results are shown for He-purged MLI and N<sub>2</sub>-purged MLI/foam insulation concepts with a packaged payload density of 56 kg/m<sup>3</sup> (Figures 5-11 and 5-12) and for N<sub>2</sub>-purged MLI/foam with a packaged payload density of 24 kg/m<sup>3</sup> (Figure 5-13).

Several general trends are evident in these charts. Figure 5-11 shows that payload placement capability curves for He-purged MLI designs did not have sharply defined maxima when either MLI thickness or percent ullage volume were varied. Hence near the optimal values of MLI thickness and percent ullage volume, payload placement capability was fairly insensitive to small changes in either ullage volume or MLI thickness. However, for N<sub>2</sub>-purged MLI/foam insulations, reference to Figures 5-12 and 5-13 shows that payload placement capability was much more sensitive to foam thickness in the region of the optimal value. Hence for LTPS designs utilizing MLI/foam tank insulation, greater modeling accuracy is required to optimize insulation design for maximum payload mass.

In all cases analyzed, it was found that payload mass was not highly sensitive to percent ullage volume in the region of the optimal value.

The primary objective of the insulation optimization analysis was to evaluate how MLI/foam interface temperature affected LTPS performance. The payload placement capability of LTPS vehicles utilizing N<sub>2</sub>-purged MLI/foam insulation were compared with the performance of LTPS vehicles utilizing conventional He-purged MLI. In each case, the insulation system (insulation thickness) and percent ullage volume were optimized for maximum LTPS payload placement capability. As indicated in Table 5-2, four LTPS vehicles were optimized for each of three payload packaging densities (56 kg/m<sup>3</sup>, 40 kg/m<sup>3</sup> and 24 kg/m<sup>3</sup>). Four unique insulation designs were analyzed. One (the baseline for comparison), was He-purged MLI. The other three were N<sub>2</sub>-purged MLI/foam insulations, in which the MLI/foam interface was assumed to be maintained at either 144°K, 200°K or 244°K during purge operations prior to launch. In addition, one LTPS vehicle was optimized for BX250A foam to assess its benefits relative to the baseline foam, Rohacell 31.

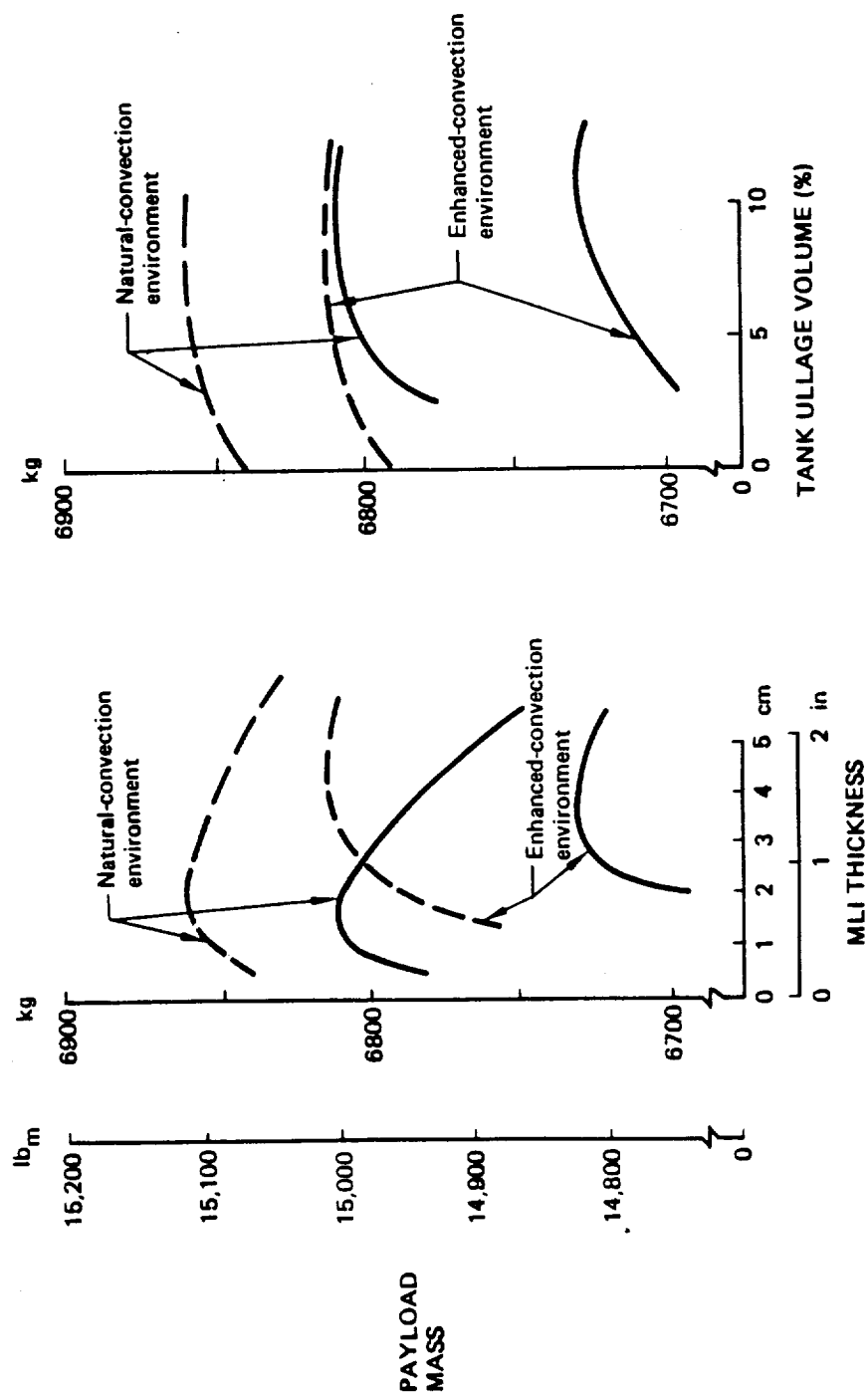
The effect of MLI/foam interface temperatures on payload placement capabilities of optimized LTPS vehicles are shown in Figures 5-14, 5-15 and 5-16 for payload packaging densities of 56, 40, and 24 kg/m<sup>3</sup>. The predicted performances of optimized LTPS vehicles utilizing He-purged MLI are shown in each chart for comparison purposes. Predicted results for the natural-convection purge enclosure conditions are denoted by the solid curves and the dashed curves represent the predictions for the enhanced convection environment.

Figures 5-14 through 5-16 illustrate the following predicted trends:

- a. The assumed heat transfer conditions in the purge enclosure during ground hold can have a large impact on LTPS payload capacity. The greatest impact occurs for He-purged MLI or when the interface temperature of the MLI/foam combination exceeds 160°K.
- b. Generally, for MLI/foam combinations, the forced-convection purge enclosure environment condition lead to predicted payload mass greater than the value predicted for the natural convection environment.

• HELIUM-PURGED MLI

---  $\text{LO}_2$  TANKS  
 —  $\text{LH}_2$  TANKS



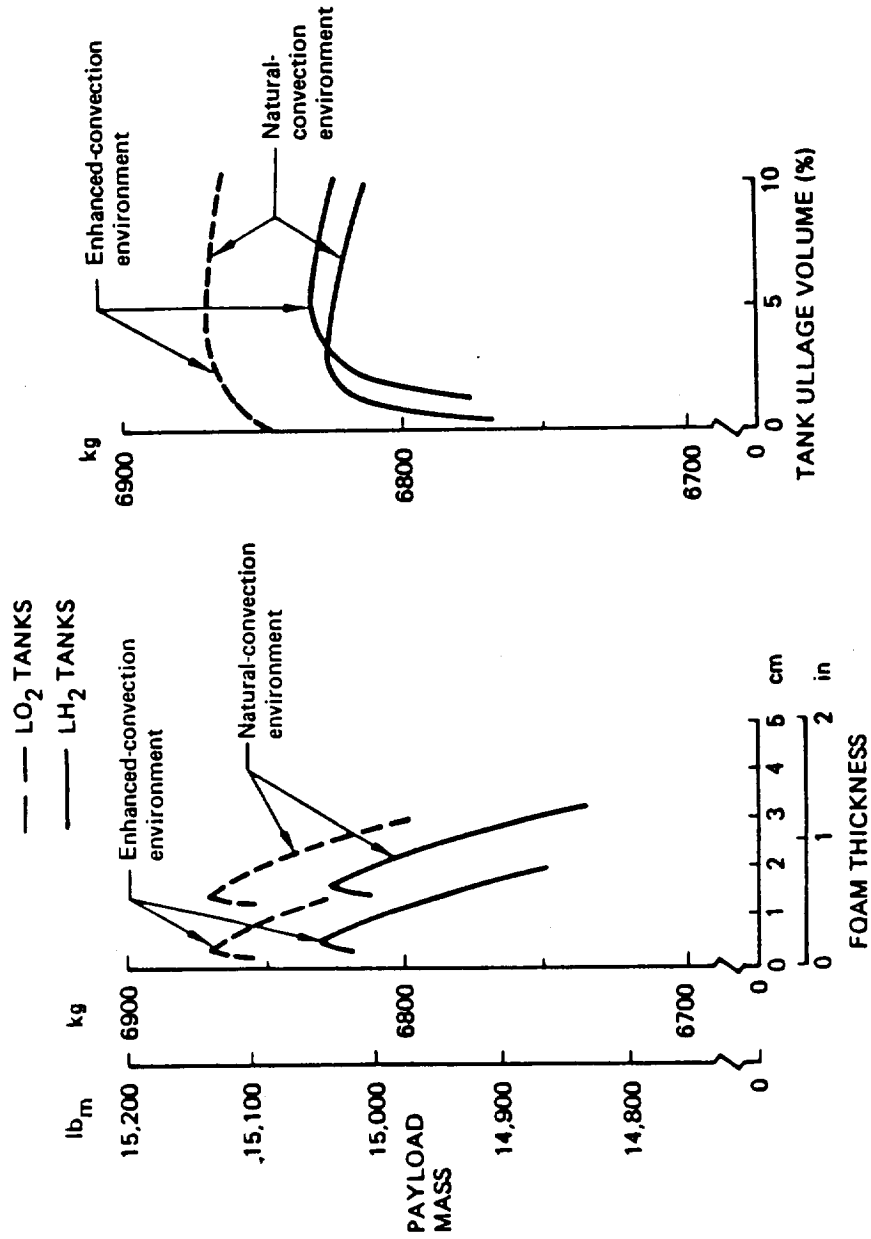
(a) EFFECT OF VARYING MLI THICKNESS FOR THE OPTIMUM ULLAGE VOLUME

(b) EFFECT OF VARYING ULLAGE VOLUME FOR THE OPTIMUM MLI THICKNESS

Figure 5-11: Effect of MLI Thickness and Ullage Volume on Payload Mass for Helium-Purged MLI for  $56 \text{ Kg/m}^3$  ( $3.5 \text{ lb}_m/\text{ft}^3$ ) Payload Packaged Density



- NITROGEN-PURGED MLI/ROHACELL 31 FOAM
- 144 K (-200 °F) MLI/FOAM INTERFACE TEMPERATURE



(a) EFFECT OF VARYING FOAM THICKNESS FOR THE OPTIMUM ULLAGE VOLUME

(b) EFFECT OF VARYING ULLAGE VOLUME FOR THE OPTIMUM FOAM THICKNESS

Figure 5-12: Effect of Foam Thickness and Ullage Volume on Payload Mass for Nitrogen-Purged MLI/Foam Insulation — 56 Kg/m<sup>3</sup> (3.5 lb<sub>m</sub>/ft<sup>3</sup>) Payload Packaged Density

- NITROGEN-PURGED MLI/ROHACELL 31 FOAM
- 144 K (-200 °F) MLI/FOAM INTERFACE TEMPERATURE

--- LO<sub>2</sub> TANKS  
 --- LH<sub>2</sub> TANKS

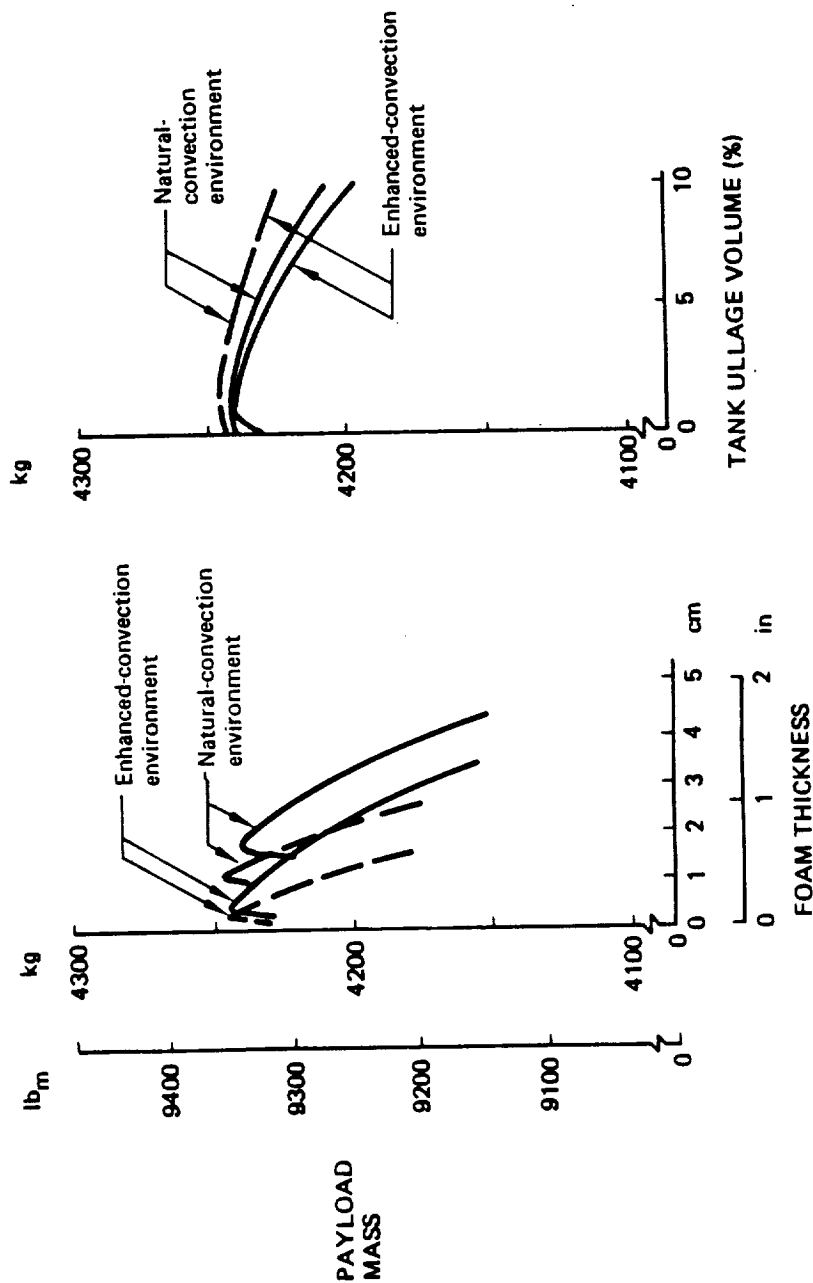


Figure 5-13: Effect of Foam Thickness and Ullage Volume on Payload Mass for Nitrogen-Purged MLI/Foam Insulation - 24 Kg/m<sup>3</sup> (1.5 lb<sub>m</sub>/ft<sup>3</sup>) Payload Packaged Density

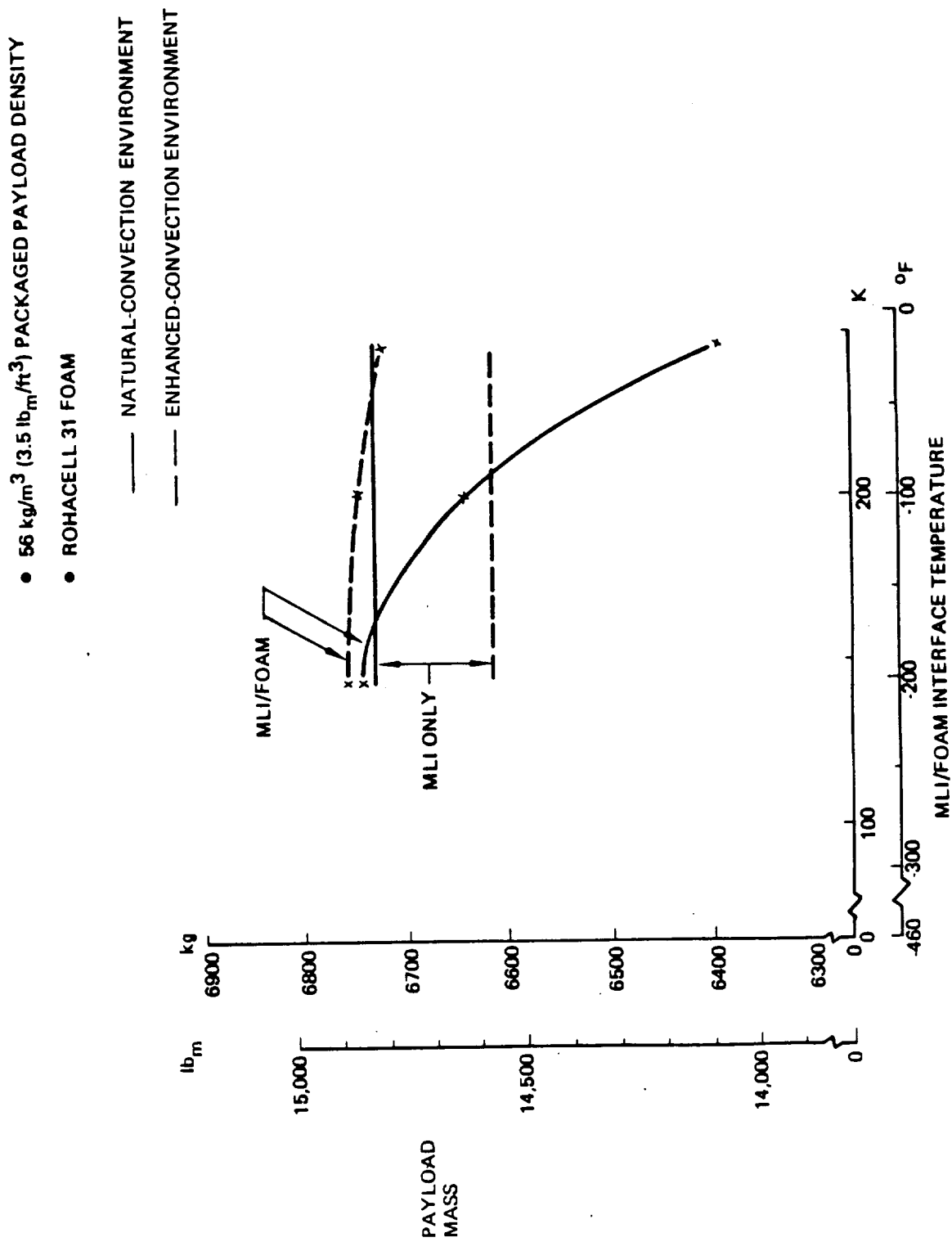


Figure 5-14: Effect of MLI/Foam Interface Temperature on Optimized Payload Mass – 56 Kg/m<sup>3</sup> (3.5 lb<sub>m</sub>/ft<sup>3</sup>) Payload Packaged Density

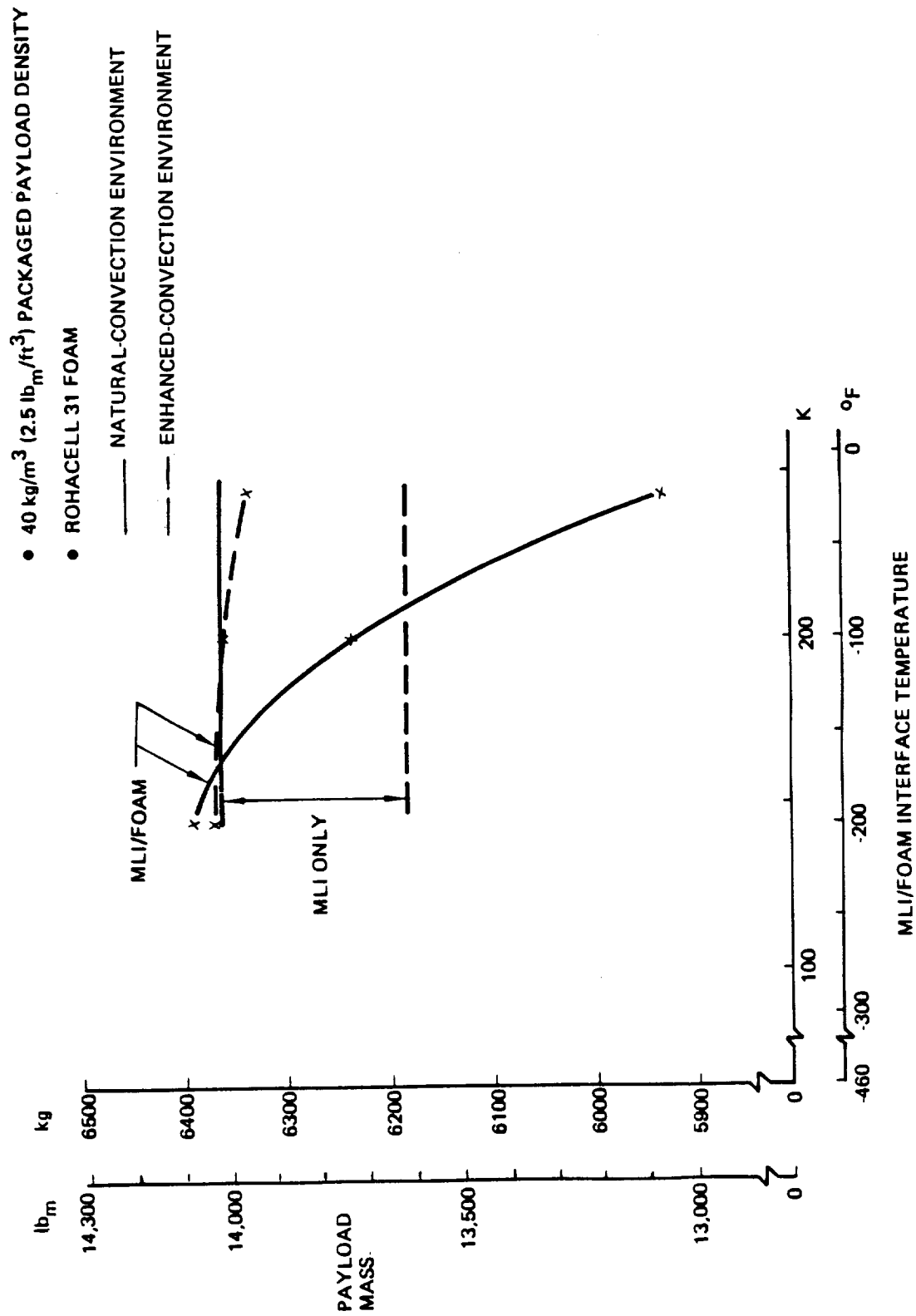


Figure 5-15: Effect of MLI/Foam Interface Temperature on Optimized Payload Mass –  $40 \text{ Kg/m}^3$  ( $2.5 \text{ lb}_m/\text{ft}^3$ ) Payload Packaged Density

- 24 kg/m<sup>3</sup> (1.5 lb<sub>m</sub>/ft<sup>3</sup>) PACKAGED PAYLOAD DENSITY
  - ROHACELL 31 FOAM
- NATURAL-CONVECTION ENVIRONMENT  
 - - - - - ENHANCED-CONVECTION ENVIRONMENT

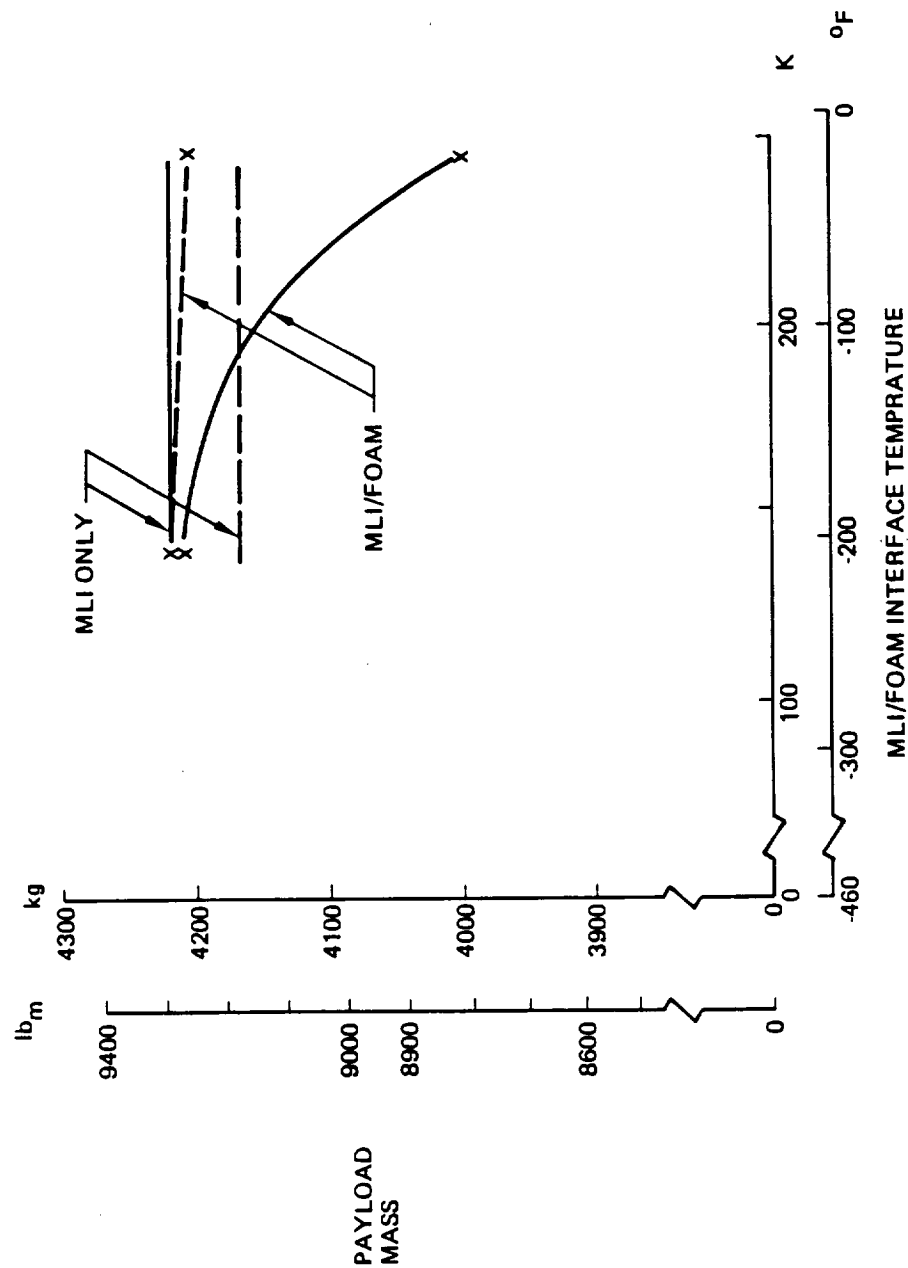


Figure 5-16: Effect of MLI/Foam Interface Temperature on Optimized Payload Mass – 24 Kg/m<sup>3</sup> (1.5 lb<sub>m</sub>/ft<sup>3</sup>) Payload Packaged Density

- c. For He-purged MLI cases, the natural-convection purge enclosure environment condition always lead to the greatest payload mass.
- d. MLI/foam combinations in which the interface temperature was maintained below 150°K actually improve LTPS payload placement capability for higher density payloads. For low-density (24 kg/m<sup>3</sup>) payloads, LTPS payload placement capabilities for MLI and MLI/foam insulations were essentially equal for foam interface temperatures below 170°K and an enhanced convection environment in the purge enclosure.

Figure 5-17 shows the relative benefits of two candidate foam materials, Rohacell 31 and BX250A, in terms of optimized LTPS payload mass. In general, it was found that the Rohacell 31 foam lead to greater payload mass because of its lower density (30.4 kg/m<sup>3</sup> vs. 36.8 kg/m<sup>3</sup> for BX250A). Average thermal conductivities and specific heats of the two foams were essentially identical (see Figures 2-1 and 2-2).

Tables 5-3 and 5-4 contain summaries of the 26 payload-optimized LTPS propellant tank insulation designs identified in the insulation optimization analysis. Table 5-3 summarizes the results for natural-convection purge enclosure environments and Table 5-4 summarizes the results for the enhanced convection cases. In interpreting the results in Table 5-3, it should be remembered that true natural convection conditions would be very difficult to achieve in the purge enclosure. Forced convection currents due to purge gas exiting the MLI moving toward the enclosure exit would probably be large enough to affect the heat transfer environment.

For each LTPS, tank volume, percent ullage volume, optimum values of foam and MLI thickness, and propellant vent loss and mass consumed by the main impulse engine are shown. In addition, the LTPS mass and length are given and maximum payload mass is provided.

• 40 kg/m<sup>3</sup> (2.5 lb<sub>m</sub>/ft<sup>3</sup>) PACKAGED PAYLOAD DENSITY

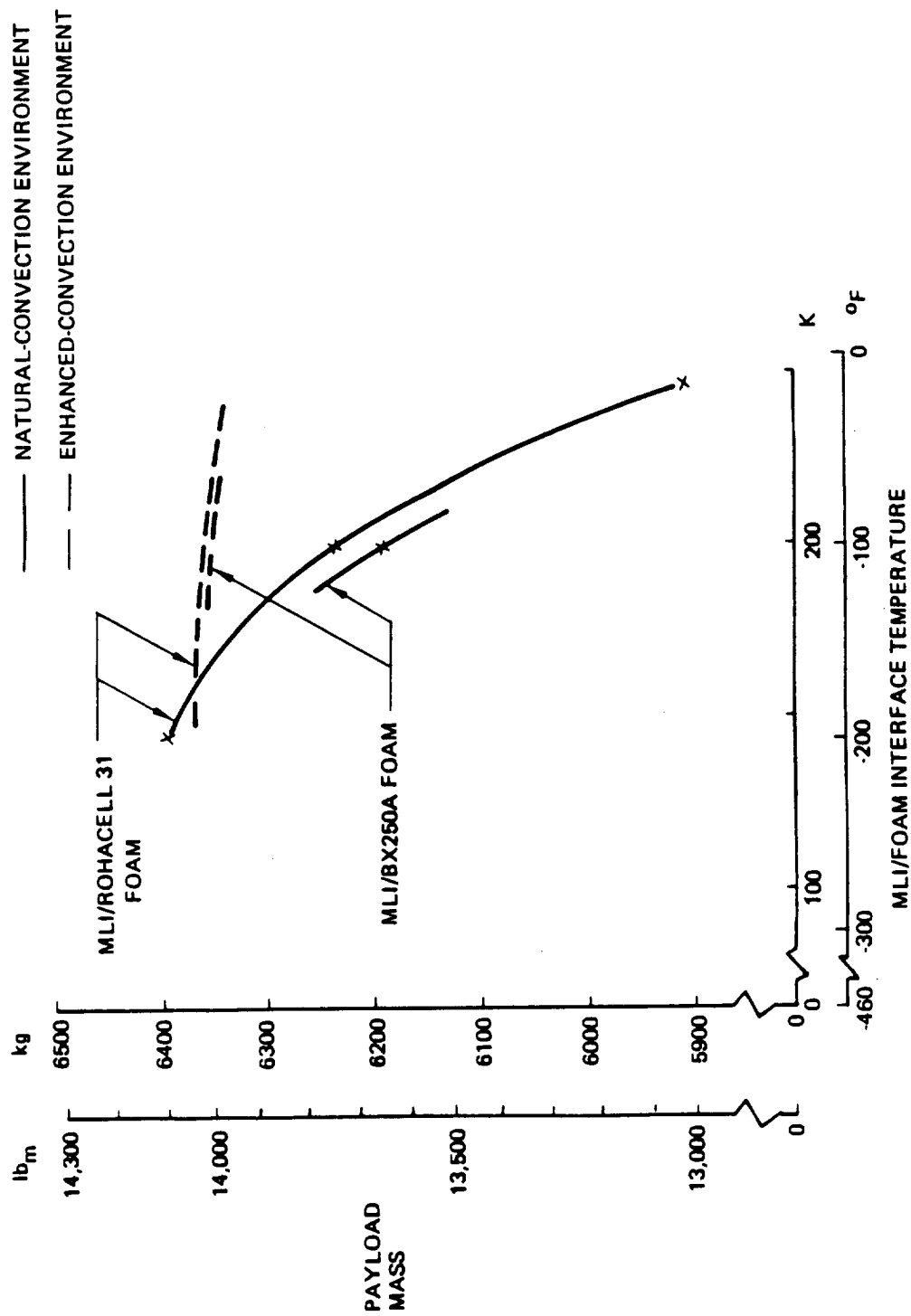


Figure 5-17: Comparison of Optimized LTPS Payload Mass for Insulations Using BX250A and Rohacell 31 Foams

PACKAGED DENSITY Kg/m <sup>3</sup> (lb <sub>m</sub> /ft <sup>3</sup> )	TYPE	MLI/FOAM INTERFACE TEMPERATURE K (F)	TYPE TANK	TANK VOLUME m <sup>3</sup> (ft <sup>3</sup> )	TANK ULLAGE VOLUME %	INSULATION THICKNESS cm (in.)		EXPENDED PROPELLANTS Kg (lb <sub>m</sub> )		LTPS		PAYLOAD	
						MLI	FOAM	LOST	MAIN IMPULSE	BURNOUT MASS Kg (lb <sub>m</sub> )	STAGE LENGTH m (ft)	ORBITER BAY LIMITATION	MASS Kg (lb <sub>m</sub> )
56 (3.5)	MLI	N/A	LH <sub>2</sub> — LO <sub>2</sub>	41.4 (1481) — 14.8 (522)	9.5 — 7.7 —	1.78 (0.70) — 2.03 (0.80)	0 — 0 —	364 (803)	1767 (38074)	2610 (5754)	7.92 (25.98)	MASS	6734 (14846)
	MLI/ ROHACELL 31	144 (200)	LH <sub>2</sub> — LO <sub>2</sub>	38.2 (1348) — 14.1 (498)	3.3 — 4.2 —	0.97 (0.38) — 1.17 (0.46)	1.78 (0.70) — 1.52 (0.60)	405 (893)	17254 (38045)	2569 (5664)	7.74 (23.39)	MASS	6746 (14872)
	MLI/ ROHACELL 31	200 (100)	LH <sub>2</sub> — LO <sub>2</sub>	38.1 (1344) — 13.7 (483)	2.8 — 3.0 —	0.76 (0.30) — 0.71 (0.28)	4.83 (1.90) — 5.66 (2.23)	444 (979)	17239 (38012)	2865 (6318)	7.92 (25.98)	MASS	6646 (14652)
	MLI/ ROHACELL 31	244 (20)	LH <sub>2</sub> — LO <sub>2</sub>	38.1 (1344) — 13.7 (483)	1.8 — 1.8 —	0.61 (0.24) — 0.71 (0.28)	11.94 (4.70) — 16.00 (6.30)	489 (1078)	17237 (38008)	2865 (6316)	8.41 (27.58)	MASS	6391 (14096)
40 (2.5)	MLI	N/A	LH <sub>2</sub> — LO <sub>2</sub>	37.2 (1313) — 14.0 (494)	0.5 — 1.3 —	1.32 (0.52) — 0.76 (0.30)	0 — 0 —	486 (1072)	17084 (37670)	3007 (6629)	6.89 (22.60)	VOLUME	6394 (14096)
	MLI/ ROHACELL 31	144 (200)	LH <sub>2</sub> — LO <sub>2</sub>	36.4 (1284) — 13.6 (480)	0.6 — 1.4 —	0.97 (0.38) — 0.91 (0.36)	1.78 (0.70) — 1.12 (0.44)	531 (1171)	16956 (37388)	2853 (6290)	6.86 (22.50)	VOLUME	6395 (14098)
	MLI 8X250A	200 (100)	LH <sub>2</sub> — LO <sub>2</sub>	36.3 (1281) — 13.7 (483)	0.6 — 1.3 —	0.76 (0.30) — 0.58 (0.23)	4.83 (1.90) — 4.32 (1.70)	657 (1449)	16959 (37395)	2940 (6482)	7.10 (23.29)	VOLUME	6325 (13944)
	MLI/ ROHACELL 31	244 (20)	LH <sub>2</sub> — LO <sub>2</sub>	36.4 (1284) — 13.7 (483)	0.5 — 0.9 —	0.61 (0.24) — 0.61 (0.24)	5.77 (2.27) — 12.52 (4.93)	656 (1446)	17024 (37531)	3034 (6689)	7.16 (23.48)	VOLUME	6192 (13653)
24 (1.5)	MLI	N/A	LH <sub>2</sub> — LO <sub>2</sub>	27.4 (967) — 10.3 (363)	0.9 — 0.9 —	1.27 (0.50) — 0.51 (0.20)	0 — 0 —	488 (1076)	12398 (27333)	2627 (5791)	5.85 (19.19)	VOLUME	4219 (9301)
	MLI/ ROHACELL 31	144 (200)	LH <sub>2</sub> — LO <sub>2</sub>	26.8 (946) — 9.9 (349)	1.0 — 1.2 —	0.97 (0.38) — 0.91 (0.36)	1.78 (0.70) — 1.12 (0.44)	459 (1012)	12268 (27046)	2477 (5461)	5.85 (19.19)	VOLUME	4211 (9284)
	MLI/ ROHACELL 31	200 (100)	LH <sub>2</sub> — LO <sub>2</sub>	26.8 (946) — 9.9 (349)	0.8 — 1.0 —	0.74 (0.29) — 0.58 (0.23)	4.80 (1.89) — 4.32 (1.70)	555 (1224)	12294 (27103)	2505 (5523)	6.00 (19.68)	VOLUME	4161 (9173)
	MLI/ ROHACELL 31	244 (20)	LH <sub>2</sub> — LO <sub>2</sub>	27.0 (953) — 10.1 (356)	0.5 — 0.7 —	0.61 (0.24) — 0.51 (0.20)	11.94 (4.70) — 12.32 (4.85)	620 (1367)	12421 (27383)	2803 (6179)	6.46 (21.19)	VOLUME	3987 (8790)

Table 5-3: Optimum LTPS Conceptual Design Summary for Natural-Convection Ground-Hold  
Purge Enclosure Environments



PACKAGED DENSITY Kg/m <sup>3</sup> (lb <sub>m</sub> /ft <sup>3</sup> )	TYPE	MLI/FOAM INTERFACE TEMPERATURE, K (°F)	TYPE TANK	TANK VOLUME, m <sup>3</sup> (ft <sup>3</sup> )	TANK ULLAGE VOLUME, %	INSULATION THICKNESS, cm (in)		EXPENDED PROPELLANTS, Kg (lb <sub>m</sub> )		LTPS		PAYLOAD	
						MLI	FOAM	LOST	MAIN IMPULSE	BURNOUT MASS Kg (lb <sub>m</sub> )	STAGE LENGTH, m (ft)	ORBITER BAY LIMITATION	MASS, Kg (lb <sub>m</sub> )
56 (3.5)	MLI	N/A	LH <sub>2</sub> — LO <sub>2</sub>	40.2 (1419) — 15.1 (533)	9.0 — 8.0 —	5.72 (2.25) — 4.32 (1.70)	0 — 0 —	337 (1743)	17272 (38078)	2767 (6078)	8.11 (26.60)	MASS	6617 (14588)
	MLI/ ROHACELL 31	144 (200)	LH <sub>2</sub> — LO <sub>2</sub>	39.0 (1376) — 14.4 (508)	5.4 — 5.6 —	1.52 (0.60) — 1.81 (0.76)	0.56 (0.22) — 0.41 (0.16)	322 (1820)	17264 (38060)	2677 (5881)	7.77 (25.49)	MASS	6760 (14903)
	MLI/ ROHACELL 31	200 (100)	LH <sub>2</sub> — LO <sub>2</sub>	38.9 (1373) — 14.4 (508)	4.9 — 5.5 —	1.14 (0.45) — 1.37 (0.54)	1.14 (0.46) — 1.07 (0.42)	386 (851)	17260 (38051)	2580 (5688)	7.77 (25.49)	MASS	6749 (14879)
	MLI/ ROHACELL 31	244 (20)	LH <sub>2</sub> — LO <sub>2</sub>	39.2 (1383) — 14.4 (508)	5.0 — 5.4 —	0.71 (0.28) — 0.89 (0.35)	1.83 (0.72) — 1.93 (0.76)	422 (1930)	17250 (38029)	2585 (5688)	7.80 (25.58)	MASS	6718 (14811)
	MLI	N/A	LH <sub>2</sub> — LO <sub>2</sub>	36.6 (1292) — 14.1 (498)	1.1 — 1.3 —	6.10 (2.40) — 5.08 (2.00)	0 — 0 —	328 (723)	17208 (37937)	3239 (7141)	6.89 (22.60)	VOLUME	6186 (13638)
40 (2.5)	MLI/ ROHACELL 31	144 (200)	LH <sub>2</sub> — LO <sub>2</sub>	35.6 (1262) — 13.8 (487)	0.8 — 1.6 —	1.32 (0.52) — 1.19 (0.47)	0.48 (0.19) — 0.25 (0.10)	429 (1946)	17036 (37558)	2931 (6462)	6.89 (22.60)	VOLUME	6370 (14043)
	MLI/ ROHACELL 31	200 (100)	LH <sub>2</sub> — LO <sub>2</sub>	36.7 (1295) — 13.8 (487)	0.8 — 1.6 —	0.98 (0.39) — 0.89 (0.35)	0.99 (0.39) — 0.69 (0.27)	467 (1030)	17029 (37542)	2928 (6455)	6.89 (22.60)	VOLUME	6361 (14023)
	MLI/ BX250A	200 (100)	LH <sub>2</sub> — LO <sub>2</sub>	36.8 (1299) — 13.9 (490)	0.8 — 1.6 —	0.94 (0.37) — 0.84 (0.33)	1.12 (0.44) — 0.67 (0.26)	482 (1063)	17044 (37576)	2949 (6501)	6.92 (22.70)	VOLUME	6363 (14006)
	MLI/ ROHACELL 31	244 (20)	LH <sub>2</sub> — LO <sub>2</sub>	36.8 (1299) — 13.9 (490)	0.8 — 1.6 —	0.88 (0.35) — 0.56 (0.22)	1.75 (0.69) — 1.22 (0.48)	577 (1272)	17016 (37511)	2924 (6446)	6.96 (22.80)	VOLUME	6338 (13973)
	MLI	N/A	LH <sub>2</sub> — LO <sub>2</sub>	28.0 (999) — 10.6 (374)	0.9 — 0.1 —	3.18 (1.25) — 2.79 (1.10)	0 — 0 —	363 (778)	12686 (27746)	2853 (6290)	5.97 (19.58)	VOLUME	4165 (9182)
24 (1.5)	MLI/ ROHACELL 31	144 (200)	LH <sub>2</sub> — LO <sub>2</sub>	27.0 (953) — 10.1 (356)	1.2 — 1.1 —	1.17 (0.46) — 1.09 (0.43)	0.43 (0.17) — 0.23 (0.09)	306 (873)	12362 (27263)	2564 (5653)	5.85 (19.19)	VOLUME	4218 (9299)
	MLI/ ROHACELL 31	200 (100)	LH <sub>2</sub> — LO <sub>2</sub>	27.0 (953) — 10.1 (356)	1.2 — 1.2 —	0.97 (0.38) — 0.81 (0.32)	0.87 (0.34) — 0.64 (0.25)	423 (933)	12350 (27227)	2552 (5616)	5.85 (19.19)	VOLUME	4214 (9290)
	MLI/ ROHACELL 31	244 (20)	LH <sub>2</sub> — LO <sub>2</sub>	27.2 (960) — 10.1 (356)	1.0 — 1.3 —	0.66 (0.26) — 0.53 (0.21)	1.70 (0.67) — 1.17 (0.46)	607 (1338)	12338 (27200)	2553 (5628)	5.88 (19.29)	VOLUME	4206 (9273)

Table 5-4: Optimum LTPS Conceptual Design Summary for Enhanced-Convection Ground-Hold  
Purge Enclosure Environments



## 6.0 EXPERIMENTAL PROGRAM PLAN

Task III in the present program was the development of a preliminary plan to experimentally evaluate the relative performance of MLI-plus-foam and MLI-only insulation systems and to experimentally verify the insulation performance predictions. The development of the plan required selection of a testing approach and determination of the particular parameters and measurement ranges required to meet the test objectives. Supporting the development of the plan was a preliminary design effort for those hardware items unique to the test program. Finally, a cost estimate for the experimental program was formulated.

### 6.1 EXPERIMENTAL APPROACH

The approach to the Experimental Program Plan represents a compromise between a test designed for maximum emphasis on measurement of undisturbed one-dimensional heat flow through the tank wall insulation, and a test designed for full simulation of all thermal influences in a LTPS application. The first extreme would typically be planned around a guarded flat plate calorimeter while the other extreme would involve a full scale cryogenic tank, with realistic full-scale supports, plumbing, insulation attachments, etc. The approach selected also represents a compromise in costs and potential benefits between the two possible extremes.

The approach selected for the program plan uses a half-scale liquid hydrogen tank, based on the shape and size of the tank for the 40 kg/m<sup>3</sup> payload density LTPS design from Task II. The choice of a half-scale tank was felt to be an appropriate compromise between a full scale tank with its greater fabrication and handling costs and a limited choice of vacuum chambers, and a smaller tank with its less representative simulation in terms of area/volume ratio, relative contribution of discrete heat leaks, and less realistic insulation configuration.

The ellipsoidal tank shape chosen will exhibit wetted area versus liquid level behavior similar to that of the full scale tank and will afford an opportunity to gain experience in designing and installing insulation on a tank of this shape. A boilerplate rather than flightweight tank was selected, to reduce design, qualification, handling, and safety costs. The effect on the test results of the difference in thermal characteristics between a boilerplate and a flightweight tank is expected to be insignificant.

The test tank supports, plumbing penetrations, and insulation joints and fasteners will be designed to perform their primary function with a minimum heat leak to the tank. This approach, rather than simulated full scale features, was selected in view of the main test objective of evaluating basic insulation performance.

A purge bag, mounted in close proximity to the tank insulation outer surface, will be used. This approach, rather than a simulated compartment purge, will minimize the volume to be purged and will simplify the purge container design by keeping the thermal environment shroud and most of the tank support structure outside the purge volume. It was felt that this concept is most likely to be employed in an actual spacecraft as well.

The tanks external thermal environment will be controlled with an electrically heated thermal shroud. The use of electrical resistance heaters avoids potential problems with selection of a heat exchange fluid suitable for the desired temperature and with potential leakage inside the vacuum chamber. The desired low temperatures of the shroud will be achieved by reducing or terminating power to the resistance heaters and allowing the chamber cryogenic shroud to cool the thermal shroud to the desired temperature.

The experimental program was planned around the use of an existing vacuum chamber which will be installed at the Boeing Tulalip Test Site. This facility has all provisions for cryogenic handling and safety required for the tests. The chamber will include an internal liquid nitrogen shroud to aid in achieving the required vacuum. A schematic of the test article, in its transportation and handling stand, installed in the vacuum chamber, is shown in Figure 6-1.

Two complete tests will be performed: one with the tank insulated with an MLI-plus-foam system and the second with an MLI-only system. The test sequence will be the same for each test and will be a simulation of the mission timeline defined in Table 3-3, with deviations dictated by limitations of the facility or the test article, and by objectives of the test. Stabilized thermal conditions will be attained and held to permit accumulation of reliable data at the ground hold and on-orbit conditions. Additionally, the launch and ascent transition in pressure and temperature will be simulated in real time.

The approach to determining the performance of propellant tank insulation systems is to employ a combination of calorimetry and temperature measurement. Calorimetry will provide the overall system heat leak, including that from tank supports, lines and penetrations, as well as the insulation system. Since heat leaks through tank supports, lines and penetrations will depend on the design of the test article, it is necessary to determine the heat leak attributable to these design-dependent elements in order to evaluate insulation system performance.

Heat leak through the insulation system will be calculated by subtracting the heat leak through insulation penetrations from the total tank heat leak. Temperature gradients along struts, lines, and insulation support hardware will be measured and thermal analysis modeling used to calculate heat fluxes. Care will be taken to use materials of known thermophysical properties in the construction of hardware penetrating the foam and MLI. Multilayer insulation will cover all tank support hardware, service lines and the suspension system to minimize environmental heating under vacuum conditions.

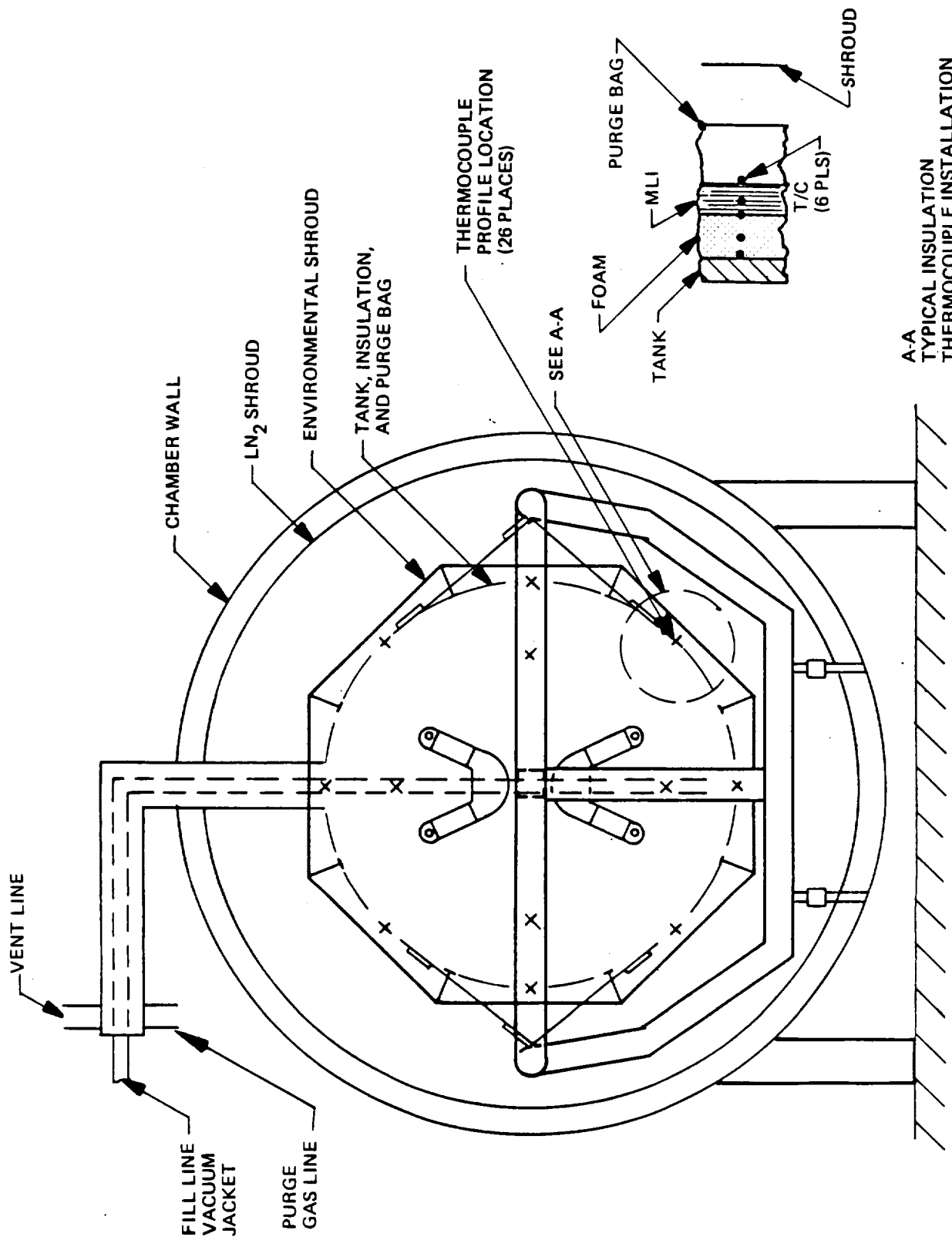
Thin flat plate calorimeters and thermocouples will be used between MLI and foam layers to measure insulation performance. Since the calorimeter thermal mass will be much greater than the insulation thermal mass, the calorimeter temperature will lag that of the insulation. The rate of decrease in calorimeter temperature after the MLI has been evacuated will be input to an analytical model and insulation effective conductance predicted. Thermocouples with low-mass attachments to the insulation will indicate temperature profiles, providing measurement of instantaneous heat flow under steady-state conditions.

## **6.2 EXPERIMENT PLAN**

### **6.2.1 Test Preparations**

A number of design, analysis, fabrication, and installation tasks are necessary to ready the test article and laboratory facilities. These tasks, identified and scoped in a preliminary manner for the purpose of cost estimates, are:

1. Detailed test plan development.
2. Pre-test predictions of insulation performance and heat leaks.
3. Detailed design of the test article.
  - o Tank
  - o Support System
  - o Insulation Systems
  - o Purge Bag



A-A  
TYPICAL INSULATION  
THERMOCOUPLE INSTALLATION  
(MLI-PMS-FOAM INSULATION SHOWN)

Figure 6-1: Test Configuration Schematic

- o Fill and Vent Plumbing
- 4. Detailed design of instrumentation system.
- 5. Detailed design of laboratory facility modifications and additions.
  - o Mechanical
  - o Vacuum
  - o Cryogenic
  - o Purge Gas
  - o Electrical
- 6. Design and fabrication of thermal shroud.
- 7. Design and fabrication of transportation and handling stand.
- 8. Tank fabrication and proof testing.
- 9. Support structure fabrication and proof testing.
- 10. Design and fabrication of insulation tooling.
- 11. Fabrication and installation of insulation and purge bag.
- 12. Fabrication and installation of laboratory facility hardware.
  - o Mechanical
  - o Vacuum
  - o Cryogenic
  - o Purge Gas
  - o Electrical
- 13. Procurement and installation of instrumentation system.
- 14. Test article installation.
- 15. Systems check-out and instrumentation calibration.

The development of the detailed test plan will include preparation of a test procedure document. This document will specify all safety and acceptance requirements and will include a step by step procedure for the preparation and conduction of the tests. Any changes to this document required during the test will be recorded in the "Official Test Copy." Such changes will be made only with the approval of the Test Director.

The test procedure document will contain sections defining the actions necessary to be taken for a test hold condition as well as the emergency backout procedures for critical component failures. All possible failure modes cannot be covered by procedure, however, a generalized backup plan will be developed for the known test parameters.

All safety requirements and considerations will be called out in the test procedures. The call out will be in a general section at the beginning of the procedure or, if specific requirements exist, as procedural steps in the operational portion of the procedure.

Safety will be a basic consideration in all aspects of the program, from design through final securing of the test site. Standard Boeing-approved Test Laboratory Safety Instructions will be followed. The facility design will contain a number of reviews in which both personnel and equipment safety will be addressed. Major safety design considerations are listed below:

- a. Fail safe mode of operation.
- b. Power interrupt/failure will not cause a system failure.
- c. All control functions will be manually initiated, computer controlled and have a manual backup.
- d. Lines will be designed for worst case flow conditions and will be pressure-relieved for system and personnel safety.

- e. Any multiple valve systems will be designed such that one valve always remains in a system safe position.
- f. H<sub>2</sub> detectors will be constantly monitored by the data system.
- g. A failure analysis review will be conducted to verify design.

Before each test there will be a Test Readiness Review in which all aspects of the test will be discussed. This review must be completed to all participants' satisfaction before proceeding into the test.

The detailed design, planning, and prediction tasks will utilize the preliminary work performed in the present program and carry that work to the level required to fabricate hardware and commit the laboratory to the tests. The total modifications and additions required to prepare the existing Boeing facility for the tests were identified but that work required to provide basic mission-simulation cryogenic tank testing capability was not included in the cost estimate. Thus, only those modifications and set-up tasks required to install the particular tank and its related systems were charged to the experimental program.

### 6.2.2 Test Sequence

The planned order of the two major tests is to test the MLI-plus-foam insulation first and the MLI-only system second. This plan allows installation of the more complex insulation system in the fabrication shop rather than in the less controlled environment of the test site. This sequence also permits reuse of the MLI blankets as the MLI-only system after their use as the outer insulation component in the MLI-plus-foam system.

After the first test, all insulation will be removed from the tank. The MLI blankets will be returned to the clean room where they were fabricated and trimmed for reinstallation directly on the tank. They will then be vacuum outgassed, packaged, and returned to the tank for installation as the MLI-only system. The decision as to retain the tank at the test site or return it to the fabrication shop for insulation change-over will be made as part of the detailed test plan.

The timeline for the main tests is shown in Figure 6-2. The events for the two tests are the same except for the selection of dry nitrogen or helium (indicated by the entries "Dry N<sub>2</sub>/He" in the Purge System column), as required for purging the MLI-plus-foam or MLI-only systems, respectively. Some of the undefined time intervals may differ between the tests of the two insulation systems, as stabilization times may differ. Some of the undefined time points and intervals will be determined after development of the detailed test plan and completion of pre-test heat flow predictions, and others must remain open, to be determined as the tests progress. For the purpose of program cost estimates a 6-day (144-hr) duration was assumed for each of the tests.

The chamber depressurization, indicated during the Launch Simulation Phase in Figure 6-2, will follow, as closely as permitted by facility capability, the pressure history shown in Figure 6-3. This profile, based on STS-III measured cargo bay pressure, with a logarithmic extension, is the same as was used for the Task II trade study analyses discussed in section 4.0 of this report. The repressurization profile at the end of the test is not defined but will be determined so as to assure test article integrity and facility capability.

The thermal shroud temperature profile from the beginning of depressurization through time point,  $t_4 + 54$ , follows the body shell temperature history used for Task I and II

Phase	Time (hr)	System Status or Event			
		Chamber	Shroud	Tank	Purge System
Purge and Chill	$t_0$	Close, GN <sub>2</sub> Purge, 760 Torr	No Heat	GN <sub>2</sub> Purge	GN <sub>2</sub> Purge
	$t_1$				
	$t_1 + 5$			Cold GH <sub>2</sub> Purge	Dry N <sub>2</sub> /He Purge
LH <sub>2</sub> Fill	$t_2$			LH <sub>2</sub> Fill	
Ground Hold Stabilization	$t_3$		311 °K (100 °F)	Full, Top Continuously	
	$t_4$		311 °K (100 °F)	Stable Temp. & Boil-Off	
Ground Hold Simulation	$t_4 + 4$	Begin Depress	311 °K (100 °F)	Continue Topping	End Purge, Open Vent
Launch Simulation	$t_4 + 6$	10 <sup>-5</sup> Torr	267 °K (20 °F)	Top Periodically	
Orbit Stabilization	$t_4 + 19$		256 °K (0 °F)		
	$t_4 + 24$		244 °K (-20 °F)		
	$t_4 + 49$		244 °K (-20 °F)		
	$t_4 + 54$		200 °K (-100 °F)		
Orbit Simulation	$t_5$		200 °K (-100 °F)	Stable Temp.	
	$t_5 + 2$		200 °K (-100 °F)	Recover LH <sub>2</sub>	
Recovery & Shut-Down	$t_6$		311 °K (100 °F)	GN <sub>2</sub> Purge	Dry N <sub>2</sub> /He Purge
	$t_7$	Repressurize			
	$t_8$	760, Torr, Open	No Heat	Ambient Temp.	Off

Figure 6-2: Test Timeline



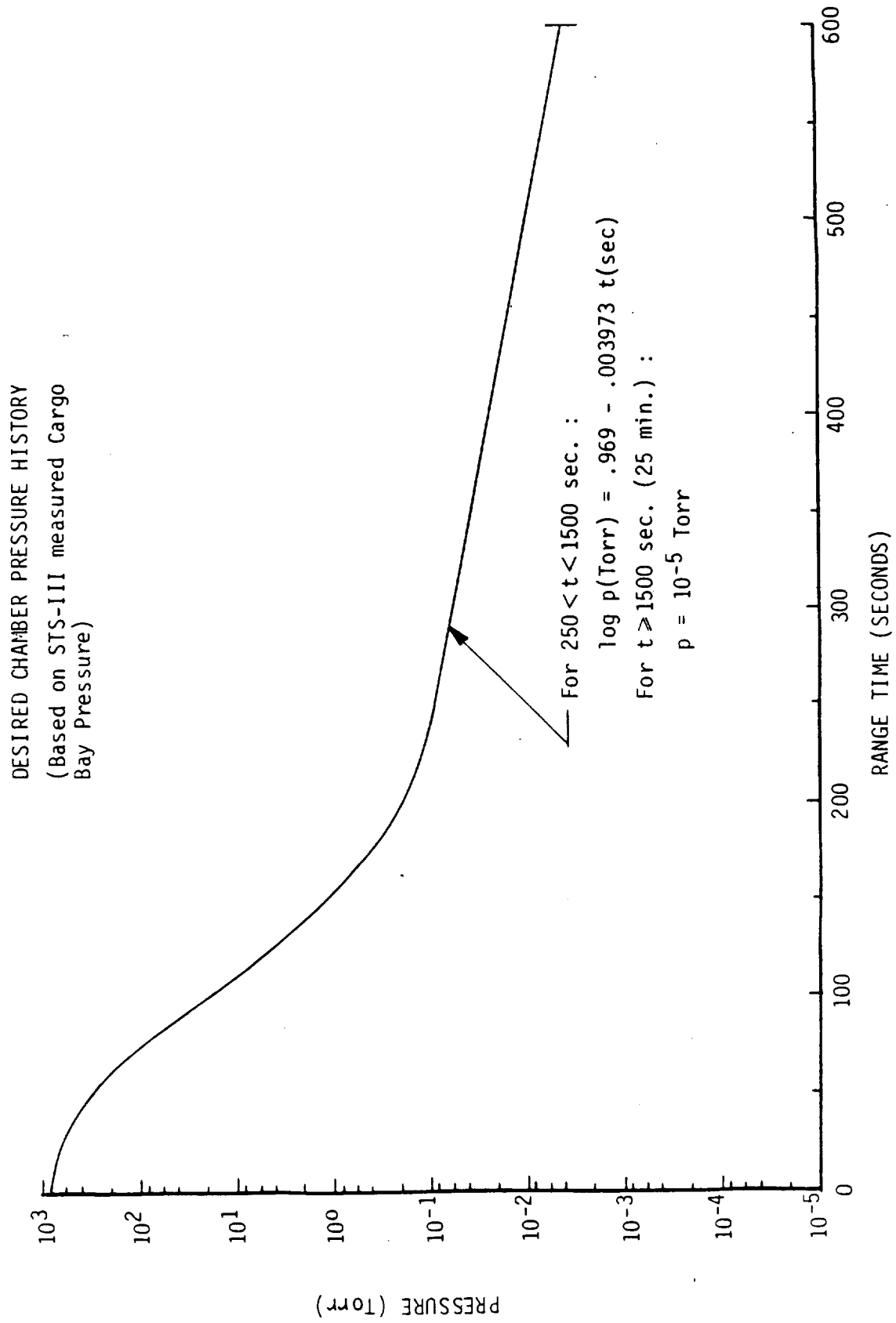


Figure 6-3: Desired Chamber Pressure History (Based on STS-III Measured Cargo Bay Pressure)

analyses. The shroud temperature profile from  $t_4$  into the Orbit Simulation phase is shown in Figure 6-4. The shroud temperature will be brought back up to 311°K condition prior to repressurization at the end of the test, in order to minimize possibilities of condensation in the MLI.

During the Ground Hold Stabilization and Ground Hold Simulation phases of the test the tank will be topped continuously with liquid hydrogen. It was anticipated that the area/volume ratio of the half-scale tank and the relative significance of the support and plumbing penetration heat leaks are such that boil-off rates up to 68 kg/hr will be experienced during these phases. It was felt that the resulting rapid change in liquid level of a non-topped tank would preclude attaining a stable thermal condition. Therefore, continuous topping was concluded to be the only choice during these phases.

Boil-off rates are expected to be much lower, i.e., in the neighborhood of 0.454 kg/hr during the Orbit Stabilization and Orbit Simulation Phases. Therefore it was concluded that periodic topping of the tank would be a suitable procedure, with quasi-stable conditions reached between each periodic topping. The preliminary replenishment criterion is to refill the tank when the ullage volume reaches 2% of the total volume, which is equivalent to approximately 10% of the tank internal surface area and approximately 15.2 cm of space between the liquid surface and the top of the tank. Periodic topping of the tank will continue through the Orbit Simulation Phase, if necessary to satisfy the above criterion.

The purge system schedule in Figure 6-2 begins by employing laboratory-grade nitrogen. At the  $t_1$  time point, the chart shows a change to helium for the MLI-only insulation and, to dry nitrogen (Dry  $N_2$ ) for the MLI-plus-foam system. The dry nitrogen is that with less than 140 ppm of moisture, required for the 244°K minimum insulation interface temperature. The preliminary design of the facility gas system, however, includes only one gaseous nitrogen supply system, and it is planned that all nitrogen used will meet the moisture content limit specified for the insulation purge. The preliminary plan specifies a five hour dry-nitrogen or helium purge before beginning to chill the tank to liquid hydrogen temperature. This period will be reevaluated in the detailed plan, after the purge system detail design is complete.

The purge schedule in Figure 6-2 indicates the opening of a vent, coincident with the end of purge flow and beginning of chamber pumpdown at  $t_4 + 4$ . The venting of the purge gas will be to the chamber interior, both during active purge flow and during chamber depressurization. When the purge bag design is completed, it may be found that the bag vent area is sufficient to accommodate outflow during depressurization and that vent valves are not needed.

Insulation purge will be resumed during repressurization and tank warm-up at the end of the test, in order to prevent condensation in the MLI.

### 6.2.3 Measurements

The primary measurements, to meet the objectives of the experimental program, will be; 1) flow rate of the boiled-off hydrogen, and 2) temperatures through the thickness of the insulation. The former will provide the basis for evaluating the total heat flow to the tank and the latter will provide an indication of heat flux through the insulation.

Valid interpretation of boil-off rate measurements will require supplemental measurement of temperatures of the liquid in the tank, temperature and pressure in the tank ullage space, and temperature and pressure at the point of flow measurement. Liquid level in the tank must also be measured.

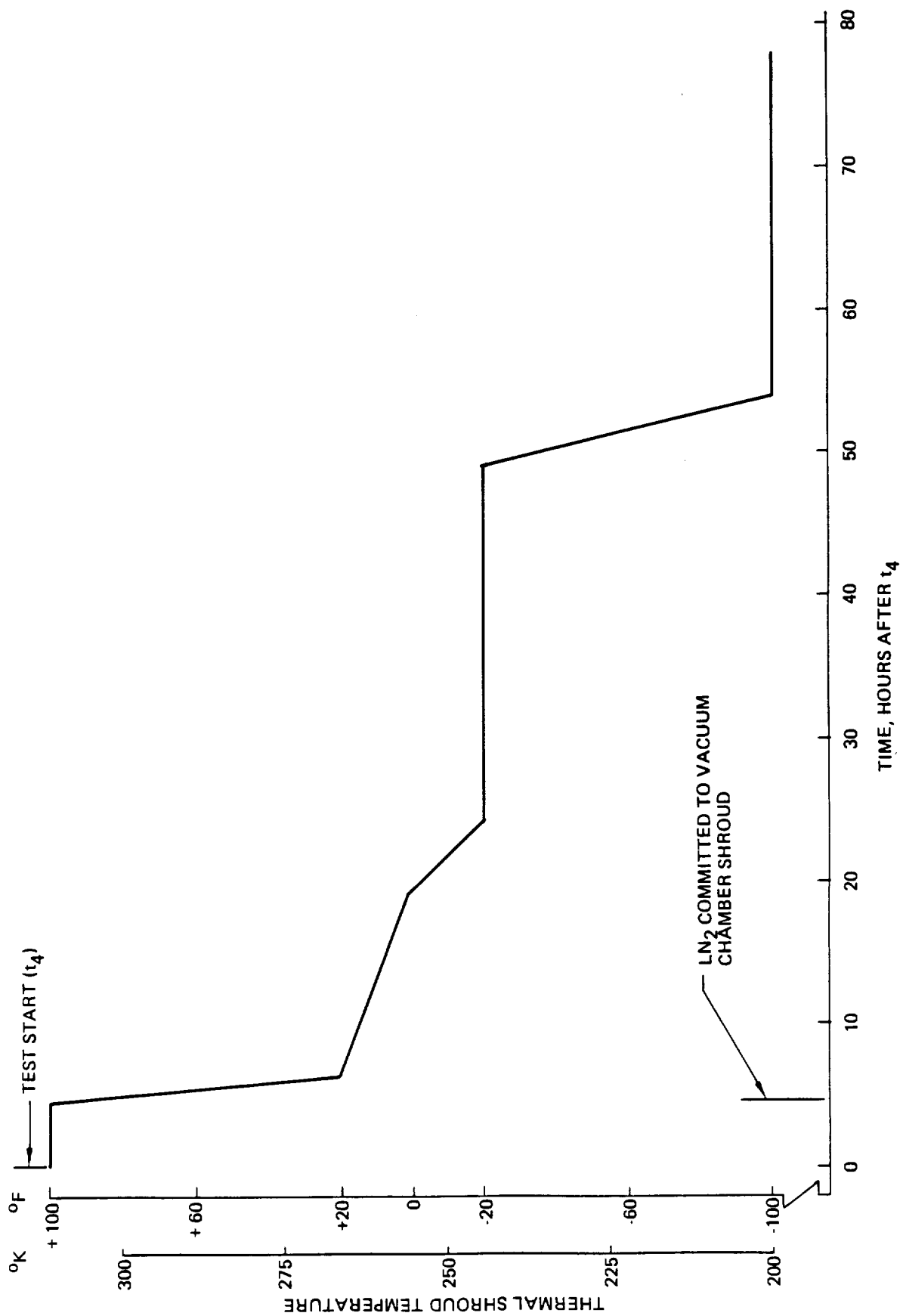


Figure 6-4: Thermal Shroud Temperature Versus Time

Temperature profiles through the tank insulation are desired at a number of locations over the tank in order to assess the effects of non-uniformities in external (thermal shroud) boundary temperatures or in tank wall temperatures. Although neither of these non-uniformities are planned, each is possible, due to external convection and liquid hydrogen stratification, respectively. Non-uniform purging of the MLI and other deviations from ideal insulation characteristics, such as variations in layer density, variation in contact intimacy between tank and foam, foam and MLI, etc., are expected to cause temperature profiles to vary from point to point. Temperature measurements on the purge bag will also be required to evaluate local heat flow.

To further aid in evaluating insulation heat flow, measurements will be required to assess the heat flow through discrete heat leaks such as support straps and plumbing penetrations. Temperatures measured at selected locations along the major heat paths through these components will supplement theoretical predictions of their heat leak contributions.

A number of measurements will be required to monitor performance of various test systems and verify that prescribed test parameters were achieved. These measurements include chamber pressure, thermal shroud temperatures, liquid hydrogen fill flow rate, purge gas flow, and purge space pressure. Additional measurements required to monitor facility systems from a performance or safety standpoint will be defined in the course of detailed test planning and facility design.

Preliminary predictions were made for ranges of some of the major test variables to be measured, to aid in selection and cost estimation for instrumentation. Liquid hydrogen boil-off rates are expected to range from near zero to 72.6 kg/hr. Temperatures in the foam insulation may vary from 20.6°K to 267°K and in the MLI insulation, from 20.6°K to 322°K. Liquid levels in the tank must be measured over the full depth of the tank and to an accuracy of  $\pm 3.8$  cm over the upper 25% of the liquid level range. Test chamber and purge space pressures will range from 760 torr down to possibly as low as  $10^{-6}$  torr. The thermal shroud temperature requirements are from 200°K to 311°K. A maximum power level of 9 KW to the thermal shroud heaters will be required. Tank internal pressures up to 17.2 N/cm<sup>2</sup> are expected. The wide range of some of the variables to be measured will require more than one type of instrument to provide data over the range. Other measurement ranges will be discussed in a later section on instrumentation.

#### **6.2.4 Analysis and Conclusions**

The Experiment Plan includes provisions for pre-test and post-test theoretical analyses of insulation system and overall cryogenic tank thermal performance. Products of these analyses will include predictions of temperature profiles through the insulation and purge bag system and over critical sections of support and plumbing system components. Additionally, predictions of overall heat leak and boil-off, together with individual component contributions to this heat leak, will be made. The theoretical predictions will employ analytical models, solution tools and techniques similar to those used in the Task I and II analyses described in this report.

The pre-test analysis will support the detailed test plan and detailed design activities, aiding in sizing gas and cryogen lines, selecting instrumentation locations and ranges, and establishing time line events. The pre-test analyses results are also expected to identify deficiencies in the thermal design of the test article, permitting design changes to reduce heat leaks. Finally, provided the tests are completed according to planned procedures and boundary conditions, the pre-test analyses are central to the experimental program objective of verifying the Task I full scale predictions.

The test results will provide an opportunity for empirically adjusting the model, properties, or assumptions employed in the theoretical predictions. The post-test analyses will evaluate these adjustments to achieve improved correlations between experimental and theoretical insulation performance figures. The post-test analyses will also take into account deviations in the actual test parameters, relative to the planned values and procedure.

The integrity of the insulation system in the post-test state will be evaluated by inspection of the removed components. The foam in particular will be examined for attachment pad bond failures, cracking, cell collapse or expansion, and other evidence of damage.

The results of the Analysis and Evaluation Task will be used to form conclusions regarding insulation performance, prediction capability, and test techniques. Recommendations will be made regarding further improvements in analytical predictions, insulation system design, and laboratory test procedures.

### **6.3 EXPERIMENTAL HARDWARE DESIGN**

Preliminary designs for experimental program hardware were developed for aiding the formulation of realistic cost estimates. Although a number of design decisions were beyond the scope of the present effort, an attempt was made to resolve those issues that would have a major impact on program costs. Preliminary or conceptual designs were made for the test tank and its support and handling hardware, the tank insulation systems, the laboratory system modifications, and the instrumentation system.

#### **6.3.1 Cryogenic Tank**

The tank design is shown in Figure 6-5. Figures 6-6 and 6-7 are the supporting parts list and construction notes, respectively. The boilerplate tank will be fabricated from 7.87mm 6061-0 aluminum alloy plates. The ellipsoidal heads are shown in the drawing as built up from preformed welded gores but spinning is an alternate means of forming. The tank features a single opening, at the top, closed with a flat cover, which includes the transition coupling. This coupling will accommodate all fill, vent, and sensor lines to the tank interior. The drawing shows a 6.35 cm diameter coupling, but this size may be changed after completion of the facility system detailed design identifies required tubing and wire bundle sizes. An indium seal is provided to seal the cover.

#### **6.3.2 Tank Support System**

After delivery of the tank from the fabricator the tank will be mounted in a transportation and handling stand and will remain in the stand for the remainder of the program. The stand design, shown in Figure 6-8, is patterned after that of Reference 18, and is sized to fit into the vacuum chamber. The stand design features a tank mounting ring which may be rotated in the stand frame approximately +40 degrees to facilitate access to lower surfaces of the tank. Removable braces will lock this ring in the level position when movement is not required for insulation installation and other work. The stand will be constructed from steel pipe and plate and will be cleaned and coated with low-outgassing paint suitable for the vacuum chamber environment. The dollies shown in the figure will be removed prior to vacuum chamber installation to minimize contamination.

The tank will be supported in the stand by 16 Kevlar/epoxy tension straps, illustrated in Figure 6-9. Kevlar was chosen for its low thermal conductivity and high elastic modulus and will be employed in a unidirectional tape lay-up. Bonded titanium end fittings will complete each strap, and turnbuckles will join the 16 support straps to welded steel spider



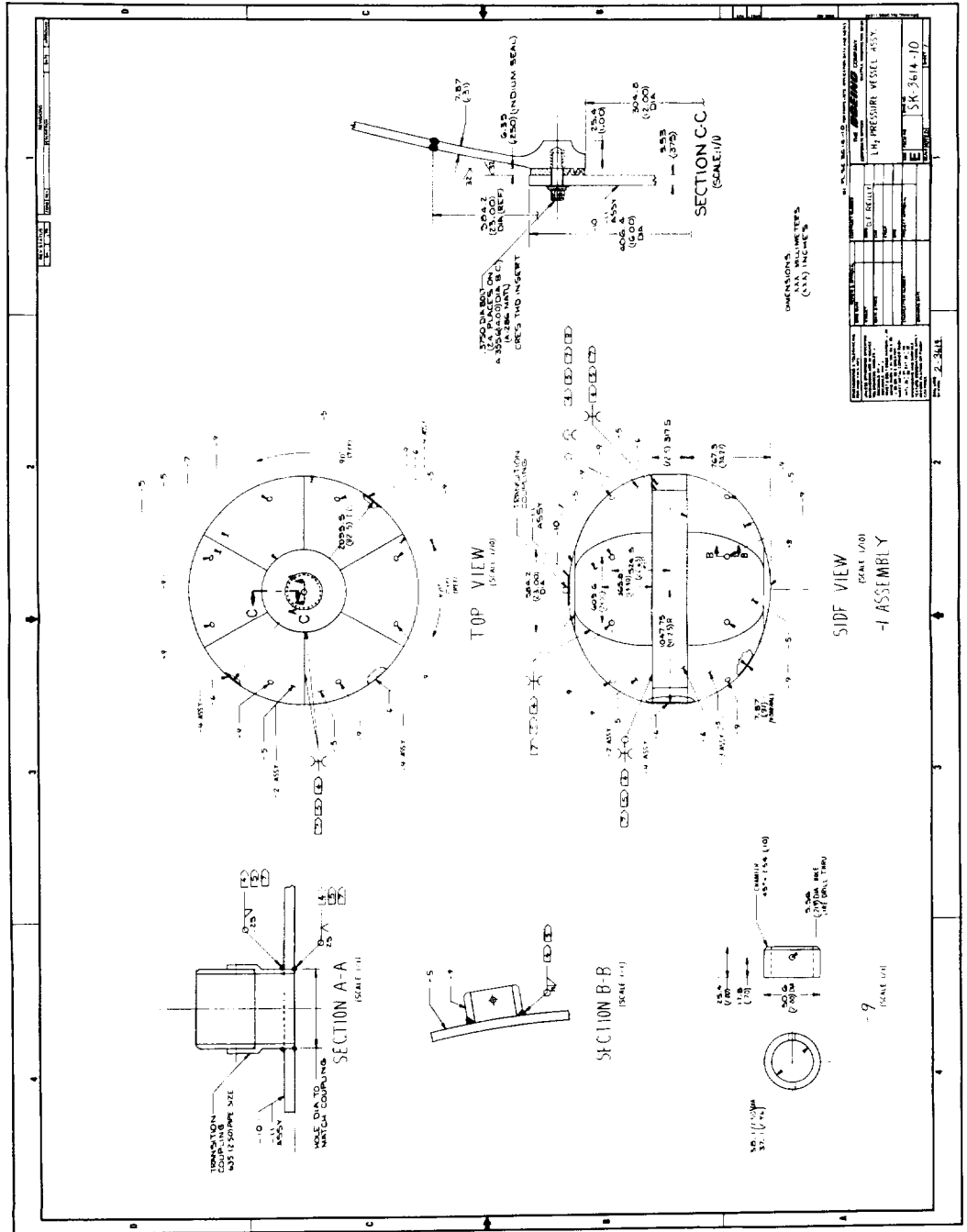






**Figure 6-6: Test Tank Parts List**

[illegible]





CO	
----	--

THE  
**BOEING**

CORPORATE OFFICES  
SEATTLE, WASHINGTON 98124



SEATTLE, WASHINGTON 98124

**CONTRACT NUMBER**

CODE IDENT
------------

**PLSK-3614-10**

REV

REV

## NOTES

- 15 Test requirements: The supplier shall test the pressure vessel and provided certified test results to show compliance with the requirements listed below:
- A) Cold Shock — Cold shock with liquid nitrogen.
  - B) Proof Pressure Test — Hydrostatic proof pressure test to 25.9 N/cm<sup>2</sup> (37.5 psi) with deionized water at room temperature.
  - C) Weld Seam Check —
- NOTE: Remove cap (Note 9) during test.
- Helium leak check weld seams incrementally using a vacuum cup arrangement connected to 5 psi at room temperature. After complete check of weld seams, repair as necessary. Repeat tests A, B, C after repairs.



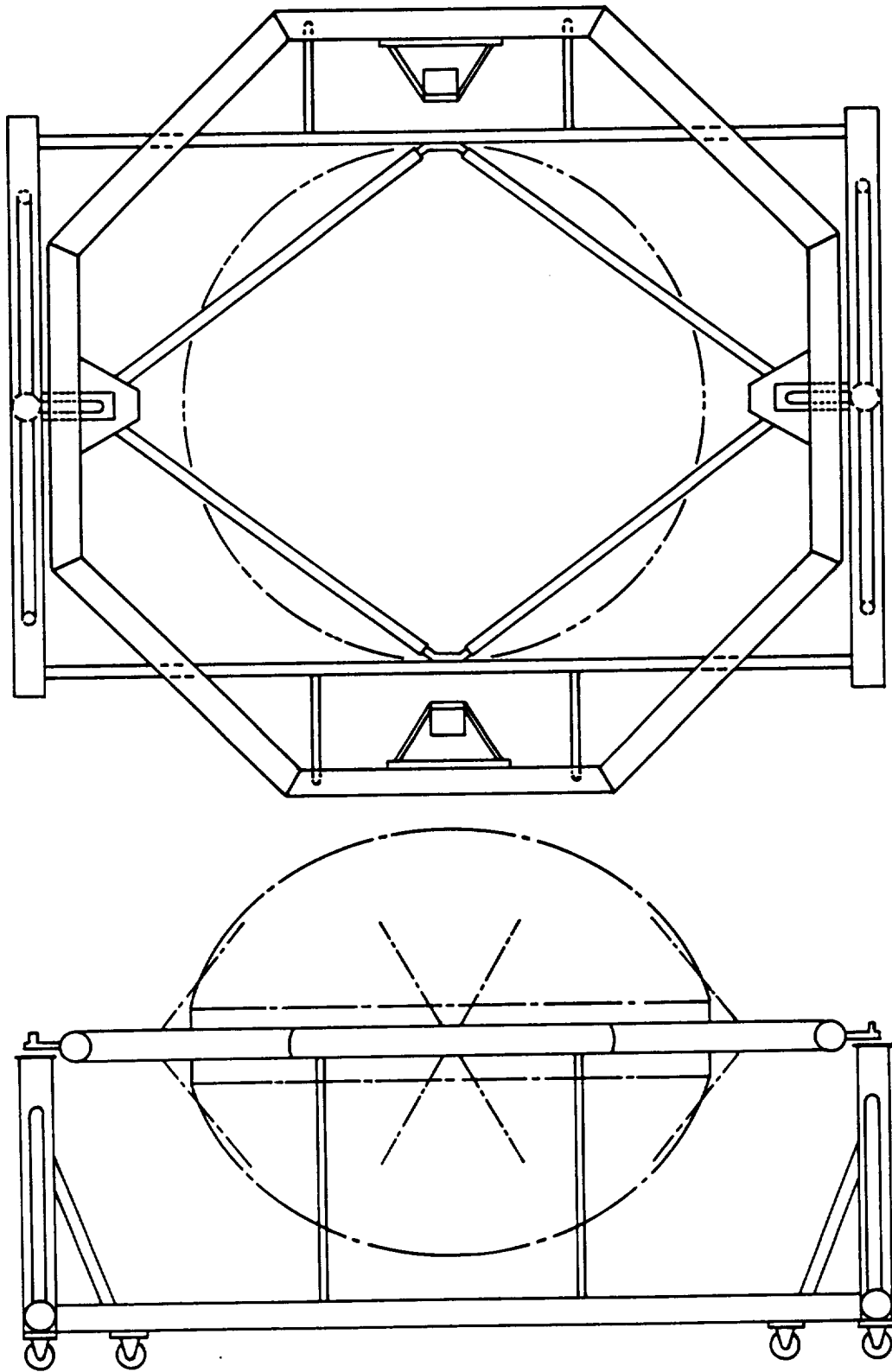


*Figure 6-8: Tank Transportation and Handling Stand*

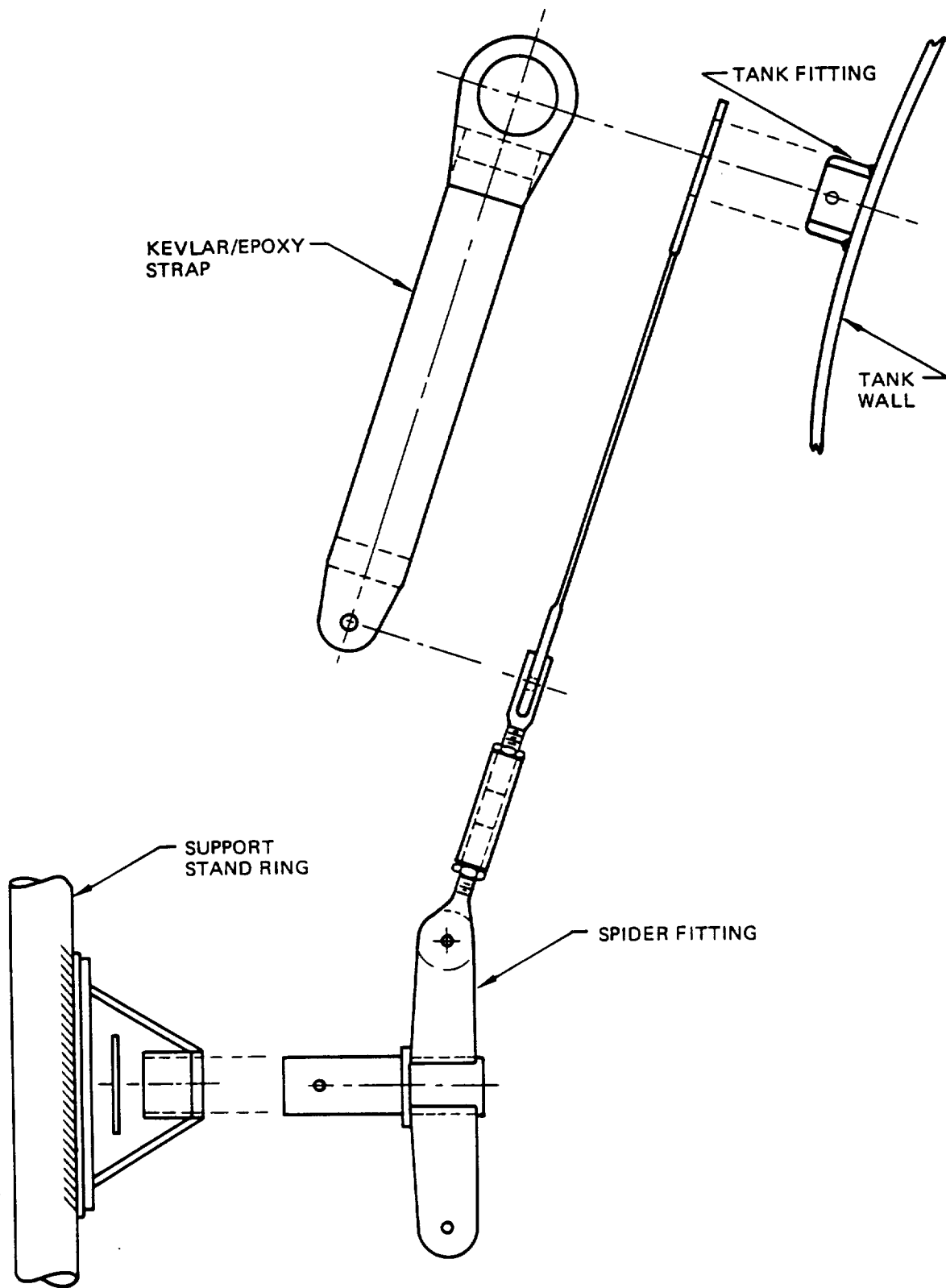


*Figure 6-9: Tank Support Straps*

fittings which attach to brackets at four points on the stand support ring. The straps and associated fittings will be sized in the course of the detailed design task.

The tank and its thermal shroud, mounted in the transportation and handling stand, are illustrated in Figure 6-10. Consideration will be given to removal of the eight upper straps during the vacuum chamber tests to reduce heat leak to the tank. This advantage must be weighed against problems of access and disturbance to the insulation and purge bag.

### **6.3.3. Thermal Shroud**

The thermal shroud will be constructed of 0.32 cm aluminum sheet, attached to the stand support ring with brackets for easy installation and removal for tank access. The panels may be either curved, as shown in Figure 6-10, or flat segments. Gaps will be provided between adjacent panels, adequate for free venting of the enclosed space but small enough to cause negligible disturbance to uniform radiation exchange between the tank and the shroud.

Heating of the thermal shroud will be accomplished with Nichrome ribbon resistance heaters bonded to the panels. Resistance heaters were chosen over fluid heat exchangers for several reasons. The required shroud temperature range of 200°K to 311°K would make the choice of a liquid fluid difficult. A gaseous circulating fluid would be undesirable because of anticipated problems in temperature uniformity due to the characteristic low thermal capacitance of gases. Any fluid system was expected to be difficult to design and install for leak-free operation in a vacuum chamber. Low temperature of an electrical resistance-heated shroud will be obtained by reducing or shutting off power to the heaters and allowing the chamber cryogenic shroud to cool the thermal shroud by radiation. Power to the thermal shroud may have to be reduced or shut off during part of the pump-down period to reduce the possibility of corona arcing.

### **6.3.4 Insulation System(s)**

Insulation design concepts are shown schematically in Figure 6-11. The MLI-foam system (Figure 6-11(a)) will employ two layers of 2.54 cm thick Rohacell 31 foam panels, formed to match the tank surface contour, and two 44-layer MLI blankets. Foam panels will be chamfered at their edges to accommodate differential thermal shrinkage between the tank wall and the foam. The MLI blankets will have single-step lap joints to reduce joint heat leaks. Between the foam and MLI blanks will be a single layer of Kapton film with all seams and penetrations sealed, to prevent gases trapped beneath and within the foam from contaminating the MLI. The MLI blankets will consist of 0.00076 cm (0.30 mil) double-aluminized Kapton film and B4A Dacron net spacers.

Figure 6-11(b) illustrates the MLI-only insulation concept. The same MLI blankets that form the outer part of the MLI-foam system will be used for the MLI-only system. The MLI-foam system will be installed and tested first, and the MLI blankets will be trimmed prior to reinstallation as the MLI-only system.

The purge bag, shown in Figure 6-11(b) is a laminated reinforced Kapton film supported approximately 10 cm (4 inches) from the outer surface of the insulation. The edges of the purge bag sheets will be joined by taping. Arrangements of gas feed to the bag, gas feed to the MLI interstices, and venting will be determined in the purge system detailed design. The purge bag will be supported on stand-off posts attached to the insulation or tank, or from ties to the thermal shroud panels.

Assembly of foam panels and MLI blankets on the tank is shown in Figure 6-12. Joints in all adjacent layers are staggered so that no two adjacent seams are superimposed. The

TANK INSULATION AND PURGE BAG NOT SHOWN

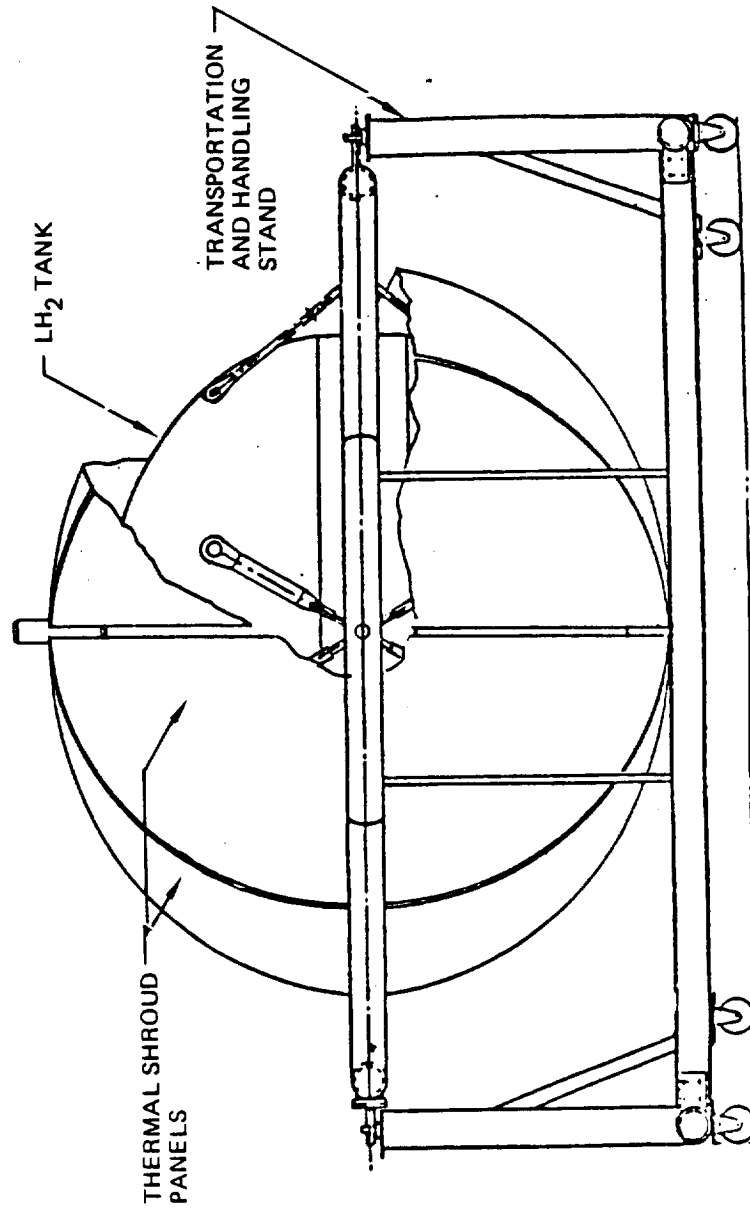


Figure 6-10: Tank and Thermal Shroud in Stand



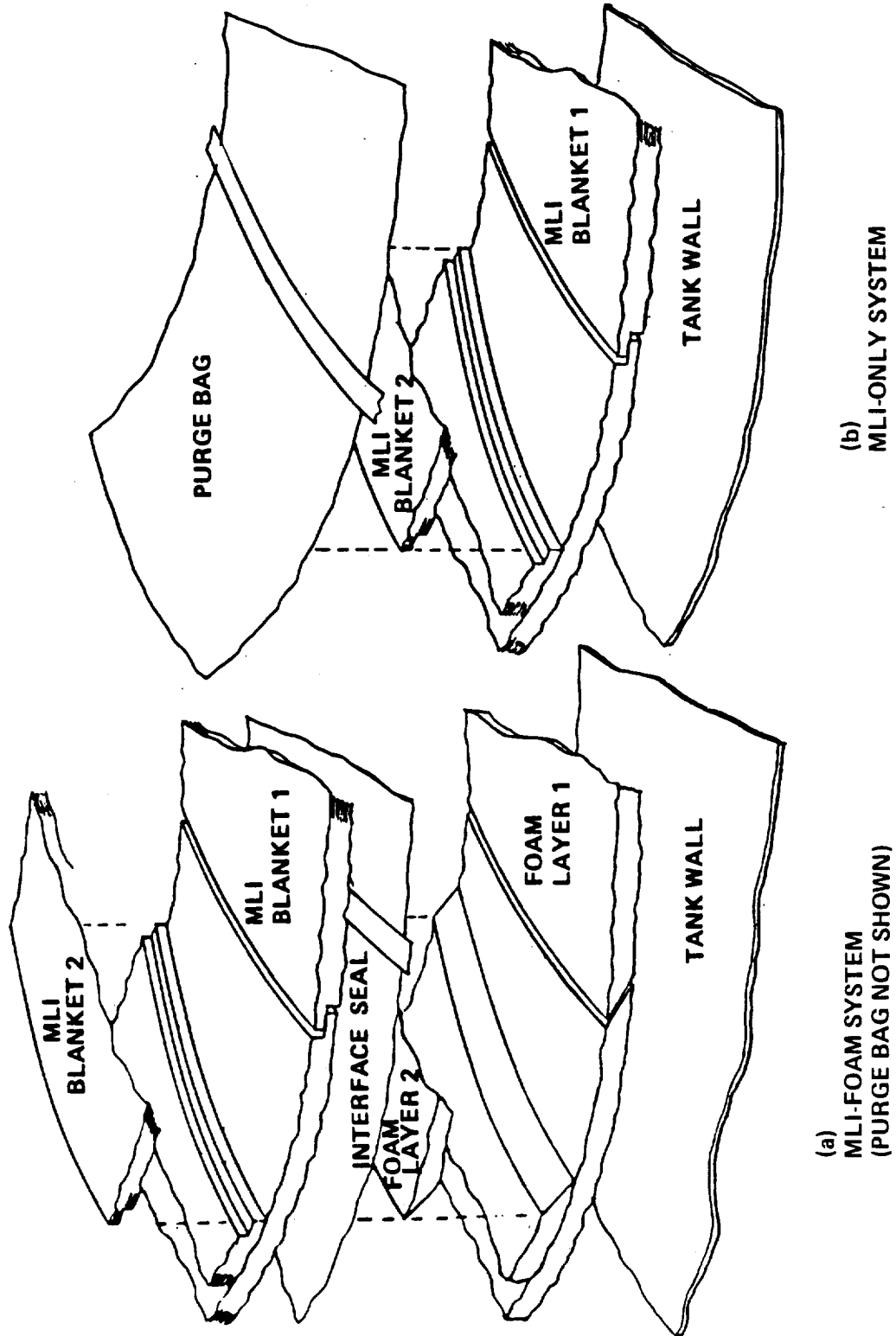


Figure 6-11: Insulation Design Concepts

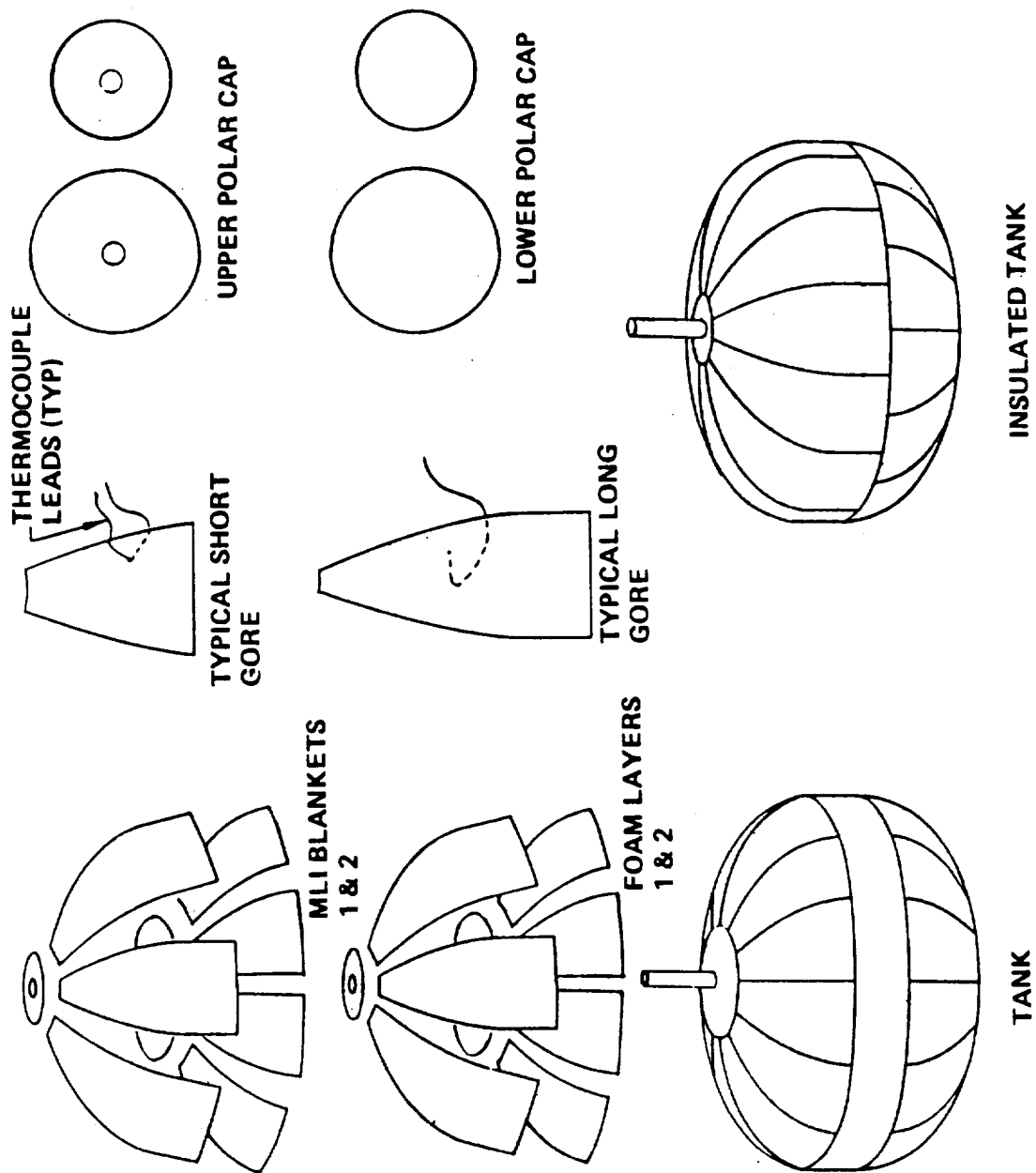


Figure 6-12: Insulation Installation

figure does not shown penetrations that will be required for support straps or details such as closures at these penetrations, MLI wraps on the straps and fittings, and MLI wraps at the plumbing penetration.

Tooling for the foam panels will consist of male fiberglass/epoxy molds and either similar female molds or a vacuum bag. Forming from flat stock sheets will be accomplished in a hot water bath or in a low temperature (170-190°C) autoclave, as described in Rohacell vendor publications. Fiberglass/epoxy templates will be fabricated for use as guides for trimming the panels to shape.

The MLI blankets will be laid up on fiberglass/epoxy male forms similar to the molds used to form the foam panels. The trim templates for initial trimming and retrimming the MLI blankets will also be fiberglass/epoxy, similar to those used for the foam.

The layers of the MLI blankets will be held together by Nylon pin fasteners such as the one shown in Figure 6-13. The button retainers for these fasteners snap into position on the pin shaft and can be permanently fixed by fusing the shaft to the button with a soldering iron. These fasteners not only retain the layers but provide a means of lacing (with Dacron thread) to secure adjacent blanket panels at joints. So laced, the MLI blankets will form a complete enclosure, requiring only minimum attachment of foam or inner MLI blankets to the tank. This arrangement of MLI blanket assembly is the same as that successfully used in the program of Reference 18.

After forming, lay-up, and trimming of the foam and MLI panels, the panels will be pre-conditioned in a vacuum chamber to remove contaminants and packaged in sealed containers with dry nitrogen until installed on the tank. Insulation thermocouples will be installed and wires routed and attached as insulation panels are installed on the tank, as shown in Figure 6-14.

Foam panels will be attached to the tank by either bonding or by means of Nylon hook-and-pile pads. If development tests provide that foam attachment by hook-and-pile pads will not lead to cryopumping and insulation performance degradation, this method will be used because it will ease the problem of foam removal. Patches of pile material will be bonded to the tank surface and the mating hook patches will be bonded to the foam panels. This means of attachment will provide for ease of adjustment and removal of the foam panels and will allow yielding at the mounting points needed to accommodate the thermal expansion difference between the foam and the tank. The outer foam panels will be attached to the inner layer in the same manner and then will be covered with a sealant to preclude cryopumping of the GN<sub>2</sub> purge gas. The MLI blankets will be attached to the tank, the foam, or to each other in a similar fashion. On the MLI blankets the hook or pile pads will be bonded to the heads or buttons of the fasteners shown in Figure 6-13.

### **6.3.5 Test Facility**

The laboratory facility assumed for planning and costing the experimental program is an existing vacuum chamber to be located at one of the test pads at the Boeing Tulalip Test Site. Cryogenic facilities, power, safety, control, and handling services are available at the site, located within 50 miles of the plant where engineering and fabrication work will take place.

The vacuum chamber is a 3.7 meter diameter horizontal-access cylinder, shown in Figure 6-15. Rails will be installed in the chamber to permit the insertion and securing of the test article in its transportation and handling stand. Installation of a liquid nitrogen cryogenic shroud along the inner walls of the chamber will also be required but is not considered as chargeable to the Experimental Program. Although the required cryogenic,

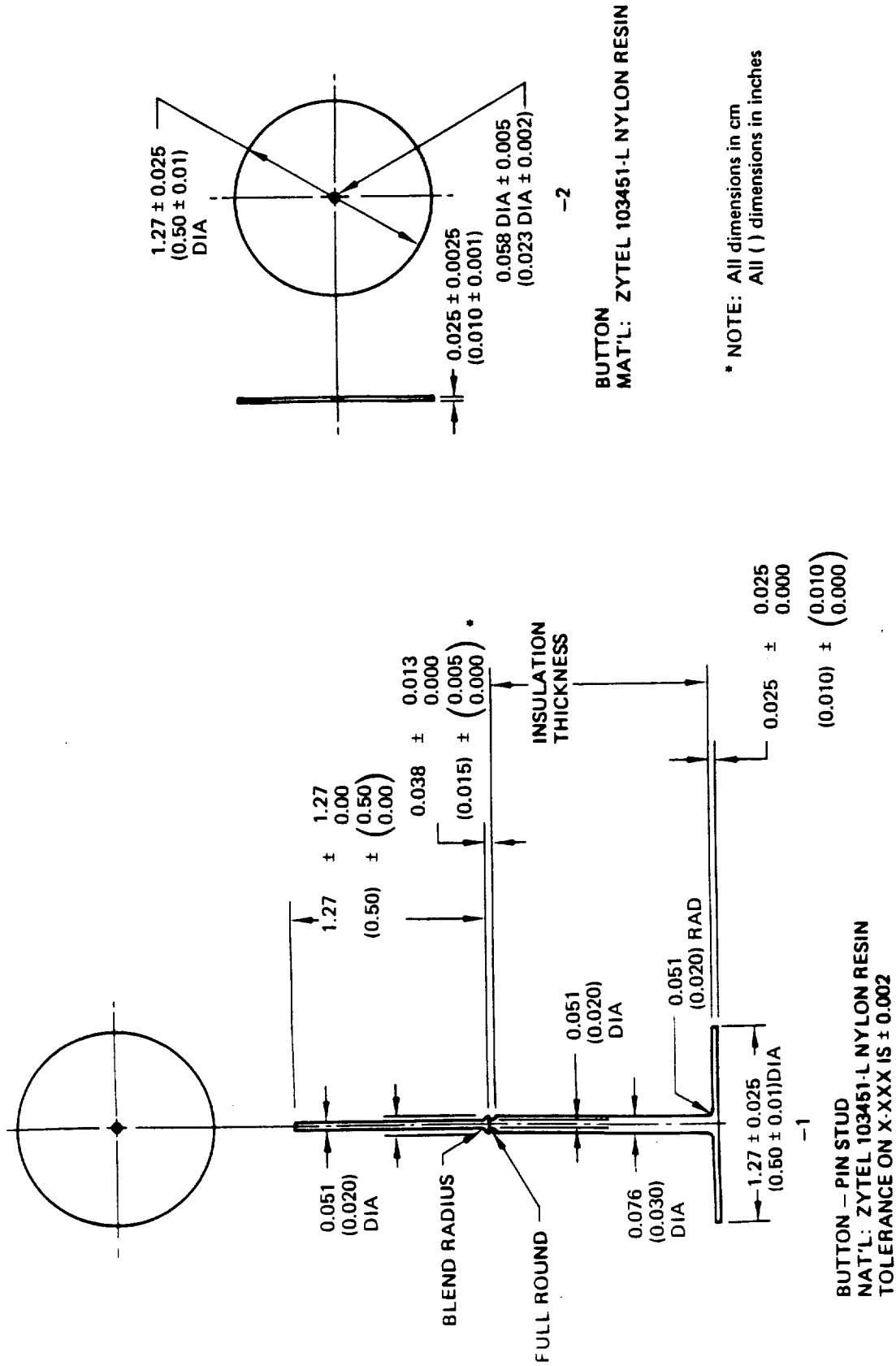


Figure 6-13: Typical Fastener for MLI Insulation

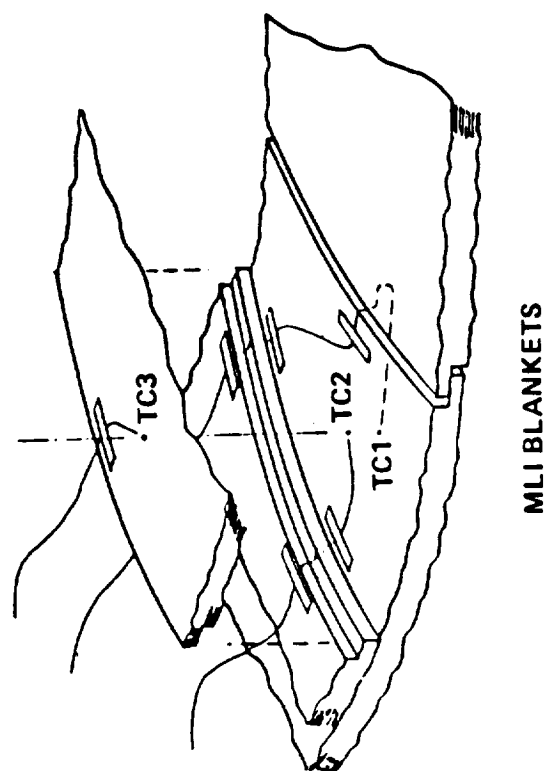
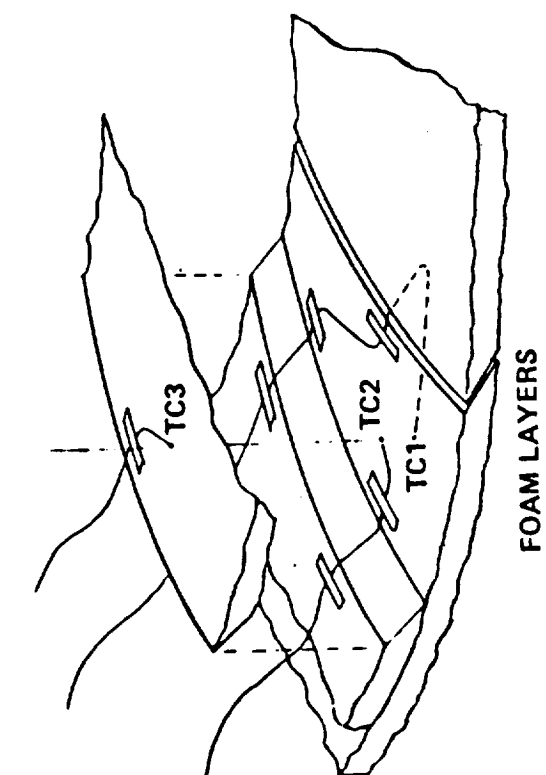


Figure 6-14: Insulation Assembly Typical Thermocouple Set Installation and Wire Routing

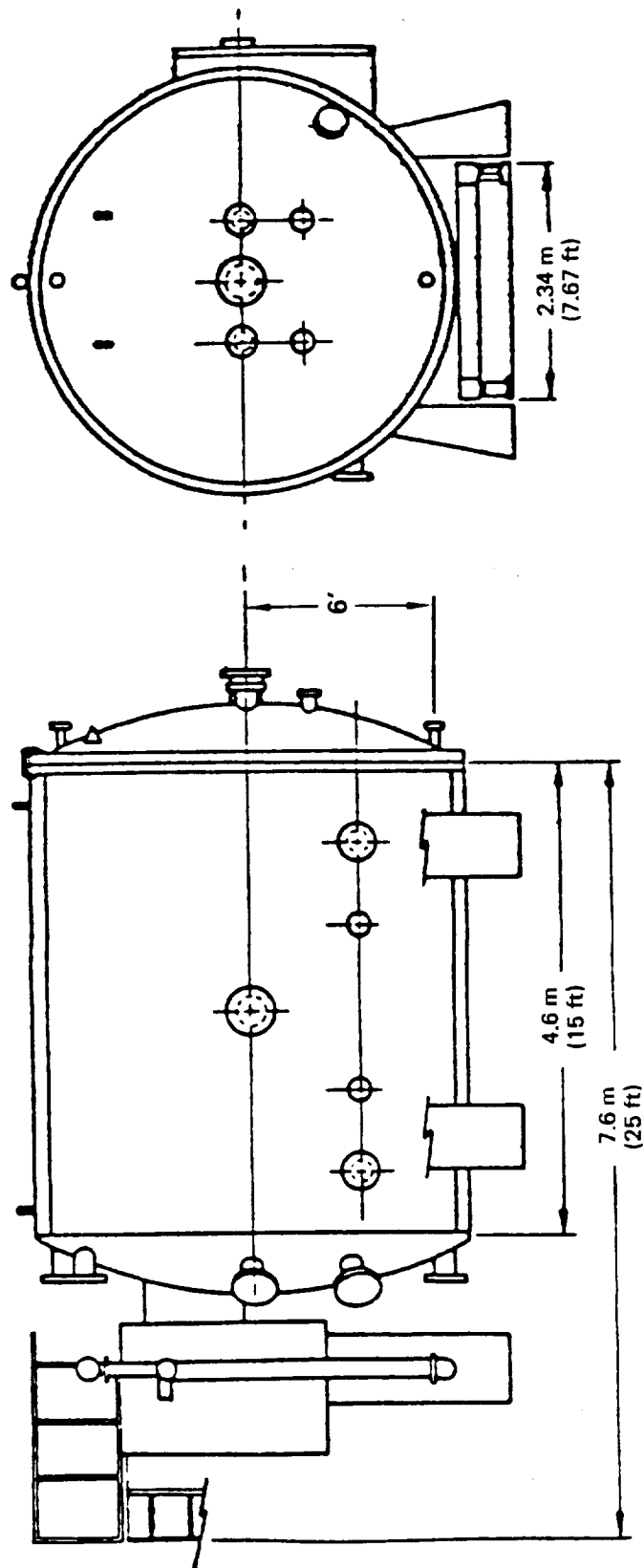


Figure 6-15: Vacuum Chamber

gas, power, and data acquisition systems are available at the test facility, a significant amount of design, fabrication, installation, checkout, and calibration work, unique to this particular program, will be required to test the tank in this chamber.

A schematic layout of test facility cryogenic, gas, vacuum, electrical, and data acquisition systems was developed to aid in estimating facility modification, set-up and calibration costs. This layout and basic facility requirements are shown in Figure 6-16. Individual lines, pumps, valves, tanks, etc., were not sized, but the layout plan provided a basis for an overall estimate of components and materials, as well as design and fabrication effort, required to prepare the facility for testing.

The test tank pressure control and hydrogen boil-off flow measuring and vent system is a key part of the facility system. Layout of this part of the system is shown in more detail in Figure 6-17. Multiple circuits and devices are required for the back pressure control and boil-off flow rate measurement because of the wide variation in heat flow to the tank between ground hold (sea level pressure and MLI purge) simulation and orbit (space vacuum) simulation.

### **6.3.6 Instrumentation System**

Approximately 300 channels of instrumentation will be used to control and monitor the pressure gages, flow meters, and temperature sensors for the tests. In addition to measuring the performance of the test article, the system will include sensors placed at strategic points to monitor the function of the various facility systems. A list of instrumentation for primary test measurements appears in Table 6-1. This list does not include those instruments that are considered as permanent components in the facility systems to monitor and control their performance.

Determination of the hydrogen boil-off flow rate is the single most important instrumentation requirement for the program and a difficult one to satisfy accurately because of the expected wide range of flow rates. Three separate flow meter systems are planned, operating over different but overlapping measurement ranges. Final selection of particular devices requires further study, as part of the detailed test planning. Instruments considered for this application include hot film anemometers, Matheson mass flow meters, wet test meters, and Hastings-Radist mass flow meters, such as were planned for use in the program of Reference 18.

A back pressure control system will be used to maintain a constant pressure in the tank and a constant hydrogen saturation temperature. A silicon diode thermometer tree with 50 sensors will be used to measure liquid and gas temperatures within the tank and to determine liquid level. All wires into the tank will be routed through the guarded connector to minimize heat leak.

Temperature sensors will be attached through the insulation layers and on the purge bag at 26 locations. Silicon diode thermometers will be used on the tank wall and Type "E" chromel-thermocouples will be used within the insulation and on the purge bag. Sensor lead wires, except for those to thermocouples on the purge bag and insulation outer surface, will be routed so as to minimize absorption of radiant heat from the thermal shroud.

The thermal shroud will be divided into 28 heat zones for use of independently monitored and controlled heater arrays. The shroud zones will be initially heated to follow the temperature profile of Figure 6-4 and adjusted to provide a uniform distribution of insulation surface temperatures.





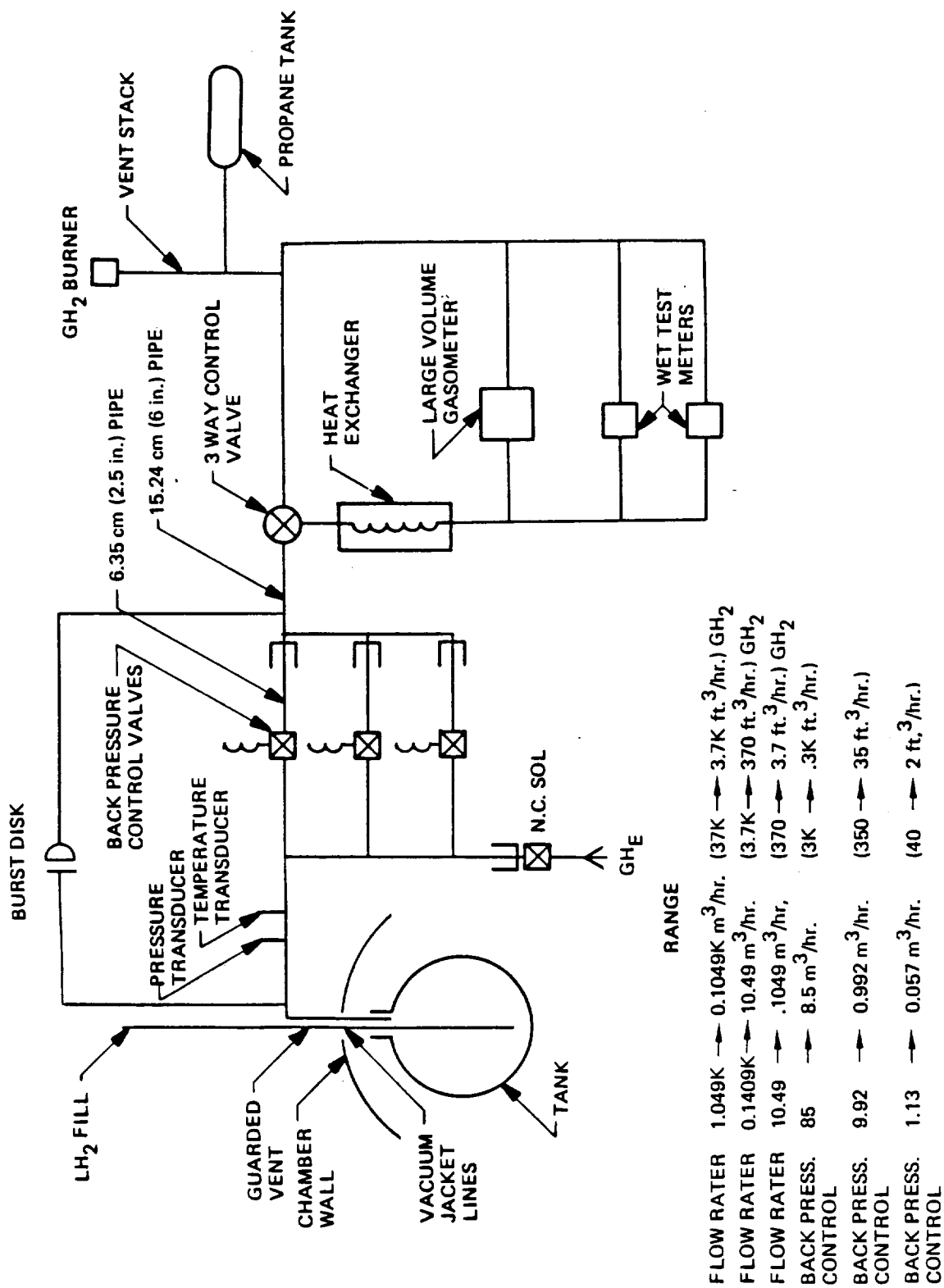


Figure 6-17: Hydrogen Back Pressure and Vent System

Description	Tolerance	Instru.	Qty
Temperature survey of tank insulation and tank surface (18 positions)	(Typ) $\pm 0.05^{\circ}\text{K}$ ( $\pm 0.1^{\circ}\text{F}$ ) on tank @ $22^{\circ}\text{K}$ ( $40^{\circ}\text{R}$ )	Silicon diode	18
	(Typ) $\pm 0.5^{\circ}\text{K}$ ( $\pm 1.0^{\circ}\text{F}$ ) in insula. @ $39^{\circ}\text{K}$ ( $70^{\circ}\text{R}$ )	Thermal-couple Type "E"	108
Temperature survey of tank supports and tank connections	Typ	Silicon diode	36
16 support (2 SD-4 T/C)	Typ	"E" T/C	68
2 wire bundles (2 T/C)			
2 supply and vent lines (2 SD)			
Radiant heat shroud temp w/control feedback (4 junctions average)	Typ	"E" T/C	29
Chamber pressure			
• Barratron — 760 torr - 1 torr	$\pm 1\%$	Barratron	1
• UHV — $1 \times 10^{-3}$ torr - $1 \times 10^{-11}$	$\pm 20\%$	UHV	1
• Grandvill Phillips — 760 torr - $1 \times 10^{-3}$	$\pm 10\%$	GP	1
Tank static pressures and control	$\pm 1\%$	Barratron	1
Fill line temp	Typ	Silicon diode	1
Purge line temp	Typ	"E" T/C	1
Vent line temp	Typ	Silicon diode	1
Diffusion pump temp	Typ	T/C	1
LN <sub>2</sub> shroud temp	Typ	T/C	8
Tank LN <sub>2</sub> level	$\pm 1^{\circ}\text{F}$	Silicon diode	50
GH <sub>2</sub> vent rate	$\pm 1\%$		3
Purge blanket pressure	$\pm 1\%$ scale	MKS Barratron 0-3 torr diff head	1
Blanket flow rate	$\pm 1\%$	Fisher-Porter flow meter	1

Table 6-1: Instrumentation List

All calorimeter and flow rate instruments will be calibrated to  $\pm 1\%$  of reading. The remaining instrumentation will be  $\pm 1\%$  full scale.

Calibration of the flow rates, back pressure controller, and calorimeter thermocouples will require special procedures and test fixtures. Additionally, an installation technique will have to be developed to insure repeatable thermocouple readings at the desired accuracy of  $0.5^\circ\text{K}$ .

All data lines will be routed through a control system for storage on an 8 track tape. The data sample rate of once/second will be controlled by this equipment. During the simulated launch period, selected monitors will be continuously recorded to provide transient data. Control system will provide real time monitoring of all active measurements and control functions.

## 6.4 COST ESTIMATES

The cost estimate for the Experimental Program was developed by integrating two basic approaches to defining the magnitude of the program effort. In the first approach, a list of individual tasks constituting the program was formulated and costs in terms of labor, materials, and other expenses were estimated for each task. The tasks included all those necessary to plan the program, administer and manage it, prepare for the tests, carry out the tests, and evaluate and report the results. The test preparation tasks were summarized in section 6.2.1. The second approach took into account the sequential dependence and completion time required for the program tasks and led to a schedule of program activities. The core of this schedule, the portion describing the direct preparation and execution of the tests, was formulated first and is illustrated in Figure 6-18. Periods for detailed planning and early design work and the beginning of the program, and for evaluation and reporting at the end, were added to the core schedule.

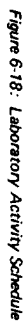
Review of the task labor requirements permitted adjustment of the schedule in order to avoid large variations in manning levels and to aid in efficient management, direction, and coordination. It was concluded from this exercise that a 24 month duration was appropriate for the program, setting the stage for a final summation of program cost estimates.

Cost estimates were formulated in 1982 dollars. Labor costs were developed from estimates of the actual hours required to perform the tasks and burdened labor rates, which included all overhead and distributed costs except the program fee. Costs of materials, dedicated equipment, and purchased components were estimated from vendor quotes, available price lists, or recent experience. Scrap allowances were added to material quantities where they could be computed, e.g., to film, net, and foam stock for insulation fabrication. Following standard Boeing practice, an additional yield factor of 1.25 was applied to all raw material quantities as an allowance for additional scrappage, rejection, or damage. The yield factor was not applied to specifically identified equipment items or completed components expected to be covered by specifications and performance guarantees.

Test consumables, i.e., cryogenes, gases, solvents, cleaners, and lubricants, were all considered as overhead items and thus do not appear in the cost estimates.

Estimation of labor, material, and component costs relied heavily on experience from two recent programs at Boeing. The first was that of Reference 18, which included many preparation tasks, hardware items, and test procedures similar to those identified for the present planned program. Cost data from the program of Reference 18, however, is approximately 10 years old. Where these data were used, a factor of 2.0 was applied to







adjust to 1982 dollars. The second source of useful cost data was the ongoing Boeing Cryogenic Propulsion IR&D program, in which plans are being developed for a test of a liquid hydrogen tank in the same facility selected for the present planned program. Except in cases where price quotes were already available, the scope and time scheduled for the Task III effort did not permit a formal request for quote and supplier selection process for procured items.

For the purpose of labor dollar estimates, five categories of labor were identified, and hourly rates for each category selected on the basis of the average skill level deemed appropriate for the tasks of the program.

Contract administration and program utility and housekeeping support were considered overhead items and are accounted for as part of the burdened rates for direct labor.

Costs for computer time, required for the pre- and post-test thermal analyses, were estimated on the basis of experience with similar analyses carried out in Tasks I and II of the present program.

Travel costs for personnel travel to the test site for those employees not assigned to that location were computed based on \$0.20 per mile. Travel costs for presentations at NASA Lewis Research Center were based on recent actual costs for similar trips. Each of these three visits was assumed to involve three persons spending one working day at Cleveland.

The liquid hydrogen tank pressure vessel is a significant item in the hardware cost estimate for the program. Its fabrication cost was estimated two ways and the lower of the two used in the final estimate. The preliminary design drawing (Figures 6-5 through -7) was submitted to Boeing Aerospace Manufacturing Organization for a formal estimate. At the same time an informal estimate was made, based on the cost of the tank for the program of Reference 18, as produced by an independent fabricator. An arbitrary \$1000 was added to the independent fabricator's cost to account for shipping.

The program fee was set at 7% of the total cost.

## **6.5 PROGRAM SCHEDULE AND COSTS**

The breakdown and schedule of program tasks, at the level used for cost estimating, was judged too detailed for convenient display on a single chart. Therefore, for summary documentation purposes, the tasks were organized into four major categories. These categories are engineering and administration, fabrication and assembly, facility preparation, and test activities. Charts showing the schedule and cost summaries for tasks under these four categories are presented as Figure 6-19 through 6-22. These charts show all costs except the program fee.

In Figure 6-19 the non-labor costs apply to travel for technical direction and coordination and for reporting, and computer charges for the analysis tasks. The reporting task schedule does not show monthly progress reports but the cost of preparing these was included in the labor estimate.

The non-labor entries for the fabrication and assembly tasks, Figure 6-20, are all for material or hardware procurement. No labor cost is shown for the tank fabrication since it was assumed as a outside procurement item. Labor for proof tests of the tank (Figure 6-7, Note 15) is included in the test task category, Figure 6-22, although the tests would probably be performed by the fabricator and added to the cost of the tank.

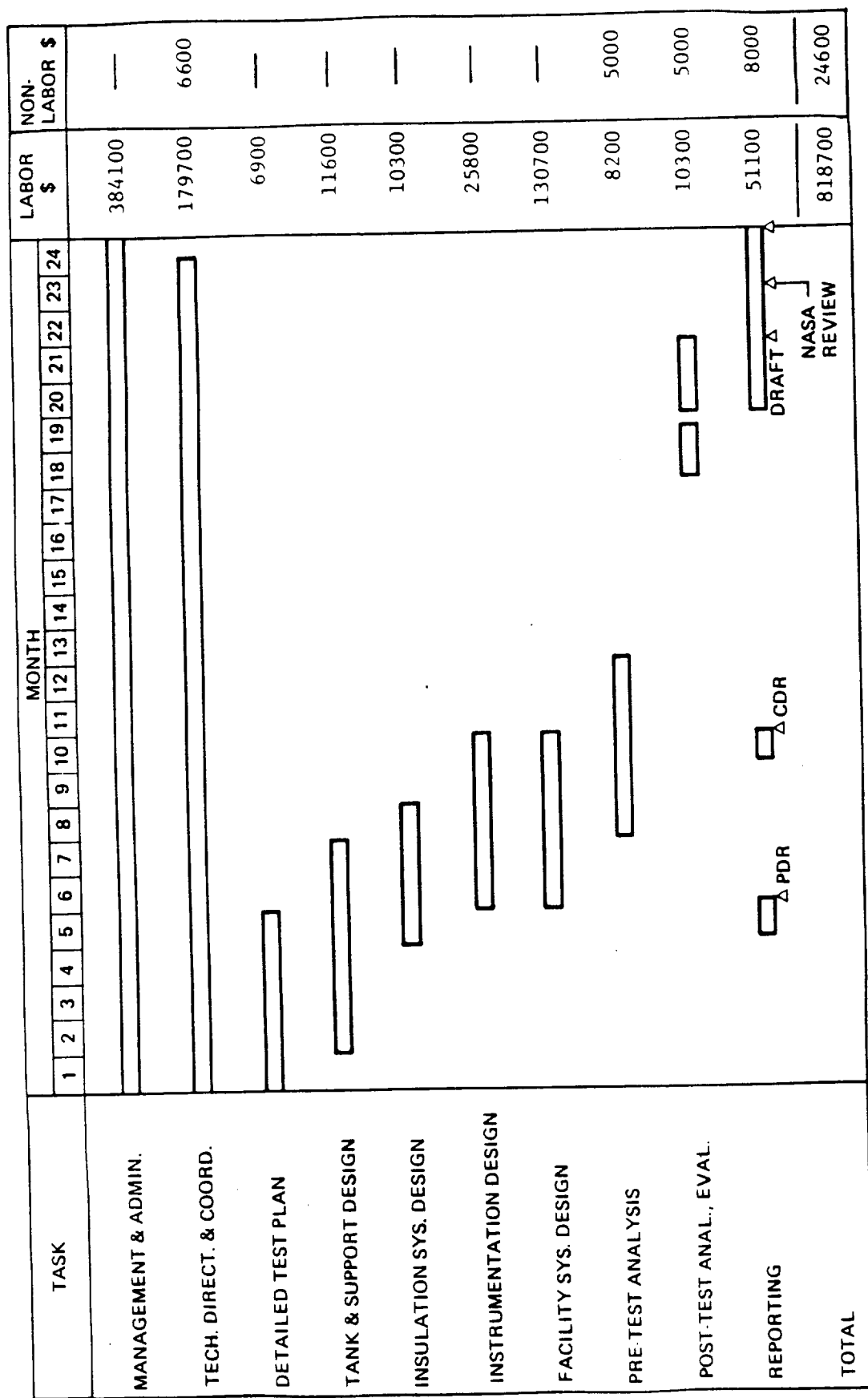


Figure 6-19: Experimental Program Task Breakdown — Engineering and Administration



TASK	MONTH																								LABOR \$	NON-LABOR \$
	1	2	3	4	5	6	7	8	9	10	11	12	13	14	15	16	17	18	19	20	21	22	23	24		
TANK FAB.																									—	41000
TANK SUPPORT SYS. FAB.																									15400	1300
MLI BLANKET FAB.																									37400	60400
FOAM PANEL FAB.																									14800	6000
TRANS. & HANDLING STAND																									18400	1500
INS. INSTALL., REMOVAL																									8300	
INSTRU. SYS. FAB.																									39100	60400
TEST ART. ASSEMB. & INSTALL.																									103800	—
TEAR-DOWN																									22300	—
TOTAL																									259500	170600

Figure 6-20: Experimental Program Task Breakdown — Fabrication and Assembly

TASK	MONTH																								LABOR \$	NON-LABOR \$
	1	2	3	4	5	6	7	8	9	10	11	12	13	14	15	16	17	18	19	20	21	22	23	24		
SITE PREPARATION																									53200	4800
CHAMBER LOC. & MOD.																									58800	5000
CHAMBER CLEAN, CONDITION																									54100	-
THERMAL SHROUD																									39900	23400
VACUUM SYSTEM																									34400	6900
CRYOGENIC SYSTEM																									36200	11000
PURGE SYSTEM																									33200	7000
ELECTRICAL SYSTEM																									18200	5000
DATA ACQUIS. SYSTEM																									19100	-
TOTAL																									347100	63200

Figure 6-21: Experimental Program Task Breakdown -- Facility Preparation

TASK	MONTH																								LABOR \$	NON-LABOR \$	
	1	2	3	4	5	6	7	8	9	10	11	12	13	14	15	16	17	18	19	20	21	22	23	24			
TANK PROOF TEST (CODE)																										24700	—
SUPPORT SYS. COMP. TESTS																										5000	300
MLI LAY-UP TRIALS																										1000	—
FOAM FORMING TRIALS																										1000	—
PUMP SYS. TESTS																										37700	—
CRYO. SYS. TESTS																										37700	—
INSTRU. CALIB.																										40900	—
PURGE SYS. TESTS																										37700	—
MAIN TESTS																										134000	—
POST-TEST INS. SYS. EXAM.																										1500	—
TOTAL																										321200	300

Figure 6-22: Experimental Program Task Breakdown — Test Activities

The facility preparation tasks of Figure 6-21 are those considered unique to the planned program and do not include capital expenses that might be required to provide basic facility capability, not chargeable to this program.

The test activity tasks of Figure 6-22 include all development, proof, checkout, and calibration tests; fabricability demonstrations; and material examinations; as well as the main cryogenic tank heat flow tests. The cost of support system component tests was allotted to non-labor costs for material for specimens to be tested before finalizing the tank support strap design. Costs for materials used in the foam and MLI fabricability demonstrations were included in the total costs of these materials tabulated in Figure 6-20.

Summation of costs from the four task categories, plus the program fee, is as follows:

Engineering and administration	\$ 843,300
Fabrication and assembly	\$ 430,100
Facility preparation	\$ 410,300
Test activities	\$ 321,500
Fee	\$ 140,400
Total	\$2,145,600

The total labor required is 39,200 hours and the cost breakdown by major cost sources is:

Labor	\$1,746,500
Material (including equipment and purchased components)	\$ 233,100
Computer	\$ 10,000
Other non-labor	\$ 15,600
Fee	\$ 140,400
Total	\$2,145,600

The program cost estimate was developed largely from a technical viewpoint, as a summation of its various component parts. It was not subjected to a critical management and cost control review appropriate to final costing of a program of its magnitude. Inputs were furnished independently by a number of contributors. It is quite possible that a closer integration of tasks and a more detailed definition of program flow and resource requirements would disclose and eliminate duplication or reduce idle time that may presently exist in the schedule.

On the other hand, as with any research program, there exist a number of high risk areas in the plan. Greater than anticipated problems in these areas could lead to significant increases in costs if program objectives and schedule are to be met. Risk areas include the design and performance of the MLI purge system, integrity of the foam when subjected to the range of pressures and temperatures required, and the ability to achieve desired vacuum levels, particularly within the MLI, with the many potential contamination sources present. Other potential problems are the ability to accurately measure boil-off rates over the wide range required, achievement of adequate thermal stability in the tank to permit meaningful interpretation of measured boil-off, and accurate assessment of discrete heat leaks to permit valid comparison of basic insulation heat flow. Overall, the program cost estimate is felt to represent a reasonable mean between possible reductions and potential additional costs. A large uncertainty, however, possible  $\pm 20\%$ , must be recognized, at least until a more detailed plan is accomplished.

## 6.6 TEST PROGRAM RECOMMENDATIONS AND ALTERNATIVE PLANS

Alternative test programs or design variations were considered very briefly with the goal of meeting all or some of the planned objectives at a reduced cost. Since a large part of the cost is in preparing the test facility, large cost reductions did not appear possible without a major change in test approach. It should be pointed out that the present plan, with its sub-scale tank, will not provide direct verification of the Task I performance predictions, and thus compromises to some degree that objective.

A further reduction in liquid hydrogen tank size could reduce the cost of the tank, particularly if forming of the tank heads by spinning, as opposed to the present welded preformed-gore fabrication, is made possible. Further savings would accrue through reductions in the material quantities required for insulation, the support stand, and the thermal shroud. All of these reductions, however, would be a relatively small percentage of total cost. The disadvantages of greater relative heat leak from penetrations and other local effects, and the greater departure from full scale are felt to outweigh the savings if the tank size is significantly reduced. If a change to spun tank heads is possible with only a small reduction in tank size, this modification is recommended.

A single test, that of the MLI-plus-foam system, was considered. This variation would shorten the program by approximately 1½ months and reduce the labor by the hours required for the eliminated test, insulation re-work, and associated pre- and post-test analyses. Test article fabrication, materials, and facility preparation, however, remain unchanged. The potential value of the information lost with this change is very great. With the potential difficulty in accurately evaluating the discrete heat leaks, an experimental comparison between the total heat flow with the MLI-plus-foam system and the MLI-only system may be the most accurate way of evaluating the performance of the former system. The deletion of the MLI-only test is therefore not recommended.

At the limit of tank down-sizing is a change to a flat plate calorimeter type test. Much of the preparation, analysis, and support activity for such a test would be on a much smaller scale than that of the present plan. The cost of such a program would, therefore, be much less than the present estimate. Properly designed, such a test would provide the clearest evaluation of heat flow through the basic tank wall insulation. No other information, such as penetration heat leaks, effects of tank liquid level, stratification, and pressure variations, or realistic insulation temperature distributions would be obtained, however. No experience would be gained in designing, fabricating, and operating insulation and purge systems on a real tank shape. The benefit of hardware and facility systems which could be carried over to future, even more realistic experimental programs, would be lost. A flat plate calorimeter test can be recommended as an adjunct or a preliminary to the present planned program but not as a substitute for it.

Substitution of liquid nitrogen for liquid hydrogen as the test cryogen would yield a moderate reduction in complexity and costs of certain test facility components, systems, and safety provisions. Some of the program risks would be reduced but much of the test realism would be lost. Temperature profiles would be altered so as to seriously degrade the validity of the Task I analysis verification. Assessment of the ability of the MLI purge to prevent condensation would be eliminated for all practical purposes. The relatively small cost saving from this alternative is not considered worth the loss in program value.



## 7.0 STUDY CONCLUSIONS AND RECOMMENDATIONS

The results of this study have shown potential benefits can be derived from the application of a foam substrate beneath cryogenic propellant tank multilayer insulation. Specific benefits are; 1) increased payloads for LTPS; and 2) reduced operational complexity due to the use of Orbiter cargo bay N<sub>2</sub> purge gas for MLI purging. In order to gain the benefit of increased payload mass when compared to MLI-only, it was found to be necessary to specify enhanced convection heat transfer in the purge enclosure. The enhanced convection environment provided increased thermal coupling between the warm Orbiter cargo bay and the outer layer of the propellant tank MLI. Therefore, the outer layer of the MLI was considerably warmer than it was for the case in which natural convection was assumed to occur in the purge enclosure. Less MLI and less foam were therefore required to achieve the desired MLI/foam interface temperature. Comparison of typical calculated foam and MLI thicknesses showed that optimized combination insulation thicknesses for natural convection conditions were typically 30 to 500% times greater than those for enhanced convection conditions. A true natural convection environment in the purge enclosure, however, would be difficult to achieve. This condition represents an extreme and was used to bound the problem of defining insulation designs.

A number of grades of N<sub>2</sub> were investigated as potential purge gases. The gas used to purge the Orbiter cargo bay has a dew point of slightly less than 244°K (-21°K). MLI/foam combinations designed for this dew point resulted in the largest payload penalties of all combination insulations investigated. However, for enhanced convection ground hold purge enclosure environments, even the insulation designed for the maximum MLI/foam interface temperature outperformed MLI-only on the basis of LTPS payload delivery capability. The payoff of using MLI/foam combination insulations was the greatest for the LTPS designed for the larger payload densities of 56 kg/m<sup>3</sup> (3.5 lbm/ft<sup>3</sup>) and 40 Kg/m<sup>3</sup> (2.5 lbm/ft<sup>3</sup>).

In general, however, considering all payload densities, the best MLI/foam interface temperature, from the standpoint of LTPS payload mass, was 144°K (-200°F). This temperature was the lowest value investigated. The difference in predicted LTPS payload capacity in going from a 144°K (-200°F) interface temperature to 244°K (-20°F) was only about 42 kg (93 lbm). Therefore the payload penalty incurred in selecting the higher interface temperature appears to be acceptable because Orbiter bay purge gas could then be used for MLI purging.

For low density payloads, the use of either MLI/foam or MLI-only insulations resulted in almost identical LTPS payload capacities. However, the benefits of being able to use Orbiter bay purge gas for MLI purging warrant the selection of MLI/foam insulations for low-density payload LTPS applications as well as for high-density payloads.

For high-density payload (payload mass-limited) cases, the two factors having the greatest influence on optimum MLI/foam insulation thickness were insulation mass and propellant boiloff. The optimum thickness occurred at the point at which the combined impact of insulation mass and propellant vent loss resulted in maximum payload capacity. The effect of insulation heat leak on tank self-pressurization and additional propellant for the 5 minute contingency countdown hold had little impact on the optimum insulation thickness.

In the case of moderate and low-density payload LTPS designs, MLI/foam thickness and tank volume had the greatest impact on the optimum insulation design. Tank volume was dependent on insulation performance because mission-integrated heat leak determined the amount of tank oversizing required to provide volume for propellants lost through venting.

The optimum insulation design occurred at the point at which the combined impact of insulation thickness and tank volume resulted in the shortest LTPS.

Estimated program cost for fabricating and testing both a MLI-only and a MLI/foam insulated  $\frac{1}{2}$  scale tank is 2.1 million dollars. The use of an existing tank as the test article would reduce program cost by \$50,000. The cost of performing the necessary testing is slightly more than \$320,000. Engineering and facility preparation were the other primary program labor cost items.

Facility preparation costs were based on an estimate of the labor, equipment, and materials required to prepare the existing Boeing hazardous test vacuum chamber for testing. Hence, the 0.41 million dollar cost estimated for this effort is valid for only the Boeing facility. These costs could be considerably less or more, depending on the test site ultimately selected.

In summary, the principal study results were:

## TASKS I AND II

- a. The purge enclosure heat transfer environment had a significant impact on insulation design because it determined MLI/foam insulation thickness and affected ground hold heat leak.

A natural convection environment (essentially stagnant gas conditions) was found to result in the highest LTPS payload mass delivery capability for He-purged tank insulation designs. An enhanced convection environment, in which warm purge gas was circulated in the purge enclosure, resulted in the highest LTPS payload mass for  $N_2$ -purged MLI/foam insulation designs.

- b. In comparing payload capabilities of LTPS utilizing MLI-insulated tanks with those utilizing MLI/foam, the use of MLI/foam was found to increase payload mass for cases in which enhanced convection was assumed to exist in the purge enclosure.
- c. In comparing payload capabilities of LTPS utilizing MLI-insulated tanks with those utilizing MLI/foam, the use of MLI/foam decreased payload mass for cases in which natural convection conditions were assumed to exist in the purge enclosure.
- d. In comparing payload capabilities of LTPS utilizing MLI/insulated tanks with those utilizing MLI/foam, for both purge enclosure environments, it was found the use of MLI/foam would give the highest payload mass for certain cases. For LTPS with the highest payload density of  $56 \text{ kg/m}^3$  ( $3.5 \text{ lbm/ft}^3$ ) the use of MLI/foam and an enhanced convection purge enclosure environment always resulted in highest payload masses.

For LTPS with the lowest payload density of  $24 \text{ kg/m}^3$  ( $1.5 \text{ lbm/ft}^3$ ) the use of MLI/foam and either a forced or natural convection purge enclosure environment always resulted in payload masses less than the MLI-only design with a natural convection purge enclosure.

- e. For MLI/foam combination insulations designed for an enhanced-convection purge environment, the  $LH_2$  tank foam substrate thicknesses ranged from a minimum of 0.43 cm (0.17 in) to a maximum of 1.83 cm (0.72 in) for all MLI/foam interface temperatures studied. The least foam was required for the lowest interface temperature, 144°K (-200°F), and the most foam was required for the highest interface temperature, 244°K (-20°F).  $LO_2$  tank foam thicknesses varied from 0.23 cm (0.09 in) to 1.93 cm (0.76 in).



- f. For MLI/foam combination insulations designed for a natural convection purge environment, the LH<sub>2</sub> tank foam substrate thicknesses ranged from 1.78 cm (0.71 in) for a 144°K (-200°F) interface temperature to 12 cm (4.7 in) for a 244°K (-20°F) interface temperature. LO<sub>2</sub> tank foam thicknesses varied from 1.12 cm (0.44 in) to 16 cm (6.3 in).
- g. Optimum LH<sub>2</sub> and LO<sub>2</sub> tank MLI thicknesses for He-purged insulations designed for a natural convection purge enclosure environment ranged from 2.03 cm (0.81 in) to 0.51 cm (0.21 in).
- h. Optimum LH<sub>2</sub> and LO<sub>2</sub> tank MLI thicknesses for He-purged insulations designed for an enhanced convection purge enclosure environment ranged from 6.1 cm (2.4 in) to 2.79 cm (1.1 in).
- i. From the standpoint of maximum payload mass, the best MLI/foam interface temperature is 144°K (-200°F). However, for combination insulations designed for the forced or enhanced convection purge enclosure environment, the loss in payload mass in going from 144°K (-200°F) to 244°K (-20°F) was only a maximum of 42 kg (93 lbm).
- j. The two principal factors which determined the optimum insulation design for high-density payload LTPS were propellant vent loss mass and insulation mass.
- k. The two principal factors which determined the optimum insulation design for low-density payload LTPS were propellant tank length and insulation thickness.

### TASK III

- a. A ½-scale LH<sub>2</sub> tank calorimetric test was defined to measure MLI/foam insulation performance. Total tank heat leak would be determined by measuring vent mass flow rate during simulated ground hold, ascent, and orbital conditions. Both MLI/foam and MLI-only insulations would be tested.
- b. The test program was estimated to require two years to complete. This program schedule included the design and fabrication of the test tank.
- c. Estimated test program cost, including labor and materials was 2.1 million dollars.
- d. Total program labor costs were 1.75 million dollars for the estimated requirement of 39200 hours.
- e. Engineering and administration costs totaled 0.833 million dollars. Test hardware fabrication and assembly costs were 0.43 million dollars, including 0.23 million dollars for materials, equipment and purchased components. Facility preparation cost was 0.41 million dollars and the cost of testing was 0.32 million dollars.

Based on the results of this study, areas for additional study have been identified. The additional studies should be made to finalize the relative merits of MLI versus MLI/foam insulations for a particular propulsion system and its associated mission or other similar Shuttle-transportable cryogenic tankage. These studies should address:

- o the effect of a different mission timeline, e.g. what if a seven-day hold on LEO was required,
- o advantages of applying a non-uniform foam thickness to the tanks,
- o the influence of different ground-hold conditions for a different LTPS configuration,

- o benefits of a decreased MLI layer density,
- o design techniques to preclude N<sub>2</sub> condensation on penetrations.

The benefits of MLI/foam insulations should be verified by test. In addition to validating predicted performance, hardware fabrication and testing are needed to address the following issues:

- a) How much moisture condensation and freezing can be allowed in the N<sub>2</sub>-purged MLI?
- b) What is the heat transfer performance effect of condensibles trapped in the seams and interstices of the foam?
- c) What additional costs are incurred by including the foam substrate?

## APPENDIX A

### RADIATION INTERCHANGE FACTOR AND ENVIRONMENTAL HEATING ANALYSIS PROGRAMS

A Boeing-proprietary computer program, RADSIM, was used in this study to predict radiation interchange factors between the Orbiter cargo bay, LTPS and LSS payload surfaces. A brief description of this program follows: The Radiation Simulation (RADSIM) program is a computer program which uses a Monte Carlo ray trace technique to calculate radiation exchange factors (Script-F's). The basic RADSIM program was developed by Dr. R. C. Corlett of Boeing. Minor modifications to the basic program have been made and the checkout and debugging of the computer code performed. The present version of RADSIM (version 4) is compatible with another Boeing-proprietary computer program, the Orbital Payload Environmental Radiation Analyzer (OPERA) program.

RADSIM incorporates radiation simulation at two wavelengths. The user may specify either diffuse emission at wavelength 1 or normal emission at wavelength 2. In general wavelength 1 is used for infrared radiation and wavelength 2 for solar radiation. The diffuse emission option is then used in determining the radiation exchange factors (Script-F's) between the model surfaces. The normal emission option can be used, along with a solar simulator emitting surface, to determine the radiation exchange factors between the model surfaces and the sun. However, for most cases, the solar calculations are made in a more appropriate manner with the OPERA.

Five (5) types of primary surfaces can be used to describe the vehicle geometry. These surfaces consist of trapezoids and segments of cylinders, cones, discs, and spheres. The primary surfaces can be subdivided into nodes to match that of the thermal math model. At present RADSIM will accept up to 700 primary surfaces and 1000 nodes. OPERA will accept up to 500 primary surfaces and 700 nodes.

RADSIM and OPERA calculations utilize both the infrared and solar radiative properties of the model nodes. The infrared and solar reflectivities can be specified as diffuse, specular, or a combination of diffuse and specular. In addition, nodes can be specified as adiabatic (i.e., floating at the radiative environment temperature). Adiabatic nodes are characterized as one- or two-sided and as isothermal or local adiabatic surfaces.

RADSIM prints out Script-F values from the emitting nodes to each model node. In addition, the program prints out the estimated statistical uncertainty in the Script-F value, product of area and Script-F, and the reverse Script-F value. RADSIM also generates an auxiliary disc file which contains the results in a format that can be used by utility programs. These utility programs put the results in a form suitable for direct use in a thermal analyzer program.

OPERA was used in this study to predict total thermal radiation heat flux on LTPS surfaces. The predicted flux included direct solar, direct earth IR and direct earth albedo fluxes as well as the total flux from these sources reflected by the Orbiter and LSS payload surfaces onto the LTPS. The OPERA program was developed to calculate environmental (solar, planet emission and albedo) heat loads for complex orbiting vehicles. The improvement that OPERA offers over previous orbital heat load programs is the inclusion of blockage and reflected (diffuse and/or specular) radiation.

The OPERA heat load calculations are based on a Monte carlo ray tracing technique which determines the radiation exchange factor (Script-F) with the environmental source (sun,

planet emission and albedo). RADSIM was modified and incorporated into OPERA to perform the Script-F calculations. Another existing program, SPARAD (Space Radiation) was modified and incorporated into OPERA to perform the orbit mechanics calculations.

OPERA uses the Script-F arrays to determine the environmental heat load on each nodal surface. A nodal heat load-time array is generated by OPERA for direct use with BETA (Boeing Engineering Thermal Analyzer) or SINDA (Systems Improved Numerical Differencing Analyzer) in the determination of the temperature-time profile of the complete thermal model. OPERA was also written such that it could be used directly as a subroutine to BETA.

OPERA calculates the geometric relationship between vehicle, sun and planet for both circular and elliptical orbits as a function of orbit position and time. The vehicle orientation can be specified as one of twenty-four (24) standard planet oriented or twenty-four (24) standard sun oriented cases. Other orientations can be specified as any fixed inertial orientation or a subroutine can be used to specify any orientation desired. In addition, a spinning vehicle can also be specified.

At present OPERA will calculate heat loads for up to forty (40) orbit output points in a single run. These output points can be specified as evenly spaced in mean anomaly (time) or the user can directly input the orbit output points to be used. The user may also specify that terminator and/or shadow crossing points be included in the output points.

At each orbit point, OPERA calculates each component of the environmental heat load on the vehicle model nodes. The user can specify any combination of solar, albedo and planet IR sources to be used in this heat load calculation. The calculations include the effects of blockage and reflection of the incident radiation.

OPERA prints out the Script-F values from each node to the specified environment source at each orbit output point. Heat load arrays are printed out for each environment source as well as the total for all sources on each node.

OPERA will also store the heat load arrays on disc files in a format that can be used by a thermal analyzer (e.g., SINDA). OPERA will also generate disc files which can be used to plot the vehicle geometry, nodal heat loads as a function of time, and the vehicle orbit.

## APPENDIX B

### TANK SUPPORT STRUT OPTIMIZATION

#### Symbols

A	Tank surface area $\sim m^2$
$A_0$	Baseline tank surface area $\sim m^2$
$f_1(V)$	Function relating mass of tank membranes, weld lands, etc. to volume
$f_2(V)$	Function relating mass of support ring, struts, and other support hardware to tank volume
I	Tank support strut cross sectional moment of inertia $\sim cm^4$
L	Strut length $\sim cm$
r	Radius of tank cylindrical section $\sim m$
$r'$	Toroidal tank minor radius $\sim m$
$r'_0$	Baseline toroidal tank minor radius $\sim m$
$r_1$	Strut outside radius $\sim cm$
$r_2$	Strut inside radius $\sim cm$
t	Thickness of $LH_2$ tank cylindrical section wall $\sim m$
$t_b$	Wall thickness of buckling-designed strut $\sim cm$
$t_0$	Baseline tank support strut wall thickness $\sim cm$
$t_s$	Strut wall thickness $\sim cm$
$t_t$	Wall thickness of tension - designed strut $\sim cm$
$t_w$	New calculated strut wall thickness as determined by total loaded tank weight $\sim cm$
V	New tank volume $\sim m^3$
$V_0$	Tank volume from baseline OTV (Reference 1) $\sim m^3$
W	LTPS loaded tank weight $\sim kg$
$W_A$	Calculated value of weight for $LO_2$ tank membranes, weld lands, tolerances, etc., based on weight - surface area relationship $\sim kg$
$W_0$	Reference 1 OTV loaded tank weight $\sim kg$
$W_r$	Calculated value of weight for $LO_2$ tank membranes, weld lands, tolerances, etc., based on weight - radius of curvature relationship $\sim kg$
$W_1$	Weight of tank membranes, weld lands, tolerances, manholes, local beef-ups, etc., for Reference 1 OTV tank $\sim kg$
$W_2$	Weight of support ring, struts and other support hardware for Reference 1 OTV tank $\sim kg$
$\rho$	Density of tank wall material $\sim kg/m^3$

For Task II, the heat leak to the cryogenic tanks attributed to the tank support struts was initially based directly on the support strut designs for the orbital transfer vehicle (OTV) of Reference 1. For the three Thermal Math Models investigated in Task IIB it was decided that a more realistic representation would result if the support strut design took into account the variation in strut properties as determined by structural requirements, an approximate weight optimization, and variations in configuration geometry. Configuration geometry affects allowable strut length, and total tank weight can affect strut cross sectional area, leading to differences in strut conductances from those of the OTV baseline. Strut length can affect payload weight allowance through strut weight and through thermal conductance influence on propellant boil-off.

It was further decided that the configuration influence on strut sizing, and thus on strut heat leak, would be established for only one set of nominal characteristics for each of the three payload density configurations. Effects of differences in insulation design, either from the various prescribed purge gas temperatures or from variations to optimize the

designs, are expected to have a minimal effect on strut sizing. The exclusion of strut resizing from insulation design iterations contributed to keeping the optimization effort in scope.

Ground rules adopted for tank support strut sizing for the 3 LTPS configurations are listed below:

1. Retain number of struts per tank from the OTV design.
2. Retain the outside diameter of struts from the OTV design.
3. Struts are tangent to the tank contour at the attachment ring.
4. With the OTV struts as baseline, vary strut wall thickness with tank weight and strut length, to establish minimum acceptable wall thickness based on the worst case conditions determined from either tension or buckling-stability-design criteria.
5. On the LH<sub>2</sub> tanks, retain existing OTV design strut angle configuration.
6. On the LO<sub>2</sub> tanks, retain end-to-end strut configuration (maintain common attachment point for adjacent struts at the body shell and the tank support ring).

A one-time optimization study, utilizing the preceding ground rules, was conducted to determine strut lengths to minimize the payload mass penalty associated with the hydrogen and oxygen tank support systems for each LTPS configuration. The payload mass penalty accounted for propellant boil-off attributed to strut heat leak and that associated with the strut mass. Where the optimized strut length was greater than the allowable lengths imposed by LTPS avionics ring geometric constraints, the largest allowable strut length was selected. Table B1 lists the final strut lengths which were used to establish strut wall thicknesses and, subsequently, strut thermal conductances.

The tank weight affecting strut sizing was taken as the total loaded tank weight. It was then assumed that the strut wall thickness would vary in direct proportion to the tank weight.

Thus,

$$\frac{t_w}{t_o} = \frac{W}{W_o} \quad (B-1)$$

- $t_w$  = new strut wall thickness as determined by tank weight.
- $t_o$  = strut wall thickness for OTV strut design.
- $W$  = loaded tank weight, LTPS configuration.
- $W_o$  = loaded tank weight, corresponding OTV tank.

Additional groundrules adopted for the tank support strut optimization analysis are as follows:

1. Use the OTV (Reference 1) tank volumes and weights as baselines.
2. LH<sub>2</sub> tank will always have a cylindrical section and only this section changes with volume.
3. Membrane weight vs. volume for the LH<sub>2</sub> tank varies directly with area of constant gage cylindrical section.

Configuration	Tank	Vol. m <sup>3</sup> (ft <sup>3</sup> )	Struct. Wt. Kg (lb)	Ins. Wt. Kg (lb)	Prop. Wt. Kg (lb)	Tot. Wt. Kg (lb)	Strut Length cm (in.)	t <sub>b</sub> cm (in.)	t <sub>t</sub> cm (in.)	t <sub>design</sub> cm (in.)
OTV	LH <sub>2</sub>	38.47 (1357.6)	230 (507)	41 (90)	3125 (6889)	3396 (7486)	50.5 (19.9)			.0889 (.035)
	LO <sub>2</sub>	13.70 (483.5)	189 (416)	20 (45)	17967 (39611)	18177 (40072)	68.3 (26.9)			.168 (.066)
56 Kg/m <sup>3</sup> Pay. Den. (3.5 lb/ft <sup>3</sup> )	LH <sub>2</sub>	38.50 (1358.6)	198 (436)	166 (365)	2557 (5637)	2920 (6438)	12.4 (4.9)	.00462 (.00182)	.0932 (.0367)	.0932 (.0367)
	LO <sub>2</sub>	13.85 (488.6)	173 (381)	84 (186)	14702 (32413)	14960 (32980)	143.3 (56.4)	.607 (.00182)	.1379 (.0367)	.607 (.0367)
40 Kg/m <sup>3</sup> Pay. Den. (2.5 lb/ft <sup>3</sup> )	LH <sub>2</sub>	27.32 (964.0)	198 (436)	166 (365)	2557 (5637)	2920 (6438)	12.4 (4.9)	.00462 (.00182)	.0932 (.0367)	.0932 (.0367)
	LO <sub>2</sub>	9.82 (346.7)	173 (382)	127 (281)	14702 (32413)	15003 (33076)	52.6 (20.7)	.0820 (.0323)	.1384 (.0545)	.1384 (.0545)
24 Kg/m <sup>3</sup> Pay. Den. (1.5 lb/ft <sup>3</sup> )	LH <sub>2</sub>	48.77 (1720.8)	163 (359)	133 (294)	1814 (4000)	2111 (4653)	41.7 (16.4)	.0376 (.0148)	.0564 (.0222)	.0564 (.0222)
	LO <sub>2</sub>	16.64 (587.3)	148 (327)	104 (229)	10433 (23000)	10685 (23556)	35.1 (13.8)	.0259 (.0102)	.0986 (.0388)	.0986 (.0388)

Table B1: Tank Support Strut Sizing

4. Ellipsoidal LO<sub>2</sub> tank membrane weight varies with tank surface area in accordance with a spherical area/volume ratio.
5. Toroidal LO<sub>2</sub> tank membrane weight varies with area for change in volume accomplished through a change in minor diameter only (outside diameter remains constant).
6. For all LO<sub>2</sub> tanks, include weight change due to membrane gage change required by change in radius of curvature.
7. Assume weight increments for weld lands, tolerances, manhole and local beef-ups vary in proportion to membrane weight changes.
8. Assume weights of non-containment items (support ring, strut fittings, etc.) vary with changes in total loaded tank weight.

For the LH<sub>2</sub> tank,

$$\frac{W}{W_1+W_2} = f_1(V) \frac{W_1}{W_1+W_2} + f_2(V) \frac{W_2}{W_1+W_2} \quad (B-2)$$

where

- $W_1$  = weight of membranes, weld lands, tolerances, manhole, local beef-ups, for OTV tank.
- $W_2$  = weight of support ring, struts, other support hardware, for OTV tank.
- $f_1(V)$  = direct factor on weight from volume variations.
- $f_2(V)$  = effect of volume variations through containment vessel weight change.

Under groundrules (2), (3), (7), and (8),

$$f_1(V) = 1 + \frac{\Delta W_1}{W_1} = 1 + \frac{2t\rho\Delta V}{rW_1} = 1 + \frac{2V_0 t \rho \left(\frac{V}{V_0} - 1\right)}{W_1 r} \quad (B-3)$$

$$f_2(V) = \frac{W_0 + \Delta W_1}{W_0} = \frac{W_0 + \frac{2V_0 t \rho \left(\frac{V}{V_0} - 1\right)}{r}}{W_0} \quad (B-4)$$

where

- $t$  = thickness of cylindrical section wall
- $\rho$  = density of wall material
- $V$  = new tank volume
- $V_0$  = tank volume of baseline OTV tank
- $r$  = radius of cylindrical section
- $W_0$  = loaded tank weight, corresponding to baseline OTV tank

For the properties and dimensions of the baseline LH<sub>2</sub> tank (Reference 1),

$$\frac{W}{W_1+W_2} = .33776 + .66224 \frac{V}{V_0} \quad (B-5)$$



For the ellipsoidal LO<sub>2</sub> tank,

$$\frac{W}{W_1+W_2} = f_1(V) \frac{W_1}{W_1+W_2} + f_2(V) \frac{W_2}{W_1+W_2} \quad (B-6)$$

where the nomenclature is defined as before.

Here,

$$f_1(V) = 1 + \frac{\Delta W_1}{W_1} = \frac{W_A}{W_1} + \frac{W_r}{W_1} - 1 = \left(\frac{V}{V_o}\right)^{2/3} + \left(\frac{V}{V_o}\right)^{1/3} - 1 \quad (B-7)$$

where,

$$\begin{aligned} W_A &= \text{new } W_1 \text{ as affected by change in surface area} \\ W_r &= \text{new } W_1 \text{ as affected by change in radius of curvature} \\ f_2(V) &= \frac{W_o + \Delta W_1}{W_o} = \frac{W_o + W_1 \left( \left(\frac{V}{V_o}\right)^{2/3} + \left(\frac{V}{V_o}\right)^{1/3} - 2 \right)}{W_o} \end{aligned} \quad (B-8)$$

Again, incorporating the values for the baseline LO<sub>2</sub> tank,

$$\frac{W}{W_1+W_2} = .45929 \left(\frac{V}{V_o}\right)^{2/3} + .45929 \left(\frac{V}{V_o}\right)^{1/3} + .081414 \quad (B-9)$$

For the toroidal LO<sub>2</sub> tank, with a fixed outside diameter (Groundrule (5)), and baseline dimensions and weights taken from the Task I, 40 kg/m<sup>3</sup> (2.5 lb/ft<sup>3</sup>) payload density toroidal LO<sub>2</sub> tank configuration (Figure 3-8).

$$f_1(V) = 1 + \frac{\Delta W_1}{W_1} = \frac{W_A}{W_1} + \frac{W_r}{W_1} - 1 = \left(\frac{V}{V_o}\right)^{1/2} + \left(\frac{V}{V_o}\right)^{1/2} - 1 \quad (B-10)$$

where

$$\begin{aligned} A &= \text{new tank surface area} \\ A_o &= \text{baseline tank surface area} \\ r &= \text{new tank minor radius} \\ r_o &= \text{baseline tank minor radius} \end{aligned}$$

$$f_2(V) = \frac{W_o + W_1}{W_o} = \frac{W_o + W_1 \left( 2 \left(\frac{V}{V_o}\right)^{1/2} - 2 \right)}{W_o} \quad (B-11)$$

Then, for the toroidal LO<sub>2</sub> tanks,

$$\frac{W}{W_1+W_2} = .91858 \left( \frac{V}{V_0} \right)^{1/2} + .081414 \quad (B-12)$$

Since the insulation system of primary interest in the current program, the MLI/Foam system, results in considerably greater tank insulation weights than the MLI-only system of the OTV, the insulation weights were excluded from the preceding weight-versus-volume relations. Instead, conservative estimates of MLI/Foam weights for the individual tanks were added after computation of volume-determined tank structural weights.

Tank mass versus tank volume trend relationships (Equations (B-1), (B-2), and (B-3)), are plotted in Figure 5-4. Although the mathematical expressions differ for the ellipsoidal and the toroidal LO<sub>2</sub> tanks, for a moderate range of (V/V<sub>0</sub>), the plotted curves are practically equivalent and are so shown in the figure. For the baseline and groundrules used, the center opening of the toroidal tank vanishes at V/V<sub>0</sub> = 1.761, setting an upper limit on the toroidal LO<sub>2</sub> tank curve. Tank structural weights taken from these relationships are shown in Table B1.

The effect of strut length on wall thickness for a buckling-stability-designed strut was based on an assumed constant buckling criticality. For this,

$$\frac{I}{L^2} = \text{const.} \quad (B-13)$$

and

$$I = 1/4 \pi (r_1^4 - r_2^4), \text{ for a circular tube} \quad (B-14)$$

- I = moment of inertia of strut section
- L = strut length
- r<sub>1</sub> = outside radius of strut section
- r<sub>2</sub> = inside radius of strut section

From the expression for I, with

$$\begin{aligned} t_s &= r_1 - r_2 \\ t_s &\ll r_1, \\ I &\approx \pi r_1^3 t_s \end{aligned}$$

and therefore,

$$\frac{\pi r_1^3 t_s}{L^2} = \text{const.} \quad (B-15)$$

Thus, for constant buckling criticality, t<sub>s</sub> is proportional to L<sup>2</sup>.

The final strut wall thickness is found from:

$$t_b = t_0 \left( \frac{L}{L_0} \right)^2 \frac{W}{W_0}, \text{ buckling-designed} \quad (B-16)$$

$$t_t = t_o \frac{W}{W_o} , \quad \text{tension-designed} \quad (B-17)$$

Results of application of these relationships to the 3 configurations are shown in Table B1. Table B2 summarizes the final strut lengths, wall cross section areas and conductivity expressions.

Stowed Payload Density, kg/m <sup>3</sup> (lb <sub>m</sub> /ft <sup>3</sup> )									
Tank Type	Strut Material	Strut Conductivity – Temperature Dependence W/m-K (BTU/hr-ft-°F)	No. Struts	56 (3.6)			40 (2.5)		
				Area, * cm <sup>2</sup> (in <sup>2</sup> )	Length, cm (in)	Area, cm <sup>2</sup> (in <sup>2</sup> )	Length, cm (in)	Area, cm <sup>2</sup> (in <sup>2</sup> )	Length, cm (in)
Hydrogen	Fiberglass/ Epoxy	0.086 + 1.98 x 10 <sup>-3</sup> T (0.342 + 6.35 x 10 <sup>-4</sup> T)	24	44.6 (6.92)	12.4 (4.9)	44.6 (6.92)	12.4 (4.9)	27.0 (4.18)	41.7 (16.4)
Oxygen	Graphite/ Epoxy	0.138 + 0.146T (21.7 + 0.047T)	32	310 (48.1)	143 (56.4)	70.7 (11.0)	52.6 (20.7)	50.3 (7.80)	35.1 (13.8)

\* Cross section area of all support struts

Table B2: Support Strut Thermal Configuration(s)

## APPENDIX C

### TRADE PROGRAMS FOR LTPS SIZING AND INSULATION OPTIMIZATION

Two interactive computer programs were written to assess the LTPS payload capacity. Program development was based on the methods presented in section 5.

Figure C-1 illustrates the typical input required and the detailed output supplied by each program. As such, the output provides:

- o Intermediate calculations, if requested
- o The effect of thermal loads on LTPS design features
- o An itemized propellant inventory
- o Mass and volume statements for the LTPS conceptual design and LSS payload
- o A summary of the input data and the LTPS deliverable LSS mass.

Note that an abbreviated output option is available, which only gives the last six lines.

Figures C-2 and C-3 present the two interactive programs. Program TRADE as initially written was used to evaluate the insulation integrated performance for natural-convection ground-hold environments. This program was subsequently simplified to reflect enhanced-convection ground-hold environments, and it was, therefore, named TRADE2.

Each program contains numerous comment statements, that aided in program development. They also serve to help the interested reader in understanding the program(s).

Do you want calculation details? yes  
 packaged payload density= 2.5  $\text{lb}_m/\text{ft}^3$   
 type tank (hydrogen or oxygen): hydrogen  
 tank ullage volume at t-4 min.= 2.0 %  
 Do you want nitrogen or helium purge gas? nitrogen  
 type foam (Rohacell 31 or BX 250A): Rohacell 31  
 Minimum allowable interface temperature= -200.  $^{\circ}\text{F}$   
 foam thickness (inches)= 2.0  
 END OF INPUT DATA

type tank= EH  
 maximum foam temperature=  $-0.44385\text{E}+02$   $^{\circ}\text{F}$   
 foam resistance=  $0.337738\text{E}+02$   $\text{Hr}\cdot\text{ft}^2\cdot^{\circ}\text{F}/\text{BTU}$   
 MLI thickness=  $0.3263\text{E}+00$  feet  
 minimum MLI surface temperature=  $0.9062\text{E}+01$   $^{\circ}\text{F}$   
 MLI resistance=  $0.3166\text{E}+02$   $\text{Hr}\cdot\text{ft}^2\cdot^{\circ}\text{F}/\text{BTU}$   
 minimum conductance=  $0.152819\text{E}-01$   $\text{Hr}\cdot\text{ft}^2\cdot^{\circ}\text{F}/\text{BTU}$   
 minimum interface temperature calculated=  $-0.2000\text{E}+03$   $^{\circ}\text{F}$

ground-hold insulation flux=  $0.69377\text{E}+01$   $\text{BTU}/\text{Hr}\cdot\text{ft}^2$   
 average foam temperature=  $-0.27117\text{E}+03$   $^{\circ}\text{F}$   
 average interface temperature=  $-0.19348\text{E}+03$   $^{\circ}\text{F}$   
 average MLI temperature=  $-0.71901\text{E}+02$   $^{\circ}\text{F}$   
 average transition heat flux=  $0.46663\text{E}-01$   $\text{BTU}/\text{ft}^2\cdot\text{Hr}$   
 due to ground-hold conditions=  $0.15032\text{E}+00$   $\text{BTU}/\text{ft}^2$   
 due to foam cooling=  $0.20121\text{E}+01$   $\text{BTU}/\text{ft}^2$   
 (foam capacitance=  $0.41850\text{E}-01$ )  $\text{BTU}/\text{lb}_m\cdot^{\circ}\text{F}$   
 due to MLI cooling and heat leak=  $0.64718\text{E}-01$   $\text{BTU}/\text{ft}^2$   
 (MLI transition heat flux=  $0.12956\text{E}-02$ )  $\text{BTU}/\text{Hr}\cdot\text{ft}^2$   
 due to deployed-LEO hold=  $0.61809\text{E}+00$   $\text{BTU}/\text{ft}^2$   
 (MLI heat flux for LEO hold=  $0.56190\text{E}-01$ )  $\text{BTU}/\text{Hr}\cdot\text{ft}^2$   
 orbit-transfer insulation flux=  $0.47762\text{E}-01$   $\text{BTU}/\text{Hr}\cdot\text{ft}^2$

Hydrogen/Oxygen tank heat leak due to:  
 penetrations= 100.0/ 74.0  $\text{BTU}/\text{Hr}$   
 struts for the mission phases,  
 ground-hold and initial ascent= 12.8/ 247.0  $\text{BTU}/\text{Hr}$   
 tank-unlock to 60 hours= 10.9/ 203.0  $\text{BTU}/\text{Hr}$   
 LTPS ignition to disposal orbit= 8.9/ 183.0  $\text{BTU}/\text{Hr}$

7 iterations were made  
 starting last iteration values-  
 stage length= 23.811  
 area-weighted insulation mass=  $0.1031\text{E}+01$   $\text{lb}_m/\text{ft}^2$   
 tank geometry:  
 height= 13.409 ft  
 area= 587.483  $\text{ft}^2$   
 volume= 1257.830  $\text{ft}^3$   
 propellant inventory:  
 propellant load= 5383.60  $\text{lb}_m$   
 4 minute boil-off= 1.44  $\text{lb}_m$   
 5 minute boil-off= 1.80  $\text{lb}_m$   
 maximum tank pressure= 19.255 psia  
 vapor ullage at lock-up= 2.07 %  
 tank ullage at lock-up= 2.03 %  
 (tank ullage at t-4 min.= 2.00) %  
 (4 minute boil-off= 1.444)  $\text{lb}_m$   
 (reduced propellant density= 4.367)  $\text{lb}_m/\text{ft}^3$   
 (tank volume= 1257.83)  $\text{ft}^3$   
 constant= 142.0  $\text{psig}\cdot\text{lb}_m$   
 propellant heating rate= 3937.0  $\text{BTU}/\text{Hr}$   $\text{BTU}$   
 propellant mass= 5382.2  $\text{lb}_m$   
 oxygen tank weight= 370.5  $\text{lb}_m$   
 hydrogen tank weight= 392.2  $\text{lb}_m$

Figure C-1: Example of TRADE Program(s) Input and Output

new iteration values-			
propellant inventory:	hydrogen	oxygen	lb <sub>m</sub>
propellant load=	5383.	32123.	lb <sub>m</sub>
4 minute boil-off=	1.44	0.24	lb <sub>m</sub>
5 minute boil-off=	1.80	0.30	lb <sub>m</sub>
pre-propulsive boil-off=	44.80	187.67	lb <sub>m</sub>
burned for delta-U=	5245.16	31470.96	lb <sub>m</sub>
vented during transfer=	39.27	154.20	lb <sub>m</sub>
start/stop losses=	10.00	63.00	lb <sub>m</sub>
residuals=	14.00	86.00	lb <sub>m</sub>
loading uncertainty=	26.92	160.61	lb <sub>m</sub>
tank geometry:			
volume=	1257.78	454.79	ft <sup>3</sup>
insulation thickness=	0.493	0.000	ft
area=	567.47	909.53	ft <sup>2</sup>
height=	13.409	4.352	ft
previous value of payload mass=	13510.3		lb <sub>m</sub>
new payload mass=	13510.5		lb <sub>m</sub>
mass limited payload=	15769.8		lb <sub>m</sub>
ASE mass=	5612.0		lb <sub>m</sub>
LTPS burnout mass=	6403.1		lb <sub>m</sub>
(prime burnout mass=		4377.0)	lb <sub>m</sub>
(insulation mass=		585.2)	lb <sub>m</sub>
(body shell mass=		388.6)	lb <sub>m</sub>
(tank weights=		762.7)	lb <sub>m</sub>
(loading uncertainty propellants=		187.5)	lb <sub>m</sub>
(contingency hold boil-off=		2.1)	lb <sub>m</sub>
(residual propellants=		100.0)	lb <sub>m</sub>
expended propellants=	37215.1		lb <sub>m</sub>
(vent losses before ignition=		232.5)	lb <sub>m</sub>
(propellants burned=		36716.1)	lb <sub>m</sub>
(vent losses after ignition=		193.5)	lb <sub>m</sub>
(start/stop losses=		73.0)	lb <sub>m</sub>
volume limited payload=	13510.5		lb <sub>m</sub>
payload density=	2.50		lb <sub>m</sub> /ft <sup>3</sup>
payload volume=	5404.21		ft <sup>3</sup>
(new stage length=		23.81)	ft
(stage length w/o insulated tanks=		6.05)	ft
(hydrogen tank length=		13.409)	ft
(length w/o insulation=		11.394)	ft
(oxygen tank length=		4.352)	ft
(length w/o insulation=		4.352)	ft
type insulated tank:	EH		
minimum interface temperature=	-200.0	deg F	
foam thickness=	2.0000	inches	
MLI thickness=	3.0153	inches	
ullage volume at t=4 minutes=	2.00	x	
payload mass=	13510.3	pounds	

Figure C-1: Example of TRADE Program(s) Input and Output (Concluded)

```

C      This interactive program assesses the impact of insulation
C      systems on the LTPS payload capacity. Insulation systems
C      are either helium purged MLI or nitrogen-purged MLI/foam
C      insulations.
C      English units (Btu, lb, ft, deg F and Hr) are used throughout
C      the program, except where noted.
C      Nomenclature-
C          PLMASS: payload mass
C          PLDEN: payload density
C          TYPET: type tank; either ellipsoidal hydrogen (EH), ellipsoidal
C                  oxygen (EO), or toroidal oxygen (TO)
C          TYPEG: type purge gas; either nitrogen or helium
C          TYPEOT: type LO2 tank; either toroidal or ellipsoidal
C          TYPEF: type foam; either Stepan BX 250 A or Rohacell 31
C          DENF: foam density
C          DELF: foam thickness
C          DELM: MLI thickness
C          TTANK: tank temperature
C          THM: minimum outside surface temperature of MLI
C          THA: average
C          TIM: minimum MLI/foam interface temperature
C          TIA: average
C          S4: tank ullage volume at 4 minutes before launch
C
C      TYPE 2
C      FORMAT(' Do you want calculation details?',S)
C      ACCEPT 3, DETAILS
C      FORMAT(A1)
C
C      ASSIGN INDEPENDENT VARIABLES
C      TYPE 5
C      FORMAT(' packaged payload density= ',S)
C      ACCEPT 6, PLDEN
C      FORMAT(F10.0)
C      TYPEOT='N'
C      IF(PLDEN.EQ.1.5 .OR. PLDEN.EQ.2.5) TYPEOT='T'
C      IF(PLDEN.EQ.3.5) TYPEOT='E'
C      IF(TYPEOT.EQ.'N') GO TO 4
C
C      TYPE 12
C      FORMAT(' Type tank (hydrogen or oxygen): ',S)
C      ACCEPT 13, TYPET
C      FORMAT(A1)
C      IF(TYPET.EQ.'O' .OR. TYPET.EQ.'o') THEN
C          TTANK=-290.
C          TYPET='TO'
C          IF(TYPEOT.EQ.'E') TYPET='EO'
C          GO TO 19
C      ENDIF
C      TTANK=-423.
C      IF(TYPET.EQ.'H' .OR. TYPET.EQ.'h') TYPET='EH'
C      IF(TYPET.NE.'EH' .AND. TYPET.NE.'EO' .AND. TYPET.NE.'TO') GO TO 11
C
C      TYPE 22
C      FORMAT(' tank ullage volume at t-4 min.= ',S)
C      ACCEPT 23, S4
C      FORMAT(F10.0)
C      SELECT INSULATION CONCEPT
C      TYPE 31
C      FORMAT(' Do you want nitrogen or helium purge gas?',S)
C      ACCEPT 32, TYPEG
C      FORMAT(A1)

```

Figure C-2: TRADE Computer Program Listing



```

C      IF(TYPEQ.EQ.'H' .OR. TYPEQ.EQ.'h') THEN
C      -FOR HELIUM PURGED MLI AND NO FOAM
      TYPEQ='H'
      TIM=TTANK
40     TYPE 41
41     FORMAT(' MLI thickness (inches)= ',3)
      ACCEPT 42, DELM
42     FORMAT(F10.0)
      DELM=DELM/12.
      DELF=0.
      TYPE 91
      GO TO 200
      ENDIF
C      -FOR NITROGEN PURGED MLI WITH A FOAM SUBSTRATE
      TYPEQ='N'
61     TYPE 62
62     FORMAT(' type foam (Rohacell 31 or BX 250A): ',3)
      ACCEPT 63, TYPEF
63     FORMAT(A1)
      TEST='N'
      IF(TYPEF.EQ.'R' .OR. TYPEF.EQ.'r') TYPEF='R'
      IF(TYPEF.EQ.'B' .OR. TYPEF.EQ.'b') TYPEF='B'
      IF(TYPEF.EQ.'R' .OR. TYPEF.EQ.'B') TEST='OK'
      IF(TEST.EQ.'N') GO TO 61
      DENF=1.9
      IF(TYPEF.EQ.'B') DENF=2.3
71     TYPE 72
72     FORMAT(' Minimum allowable interface temperature= ',3)
      ACCEPT 73, TIM
73     FORMAT(F10.0)
81     TYPE 82
82     FORMAT(' foam thickness (inches)= ',3)
      ACCEPT 83, DELF
83     FORMAT(F10.0)
      DELF=DELF/12.
90     TYPE 91
91     FORMAT(' END OF INPUT DATA'//)
C
      GFLX=0.
      PLMASS=0.
C      SEE IF ENOUGH MLI HAS BEEN ADDED TO SATISFY THE
C      MINIMUM INTERFACE TEMPERATURE REQUIREMENT
      FK=FOAMK(TYPEF,TIM,TTANK)
      RF=DELF/FK
      TFMAX=THMIN(TYPET,(1./RF))
      IF(TFMAX.LT.TIM) THEN
        TYPE 99
99     FORMAT(' !!!not enough foam to satisfy the minimum ',
+           'interface temperature requirement!!! '//)
      GO TO 9000
      ENDIF
C
C
C      FIND A SATISFACTORY MLI THICKNESS
      DELTA=10./60.
      DELM=-DELTA
      DO 190 I=1,200
      DELM=DELM + DELTA
      THM=TIM+50.
C      DETERMINE THE MINIMUM MLI SURFACE TEMPERATURE PREDICTED
C      BY THE THERMAL MATH MODEL (THM) BY VARYING THE MLI THICKNESS

```

Figure G-2: TRADE Computer Program Listing (Continued)

```

DO 105 J=1,50
THMO=THM
GK=GASK(TYPEG,THMO,TIM)
RM=DELM/GK
GMIN=1./(RF+RM)
THM=THMIN(TYPET,GMIN)
IF(ABS(THM-THMO).LT.0.001) GO TO 109
105 CONTINUE
TYPE 108, J, GMIN,DELM, THMO,THM
108 FORMAT(14,1X, 'iterations performed',
+ /' !!!the minimum MLI surface ',
+ /' temperature was not found!!!',
+ /' GMIN= 'E15.7,
+ /' DELM= 'E12.4,
+ /' OLD MINIMUM TEMPERATURE= ' E15.7,
+ /' NEW " " = ' E15.7/)
GO TO 9000
109 CONTINUE
C SEE IF ENOUGH FOAM HAS BEEN ADDED TO ATTAIN THE DESIRED
C MINIMUM INTERFACE TEMPERATURE
TITEST=TTANK + RF/(RF+RM)*(THM-TTANK)
IF(ABS(TITEST-TIM).LT.0.001) GO TO 199
IF(TITEST.GT.TIM .AND. DELTA.GT.0.) GO TO 190
IF(TITEST.LT.TIM .AND. DELTA.LT.0.) GO TO 190
DELTA=-DELTA/2.
190 CONTINUE
TYPE 198, 1
198 FORMAT(14, 'iterations performed',
+ /' !!!insufficient iterations performed to attain ',
+ /' the desired minimum interface temperature!!!'/)
199 CONTINUE
C
C
C PREDICT THE INSULATION HEAT FLUX DURING GROUND-HOLD (GFLX)
C AND ON-ORBIT MISSION PHASES OF: DEPLOYED ON LEO (SFLX) AND
C LEO TO DISPOSAL ORBIT TRANSFER (SFLXOT).
200 IF(TYPEG.EQ.'H') THEN
C CALCULATIONS TO DETERMINE THE HELIUM PURGED MLI GROUND-HOLD FLUX
C USE A CONDUCTANCE DEFINED BY 1/MLI THICKNESS (INVERSE INCHES)
GMIN=1./(DELM*12.)
ENDIF
GFLX=GRFLX(TYPET,GMIN,TYPEG)
SFLX=SPFLX(DELM)
C=0.85
IF(TYPET.EQ.'EO' .OR. TYPET.EQ.'TO') C=0.91
SFLXOT=C*SFLX
IF(TYPEG.EQ.'H') GO TO 291
C PREDICT THE TIME-AVERAGE INSULATION FLUX FROM TANK UN-LOCK
C TO INITIATION OF ORBIT TRANSFER (90 SEC TO 61 HR): TFLX
C INITIALLY FIND THE AVERAGE GROUND-HOLD MLI AND FOAM
C TEMPERATURES (TMA & TFA)
TFA=-500.
TIA=-500.
TMA=-500.
DO 290 I=1,3
IF(I.EQ.1) THEN
DELTA=DELF
TC=TTANK
ENDIF
IF(I.EQ.2) TC=TFA
IF(I.EQ.3) THEN

```

Figure C-2: TRADE Computer Program Listing (Continued)

```

DELTA=DELM
TC=TIA
ENDIF
DELT=100.
THO=TC-DELT
TKI=GFLX*(DELTA/2.)
DO 210 I=1,100
TH=THO+DELT
IF(III.EQ.3) THEN
GK=GASK(TYPEG,TH,TC)
TEST=GK*(TH-TC)
GO TO 209
ENDIF
FK=FOAMK(TYPEF,TH,TC)
TEST=FK*(TH-TC)
209 IF(ABS(TEST-TKI).LT.0.0001) GO TO 220
IF(TEST.LT.TKI .AND. DELT.GT.0.) GO TO 210
IF(TEST.GT.TKI .AND. DELT.LT.0.) GO TO 210
DELT=-DELT/2.
210 THO=TH
TYPE 211, II,I, DELT,THO,TH,TC,TEST
211 FORMAT(' II='14,4X,14' iterations performed',
+ '/' '!!!insufficient number of iterations performed to ',
+ '/' 'determine the average insulation temperature!!!',
+ '/' DELT= 'E10.4,
+ '/' THO= 'E10.4,
+ '/' TH= 'E13.5,
+ '/' TC= 'E13.5,
+ '/' TEST= 'E13.5/)
GO TO 9000
220 IF(III.EQ.1) TFA=TH
IF(III.EQ.2) TIA=TH
290 IF(III.EQ.3) TMA=TH
C FOR THESE AVERAGE TEMPERATURES, THE INTEGRATED THERMAL LOAD
C (PER SQUARE FOOT OF TANK SURFACE AREA) QTR MAY
C NOW BE FOUND.
C -DUE TO GROUND-HOLD CONDITIONS
291 QF=0.
CF=0.
TEVAC=2.8/60.
IF(TYPEG.EQ.'H') TEVAC=2.5/60.
QGTR=GFLX * (TEVAC - 90./3600.)
IF(TYPEG.EQ.'H') GO TO 292
C -DUE TO FOAM COOLING
CF=FOAMC(TFA,TTANK)
QF= DENF*DELF*CF*(TFA-TTANK)
C -DUE TO MLI COOLING AND INSULATION HEAT LEAK
292 TRMFLX=TRFLX(TYPET,DELM,TMA,TTANK,TYPEG)
QTRM=TRMFLX*(50.-TEVAC)
C -DUE TO INSULATION HEAT LEAK WHILE DEPLOYED ON LEO
QLEO=SFLX*(61.-50.)
C SUMMING TO FIND THE INTEGRATED HEAT LEAK,
QTR=QGTR+QF+QTRM+QLEO
C THE TIME-AVERAGED INSULATION FLUX IS DEFINED AS
TFLX= QTR/(61.-90./3600.)
C
C
C DETERMINE THE STRUT AND PENETRATION THERMAL LOADS
QPEN0=74.
QPENH=100.
CALL STRUTQ(PLDEN,TYPEG,QSTRH1,QSTRH2,QSTRH3,QSTRO1,QSTRO2,QSTRO3)

```

Figure C-2: TRADE Computer Program Listing (Continued)



```

WOSS=63.
WHSS=10.
WHRES=14.
WAINS=2.19*DELM + DENF*DELF
TINS=DELM*DELF
C
C   ITERATE ON THE PAYLOAD MASS
C   DO 1998 IT=1,50
C   INITIALIZE ITERATION VARIABLES
HHT=HHTN
HOT=HOTN
WHP=WHPN
WOP=WOPN
WH4=WH4N
WO4=WO4N
WH5=WH5N
WO5=WO5N
AHT=AHTN
AOT=AOTN
VHT=VHTN
VOT=VOTN
SL=SLN
PLMASS=PLMASSN
C   DETERMINE PROPELLANT DENSITIES
IF (TYPET.EQ.'EH') THEN
ODEN=70.633
DENL=4.3693
DENV=0.1004
VT=VHT
ENDIF
IF (TYPET.NE.'EH') THEN
HDEN= 4.3693
DENL=70.633
DENV=0.3365
VT=VOT
ENDIF
RDEN=REDEN(TYPET,PLDEN,S4,VT,GFLX,DENL,DENV)
IF (TYPET.EQ.'EH') HDEN=RDEN
IF (TYPET.NE.'EH') ODEN=RDEN
C   DETERMINE THE MAXIMUM TANK PRESSURE: PMAx
W4=WO4
WP=WOP-W4
CONST=1790.
VOLUME=VOT
AREA=AOT
IF (TYPET.EQ.'EH') THEN
W4=WH4
WP=WHP-W4
CONST=142.
VOLUME=VHT
AREA=AHT
ENDIF
S0= S4 + (100.*W4)/(RDEN*VOLUME)
SOV= S0 + (100.-S0)*(DENL-RDEN)/(DENL-DENV)
PMAx= 18. + CONST*(GFLX*AREA)*(90./3600.)/(SOV*WP)
C   ASSIGN A LTPS BURNOUT MASS: WBO
C   -INSULATION MASS
WINS=AOT*WAINS
IF (TYPET.EQ.'EH') WINS=AHT*WAINS
C   -FORE BODY SHELL MASS
WBS=26.34*(SL-SLB)

```

Figure C-2: TRADE Computer Program Listing (Continued)

```

C      -TANK INERT WEIGHT
      CALL WTANK(TYPET,PMAX,VHT,VOT,OTW,HTW)
      WBO=WBOP+WINS+WBS+(OTW+HTW)+.005*(WOP+WHP)+(WH5+WOS)+(WHRES+WORES)
C      DETERMINE THE PROPELLANT LOADING AT THE TERMINATION OF TOPPING
C      FOR HYDROGEN (WHP) AND OXYGEN (WOP)
      PIMP= WIMP(WBO,PLMASS,WPSCAR)
      WHIMP=PIMP/7.
      WOIMP=.8*PIMP/7.
C      ASSIGN TIME DEPENDENT PROPELLANT VENT LOSSES
      HFGH=187.
      HFGO=90.
      IF(TYPET.NE.'EH')THEN
        WO4N=(GFLX*AOOT+QPEN0+QSTRO1)*(4./60.)/HFGO
        WO5N=(GFLX*AOOT+QPEN0+QSTRO1)*(5./60.)/HFGO
        WOB1=(QTR*AOOT+(QPEN0+QSTRO2)*(61.-90./3600.))/HFGO
        WOA1=(SFLXOT*AOOT+QPEN0+QSTRO3)*(115.-61.)/HFGO
        WH4N=(QPENH+QSTRH1)*(4./60.)/HFGH
        WH5N=(QPENH+QSTRH1)*(5./60.)/HFGH
        WHB1=(QPENH+QSTRH2)*(61.-90./3600.)/HFGH
        WHA1=(QPENH+QSTRH3)*(115.-61.)/HFGH
      ENDIF
      IF(TYPET.EQ.'EH')THEN
        WH4N=(GFLX*AHT+QPENH+QSTRH1)*(4./60.)/HFGH
        WH5N=(GFLX*AHT+QPENH+QSTRH1)*(5./60.)/HFGH
        WHB1=(QTR*AHT+(QPENH+QSTRH2)*(61.-90./3600.))/HFGH
        WHA1=(SFLXOT*AHT+QPENH+QSTRH3)*(115.-61.)/HFGH
        WO4N=(QPEN0+QSTRO1)*(4./60.)/HFGO
        WO5N=(QPEN0+QSTRO1)*(5./60.)/HFGO
        WOB1=(QPEN0+QSTRO2)*(61.-90./3600.)/HFGO
        WOA1=(QPEN0+QSTRO3)*(115.-61.)/HFGO
      ENDIF
      WOPN=(WO4N+WO5N+WOB1+WOIMP+WOA1+WOSS+WORES)/0.995
      WHPN=(WH4N+WH5N+WHB1+WHIMP+WHA1+WHSS+WHRES)/0.995
C      SIZE PROPELLANT TANKS' FOR LENGTH AND AREA
      VHTN=WHPN/HDEN
      VOTN=WOPN/ODEN
      IF(TYPET.EQ.'EH')THEN
        VHTN=VHTN/(1.-S4/100.)
        THINS=TINS
        TOINS=0.
      ENDIF
      IF(TYPET.NE.'EH')THEN
        VOTN=VOTN/(1.-S4/100.)
        TOINS=TINS
        THINS=0.
      ENDIF
      CALL TANKS(PLDEN,VHTN,THINS,VOTN,TOINS,
        + AHTN,AOTN,HHTN,HOTN)
C      DETERMINE INSULATION EFFECTS ON THE STAGE LENGTH,
      DUMMY1=0.
      DUMMY2=0.
      CALL TANKS(PLDEN,VHTN,DUMMY1,VOTN,DUMMY2,
        + A1,A2,H1,H2)
C
C      DETERMINE PAYLOAD MASS FOR VOLUME-LIMITED (PLMASSV) AND
C      MASS-LIMITED (PLMASSM) CASES
      WEPROP=(WOB1+WHB1)+(WOIMP+WHIMP)+(WOA1+WHA1)+(WOSS+WHSS)
      PLMASSM= 65000. - WASE - WBO - WEPROP
      SLN=SL0+HHTN+HOTN
      PLVOL= 170. * (55.8-SLN)
      PLMASSV=PLVOL*PLDEN

```

Figure C-2: TRADE Computer Program Listing (Continued)

```

      IF (PLMASSV.LE.PLMASSM) PLMASSN=PLMASSV
      IF (PLMASSV.GT.PLMASSM) PLMASSN=(PLMASSM+PLMASS)/2.
      IF (IT.EQ.1) GO TO 1998
C     TEST FOR CONVERGENCE OF THE PAYLOAD MASS
      TEST=ABS(PLMASSN-PLMASS)
      IF (TEST.LT.1) GO TO 9000
1998  CONTINUE
      TYPE 1999, PLMASS, PLMASSN
1999  FORMAT(' !!!convergence to determine the payload mass ',
+ 'was not reached!!!',
+ '/' PLMASS= 'F12.2',
+ '/' PLMASSN= 'F12.2')
C
C
C     OUTPUT PROGRAMING:
9000  IF (DETAILS.NE.'Y' .AND. DETAILS.NE.'y') GO TO 9100
C     GIVE THERMAL MATH MODELING PREDICTIONS
      IF (TYPEG.EQ.'H') THEN
C     -FOR HELIUM PURGED MLI AND NO FOAM
      TYPE 9905, TYPET, DELM, GFLX,
+ TFLX, QGTR, QF, QTRM, TRMFLX, QLEO, SFLX,
+ SFLXOT
9905  FORMAT('/ type tank= ' A2,
+ '/' MLI thickness= '3X,E12.4' feet',
+ '/' ground-hold insulation flux= '3X,E13.5',
+ '/' average transition heat flux= '2X,E13.5',
+ '/' due to ground-hold conditions= 'E13.5',
+ '/' due to foam cooling= 'E13.5',
+ '/' due to MLI cooling and heat leak= 'E13.5',
+ '/' (MLI transition heat flux= '5X,E13.5')',
+ '/' due to deployed-LEO hold= 'E13.5',
+ '/' (MLI heat flux for LEO hold= '3X,E13.5')',
+ '/' orbit-transfer insulation flux= 'E13.5')
      GO TO 9030
      ENDIF
C     -FOR NITROGEN PURGED MLI WITH A FOAM SUBSTRATE
      TYPE 9010, TYPET, TFMAX, RF, DELM, THM, RM, GMIN, TITEST
9010  FORMAT('/ type tank= ' A2,
+ '/' maximum foam temperature= 'E13.5',
+ '/' foam resistance= '4X,E14.6',
+ '/' MLI thickness= 'E12.4' feet',
+ '/' minimum MLI surface temperature= 'E12.4',
+ '/' MLI resistance= '15X,E14.4',
+ '/' minimum conductance= 'E15.6',
+ '/' minimum interface temperature calculated= 'E12.4')
      IF (GFLX.EQ.0.) GO TO 9100
      TYPE 9020, GFLX, TFA, TIA, TMA,
+ TFLX, QGTR, QF, CF, QTRM, TRMFLX, QLEO, SFLX,
+ SFLXOT
9020  FORMAT(
+ '/' ground-hold insulation flux= 'E13.5',
+ '/' average foam temperature= '5X,E13.5',
+ '/' average interface temperature= 'E13.5',
+ '/' average MLI temperature= '6X,E13.5',
+ '/' average transition heat flux= 'E13.5',
+ '/' due to ground-hold conditions= 'E13.5',
+ '/' due to foam cooling= 'E13.5',
+ '/' (foam capacitance= '9X,E13.5')',
+ '/' due to MLI cooling and heat leak= 'E13.5',
+ '/' (MLI transition heat flux= '5X,E13.5')',
+ '/' due to deployed-LEO hold= '7X,E13.5',

```

Figure C-2: TRADE Computer Program Listing (Continued)

```

+ /' (MLI heat flux for LEO hold= '3X,E13.5')',
+ /' orbit-transfer insulation flux= 'E13.5)
  IF(TMA.LT.-425.) GO TO 9900
9030 TYPE 9031, QPENH,QPEN0, QSTRH1,QSTRO1, QSTRH2,QSTRO2,
+ QSTRH3,QSTRO3
9031 FORMAT(/' Hydrogen/Oxygen tank heat leak due to:',
+ /' penetrations= 'F6.1'/'F6.1,
+ /' struts for the mission phases,',
+ /' ground-hold and initial ascent= 'F6.1'/'F6.1,
+ /' tank-unlock to 60 hours= 'F6.1'/'F6.1,
+ /' LTPS ignition to disposal orbit= 'F6.1'/'F6.1)

C
  IF(PLMASS.EQ.0.) GO TO 9900
C
  GIVE DETAILS OF PAYLOAD ASSESSMENT
  TYPE 9050, IT, SL,WAINS,HHT,HOT,AHT,AOT,VHT,VOT,
+ WHP,WOP,WH4,WO4,WH5,WO5
9050 FORMAT(/'14' iterations were made',
+ /' starting last iteration values-',
+ /' stage length='F10.3,
+ /' area-weighted insulation mass='E13.4,
+ /' tank geometry: hydrogen'4X'oxygen',
+ /' height='17X,2F10.3,
+ /' area='17X,2F10.3,
+ /' volume='17X,2F10.3,
+ /' propellant inventory:',
+ /' propellant load='2F10.2,
+ /' 4 minute boil-off='2F10.2,
+ /' 5 minute boil-off='2F10.2)
  TYPE 9060, PMAX,
+ SOV,SO,S4,W4,RDEN,VOLUME, CONST, (QFLX*AREA), WP,
+ OTW,HTW
9060 FORMAT(
+ /' maximum tank pressure='4X,F10.3,
+ /' vapor ullage at lock-up='1X,F10.2,
+ /' tank ullage at lock-up='5X,F10.2,
+ /' (tank ullage at t-4 min.='8X,F10.2')',
+ /' (4 minute boil-off='14X,F10.3')',
+ /' (reduced propellant density='5X,F10.3')',
+ /' (tank volume='20X,F10.2')',
+ /' constant='18X,F10.1,
+ /' propellant heating rate='4X,F9.1,
+ /' propellant mass='10X,F10.1,
+ /' oxygen tank weight= 'F10.1,
+ /' hydrogen tank weight='F10.1)
  TYPE 9070, WHPN,WOPN, WH4N,WO4N, WH5N,WO5N, WHB1,WOB1,
+ WH1P,WO1P, WHA1,WOA1, WHSS,WOSS, WHRES,WORES,
+ (0.005*WHPN),(0.005*WOPN),
+ VHTN,VOTN, THINS,TOINS, AHTN,AOTN, HHTN,HOTN
9070 FORMAT(
+ /' new iteration values-',
+ /' propellant inventory: hydrogen'4X'oxygen',
+ /' propellant load='2F10.0,
+ /' 4 minute boil-off='2F10.2,
+ /' 5 minute boil-off='2F10.2,
+ /' pre-propulsive boil-off='2F10.2,
+ /' burned for delta-V='2F10.2,
+ /' vented during transfer='2F10.2,
+ /' start/stop losses='2F10.2,
+ /' residuals='2F10.2,
+ /' loading uncertainty='2F10.2,
+ /' tank geometry:',

```

Figure C-2: TRADE Computer Program Listing (Continued)



```

* /*      volume='2F10.2,
* /*      insulation thickness='2F10.3,
* /*      area='2F10.2,
* /*      height='2F10.3)
TYPE 9090, PLMASS, PLMASSN, PLMASSM, WASE,
* WBO,WBOP,WINS,WBS,(OTW+HTW),0.005*(WOPN+WHPN),(WH5N+WO5N),
* (WHRES+WORES),
* WEPROP,(WOB1+WHB1),(WOIMP+WHIMP),(WOA1+WHA1),(WOSS+WHSS),
* PLMASSV,PLDEN, PLVOL,SLN,SLO,HHTN,H1,HOTN,H2
9090  FORMAT(
* /* previous value of payload mass='F10.1,
* /* new payload mass='14X,F10.1,
* /* mass limited payload='2X,F10.1,
* /* ASE mass='15X,F10.1,
* /* LTPS burnout mass='6X,F10.1,
* /* (prime burnout mass= 'F10.1')',
* /* (insulation mass= 'F10.1')',
* /* (body shell mass= 'F10.1')',
* /* (tank weights= 'F10.1')',
* /* (loading uncertainty propellants='F10.1')',
* /* (contingency hold boil-off= 'F10.1')',
* /* (residual propellants= 'F10.1')',
* /* expended propellants='4X,F9.1,
* /* (vent losses before ignition='4X,F10.1')',
* /* (propellants burned= '4X,F10.1')',
* /* (vent losses after ignition= '4X,F10.1')',
* /* (start/stop losses= '4X,F10.1')',
* /* volume limited payload='F10.1,
* /* payload density='15X,F4.2,
* /* payload volume='10X,F10.2,
* /* (new stage length= 'F10.2')',
* /* (stage length w/o insulated tanks='F9.2')',
* /* (hydrogen tank length= 'F10.3')',
* /* (length w/o insulation= 'F10.3')',
* /* (oxygen tank length= 'F10.3')',
* /* (length w/o insulation= 'F10.3')')
C  ABBREVIATED RESULTS OF INSULATION IMPACT ON PAYLOAD CAPACITY
9100 TYPE 9101, TYPET,TIM,(DELF*12.),(DELM*12.),S4,PLMASS
9101  FORMAT(/
* /*      type insulated tank='8X,A2,
* /*      minimum interface temperature='F10.1' deg F',
* /*      foam thickness='F10.4' inches',
* /*      MLI thickness='F10.4' inches',
* /*      ullage volume at t=4 minutes='F10.2' %,
* /*      payload mass='F10.1' pounds')
C
C
C  CONTINUE WITH PROGRAM?
9900 IF(TYPEQ.EQ.'N')THEN
TYPE 9970
9970  FORMAT(///' Pick another foam thickness? ',S)
ACCEPT 9971, CASE
9971  FORMAT(A1)
IF(CASE.EQ.'Y' .OR. CASE.EQ.'y') GO TO 81
ENDIF
IF(TYPEQ.EQ.'H')THEN
TYPE 9975
9975  FORMAT(///' Pick another MLI thickness? ',S)
ACCEPT 9976, CASE
9976  FORMAT(A1)
IF(CASE.EQ.'Y' .OR. CASE.EQ.'y') GO TO 40
ENDIF

```

Figure C-2: TRADE Computer Program Listing (Continued)

```

TYPE 9980
9980 FORMAT(' Select another ullage volume? ',9)
ACCEPT 9981, CASE
9981 FORMAT(A1)
IF(CASE.EQ.'Y' .OR. CASE.EQ.'y') GO TO 21
TYPE 9990
9990 FORMAT(' Redefine optimization problem? ',9)
ACCEPT 9991, CASE
9991 FORMAT(A1)
IF(CASE.EQ.'Y' .OR. CASE.EQ.'y') GO TO 1
9999 STOP
END
C
SUBROUTINE STRUTQ(DEN,TYPEG,QH1,QH2,QH3,QO1,QO2,QO3)
IF(TYPEG.EQ.'H') GO TO 50
C
FOR NITROGEN PURGE GAS
IF(DEN.EQ.3.5) GO TO 10
IF(DEN.EQ.2.5) GO TO 20
IF(DEN.EQ.1.5) GO TO 30
C
FOR THE OXYGEN TANK
10 QO1=420.
QO2=333.
QO3=289.
C
FOR THE HYDROGEN TANK
QH1=12.5
QH2=10.9
QH3=8.9
GO TO 99
C
FOR THE OXYGEN TANK
20 QO1=247.
QO2=203.
QO3=183.
C
FOR THE HYDROGEN TANK
QH1=12.8
QH2=10.9
QH3=8.9
GO TO 99
C
FOR THE OXYGEN TANK
30 QO1=264.
QO2=217.
QO3=196.
C
FOR THE HYDROGEN TANK
QH1=13.7
QH2=11.6
QH3=9.5
GO TO 99
C
C
FOR HELIUM PURGE GAS
50 IF(DEN.EQ.3.5) GO TO 60
IF(DEN.EQ.2.5) GO TO 70
IF(DEN.EQ.1.5) GO TO 80
C
FOR THE OXYGEN TANK
60 QO1=325.
QO2=332.
QO3=289.
C
FOR THE HYDROGEN TANK
QH1= 7.5
QH2=10.9
QH3=8.9
GO TO 99
C
FOR THE OXYGEN TANK

```

Figure C-2: TRADE Computer Program Listing (Continued)

```

70  QO1=180.
    QO2=202.
    QO3=183.
C   FOR THE HYDROGEN TANK
    QH1= 7.5
    QH2=10.8
    QH3=8.9
    GO TO 99
C   FOR THE OXYGEN TANK
80  QO1=171.
    QO2=216.
    QO3=196.
C   FOR THE HYDROGEN TANK
    QH1= 8.0
    QH2=11.5
    QH3=9.5
99  RETURN
    END
C
SUBROUTINE WTANK(TYPET,PMAX,VHT,VOT,OTW,HTW)
POREF=24.
PHREF=22.
C   TANK MASSES AT THE REFERENCE PRESSURE:
C   -FOR THE HYDROGEN TANK
WHRAT=0.66224*(VHT/1721.) + 0.33776
HTW=WHRAT*507.
C   -FOR THE OXYGEN TANK
WORAT=0.45929*((VOT/587.)*(2./3.)+(VOT/587.)*(1./3.))+ 0.081414
OTW=WORAT*416.
C   DETERMINE TANK PRESSURIZATION EFFECTS ON THE TANK WEIGHTS: PEFF
IF(TYPET.NE.'EH')THEN
C   -FOR THE OXYGEN TANK
PRAT=PMAX/POREF
PEFF=0.903
IF(PRAT.GE.0.794) PEFF=0.528+0.472*PRAT
IF(PRAT.GE.1.000) PEFF=0.541+0.459*PRAT
OTW=OTW*PEFF
ENDIF
IF(TYPET.EQ.'EH')THEN
PRAT=PMAX/PHREF
PEFF=0.794
IF(PRAT.GE.0.562) PEFF=0.529+0.471*PRAT
IF(PRAT.GE.1.000) PEFF=0.222+0.778*PRAT
HTW=HTW*PEFF
ENDIF
RETURN
END
C
SUBROUTINE TANKS(PLDEN,VHT,THINS,VOT,TOINS,AHT,AOT,HHT,HOT)
C   FOR THE HYDROGEN TANK
VT=VHT
TINS=THINS
GO TO 100
10  AHT=AT
    HHT=HT
C   FOR THE OXYGEN TANK
VT=VOT
TINS=TOINS
IF(PLDEN.EQ.3.5) GO TO 100
GO TO 200
20  AOT=AT

```

Figure C-2: TRADE Computer Program Listing (Continued)

```

      HOT=HT
      GO TO 999
C     FOR ELLIPSOIDAL DOME TANKS,
C     DETERMINE THE MAXIMUM TANK VOLUME WITH NO BARREL SECTION
100    DMAX=169./12.-2.*TINS
      VNBMAX=(3.1416/6.)*(DMAX**3.)/SQRT(2.)
      IF(VNBMAX.GT.VT) GO TO 110
C     SIZE THE BARREL SECTION
      VDOMES=VNBMAX
      DTANK=DMAX
      BARA=(3.1416/4.)*DMAX**2.
      BARL=(VT-VDOMES)/BARA
      GO TO 199
C     REDUCE TANK DIAMETER TO SATISFY VOLUME CONSTRAINT
110    VDOMES=VT
      DTANK=(6.*SQRT(2.)/3.1416*VDOMES)**(1./3.)
      BARL=0.
C     DETERMINE THE TANK HEIGHT AND AREA
199    HT=BARL+DTANK/SQRT(2.)*2.*TINS
      AT=3.1416*(BARL*DTANK + 0.8116*DTANK**2.)
      IF(VT.EQ.VHT) GO TO 10
      GO TO 20
C     FOR TOROIDAL OXYGEN TANKS,
200    OR=(169./12.-2.*TINS)/2.
      ROLD=SQRT(VT/(2.*3.1416**2.*OR))
      DO 210 I=1,100
      RNEW=SQRT((VT/(2.*3.1416**2.) + ROLD**3.)/OR)
      IF(ABS(ROLD-RNEW).LT.0.0001) GO TO 220
210    ROLD=RNEW
      TYPE 211, VT,OR,ROLD,RNEW
211    FORMAT(' !!!convergence on toroidal tank minor radius ',
+ 'did not occur!!!',
+ /' VT= 'E13.5,
+ /' OR= 'E13.5,
+ /' ROLD= 'E13.5,
+ /' RNEW= 'E13.5)
220    HT=2.*RNEW*2.*TINS
      AT=4.*3.1416**2.*(OR-RNEW)*RNEW**2.
      GO TO 20
999    RETURN
      END
C
      FUNCTION WIMP(WBO,PLMASS,WPSCAR)
      WP2=WBO*(0.0229)
      WGEO=WBO+WP2+PLMASS
      WP1=WGEO*(1.823)
      WIMP=(WP1+WP2)-WSCAR
      RETURN
      END
C
      FUNCTION REDDEN(TYPET,PLDEN,S4,VT,GFLX,DENL,DENV)
C     HEAT FLUX FOR CORRELATION IS IN WATTS/SQUARE FOOT
      BO=(1.-DENL/DENV)*(0.293*GFLX)/(VT*(1.-S4/100.))
      IF(TYPET.EQ.'EH'.AND. PLDEN.NE.1.5) GO TO 10
      IF(TYPET.EQ.'EH') GO TO 40
      IF(TYPET.EQ.'EO') GO TO 20
      IF(PLDEN.EQ.2.5) GO TO 30
      IF(PLDEN.EQ.1.5) GO TO 50
10     A0=0.03353
      A1=-0.4417E-2
      A2=0.6122E-3

```

Figure C-2: TRADE Computer Program Listing (Continued)

```

      A3=-0.3048E-4
      GO TO 98
20    A0=0.1689
      A1=-0.2237E-1
      A2=0.3030E-2
      A3=-0.1508E-3
      GO TO 98
30    A0=0.1423
      A1=-0.1669E-1
      A2=0.2348E-2
      A3=-0.1201E-3
      GO TO 98
40    A0=0.02319
      A1=-0.3096E-2
      A2=0.4185E-3
      A3=-0.2062E-4
      GO TO 98
50    A0=0.1014
      A1=-0.1118E-1
      A2=0.1483E-2
      A3=-0.7375E-4
98    Y=A0+A1*S4+A2*S4**2.+A3*S4**3.
99    REDDEN=DENL + B*Y
      RETURN
      END

C      FUNCTION GASK(TYPEG,TH,TC)
      IF(TYPEG.EQ.'H') GO TO 50
C      FOR NITROGEN GAS
      A=0.01286
      B=2.6767E-5
      IF(TH.EQ.TC) THEN
      GASK=A+B*TH
      GO TO 100
      ENDIF
      TKI=A*(TH-TC) + B/2.*(TH**2.-TC**2.)
      GO TO 99
C      FOR HELIUM PURGE GAS
50    TKI=0.
      IF(TC.GT.-406.)GO TO 59
      TCI=TC
      THI=-406.
      IF(TH.LT.-406.) THI=TH
      AI=0.1428
      BI=3.044E-4
      TKI=TKI + AI*(THI-TCI) + BI/2.*(THI**2.-TCI**2.)
      IF(TH.EQ.THI) GO TO 99
39    CONTINUE
      IF(TC.GT.-244.)GO TO 69
      TCI=-406.
      IF(TC.GT.-406.) TCI=TC
      THI=-244.
      IF(TH.LT.-244.) THI=TH
      AI=0.0896
      BI=1.735E-4
      TKI=TKI + AI*(THI-TCI) + BI/2.*(THI**2.-TCI**2.)
      IF(TH.EQ.THI) GO TO 99
69    CONTINUE
      TCI=-244.
      IF(TC.GT.-244.) TCI=TC
      THI=TH

```

Figure C-2: TRADE Computer Program Listing (Continued)

```

      AI=0.0779
      BI=1.253E-4
      TKI=TKI + AI*(THI-TCI) + BI/2.*(THI**2.-TCI**2.)
99    GASK= TKI/(TH-TC)
100   RETURN
      END
C
      FUNCTION FOAMK(TYPEF,TH,TC)
      IF(TYPEF.EQ.'B') GO TO 50
C     FOR ROHACELL 31 FOAM
      IF(TH.EQ.TC) THEN
      FOAMK=0.0148 + 3.167E-5*TH
      GO TO 99
      ENDIF
      A=0.0148*(TH-TC)
      B=(3.167E-5/2.)*(TH**2.-TC**2.)
      TKI=A+B
      FOAMK=TKI/(TH-TC)
      GO TO 99
C     FOR BX 250A FOAM
50    TKI=0.
      IF(TH.EQ.TC) THEN
      FOAMK=0.0172 + 3.571E-5*TH
      IF(TH.GT.-90.) FOAMK=0.0119 - 2.345E-5*TH
      IF(TH.GT.55.) FOAMK=0.0085 + 3.777E-5*TH
      GO TO 99
      ENDIF
      THLIM=TH
      IF(TH.GT.55.) THEN
      A=0.0085*(TH-55.)
      B=(3.777E-5/2.)*(TH**2.-55.**2.)
      TKI=A+B+1.6065
      THLIM=-90.
      ENDIF
      IF(TH.GT.-90. .AND. TH.LE.55.) THEN
      A=0.0119*(TH+90.)
      B=(2.345E-5/2.)*(TH**2.-90.**2.)
      TKI=A+B
      THLIM=-90.
      ENDIF
      A=0.0172*(THLIM-TC)
      B=(3.571E-5/2.)*(THLIM**2.-TC**2.)
      TKI=TKI + A+B
      FOAMK=TKI/(TH-TC)
99    RETURN
      END
C
      FUNCTION FOAMC(TH,TC)
      IF(TH.EQ.TC) THEN
      FOAMC=1.E-10
      GO TO 99
      ENDIF
      THLIM=TH
      TKI=0.
      IF(TH.GT.-233.) THEN
      A=0.2724*(TH+233.)
      B=(8.214E-4/2.)*(TH**2.-233.**2.)
      TKI=A+B
      THLIM=-233.
      ENDIF
      A=0.1609*(THLIM-TC)

```

Figure C-2: TRADE Computer Program Listing (Continued)

```

      B=(3.430E-4/2.)*(THLIM**2.-TC**2.)
      TK1=TK1 + A*B
      FOAMC=TK1/(TH-TC)
99    RETURN
      END
C
      FUNCTION THMIN(TYPET,G)
      IF(TYPET.EQ.'EH') GO TO 10
      IF(TYPET.EQ.'EO') GO TO 20
      IF(TYPET.EQ.'TO') GO TO 30
10    THMIN=83.-5501.*G+46606.*G**2.-217731.*G**3.+371997.*G**4.
      IF(G.LE.0.125) GO TO 99
      THMIN=5.-2269.*G+4016.*G**2.
      IF(G.LE.0.214) GO TO 99
      THMIN=-222.-345.*G
      IF(G.LE.0.55) GO TO 99
      THMIN=-410.
      GO TO 99
20    THMIN=75.-5622.*G+55386.*G**2.-228533.*G**3.
      IF(G.LE.0.085) GO TO 99
      THMIN=-54.-1139.*G+1477.*G**2.
      IF(G.LE.0.25) GO TO 99
      THMIN=-219.-112.8*G
      IF(G.LE.0.6) GO TO 99
      THMIN=-280.
      GO TO 99
30    THMIN=90.-4800.*G+44412.*G**2.-177053.*G**3.
      IF(G.LE.0.082) GO TO 99
      THMIN=-27.-1134.*G+1399.*G**2.
      IF(G.LE.0.25) GO TO 99
      THMIN=-193.-140.2*G
      IF(G.LE.0.63) GO TO 99
      THMIN=-280.
99    RETURN
      END
C
      FUNCTION GRFLX(TYPET,G,TYPEG)
      IF(TYPEG.EQ.'H') GO TO 40
      IF(TYPET.EQ.'EH') GO TO 10
      IF(TYPET.EQ.'EO') GO TO 20
      IF(TYPET.EQ.'TO') GO TO 30
10    Y=447.*G+844.*G**2.-.2793E5*G**3+.1753E6*G**4.-.3414E6*G**5.
      IF(G.LE.0.158) GO TO 99
      Y=32.1+189.*G
      GO TO 99
20    Y=371.*G-1166.*G**2.+2352.*G**3.-1978.*G**4.
      IF(G.LE.0.4) GO TO 99
      Y=33.+71.*G
      GO TO 99
30    Y=314.*G-624.*G**2.
      IF(G.LE.0.25) GO TO 99
      Y=31.+39.4*G
      GO TO 99
C
40    IF(TYPET.EQ.'EH') GO TO 50
      IF(TYPET.EQ.'EO') GO TO 60
      IF(TYPET.EQ.'TO') GO TO 70
50    A=0.
      B=152.
      IF(G.GE.0.50) THEN
      A=51.6

```

Figure C-2: TRADE Computer Program Listing (Continued)

```

      B=48.7
      ENDIF
      IF(G.GE.1.67) THEN
      A=97.8
      B=21.1
      ENDIF
      IF(G.GE.3.33) THEN
      A=141.1
      B=8.10
      ENDIF
60    GO TO 80
      A=0.
      B=116.1
      IF(G.GE.0.56) THEN
      A=44.6
      B=36.5
      ENDIF
      IF(G.GE.1.82) THEN
      A=85.1
      B=14.2
      ENDIF
      IF(G.GE.4.00) THEN
      A=115.7
      B=6.70
      ENDIF
70    GO TO 80
      A=0.
      B=108.9
      IF(G.GE.0.56) THEN
      A=46.3
      B=26.2
      ENDIF
      IF(G.GE.1.82) THEN
      A=78.1
      B=8.70
      ENDIF
      IF(G.GE.4.00) THEN
      A=99.5
      B=3.40
      ENDIF
80    Y=A+B*G
C     C
99    GRFLX=Y
      RETURN
      END
C
C     FUNCTION TRFLX(TYPET,DELM,TH,TC,TYPEG)
C     FOR HELIUM PURGED MLI AND NO FOAM THE AVERAGE THERMAL LOAD THROUGH
C     THE MLI IS CORRELATED AGAINST 1/MLI THICKNESS (INVERSE INCHES).
C     THESE PREDICTIONS ARE BASED ON TMM RESULTS, WHERE THE MLI IS
C     VERY COLD DURING THE GROUND-HOLD MISSION PHASE.
      X=1./(DELM*12.)
      DELTAU=50.0652
      IF(TYPET.EQ.'EH') THEN
      Y=(3.38+6.68*X)/DELTAU
      IF(X.LT.0.2) Y=23.58*X/DELTAU
      ENDIF
      IF(TYPET.NE.'EH') THEN
      Y=(3.00+4.92*X)/DELTAU
      IF(X.LT.0.2) Y=19.92*X/DELTAU
      ENDIF

```

Figure C-2: TRADE Computer Program Listing (Continued)



```

C      IF (TYPEQ.EQ.'H') GO TO 98
C      FOR NITROGEN PURGED MLI WITH A FOAM SUBSTRATE
C      -ASSIGN A MAXIMUM AVERAGE THERMAL LOAD PREDICATED ON A SIMPLIFIED
C      ANALYSIS.
      YMAX=6.
C      -ASSIGN ITERATION PARAMETERS FOR NITROGEN PURGED MLI WITH A
C      FOAM SUBSTRATE
      DEN=DELM*(TH-TC)
      XX=3.5/1000.
      B1=57.
      A2=0.187
      B2=3.72
      IF (TYPEQ.EQ.'EH') THEN
      XX=4.2/1000.
      B1=58.
      A2=0.223
      B2=5.20
      ENDIF
C      INITIALIZE ITERATION PARAMETERS
      YTEST=0.3
      DO 90 I=1,300
      Y=YTEST
      X=Y/DEN
      A=0.
      B=B1
      IF (X.GT.XX) THEN
      A=A2
      B=B2
      ENDIF
      YTEST= A + B*(Y/DEN)
      IF (YTEST.GE.YMAX .AND. B.EQ.B2) THEN
      YTEST=YMAX
      ENDIF
      IF (ABS(Y-YTEST).LT.0.001) GO TO 98
90     CONTINUE
C      IF CONVERGENCE WASN'T REACHED-
      TYPE 91, I, DEN,XX,B1,A2,B2, Y, YTEST,X,A,B
91     FORMAT('4' iterations made',
+ /' !!!insufficient number of iterations were made ',
+ /' to determine the transition heat leak!!!',
+ /' DEN= 'E13.5,
+ /' XX= ',3X,E12.4,
+ /' B1= ',3X,F10.2,
+ /' A2= ',3X,F10.3,
+ /' B2= ',3X,F10.2,
+ /' Y= ',3X,E13.5,
+ /' YTEST= 'E13.5,
+ /' X= 'E12.4,
+ /' A= '2X,F10.3,
+ /' B= '2X,F10.2/)
98     TRFLX=Y
      RETURN
      END
C
      FUNCTION SPFLX(DELM)
      IF (DELM.EQ.0.) THEN
      SPFLX=1.E10
      GO TO 99
      ENDIF
      X=1./(DELM*12.)
      A=0.

```

Figure C-2: TRADE Computer Program Listing (Continued)

```

B=0.22
IF(X.GT.0.5) THEN
A=0.056
B=0.107
ENDIF
IF(X.GT.1.59) THEN
A=0.083
B=0.090
ENDIF
IF(X.GT.4.0) THEN
A=0.148
B=0.074
ENDIF
SPFLX= A + B*X
99 RETURN
END

```

*Figure C-2: TRADE Computer Program Listing (Concluded)*

```

C      This interactive program assesses the impact of insulation
C      systems on the LTPS payload capacity. Insulation systems
C      are either helium purged MLI or nitrogen-purged MLI/foam
C      insulations.
C      English units (Btu, lb, ft, deg F and Hr) are used throughout
C      the program, except where noted.
C      Nomenclature-
C          PLMASS: payload mass
C          PLDEN: payload density
C          TYPET: type tank; either ellipsoidal hydrogen (EH), ellipsoidal
C                  oxygen (EO), or toroidal oxygen (TO)
C          TYPEG: type purge gas; either nitrogen or helium
C          TYPEOT: type LO2 tank; either toroidal or ellipsoidal
C          TYPEF: type foam; either Stepan BX 250 A or Rohacell 31
C          DENF: foam density
C          DELF: foam thickness
C          DELM: MLI thickness
C          TH: outside surface temperature of the MLI
C          TI: MLI/foam interface temperature
C          TTANK: tank temperature
C          S4: tank ullage volume at 4 minutes before launch
C
C      TH=70.
1      TYPE 2
2      FORMAT(' Do you want calculation details?',S)
      ACCEPT 3, DETAILS
3      FORMAT(A1)
C
C      ASSIGN INDEPENDENT VARIABLES
4      TYPE 5
5      FORMAT(' packaged payload density= ',S)
      ACCEPT 6,PLDEN
6      FORMAT(F10.0)
      TYPEOT='N'
      IF(PLDEN.EQ.1.5 .OR. PLDEN.EQ.2.5) TYPEOT='T'
      IF(PLDEN.EQ.3.5) TYPEOT='E'
      IF(TYPEOT.EQ.'N') GO TO 4
11     TYPE 12
12     FORMAT(' Type tank (hydrogen or oxygen): ',S)
      ACCEPT 13, TYPET
13     FORMAT(A1)
      IF(TYPET.EQ.'O' .OR. TYPET.EQ.'o') THEN
          TTANK=-290.
          TYPET='TO'
          IF(TYPEOT.EQ.'E') TYPET='EO'
          GO TO 19
      ENDIF
          TTANK=-423.
          IF(TYPET.EQ.'H' .OR. TYPET.EQ.'h') TYPET='EH'
          IF(TYPET.NE.'EH' .AND. TYPET.NE.'EO' .AND. TYPET.NE.'TO') GO TO 11
19     TYPE 22
21     TYPE 22
22     FORMAT(' tank ullage volume at t-4 min.= ',S)
      ACCEPT 23, S4
23     FORMAT(F10.0)
C      SELECT INSULATION CONCEPT
30     TYPE 31
31     FORMAT(' Do you want nitrogen or helium purge gas?',S)
      ACCEPT 32, TYPEG
32     FORMAT(A1)
      IF(TYPEG.EQ.'H' .OR. TYPEG.EQ.'h') THEN

```

Figure C-3: TRADE2 Computer Program Listing

```

C      -FOR HELIUM PURGED MLI AND NO FOAM
      TYPEQ='H'
      TI=TTANK
40     TYPE 41
41     FORMAT(' MLI thickness (inches)= ',3)
      ACCEPT 42, DELM
42     FORMAT(F10.0)
      DELM=DELM/12.
      DELF=0.
      RF=0.
      RM=0.
      TYPE 91
      GO TO 200
      ENDIF
C      -FOR NITROGEN PURGED MLI WITH A FOAM SUBSTRATE
      TYPEQ='N'
      TYPE 62
62     FORMAT(' type foam (Rohacell 31 or BX 250A): ',3)
      ACCEPT 63, TYPEF
63     FORMAT(A1)
      TEST='N'
      IF(TYPEF.EQ.'R' .OR. TYPEF.EQ.'r') TYPEF='R'
      IF(TYPEF.EQ.'B' .OR. TYPEF.EQ.'b') TYPEF='B'
      IF(TYPEF.EQ.'R' .OR. TYPEF.EQ.'B') TEST='OK'
      IF(TEST.EQ.'N') GO TO 61
      DENF=1.9
      IF(TYPEF.EQ.'B') DENF=2.3
71     TYPE 72
72     FORMAT(' MLI/foam interface temperatures= ',3)
      ACCEPT 73, TI
73     FORMAT(F10.0)
81     TYPE 82
82     FORMAT(' foam thickness (inches)= ',3)
      ACCEPT 83, DELF
83     FORMAT(F10.0)
      DELF=DELF/12.
      RF=0.
      RM=0.
90     TYPE 91
91     FORMAT(' END OF INPUT DATA'//)
C
C
C      FIND THE MLI THICKNESS
C      -CALCULATE THE FOAM RESISTANCE (RF)
      FK=FOAMK(TYPEF,TI,TTANK)
      RF=DELF/FK
C      -DETERMINE THE GAS CONDUCTIVITY
      GK=GASK(TYPEQ,TH,TI)
C      THE MLI THICKNESS IS CALCULATED BY CONTINUITY OF HEAT FLUX
      DELM=GK*(TH-TI)*RF/(TI-TTANK)
C      THE MLI THERMAL RESISTANCE (RM) IS NOW FOUND BY
      RM=DELM/GK
C
C
C      PREDICT THE INSULATION HEAT FLUX DURING GROUND-HOLD (GFLX)
C      AND ON-ORBIT MISSION PHASES OF: DEPLOYED ON LEO (SFLX) AND
C      LEO TO DISPOSAL ORBIT TRANSFER (SFLXOT).
200    IF(TYPEQ.EQ.'H') THEN
      GK=GASK(TYPEQ,TH,TTANK)
      RM=DELM/GK
      ENDIF

```

Figure C-3: TRADE2 Computer Program Listing (Continued)

```

GINS=1./(RF+RM)
GFLX=GINS*(TH-TTANK)
SFLX=SPFLX(DELM)
C=0.85
IF(TYPET.EQ.'EO' .OR. TYPET.EQ.'TO') C=0.91
SFLXOT=C*SFLX
C
PREDICT THE TIME-AVERAGE INSULATION FLUX FROM TANK UN-LOCK
C
TO INITIATION OF ORBIT TRANSFER (90 SEC TO 61 HR): TFLX
C
INITIALLY FIND THE AVERAGE GROUND-HOLD MLI AND FOAM
C
TEMPERATURES (TMA & TFA)
TFA=-500.
TIA=-500.
TMA=-500.
IMIN=1
IF(TYPEG.EQ.'H') THEN
IMIN=3
TFA=TTANK
TIA=TTANK
ENDIF
DO 290 II=IMIN,3
IF(II.EQ.1) THEN
DELTA=DELF
TCI=TTANK
ENDIF
IF(II.EQ.2) TCI=TFA
IF(II.EQ.3) THEN
DELTA=DELM
TCI=TIA
ENDIF
DELT=100.
THIO=TCI-DELT*1.
TKI=GFLX*(DELTA/2.)
DO 210 I=1,100
THI=THIO+DELT
IF(II.EQ.3) THEN
GK=GASK(TYPEG,THI,TCI)
TEST=GK*(THI-TCI)
GO TO 209
ENDIF
FK=FOAMK(TYPEF,THI,TCI)
TEST=FK*(THI-TCI)
209 IF(ABS(TEST-TKI).LT.0.0001) GO TO 220
IF(TEST.LT.TKI .AND. DELT.GT.0.) GO TO 210
IF(TEST.GT.TKI .AND. DELT.LT.0.) GO TO 210
DELT=-DELT/2.
210 THIO=THI
TYPE 211, II,I, DELT,THIO,THI,TCI,TEST
211 FORMAT(' II='14,4X,'14' iterations performed',
+ /' !!!insufficient number of iterations performed to ',
+ /' determine the average insulation temperature!!!',
+ /' DELT= 'E10.4,
+ /' THIO= 'E10.4,
+ /' THI= 'E13.5,
+ /' TCI= 'E13.5,
+ /' TEST= 'E13.5/)
GO TO 9000
220 IF(II.EQ.1) TFA=THI
IF(II.EQ.2) TIA=THI
290 IF(II.EQ.3) TMA=THI
C
FOR THESE AVERAGE TEMPERATURES, THE INTEGRATED THERMAL LOAD
C
(PER SQUARE FOOT OF TANK SURFACE AREA) QTR MAY

```

Figure C-3: TRADE2 Computer Program Listing (Continued)

```

C      NOW BE FOUND.
      QF=0.
      CF=0.
C      -DUE TO GROUND-HOLD CONDITIONS
      TEVAC=2.8/60.
      IF(TYPEQ.EQ.'H') TEVAC=2.5/60.
      QGTR=GFLX*(TEVAC - 90./3600.)
      IF(TYPEQ.EQ.'H') GO TO 292
C      -DUE TO FOAM COOLING
      CF=FOAMC(TFA,TTANK)
      QF= DENF*DELF*CF*(TFA-TTANK)
C      -DUE TO MLI COOLING AND INSULATION HEAT LEAK
292    TRMFLX=TRFLX(TYPET,DELM,TMA,TTANK,TYPEQ)
      QTRM=TRMFLX*(50.-TEVAC)
C      -DUE TO INSULATION HEAT LEAK WHILE DEPLOYED ON LEO
      QLEO=SFLX*(61.-50.)
C      SUMMING TO FIND THE INTEGRATED HEAT LEAK,
      QTR=QGTR+QF+QTRM+QLEO
C      THE TIME-AVERAGED INSULATION FLUX IS DEFINED AS
      TFLX= QTR/(61.-90./3600.)
C
C
C      DETERMINE THE STRUT AND PENETRATION THERMAL LOADS
      QPEN0=74.
      QPENH=100.
      CALL STRUTQ(PLDEN,QSTRH1,QSTRH2,QSTRH3,QSTRO1,QSTRO2,QSTRO3)
C
C
C      ASSESS THE PAYLOAD MASS FOR THE SELECTED INSULATION CONCEPT,
      TANK CONFIGURATION, AND TANK ULLAGE VOLUME
C      INITIALIZE PARAMETERS
      IF(PLDEN.EQ.3.5) THEN
        WASE=5586.
        PLMASSN=15607.
        WBOP=4041.
        WORES=134.
        HHTN=144.5
        HOTN=92.2
        WHPN=5533.
        WOPN=32900.
        AHTN=600.
        AOTN=305.
        VHTN=1358.
        VOTN=484.
        WPSCAR=323.
C      LENGTHS: STAGE=SL, STAGE W/O TANKS OR INSULATION=SLO,
C      STAGE W/O FORE BODY SHELL=SLB
        SLN=298.8/12.
        SLO=60.9/12.
        SLB=161.6/12.
        ENDIF
        IF(PLDEN.EQ.2.5) THEN
          WASE=5612.
          PLMASSN=15239.
          WBOP=4377.
          WORES= 86.
          HHTN=144.5
          HOTN=27.4
          WHPN=5520.
          WOPN=32853.
          AHTN=600.

```

Figure C-3: TRADE2 Computer Program Listing (Continued)

```

AOTN=429.
VHTN=1358.
VOTN=489.
WPSCAR=323.
SLN=245.7/12.
SLO=72.6/12.
SLB=108.7/12.
ENDIF
IF (PLDEN.EQ.1.5) THEN
WASE=5612.
PLMASSN= 9731.
WBOP=3888.
WORES= 86.
HHTN=116.7
HOTN=22.0
WHPN=3926.
WOPN=23367.
AHTN=483.
AOTN=377.
VHTN= 964.
VOTN=348.
WPSCAR=293.
SLN=206.2/12.
SLO=66.3/12.
SLB= 96.2/12.
ENDIF
WOSS=63.
WHSS=10.
WHRES=14.
WAINS=2.19*DELM + DENF*DELF
TINS=DELM*DELF
C
C   ITERATE ON THE PAYLOAD MASS
C   DO 1998 IT=1,50
C   INITIALIZE ITERATION VARIABLES
HHT=HHTN
HOT=HOTN
WHP=WHPN
WOP=WOPN
WH4=WH4N
WO4=WO4N
WH5=WH5N
WO5=WO5N
AHT=AHTN
AOT=AOTN
VHT=VHTN
VOT=VOTN
SL=SLN
PLMASS=PLMASSN
C   DETERMINE PROPELLANT DENSITIES
IF (TYPET.EQ.'EH') THEN
ODEN=70.633
DENL=4.3693
DENV=0.1004
VT=VHT
ENDIF
IF (TYPET.NE.'EH') THEN
HDEN= 4.3693
DENL=70.633
DENV=0.3365
VT=VOT

```

Figure C-3: TRADE2 Computer Program Listing (Continued)

```

ENDIF
RDEN=REDEN(TYPET,PLDEN,S4,VT,GFLX,DENL,DENV)
IF(TYPET.EQ.'EH') HDEN=RDEN
IF(TYPET.NE.'EH') ODEN=RDEN
C DETERMINE THE MAXIMUM TANK PRESSURE: PMAX
W4=WO4
WP=WOP-W4
CONST=1790.
VOLUME=VOT
AREA=AOT
IF(TYPET.EQ.'EH') THEN
W4=WH4
WP=WHP-W4
CONST=142.
VOLUME=VHT
AREA=AHT
ENDIF
S0= S4 + (100.*W4)/(RDEN*VOLUME)
SOV= S0 + (100.-S0)*(DENL-RDEN)/(DENL-DENV)
PMAX= 18. + CONST*(GFLX*AREA)*(90./3600.)/(SOV*WP)
C ASSIGN A LTPS BURNOUT MASS: WBO
C -INSULATION MASS
WINS=AOT*WAINS
IF(TYPET.EQ.'EH') WINS=AHT*WAINS
C -FORE BODY SHELL MASS
WBS=26.34*(SL-SLB)
C -TANK INERT WEIGHT
CALL WTANK(TYPET,PMAX,VHT,VOT,OTW,HTW)
WBO=WBO+WINS+WBS+(OTW+HTW)+.005*(WOP+WHP)+(WH5+WOS)+(WHRES+WORES)
C DETERMINE THE PROPELLANT LOADING AT THE TERMINATION OF TOPPING
C FOR HYDROGEN (WHP) AND OXYGEN (WOP)
PIMP= WIMP(WBO,PLMASS,WPSCAR)
WHIMP=PIMP/7.
WOIMP=.6.*PIMP/7.
C ASSIGN TIME DEPENDENT PROPELLANT VENT LOSSES
HFGH=187.
HFGO=90.
IF(TYPET.NE.'EH') THEN
WO4N=(GFLX*AOT+QPEN0+QSTRO1)*(4./60.)/HFGO
WO5N=(GFLX*AOT+QPEN0+QSTRO1)*(5./60.)/HFGO
WOB1=(QTR*AOT+(QPEN0+QSTRO2)*(61.-90./3600.))/HFGO
WOA1=(SFLXOT*AOT+QPEN0+QSTRO3)*(115.-61.)/HFGO
WH4N=(QPENH+QSTRH1)*(4./60.)/HFGH
WH5N=(QPENH+QSTRH1)*(5./60.)/HFGH
WHB1=(QPENH+QSTRH2)*(61.-90./3600.)/HFGH
WHA1=(QPENH+QSTRH3)*(115.-61.)/HFGH
ENDIF
IF(TYPET.EQ.'EH') THEN
WH4N=(GFLX*AHT+QPENH+QSTRH1)*(4./60.)/HFGH
WH5N=(GFLX*AHT+QPENH+QSTRH1)*(5./60.)/HFGH
WHB1=(QTR*AHT+(QPENH+QSTRH2)*(61.-90./3600.))/HFGH
WHA1=(SFLXOT*AHT+QPENH+QSTRH3)*(115.-61.)/HFGH
WO4N=(QPEN0+QSTRO1)*(4./60.)/HFGO
WO5N=(QPEN0+QSTRO1)*(5./60.)/HFGO
WOB1=(QPEN0+QSTRO2)*(61.-90./3600.)/HFGO
WOA1=(QPEN0+QSTRO3)*(115.-61.)/HFGO
ENDIF
WOPN=(WO4N+WO5N+WOB1+WOIMP+WOA1+WOS+WOES)/0.995
WHPN=(WH4N+WH5N+WHB1+WHIMP+WHA1+WHSS+WHRES)/0.995
C SIZE PROPELLANT TANKS' FOR LENGTH AND AREA
VHTN=WHPN/HDEN

```

Figure C-3: TRADE2 Computer Program Listing (Continued)



```

VOTN=WOPN/ODEN
IF (TYPET.EQ.'EH') THEN
VHTN=VHTN/(1.-S4/100.)
THINS=TINS
TOINS=0.
ENDIF
IF (TYPET.NE.'EH') THEN
VOTN=VOTN/(1.-S4/100.)
TOINS=TINS
THINS=0.
ENDIF
CALL TANKS(PLDEN,VHTN,THINS,VOTN,TOINS,
* AHTN,AOTN,HHTN,HOTN)
C
DETERMINE INSULATION EFFECTS ON THE STAGE LENGTH,
DUMMY1=0.
DUMMY2=0.
CALL TANKS(PLDEN,VHTN,DUMMY1,VOTN,DUMMY2,
* A1,A2,H1,H2)
C
C
C DETERMINE PAYLOAD MASS FOR VOLUME-LIMITED (PLMASSV) AND
MASS-LIMITED (PLMASSM) CASES
WEPROP= (WOB1+WHB1)+(WOIMP+WHIMP)+(WOA1+WHA1)+(WOSS+WHSS)
PLMASSM= 65000. - WASE - WBO - WEPROP
SLN=SL0+HHTN+HOTN
PLVOL= 170. * (55.6-SLN)
PLMASSV=PLVOL*PLDEN
IF (PLMASSV.LE.PLMASSM) PLMASSN=PLMASSV
IF (PLMASSV.GT.PLMASSM) PLMASSN=(PLMASSM+PLMASSV)/2.
IF (IT.EQ.1) GO TO 1998
C
TEST FOR CONVERGENCE OF THE PAYLOAD MASS
TEST=ABS(PLMASSN-PLMASS)
IF (TEST.LT.1) GO TO 9000
1998 CONTINUE
TYPE 1999, PLMASS,PLMASSN
1999 FORMAT(' !!!convergence to determine the payload mass ',
* 'was not reached!!!',
* /' PLMASS= 'F12.2,
* /' PLMASSN= 'F12.2)
C
C
C OUTPUT PROGRAMING:
9000 IF (DETAILS.NE.'Y' .AND. DETAILS.NE.'y') GO TO 9100
C
GIVE THERMAL MODELING PREDICTIONS
TYPE 9010,TYPET, RF, DELM,TH,RM, GINS
9010 FORMAT(/' type tank= ' A2,
* /' foam resistance= '4X,E14.6,
* /' MLI thickness= 'E12.4' feet',
* /' MLI surface temperature= 'E12.4,
* /' MLI resistance= '15X,E14.4,
* /' insulation conductance= 'E15.6)
TYPE 9020, GFLX,TFA,TIA,TMA,
* TFLX, QGTR, QF,CF, QTRM,TRMFLX, QLEO,SFLX,
* SFLXOT
9020 FORMAT(
* /' ground-hold insulation flux= 'E13.5,
* /' average foam temperature= '5X,E13.5,
* /' average interface temperature= 'E13.5,
* /' average MLI temperature= '6X,E13.5,
* /' average transition heat flux= 'E13.5,
* /' due to ground-hold conditions= 'E13.5,
* /' due to foam cooling= 'E13.5,

```

Figure C-3: TRADE2 Computer Program Listing (Continued)

```

* /' (foam capacitance= '9X,E13.5')',
* /' due to MLI cooling and heat leak='E13.5',
* /' (MLI transition heat flux= '5X,E13.5')',
* /' due to deployed-LEO hold= '7X,E13.5',
* /' (MLI heat flux for LEO hold= '3X,E13.5')',
* /' orbit-transfer insulation flux= 'E13.5)
IF(TMA.LT.-425.) GO TO 9900
9030 TYPE 9031, QPENH,QPEN0, QSTRH1,QSTRO1, QSTRH2,QSTRO2,
* QSTRH3,QSTRO3
9031 FORMAT(/' Hydrogen/Oxygen tank heat leak due to:',
* /' penetrations= 'F6.1'/'F6.1,
* /' struts for the mission phases,',
* /' ground-hold and initial ascent= 'F6.1'/'F6.1,
* /' tank-unlock to 60 hours= 'F6.1'/'F6.1,
* /' LTPS ignition to disposal orbit= 'F6.1'/'F6.1)
C
C GIVE DETAILS OF PAYLOAD ASSESSMENT
TYPE 9050, IT, SL,WAINS,HHT,HOT,AHT,AOT,VHT,VOT,
* WHP,WOP,WH4,WO4,WH5,WO5
9050 FORMAT(/'14' iterations were made',
* /' starting last iteration values-',
* /' stage length='F10.3,
* /' area-weighted insulation mass='E13.4,
* /' tank geometry: hydrogen'4X'oxygen',
* /' height=',17X,2F10.3,
* /' area=',17X,2F10.3,
* /' volume=',17X,2F10.3,
* /' propellant inventory: ',
* /' propellant load='2F10.2,
* /' 4 minute boil-off='2F10.2,
* /' 5 minute boil-off='2F10.2)
TYPE 9060, PMAx,
* SOV,S0,S4,W4,RDEN,VOLUME, CONST, (GFLX*AREA), WP,
* OTW,HTW
9060 FORMAT(
* /' maximum tank pressure='4X,F10.3,
* /' vapor ullage at lock-up='1X,F10.2,
* /' tank ullage at lock-up='5X,F10.2,
* /' (tank ullage at t-4 min.='8X,F10.2')',
* /' (4 minute boil-off='14X,F10.3')',
* /' (reduced propellant density='5X,F10.3')',
* /' (tank volume='20X,F10.2')',
* /' constant='18X,F10.1,
* /' propellant heating rate='4X,F9.1,
* /' propellant mass='10X,F10.1,
* /' oxygen tank weight= 'F10.1,
* /' hydrogen tank weight='F10.1)
TYPE 9070, WHPN,WOPN, WH4N,WO4N, WH5N,WO5N, WHB1,WOB1,
* WH1P,W01P, WHA1,WOA1, WHSS,W0SS, WHRES,W0RES,
* (0.005*WHPN),(0.005*WOPN),
* VHTN,VOTN, THINS,TOINS, AHTN,AOTN, HHTN,HOTN
9070 FORMAT(
* /' new iteration values-',
* /' propellant inventory: hydrogen'4X'oxygen',
* /' propellant load='2F10.0,
* /' 4 minute boil-off='2F10.2,
* /' 5 minute boil-off='2F10.2,
* /' pre-propulsive boil-off='2F10.2,
* /' burned for delta-V='2F10.2,
* /' vented during transfer='2F10.2,
* /' start/stop losses='2F10.2,

```

Figure C-3: TRADE2 Computer Program Listing (Continued)

```

+ //      residuals='2F10.2,
+ //      loading uncertainty='2F10.2,
+ //      tank geometry:',
+ //      volume='2F10.2,
+ //      insulation thickness='2F10.3,
+ //      area='2F10.2,
+ //      height='2F10.3)
TYPE 9090, PLMASS, PLMASSN, PLMASSM, WASE,
+ WBO,WBOP,WINS,WBS,(OTW+HTW),0.005*(WOPN+WHPN),(WH5N+W05N),
+ (WHRES+W0RES),
+ WEPROP,(WOB1+WHB1),(WOIMP+WHIMP),(WOA1+WHA1),(WOSS+WHSS),
+ PLMASSV,PLDEN, PLVOL,SLN,SLO,HHTN,H1,HOTN,H2
9090 FORMAT(
+ // previous value of payload mass='F10.1,
+ // new payload mass='14X,F10.1,
+ // mass limited payload='2X,F10.1,
+ // ASE mass='15X,F10.1,
+ // LTPS burnout mass='6X,F10.1,
+ // (prime burnout mass='F10.1')',
+ // (insulation mass='F10.1')',
+ // (body shell mass='F10.1')',
+ // (tank weights='F10.1')',
+ // (loading uncertainty propellants='F10.1')',
+ // (contingency hold boil-off='F10.1')',
+ // (residual propellants='F10.1')',
+ // expended propellants='4X,F9.1,
+ // (vent losses before ignition='4X,F10.1')',
+ // (propellants burned='4X,F10.1')',
+ // (vent losses after ignition='4X,F10.1')',
+ // (start/stop losses='4X,F10.1')'
+ // volume limited payload='F10.1,
+ // payload density='15X,F4.2,
+ // payload volume='10X,F10.2,
+ // (new stage length='F10.2')',
+ // (stage length w/o insulated tanks='F9.2')',
+ // (hydrogen tank length='F10.3')',
+ // (length w/o insulation='F10.3')',
+ // (oxygen tank length='F10.3')',
+ // (length w/o insulation='F10.3')')
C ABBREVIATED RESULTS OF INSULATION IMPACT ON PAYLOAD CAPACITY
9100 TYPE 9101, TYPE T, TI, (DELF#12.), (DELM#12.), S4, PLMASS
9101 FORMAT(/
+ //      type insulated tank:'8X,A2,
+ //      MLI interface temperature='F10.1' deg F',
+ //      foam thickness='F10.4' inches',
+ //      MLI thickness='F10.4' inches',
+ //      ullage volume at t-4 minutes='F10.2' %,
+ //      payload mass='F10.1' pounds')
C
C
C CONTINUE WITH PROGRAM?
9900 IF (TYPE EQ. 'N') THEN
TYPE 9970
9970 FORMAT(///' Pick another foam thickness? ',S)
ACCEPT 9971, CASE
9971 FORMAT(A1)
IF (CASE EQ. 'Y' .OR. CASE EQ. 'y') GO TO 81
ENDIF
IF (TYPE EQ. 'H') THEN
TYPE 9975
9975 FORMAT(///' Pick another MLI thickness? ',S)
ACCEPT 9976, CASE

```

Figure C-3: TRADE2 Computer Program Listing (Continued)

```

9976  FORMAT(A1)
      IF(CASE.EQ.'Y' .OR. CASE.EQ.'y') GO TO 40
      ENDIF
      TYPE 9980
9980  FORMAT(' Select another ullage volume? ',S)
      ACCEPT 9981, CASE
9981  FORMAT(A1)
      IF(CASE.EQ.'Y' .OR. CASE.EQ.'y') GO TO 21
      TYPE 9990
9990  FORMAT(' Redefine optimization problem? ',S)
      ACCEPT 9991, CASE
9991  FORMAT(A1)
      IF(CASE.EQ.'Y' .OR. CASE.EQ.'y') GO TO 1
9999  STOP
      END

C
      SUBROUTINE STRUTQ(DEN,QH1,QH2,QH3,QO1,QO2,QO3)
C
      FOR A WARM BODY SHELL
      IF(DEN.EQ.3.5) GO TO 10
      IF(DEN.EQ.2.5) GO TO 20
      IF(DEN.EQ.1.5) GO TO 30
C
      FOR THE OXYGEN TANK
10    QO1=420.
      QO2=333.
      QO3=289.
C
      FOR THE HYDROGEN TANK
      QH1=12.5
      QH2=10.9
      QH3=8.9
      GO TO 99
C
      FOR THE OXYGEN TANK
20    QO1=247.
      QO2=203.
      QO3=183.
C
      FOR THE HYDROGEN TANK
      QH1=12.8
      QH2=10.9
      QH3=8.9
      GO TO 99
C
      FOR THE OXYGEN TANK
30    QO1=264.
      QO2=217.
      QO3=196.
C
      FOR THE HYDROGEN TANK
      QH1=13.7
      QH2=11.6
      QH3=9.5
99    RETURN
      END

C
      SUBROUTINE WTANK(TYPET,PMAX,VHT,VOT,OTW,HTW)
      POREF=24.
      PHREF=22.
C
      TANK MASSES AT THE REFERENCE PRESSURE:
C
      -FOR THE HYDROGEN TANK
      WHRAT=0.66224*(VHT/1721.) + 0.33776
      HTW=WHRAT*507.
C
      -FOR THE OXYGEN TANK
      WORAT=0.45929*((VOT/587.)*(2./3.)+(VOT/587.)*(1./3.))+ 0.081414
      OTW=WORAT*416.
C
      DETERMINE TANK PRESSURIZATION EFFECTS ON THE TANK WEIGHTS: PEFF

```

Figure C-3: TRADE2 Computer Program Listing (Continued)

```

C      IF (TYPET.NE.'EH') THEN
      -FOR THE OXYGEN TANK
      PRAT=PMAX/POREF
      PEFF=0.903
      IF (PRAT.GE.0.794) PEFF=0.528+0.472*PRAT
      IF (PRAT.GE.1.000) PEFF=0.541+0.459*PRAT
      OTW=OTW*PEFF
      ENDIF
      IF (TYPET.EQ.'EH') THEN
      PRAT=PMAX/PHREF
      PEFF=0.794
      IF (PRAT.GE.0.562) PEFF=0.529+0.471*PRAT
      IF (PRAT.GE.1.000) PEFF=0.222+0.778*PRAT
      HTW=HTW*PEFF
      ENDIF
      RETURN
      END

C
C      SUBROUTINE TANKS(PLDEN,VHT,THINS,VOT,TOINS,AHT,AOT,HHT,HOT)
C      FOR THE HYDROGEN TANK
      VT=VHT
      TINS=THINS
      GO TO 100
10     AHT=AT
      HHT=HT
C      FOR THE OXYGEN TANK
      VT=VOT
      TINS=TOINS
      IF (PLDEN.EQ.3.5) GO TO 100
      GO TO 200
20     AOT=AT
      HOT=HT
      GO TO 999
C      FOR ELLIPSOIDAL DOME TANKS,
C      DETERMINE THE MAXIMUM TANK VOLUME WITH NO BARREL SECTION
100    DMAX=169./12.-2.*TINS
      VNBMAX=(3.1416/6.)*(DMAX**3.)/SQRT(2.)
      IF (VNBMAX.GT.VT) GO TO 110
C      SIZE THE BARREL SECTION
      VDOMES=VNBMAX
      DTANK=DMAX
      BARA=(3.1416/4.)*DMAX**2.
      BARL=(VT-VDOMES)/BARA
      GO TO 199
C      REDUCE TANK DIAMETER TO SATISFY VOLUME CONSTRAINT
110    VDOMES=VT
      DTANK=(6.*SQRT(2.)/3.1416*VDOMES)**(1./3.)
      BARL=0.
C      DETERMINE THE TANK HEIGHT AND AREA
199    HT=BARL+DTANK/SQRT(2.)*2.*TINS
      AT=3.1416*(BARL*DTANK + 0.8116*DTANK**2.)
      IF (VT.EQ.VHT) GO TO 10
      GO TO 20
C      FOR TOROIDAL OXYGEN TANKS,
200    OR=(169./12.-2.*TINS)/2.
      ROLD=SQRT(VT/(2.*3.1416**2.*OR))
      DO 210 I=1,100
      RNEW=SQRT((VT/(2.*3.1416**2.) + ROLD**3.)/OR)
      IF (ABS(ROLD-RNEW).LT.0.0001) GO TO 220
210    ROLD=RNEW
      TYPE 211, VT,OR,ROLD,RNEW

```

Figure C-3: TRADE2 Computer Program Listing (Continued)

```

211  FORMAT(' !!!convergence on toroidal tank minor radius ',
+ 'did not occur!!!',
+ /' VT= 'E13.5,
+ /' OR= 'E13.5,
+ /' ROLD= 'E13.5,
+ /' RNEW= 'E13.5)
220  HT=2.*RNEW*2.*TINS
    AT=4.*3.1416**2.*(OR-RNEW)*RNEW**2.
    GO TO 20
999  RETURN
    END
C
    FUNCTION WIMP(WBO,PLMASS,WPSCAR)
    WP2=WBO*(0.0229)
    WGEO=WBO*WP2+PLMASS
    WP1=WGEO*(1.623)
    WIMP=(WP1+WP2)-WSCAR
    RETURN
    END
C
    FUNCTION REDDEN(TYPET,PLDEN,S4,VT,GFLX,DENL,DENV)
C    HEAT FLUX FOR CORRELATION IS IN WATTS/SQUARE FOOT
    BO=(1.-DENL/DENV)*(0.293*GFLX)/(VT*(1.-S4/100.))
    IF(TYPET.EQ.'EH'.AND. PLDEN.NE.1.5) GO TO 10
    IF(TYPET.EQ.'EH') GO TO 40
    IF(TYPET.EQ.'EO') GO TO 20
    IF(PLDEN.EQ.2.5) GO TO 30
    IF(PLDEN.EQ.1.5) GO TO 50
10   A0=0.03353
    A1=-0.4417E-2
    A2=0.6122E-3
    A3=-0.3046E-4
    GO TO 98
20   A0=0.1689
    A1=-0.2237E-1
    A2=0.3030E-2
    A3=-0.1508E-3
    GO TO 98
30   A0=0.1423
    A1=-0.1669E-1
    A2=0.2348E-2
    A3=-0.1201E-3
    GO TO 98
40   A0=0.02319
    A1=-0.3096E-2
    A2=0.4185E-3
    A3=-0.2062E-4
    GO TO 98
50   A0=0.1014
    A1=-0.1118E-1
    A2=0.1483E-2
    A3=-0.7375E-4
98   Y=A0+A1*S4+A2*S4**2.+A3*S4**3.
99   REDDEN=DENL + BO*Y
    RETURN
    END
C
    FUNCTION GASK(TYPEG,TH,TC)
    IF(TYPEG.EQ.'H') GO TO 50
C    FOR NITROGEN GAS
    A=0.01286

```

Figure C-3: TRADE2 Computer Program Listing (Continued)

```

      B=2.6767E-5
      IF (TH.EQ.TC) THEN
        GASK=A+B*TH
        GO TO 100
      ENDIF
      TKI=A*(TH-TC) + B/2.*(TH**2.-TC**2.)
      GO TO 99
C     FOR HELIUM PURGE GAS
50    TKI=0.
      IF (TH.EQ.TC) THEN
        GASK=8.33E-4 * (TC**0.74)
        GO TO 100
      ENDIF
      IF (TC.GT.-406.) GO TO 59
      TCI=TC
      THI=-406.
      IF (TH.LT.-406.) THI=TH
      AI=0.1428
      BI=3.044E-4
      TKI=TKI + AI*(THI-TCI) + BI/2.*(THI**2.-TCI**2.)
      IF (TH.EQ.THI) GO TO 99
59    CONTINUE
      IF (TC.GT.-244.) GO TO 69
      TCI=-406.
      IF (TC.GT.-406.) TCI=TC
      THI=-244.
      IF (TH.LT.-244.) THI=TH
      AI=0.0896
      BI=1.735E-4
      TKI=TKI + AI*(THI-TCI) + BI/2.*(THI**2.-TCI**2.)
      IF (TH.EQ.THI) GO TO 99
69    CONTINUE
      TCI=-244.
      IF (TC.GT.-244.) TCI=TC
      THI=TH
      AI=0.0779
      BI=1.253E-4
      TKI=TKI + AI*(THI-TCI) + BI/2.*(THI**2.-TCI**2.)
99    GASK= TKI/(TH-TC)
100   RETURN
      END
C
      FUNCTION FOAMK(TYPEF,TH,TC)
      IF (TYPEF.EQ.'B') GO TO 50
C     FOR ROHACELL 31 FOAM
      IF (TH.EQ.TC) THEN
        FOAMK=0.0148 + 3.167E-5*TH
        GO TO 99
      ENDIF
      A=0.0148*(TH-TC)
      B=(3.167E-5/2.)*(TH**2.-TC**2.)
      TKI=A+B
      FOAMK=TKI/(TH-TC)
      GO TO 99
C     FOR BX 250A FOAM
50    TKI=0.
      IF (TH.EQ.TC) THEN
        FOAMK=0.0172 + 3.571E-5*TH
        IF (TH.GT.-90.) FOAMK=0.0119 - 2.345E-5*TH
        IF (TH.GT.55.) FOAMK=0.0085 + 3.777E-5*TH
        GO TO 99

```

Figure C-3: TRADE2 Computer Program Listing (Continued)

```

ENDIF
THLIM=TH
IF (TH.GT.55.) THEN
A=0.0085*(TH-55.)
B=(3.777E-5/2.)*(TH**2.-55.**2.)
TKI=A+B+1.6065
THLIM=-90.
ENDIF
IF (TH.GT.-90. .AND. TH.LE.55.) THEN
A=0.0119*(TH+90.)
B=(2.345E-5/2.)*(TH**2.-90.**2.)
TKI=A+B
THLIM=-90.
ENDIF
A=0.0172*(THLIM-TC)
B=(3.571E-5/2.)*(THLIM**2.-TC**2.)
TKI=TKI + A+B
FOAMK=TKI/(TH-TC)
99 RETURN
END

C
FUNCTION FOAMC(TH,TC)
IF (TH.EQ.TC) THEN
FOAMC=1.E-10
GO TO 99
ENDIF
THLIM=TH
TKI=0.
IF (TH.GT.-233.) THEN
A=0.2724*(TH+233.)
B=(8.214E-4/2.)*(TH**2.-233.**2.)
TKI=A+B
THLIM=-233.
ENDIF
A=0.1609*(THLIM-TC)
B=(3.430E-4/2.)*(THLIM**2.-TC**2.)
TKI=TKI + A+B
FOAMC=TKI/(TH-TC)
99 RETURN
END

C
FUNCTION TRFLX(ITYPET,DELM,TH,TC,TYPEG)
C FOR NITROGEN PURGED MLI WITH A FOAM SUBSTRATE OR HELIUM PURGED
C MLI WITH A WARM BOUNDARY TEMPERATURE.
C -ASSIGN A MAXIMUM AVERAGE THERMAL LOAD PREDICATED ON A SIMPLIFIED
C ANALYSIS
YMAX=6.
C -ASSIGN ITERATION PARAMETERS
DEN=DELM*(TH-TC)
XX=3.5/1000.
B1=57.
A2=0.187
B2=3.72
IF (ITYPET.EQ.'EH') THEN
XX=4.2/1000.
B1=58.
A2=0.223
B2=5.20
ENDIF
C INITIALIZE ITERATION PARAMETERS
YTEST=0.3

```

Figure C-3: TRADE2 Computer Program Listing (Continued)



```

DO 90 I=1,300
Y=YTEST
X=Y/DEN
A=0.
B=B1
IF(X.GT.XX) THEN
A=A2
B=B2
ENDIF
YTEST= A + B*(Y/DEN)
IF(YTEST.GE.YMAX .AND. B.EQ.B2) THEN
YTEST=YMAX
ENDIF
IF(ABS(Y-YTEST).LT.0.001) GO TO 98
90 CONTINUE
C IF CONVERGENCE WASN'T REACHED-
TYPE 91, I, DEN,XX,B1,A2,B2, Y, YTEST,X,A,B
91 FORMAT('14' iterations made',
+ '/' '!!!!insufficient number of iterations were made ',
+ '/' ' to determine the transition heat leak!!!',
+ '/' DEN= 'E13.5,
+ '/' XX= ',3X,E12.4,
+ '/' B1= ',3X,F10.2,
+ '/' A2= ',3X,F10.3,
+ '/' B2= ',3X,F10.2,
+ '/' Y= ',3X,E13.5,
+ '/' YTEST= 'E13.5,
+ '/' X= 'E12.4,
+ '/' A= '2X,F10.3,
+ '/' B= '2X,F10.2/)
98 TRFLX=Y
RETURN
END
C
FUNCTION SPFLX(DELM)
IF(DELM.EQ.0.) THEN
SPFLX=1.E10
GO TO 99
ENDIF
X=1./(DELM*12.)
A=0.
B=0.22
IF(X.GT.0.5) THEN
A=0.056
B=0.107
ENDIF
IF(X.GT.1.59) THEN
A=0.083
B=0.090
ENDIF
IF(X.GT.4.0) THEN
A=0.148
B=0.074
ENDIF
SPFLX= A + B*X
99 RETURN
END

```

Figure C-3: TRADE2 Computer Program Listing (Concluded)



## APPENDIX D

### PROPELLANT EFFECTIVE TANKING DENSITY ANALYSIS

#### Symbols

$A_L$	Area of tank wall below liquid free surface $\sim m^2$
$h$	Maximum depth of liquid $\sim m$
$h_{fg}$	Heat of vaporization of propellant $\sim \text{Watt-hr/kg}$
$M^*$	Combined mass of liquid and entrained bubbles $\sim kg$
$M_L$	Mass of liquid $\sim kg$
$M_V$	Mass of vapor bubbles $\sim kg$
$\dot{M}_V$	Rate at which liquid mass is converted to vapor $\sim kg/hr$
$q_L$	Heat flux through tank wall area wetted by liquid $\sim \text{Watt}/m^2$
$r_B$	Bubble radius $\sim cm$
$S$	Percent ullage volume
$T_B$	Time required for bubble to rise from nucleation site to free surface $\sim sec$
$\bar{T}_B$	Average bubble residence time in liquid phase $\sim sec$
$\bar{V}_T$	Bubble terminal velocity $\sim cm/sec$
$\bar{v}_T$	Volume-averaged bubble terminal velocity $\sim cm/sec$
$V^*$	Tank volume below liquid free surface $\sim m^3$
$V_L$	Total volume of liquid $\sim m^3$
$V_T$	Total tank volume $\sim m^3$
$V_V$	Total volume of bubbles $\sim m^3$
$\bar{V}_B$	Average bubble velocity $\sim cm/sec$
$Z$	Depth of nucleation site below liquid free surface $\sim cm$
$\rho_L$	Liquid density $\sim kg/m^3$
$\rho_V$	Vapor density $\sim kg/m^3$
$\bar{\rho}^*$	Effective density of tanked propellant $\sim kg/m^3$

This appendix summarizes an analysis performed to estimate the influence of heat flux on the effective density of propellants residing in LTPS tanks during ground operations. Effective density is defined as the mass of liquid and vapor bubbles, excluding the ullage, divided by the volume occupied by the two phase mixture. In the analysis described herein, the volume occupied by the two phase mixture is simply the difference between total tank internal free volume and the ullage volume.

The presence of vapor, in the form of bubbles interspersed within the liquid phase, is caused by boiling at the tank walls and other solid surfaces in contact with the propellant. The higher the heat leak to the propellant/surface interface, the more rapid the boiling rate and hence the more bubbles that are present in the liquid. For a fixed liquid height in the tank, the volume occupied by bubbles displaces a certain mass of liquid phase that could otherwise be used for propulsion. Hence, it is desirable to minimize heat leak during ground hold operations.

As stated above, the effective density of tanked propellant is the mass of liquid and bubbles divided by the total volume occupied by both phases. That is

$$\bar{\rho}^* = \frac{M^*}{V^*} \quad (D-1)$$

where  $M^* = M_V + M_L$

$$V^* = V_V + V_L$$

The total mass of vapor contained in the liquid at any instant is the rate of vaporization times the residence time of bubbles within the liquid. In equation form this may be expressed as:

$$M_V = \dot{M}_V \times \bar{T}_B \quad (D-2)$$

The residence time of an individual bubble was defined for this study to be the elapsed time from which the bubble detached from the wall until it reached the free surface. This definition required the following two assumptions to be made:

- a. The bubbles rose through a layer of saturated liquid near the wall and therefore did not collapse.
- b. The bubble growth time, from inception until detachment from the wall, was small compared to the rise time.

The first assumption is reasonable because the liquid near the vertical walls will warm to saturation conditions through heat conduction and free convection. Mechanical mixing via liquid jet pumps or other devices could be used to carry subcooled liquid to the walls but such an approach would be complex and costly.

The second assumption is also reasonable because of the large size of the tanks and the high predicted heat flux levels during ground-hold (see Figures 4-23 and 4-24).

The time required for a bubble to rise to the free surface from its nucleation site at depth  $Z$  can be expressed mathematically as

$$T_B = Z/\bar{V}_B \quad (D-3)$$

To find the average rise time  $\bar{T}_B$  for all bubbles having average velocity  $\bar{V}_B$ , we must integrate over all nucleation sites and divide by the depth  $h$  of the fluid.

$$\bar{T}_B = \frac{\int_0^h Z/\bar{V}_B \, dZ}{h} \quad (D-4)$$

At this point it is necessary to make some assumptions about the size and velocity distributions of bubbles. Following the equations of Reference 20 for bubble terminal velocity in liquids under normal gravity, one can calculate velocity as a function of bubble radius. The results of this calculation for  $\text{LH}_2$  at 1 atm are shown in Figure D-1. It can be seen that predicted terminal velocity is independent of effective bubble diameter when the diameter exceeds 0.23 cm (0.1 in).

It was assumed for the purposes of simplification that diameters of most of the bubbles were larger than the value at which terminal velocity was independent of size. The justification for this assumption was based on two arguments: First, collisions between bubbles due to differing velocities will almost always result in coalescence and bubble

growth. Hence, the natural tendency during bubble rise is for the average bubble diameter to increase, and for the velocities of most bubbles to approach the size-independent value. Second, since the bubble volume and vapor mass are roughly proportional to the cube of the radius, the mass-average (or volume-average) bubble velocity is very closely equal to the size independent value. This can be shown by assuming initially that bubble size is uniformly distributed. The volume-average terminal velocity  $\bar{v}_T$  is then

$$\bar{v}_T = \frac{\int_0^{r_B} v_T r_B^3 dr_B}{\frac{r_B^4}{4}} \quad (D-5)$$

Figure D-1 shows volume-average terminal velocity approaches the size-independent velocity for  $H_2$  bubble radii greater than 0.23 cm (0.1 in). If we look at only the value of the integral of equation D-5, we find that it is very small for small diameter bubbles due to the  $r_B^3$  term. Hence, the value of volume-average terminal velocity for the entire population of bubbles is relatively insensitive to the actual size distribution of small bubbles.

Figure D-2 shows the predicted size-independent terminal velocities and corresponding minimum bubble radii as functions of tank ullage pressure for both the  $LH_2$  and  $LO_2$  tanks. These calculations were performed using the Reference 20 equations. Minimum effective bubble radius is the value of characteristic bubble dimension above which rise velocity is independent of size.

The values of terminal velocity shown in Figure D-2 were substituted into equation D-4 and average bubble rise time calculated for the  $LH_2$  and  $LO_2$  tanks of the three baseline LTPS vehicles (see Figures 3-7, 3-8 and 3-9). The independent variable for these calculations was tank percent ullage volume which determines the liquid depth,  $L$ .

Values of average rise time,  $\bar{T}_B$ , were substituted into equation D-2 and the total mass of vapor contained in bubbles was calculated as a function of percent ullage volume. In using equation D-2, the rate of vaporization,  $\dot{M}_V$ , was dependent on ullage volume because only the heat entering the tanks below the free surface contributed to boiling.  $\dot{M}_V$  can be expressed as

$$\dot{M}_V = \frac{\dot{q}_L \times A_L}{h_{fg}} \quad (D-6)$$

Substituting equation D-6 into equation D-2 and solving for  $\dot{M}_V/\dot{q}_L$  gives

$$\dot{M}_V/\dot{q}_L = \frac{A_L}{h_{fg}} \bar{T}_B \quad (D-7)$$

Figures D-3 and D-4 show the calculated values of  $\dot{M}_V/\dot{q}_L$  as a function of ullage volume for the Task II baseline LTPS  $LH_2$  and  $LO_2$  tanks.

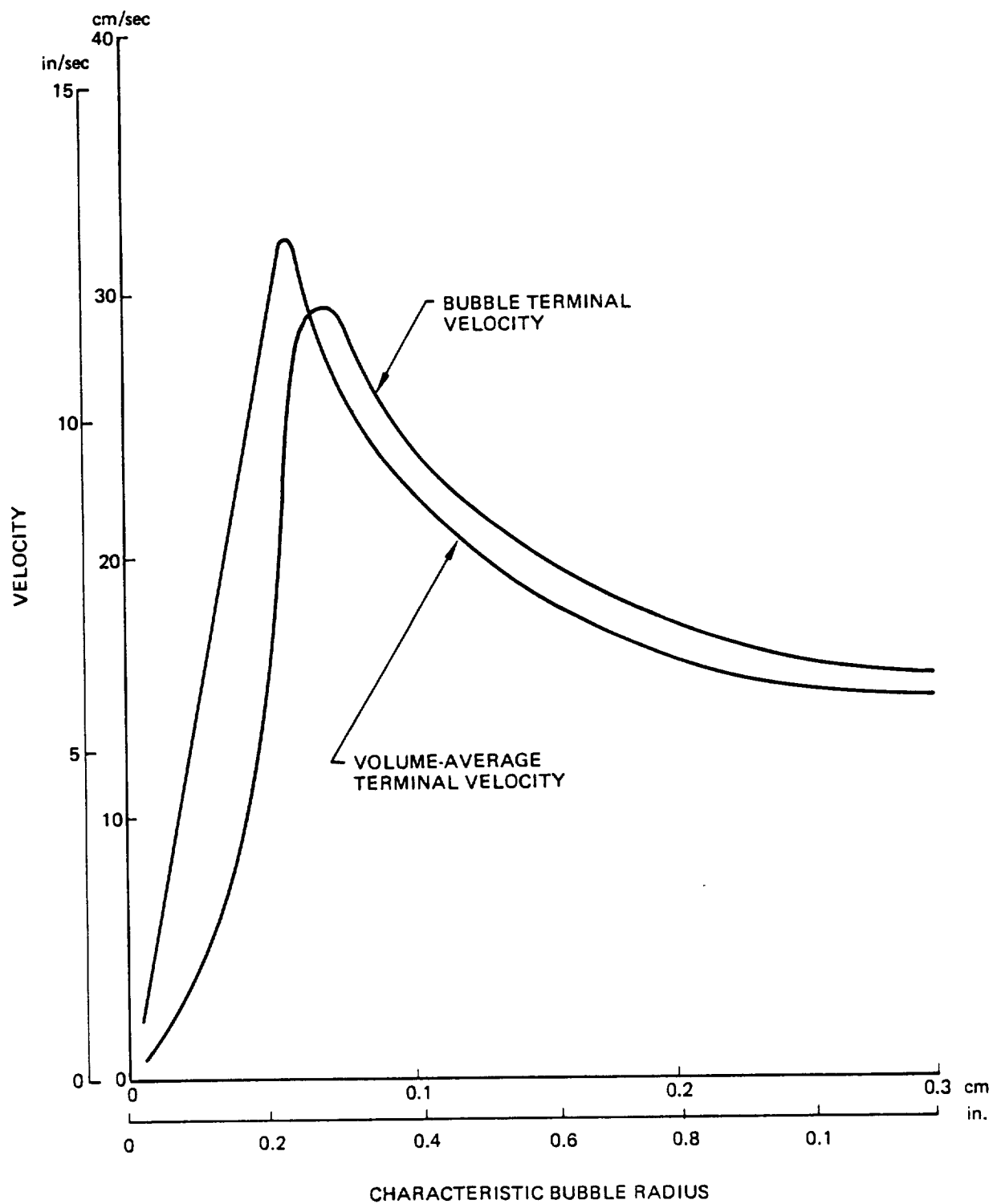


Figure D-1: Terminal Velocity and Volume – Average Velocity for Bubbles in  $LH_2$

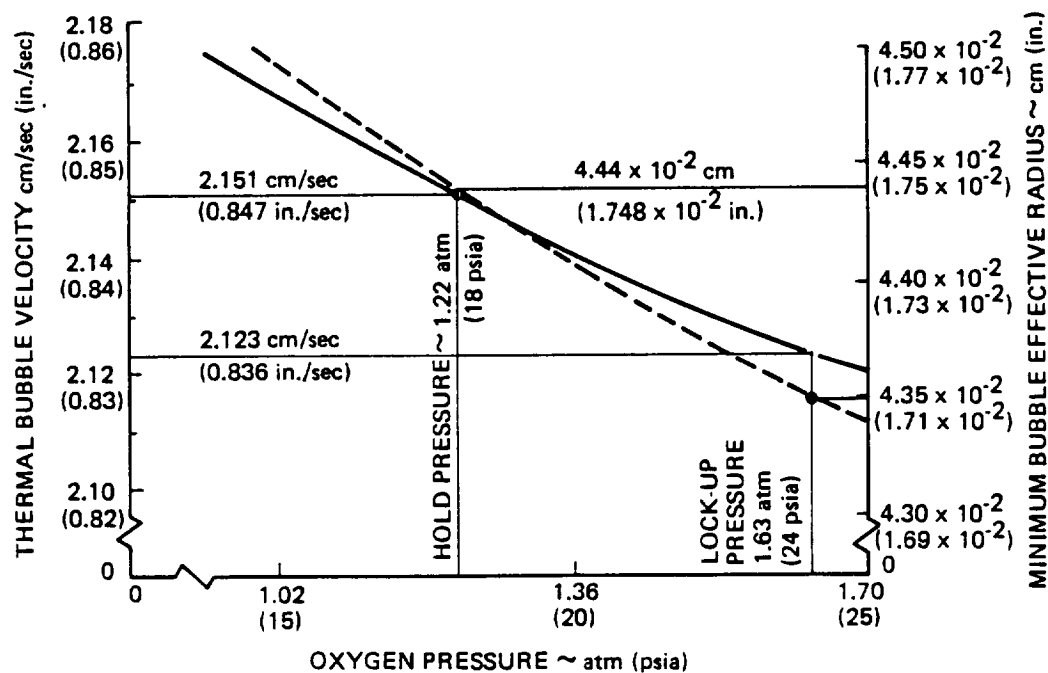
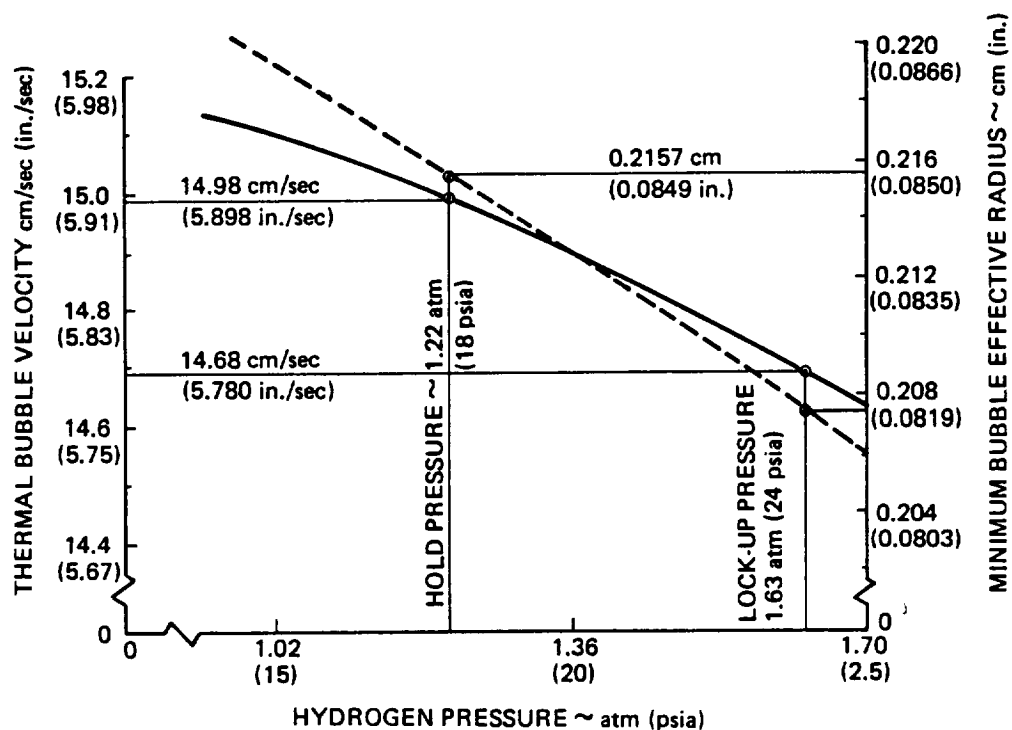


Figure D-2: Bubble Terminal Velocity and Minimum Effective Radius

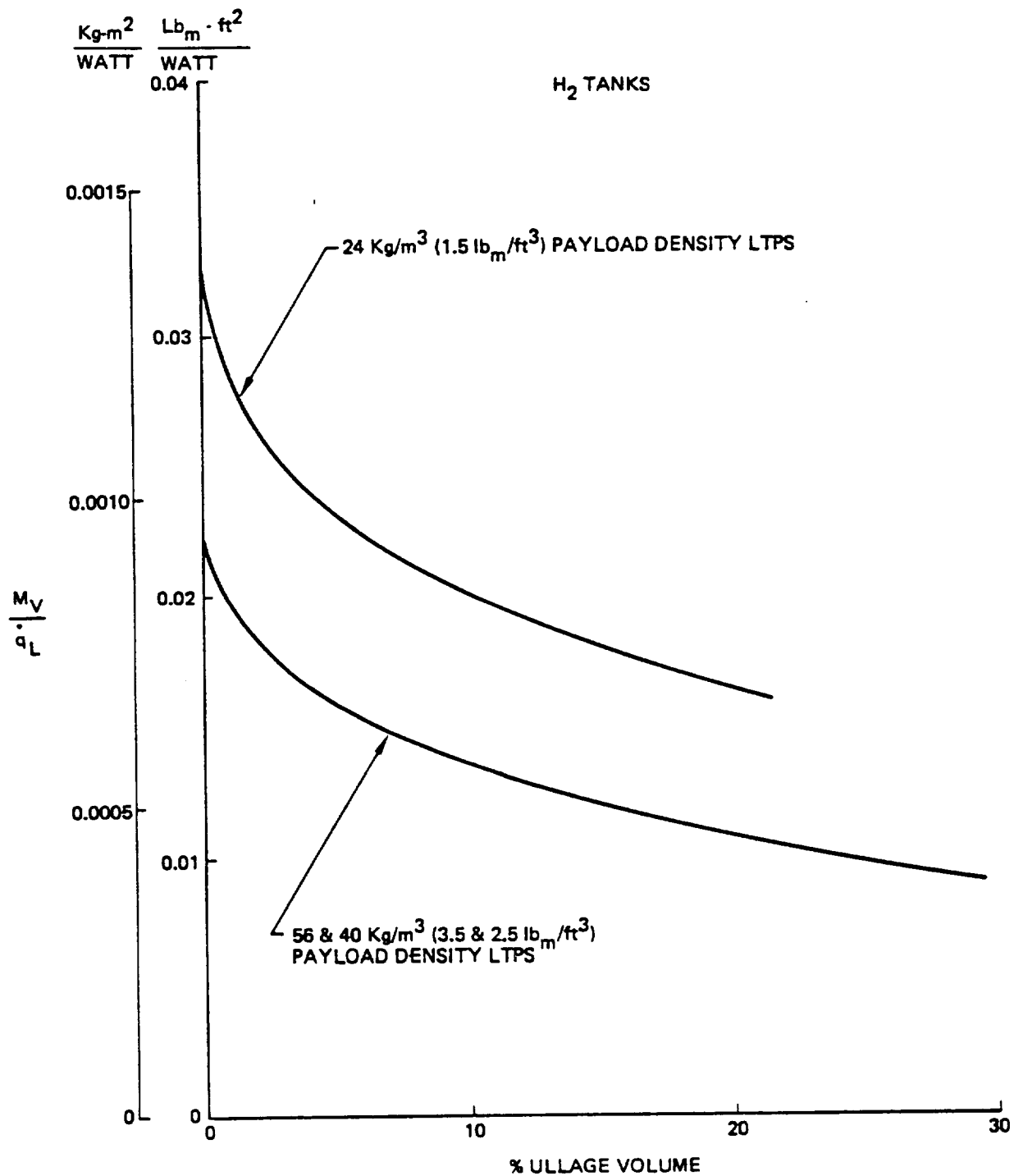


Figure D-3:  $\frac{M_V}{q_L}$  as a Function of Percent Ullage Volume for Baseline LTPS LH<sub>2</sub> Tanks



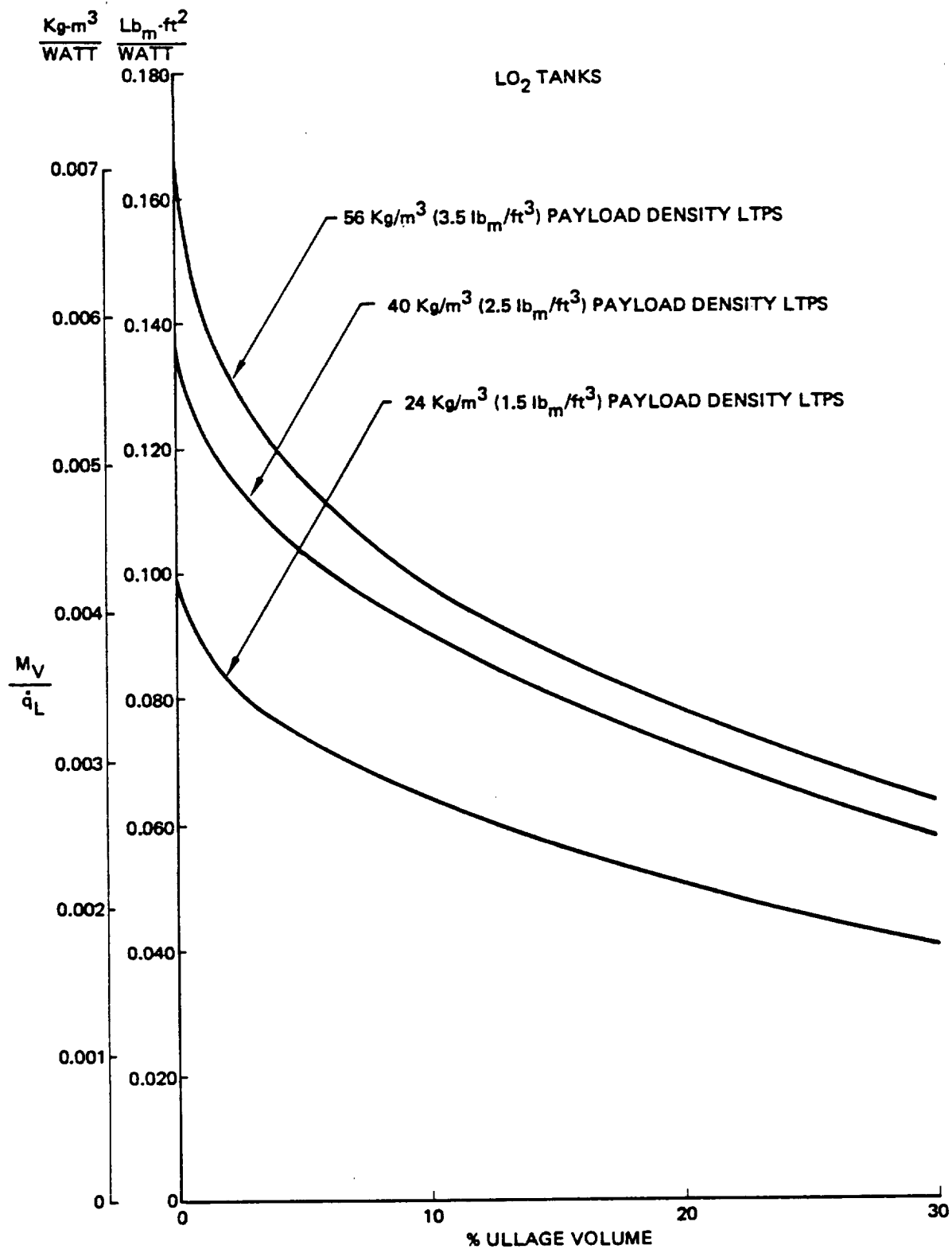


Figure D-4:  $\frac{M_V}{\dot{q}_L}$  as a Function of Percent Volume for Baseline LTDS for Tanks

Referring back to the definition of effective density  $\bar{\rho}^*$  in equation D-1, we see it can be written as

$$\bar{\rho}^* = \frac{M_V + M_L}{V^*} \quad (D-8)$$

$V^*$ , the volume below the free surface, can be related to percent ullage volume by the expression

$$V^* = \left(1 - \frac{S}{100}\right) V_T \quad (D-9)$$

The mass of liquid,  $M_L$ , below the free surface is the liquid density times the difference between the volume below the free surface and the volume of bubbles,  $V_V = \frac{M_V}{\rho_V}$ .

Therefore,  $M_L$  can be expressed as

$$M_L = \rho_L \left( \left(1 - \frac{S}{100}\right) V_T - \frac{M_V}{\rho_V} \right) \quad (D-10)$$

and equation D-8 can be rewritten as

$$\bar{\rho}^* = \frac{M_V + \rho_L \left( \left(1 - \frac{S}{100}\right) V_T - \frac{M_V}{\rho_V} \right)}{\left(1 - \frac{S}{100}\right) V_T} \quad (D-11)$$

Substituting  $(M_V/\dot{q}_L) \dot{q}_L$  for  $M_V$  into equation D-11 and rearranging gives

$$\bar{\rho}^* = \frac{\left(1 - \frac{\rho_L}{\rho_V}\right) \left(\frac{M_V}{\dot{q}_L}\right) \dot{q}_L + \rho_L}{\left(1 - \frac{S}{100}\right) V_T} \quad (D-12)$$

where

$$\left(\frac{M_V}{\dot{q}_L}\right) = f(S) \text{ see Figures D-3 and D-4}$$

$\dot{q}_L$  = function of insulation design, purge gas, and purge enclosure environment.

Equation D-12 was solved parametrically for values of percent ullage volume, with heat flux to the liquid as the independent variable. These calculations are summarized in Figures 5-5 and 5-6 for the  $24 \text{ kg/m}^3$  ( $1.5 \text{ lbm/ft}^3$ ) payload density LTPS tanks.

## APPENDIX E

### PROPELLANT TANK SELF-PRESSURIZATION MODEL

#### Symbols

a,A	empirical constants
M	mass of in tank
P	pressure
P <sub>f</sub>	pressure at end of tank lockup
P <sub>i</sub>	initial pressure
$\dot{Q}$	heat leak rate into tank
S	percent ullage volume
t	time

This appendix describes a mathematical analysis performed to predict the pressure rise in LTPS tanks during vent system lockup at launch. The analysis is based on empirical equations developed by M. H. Blatt and reported in Reference 17.

The expressions developed by Blatt to correlate measured tank pressure rise rate with heat leak, percent ullage volume and liquid mass were of the form:

$$\frac{dP}{dt} = A \left( \frac{\dot{Q}}{SM} \right)^a \quad (E-1)$$

where  $\frac{dP}{dt}$  = rate of pressure rise

If it is assumed that  $\dot{Q}$ , S, and M are constant with time during lockup, equation E-1 can be integrated and the pressure at the end of the lockup period expressed as:

$$P_f = P_i + A \left( \frac{\dot{Q}}{SM} \right)^a t \quad (E-2)$$

Values of the constant A published in Reference 17 were the following:

LH <sub>2</sub> Tanks in 1-"g" environment:	A = 100
LH <sub>2</sub> Tanks in 0-"g" environment:	A = 81
LO <sub>2</sub> Tanks in 0-"g" environment:	A = 1450

It was shown in Reference 17 that, to a good approximation, the value of a could be assumed equal to unity for a 1-"g" environment. Since the publication of Reference 17, additional studies of cryogen tank self-pressurization have been conducted. The test data from two of these studies, reported in References 21 and 22, were combined with the Reference 17 data and new correlations developed. Figure E-1 shows the correlations that were developed for LH<sub>2</sub> tanks in 1-"g". The solid line is a least squares fit of Reference 21 and 22 data. As can be seen, the expression

$$\frac{dP}{dt} = 142 \frac{\dot{Q}}{SM} \quad (E-3)$$

gives the best fit of Reference 21 and 22 data. At values of  $\dot{Q}/SM = 200$  BTU/lbm-hr, the Reference 17 data also fell reasonably close to this line. For comparison purposes, the Reference 17 correlation for LH<sub>2</sub> tank self-pressurization is shown as a dashed line labeled  $dP/dt = 100 \dot{Q}/SM$ . Also shown is an analytically derived curve for surface evaporation. For surface evaporation it is assumed all the heat leak goes into either boiling or heating the vapor in the ullage volume. The liquid phase is assumed to receive no heat and, therefore, remains isothermal at the initial temperature. The surface evaporation model represents the extreme condition which would result in the most rapid pressure rise. A condition approaching surface evaporation may actually occur in practice. The unshaded diamond data point in Figure E-1 represents measured pressure rise in the Centaur LH<sub>2</sub> tank during ground hold. This data point is fairly close to the surface evaporation line.

Figure E-2 shows the measured pressure in the Centaur LH<sub>2</sub> tank during ground hold and launch of the TC-5 flight. An initial rapid rise in pressure occurred from T-27 seconds until launch. This rise rate is approximately that predicted for surface evaporation. At launch, agitation of the liquid and resultant slosh caused the vapor pressure to collapse until thermal equilibrium was essentially established between the ullage and liquid. At this point, the pressure rise resumed.

An effective average pressure rise rate was determined by drawing a straight line between the pressure at start of lockup and the final pressure before vent valve opening. As can be seen in Figure E-2, the measured final pressure rise rate follows this line closely.

The half-shaded diamond data point shown in Figure E-1 represents the effective average pressure rise rate for the Centaur LH<sub>2</sub> tank from Figure E-2. This data point falls very close to the  $dP/dt = 100 \dot{Q}/SM$  line, but is also reasonably close to the  $dP/dt = 142 \dot{Q}/SM$ .

Based on consideration of all measured LH<sub>2</sub> tank self-pressurization measurements, including the Centaur data, it was decided to use the empirical equation

$$\frac{dP}{dt} = 142 \frac{\dot{Q}}{SM} \quad (E-4)$$

to predict LTPS LH<sub>2</sub> tank pressure rise during lockup. For the LO<sub>2</sub> tank under 1-"g" condition the following equation was used:

$$\frac{dP}{dt} = 1790 \frac{\dot{Q}}{SM} \quad (E-5)$$

The value of the constant,  $A = 1790$ , was determined by ratioing the 1-"g" and 0-"g" LH<sub>2</sub> tank pressure rise equations from Reference 17 and multiplying by the constant from the LO<sub>2</sub> tank ( $A = 1450$ ) pressure rise equation for 0-"g".

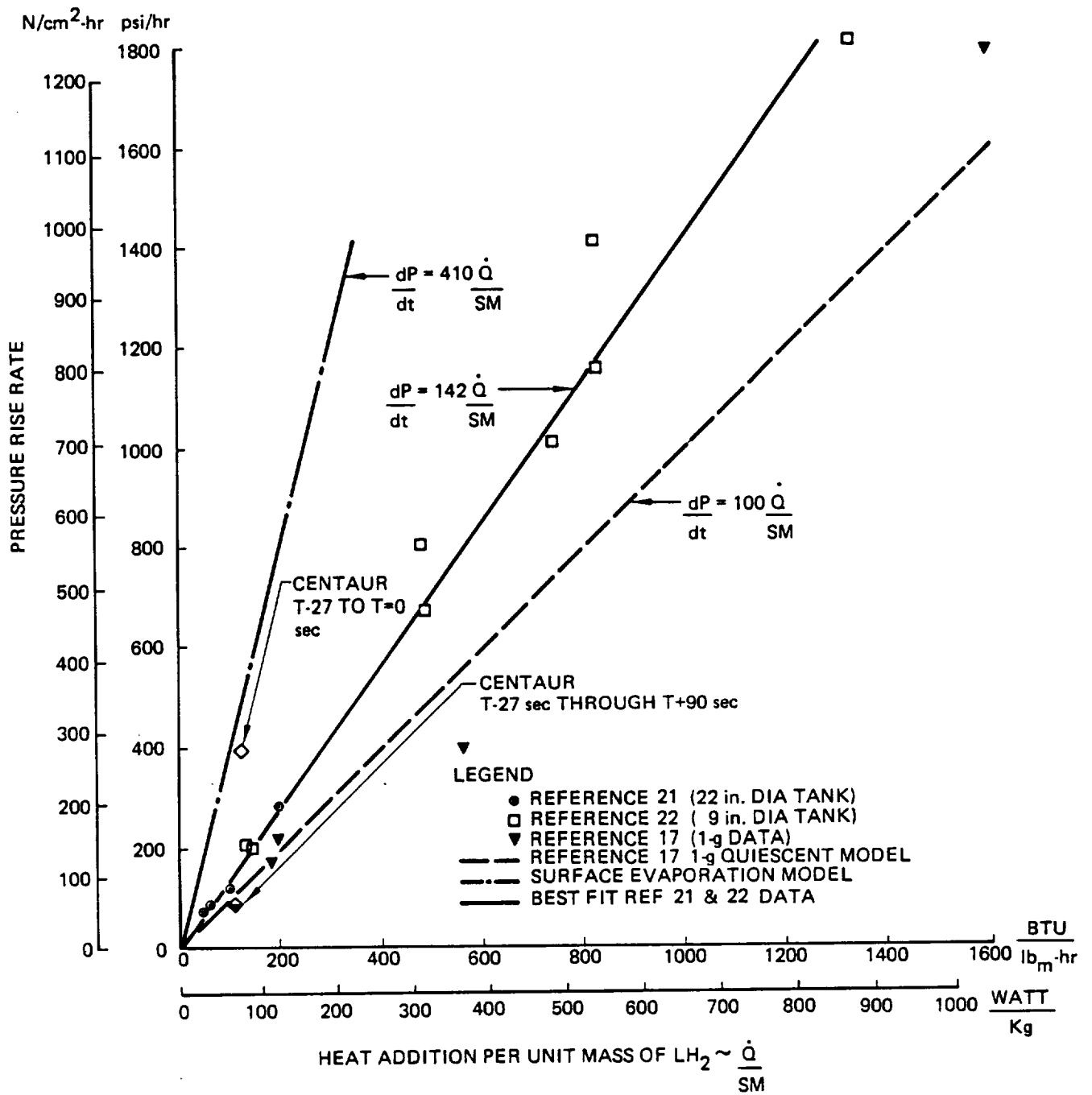


Figure E-1: Correlation of LH<sub>2</sub> Tank Self-Pressurization Data

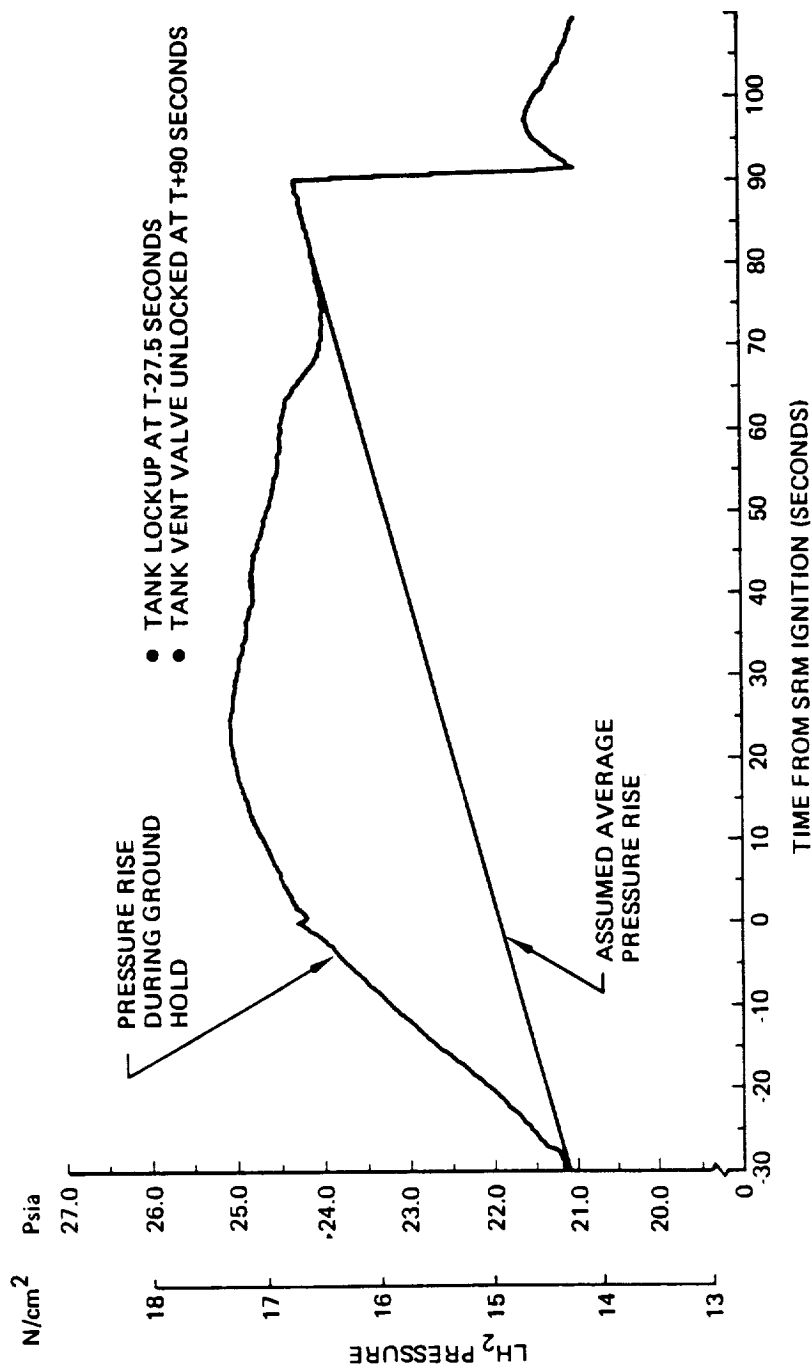


Figure E-2: Measured Pressure Rise in the Centaur 5 LH<sub>2</sub> Tank During Lockup.

**APPENDIX F**  
**SYMBOLS AND DEFINITIONS**

Abbreviations

BTU	British Thermal Units
°C	Degrees Centigrade
cm	Centimeters
°F	Degrees Fahrenheit
ft	Feet
g	Grams
in	Inches
J	Joules
°K	Degrees Kelvin
kg	Kilograms
KJ	Kilojoules
km	Kilometers
KW	Kilowatts
lbf	Pounds force
lb <sub>m</sub>	Pounds mass
m	Meters
min	Minutes
mm	Millimeters
N	Newtons
ppm	Parts per million
sec	Seconds
T	Temperature
W	Watts

## Acronyms

ASE	Airborne support equipment
DAK	Double aluminized Kapton
GEO	Geosynchronous earth orbit
He	Gaseous helium
LEO	Low earth orbit
LH <sub>2</sub>	Liquid hydrogen
LMSS	Land Mobile Satellite System
LO <sub>2</sub>	Liquid oxygen
LSS	Large space structure
LTPS	Low thrust propulsion system
MLI	Multi-layer insulation
MMU	Manned Maneuvering Unit
N <sub>2</sub>	Gaseous Nitrogen
OPERA	Orbital Payload Environmental Radiation Analyzer
OTV	Orbit transfer vehicle
PMSP	Performance and Mission Simulation Program
RADSIM	RADIation SIMulation computer program
RCS	Reaction control system
SINDA	Systems Improved Numerical Differencing Analyzer
STS	Space Transportation System
TMM	Thermal math model
TVC	Thrust vector control



## REFERENCES

1. Anon: Orbit Transfer Vehicle Concept Definition Study, Boeing Document D180-26090-3, Contract NAS8-33532, 1980.
2. Anthony, F. M., Colt, J. Z.; and Helenbrook, R. G.: Development and Validation of Cryogenic Foam Insulation for LH<sub>2</sub> Subsonic Transports, Contractor Report 3404, Contract NAS1-10969, Bell Aerospace Textron, 1981.
3. Parmley, R. T; et al.: Effect of environment on Insulation Materials, Contractor Report NAS120978, Contract NAS3-14342, Lockheed Missiles & Space Company, 1973.
4. Keller, C. W.; et al.: Thermal Performance of Multilayer Insulations, Contractor Report 134477, Contract NAS3-14377, Lockheed Missiles and Space Company, 1974.
5. Sullivan, M. R.: Hoop/Column Antenna Development Program, Large Space Antenna Systems Technology - 1982, NASA Conference Publication 2269, Part 1, 1983.
6. Anon.: Space Shuttle Payload Accommodations - Shuttle Orbiter/Cargo Standard Interfaces, JSC 07700 Volume XIV, Attachment 1 (ICD 2-19001), Revision G, NASA Lyndon B. Johnson Space Center, 1980.
7. Breakwell, J. V.: Computing Low Thrust Transfers to Synchronous Orbit, Annual Report May 1, 1980 - April 30, 1981, NASA Grant NAG 3-63, Stanford University Department of Aeronautics and Astronautics, 1981.
8. Shoji, J. M.; Ketchum, W. J.: Large Space System Cryogenic Deployment System Study, AFRPLTR-83-022, Contract FO4611-81-C-0048, 1983.
9. Springer, G. S.: Heat Transfer in Rarified Gaser, Advances in Heat Transfer, Vol. 7, Academic Press, New York, 1971, pp. 163-218.
10. Corruccini, R. J.: Calculation of Gaseous Heat conduction in Dewars, Advances in Cryogenic Engineering, Vol 3, K. D. Tammerhaus, ed. Plenum Press, New York, 196, pp. 353-366.
11. Keller, C. W.; et al.: Thermal Performance of Multilayer Insulations, Contractor Report 134477, Contract NAS3-14377, Lockheed Missiles and Space Company, 1974.
12. Sumner, I. E.; Maloy, T. E.: Transient Thermal Performance of MLI Systems During Simulated Presure Decay, NASA TND-6335, 1971.
13. Sumner, I. E.: Thermal Performance of Gaseous-Helium-Purged Tank-Mounted MLI System During Ground-Hold and Space-Hold Thermal Cycling and Exposure to Water Vapor, NASA Technical Paper 1114, 1978.
14. Walburn, A. B.: Development of a Reusable Lightweight Cryogenic Storage System, AIAA Paper 74-726, 1974.
15. Knoll, R. H.; Dewitt, R. L.: Thermal Performance of a Modularized Replaceable MLI System for a Cryogenic Stage, NASA TN D-8282, 1977.

16. Anon.: Develop and Demonstrate the Performance of Cryogenic Components Representative of Space Vehicles, Contractor Report GDC/NASA 79-003, Contract NAS8-31778, 1980.
17. Blatt, M. H.: Empirical Correlations for Pressure Rise in Closed Cryogenic Containers, AIAA Journal of Spacecraft and Rockets, Vol. 5, No. 6, June 1968, pp. 773-735.
18. Barclay, D. L.; Bell, J. E.; Brogren, E. W.; Straayer, J. W.: Lightweight Vacuum Jacket for Cryogenic Insulation, Vol. I & II, NASA Contractor Report CR 134759, Contract NAS3-15848, Boeing Aerospace Company, 1975.
19. Smith, J. P.: SINDA User's Manual, NASA Document 14690-H001-R0-00, Contract NAS9-10435, TRW, 1971.
20. North, B F.; Hill, M. E.: Conceptual Design of Two-Phase Fluid Mechanics and Heat Transfer Facility for Spacelab, NASA CR-159810, GDC CRAD-80-002, Contract NAS3-21750, General Dynamics Convair Division, 1980.
21. Aydelott, J. C.; Spuckler, C. M.: Effect of Size on Normal-Gravity Self-Pressurization of Spherical Liquid Hydrogen Tankage, NASA Technical Note, NASA TN D-5196, 1969.
22. Aydelott, J. C.: Effect of Gravity on Self-Pressurization of Spherical Liquid-Hydrogen Tankage, NASA Technical Note, NASA TN D-4286, 1967.